ERRATA SHEET

The Following Corrections and Clarifications Apply to: CORRECTIVE ACTION DECISION DOCUMENT / CORRECTIVE ACTION PLAN FOR CORRECTIVE ACTION UNIT 447: PROJECT SHOAL AREA, SUBSURFACE, NEVADA, REVISION 3, MARCH 2006

DOE Document Number: DOE/NV --1025

Revision: Rev. 3

Original Document Issuance Date: March 2006

This errata sheet was issued under cover letter from DOE on: June 8, 2006

Errata information:

In appendix E, comment response, comment response column change to read:

"DOE will provide NDEP with recent LTHMP data for their consideration on this comment. The combination of historical monitoring data and the projected contaminant boundary from the ground water model suggest that monitoring the wells requested by NDEP would not detect potential contamination. Our goal is to establish a cost effective, efficient monitoring program and the collection of data from additional wells that would provide minimal useful information seems to be unnecessary. DOE proposes to evaluate whether it would be appropriate to include these wells at a future date, once the new wells are drilled and information is obtained from them (and the other wells proposed for the monitoring system) to support the proof of concept."

In appendix E, comment response, comment/rationale column to read:

"After a review of the LTHMP data provided to us, and a comparison to MCLs, it was found that the alpha reading for well HC-2 on 3/20/97 exceeded the MCL. Alpha values have not been measured since that date at that well. Thus, no trends for this well can be determined and until additional recent data is collected, NDEP cannot, at this time, remove the request to include an existing well to the west of the emplacement cavity, but east of the hydraulic boundary, such as well HC-2. In regards to existing wells to the east of the emplacement cavity, but west of the shear zone, such as well HC-7, data from wells HC-6 and HC-7 were collected from 2/01 to 2/05 and 2/00 to 2/05, respectively. However, since 2002, the suite of analytes decreased to only Cs-137 and H-3.

While NDEP will agree to postpone a final decision as to whether it would be appropriate to include the suggested wells at a future date until the new wells are drilled and information is obtained from them, as well as, the other wells proposed for the monitoring system to support the proof of concept, please be advised that there indeed may be a request form NDEP to, at a <u>minimum, sample</u> an existing well to the east of the emplacement cavity but west of the shear zone, such as well HC-7, in addition to a well to the west of the emplacement cavity, but east of the hydraulic boundary, such as well HC-2, for a full suite of analytes, or at a <u>maximum, include in the long term monitoring network</u> for this CAU an existing well to the east of the emplacement cavity but west of the shear zone, such as well HC-7, in addition to a well to the west of the emplacement cavity, but east of the hydraulic boundary, such as well HC-2."

Nevada
Environmental
Restoration
Project

Corrective Action Decision Document/Corrective Action Plan for Corrective Action Unit 447: Project Shoal Area, Subsurface, Nevada

Controlled Copy No.: ___
Revision No.: 3

March 2006

Approved for public release; further dissemination unlimited.

Environmental Restoration
Division

U.S. Department of Energy
National Nuclear Security Administration
Nevada Site Office

Uncontrolled When Printed

Available for public sale, in paper, from:

U.S. Department of Commerce
National Technical Information Service
5285 Port Royal Road
Springfield, VA 22161
Phone: 800.553.6847
Fax: 703.605.6900
Email: *orders@ntis.gov*
Online ordering: *http://www.ntis.gov/ordering.htm*

Available electronically at *http://www.osti.gov/bridge*

Available for a processing fee to U.S. Department of Energy and its contractors, in paper, from:

U.S. Department of Energy
Office of Scientific and Technical Information
P.O. Box 62
Oak Ridge, TN 37831-0062
Phone: 865.576.8401
Fax: 865.576.5728
Email: *reports@adonis.osti.gov*

Reference herein to any specific commercial product, process, or service by trade name, trademark, manufacturer, or otherwise, does not necessarily constitute or imply its endorsement, recommendation, or favoring by the United States Government or any agency thereof or its contractors or subcontractors.

Printed on recycled paper

Uncontrolled When Printed

DOE/NV--1025--Rev. 3

CORRECTIVE ACTION DECISION DOCUMENT/CORRECTIVE ACTION PLAN FOR CORRECTIVE ACTION UNIT 447: PROJECT SHOAL AREA, SUBSURFACE, NEVADA

U.S. Department of Energy
National Nuclear Security Administration
Nevada Site Office
Las Vegas, Nevada

Controlled Copy No.: ___

Revision No.: 3

March 2006

Approved for public release; further dissemination unlimited.

Uncontrolled When Printed

CORRECTIVE ACTION DECISION DOCUMENT/CORRECTIVE ACTION PLAN FOR CORRECTIVE ACTION UNIT 447: PROJECT SHOAL AREA, SUBSURFACE, NEVADA

Approved by: Approved Signature Date: 3/23/2006

John Jones, Acting Project Manager
Offsites Project

Approved by: Approved Signature Date: 3/23/2006

Janet Appenzeller-Wing, Acting Division Director
Environmental Restoration Division

Uncontrolled When Printed

Table of Contents

List of Figures v

List of Tables ix

List of Acronyms and Abbreviations xi

Radionuclides xiv

Executive Summary ES-1

1.0 Introduction 1

1.1 Purpose 3

1.2 Scope 3

1.3 CADD/CAP Contents 4

2.0 Corrective Action Investigation Summary 6

2.1 Investigation Activities 8

2.1.1 Data Collection 8

2.1.1.1 Data Collection from 1996 to 1998 9
2.1.1.2 Data Collection from 1999 to 2003 10
2.1.1.3 Two-Well Tracer Test 11
2.1.1.4 Well Nest 12
2.1.1.5 Summary of Data Collection Results 12

2.1.2 Groundwater Flow and Contaminant Transport Modeling 22

2.1.2.1 The 1998 PSA Groundwater Model 23
2.1.2.2 The Data Decision Analysis 24
2.1.2.3 Model Purpose 24
2.1.2.4 Conceptual Model 25
2.1.2.4.1 Conceptual Flow Model 25
2.1.2.4.2 Conceptual Transport Model 28
2.1.2.5 Computer Code Selection and Verification 30
2.1.2.6 Model Design 32
2.1.2.7 Model Calibration 35
2.1.2.8 Sensitivity and Uncertainty Analysis 39
2.1.2.9 Model Verification 41
2.1.2.10 Predictive Simulations 44
2.1.2.11 Presentation of Model Results 44
2.1.2.12 Post-Audit 44
2.1.2.13 Quality Assurance/Quality Control (QA/QC) 44

Table of Contents *(Continued)*

2.1.2.13.1. Evaluation 45
2.1.2.13.2 Code Verification/Validation.....45
2.1.2.13.3 Documentation.....46
2.1.2.13.4 Peer Review 47

2.1.3 Modeling Results 47

2.2 Contaminant Boundary Determination 55

2.2.1 Land Use and the Contaminant Boundary 56

2.2.2 Relationship Between Risk and Safe Drinking Water Act Requirements 57

2.2.3 Model Uncertainty and Boundary Calculation Process 59

2.2.4 Shoal Contaminant Boundary 63

2.2.5 Boundary Through Time.....66

2.3 Compliance Boundary 66

3.0 Evaluation of Alternatives 70

3.1 Corrective Action Objectives.....70

3.2 Screening Criteria 70

3.2.1 Evaluation Criteria 71

3.3 Development of Corrective Action Alternatives 73

3.3.1 Alternative 1 - No Further Action (Without Institutional Controls).....74

3.3.2 Alternative 2 – Proof-of-Concept and Monitoring with Institutional Controls 74

3.3.3 Alternative 3 – Contaminant Control.....75

3.4 Evaluation of Alternatives 75

4.0 Recommended Alternative.....81

4.1 Proof-of-Concept 81

4.2 Monitoring 82

4.3 Institutional Controls 82

Table of Contents *(Continued)*

5.0 Implementation of the Corrective Action Plan 83

5.1 Monitoring Objectives 83

5.2 Monitoring Network 84

5.2.0 Network Design 85

5.2.0.1 Monitoring Design Tool #1 85
5.2.0.2 Monitoring Design Tool #2 92
5.2.0.3 Monitoring Design Tool #3 105
5.2.0.4 Monitoring Well Completion Interval 116
5.2.0.5 Monitoring Design Summary 121

5.2.1 Monitoring Frequency 123

5.2.2 Monitoring Analytes and Parameters....123

5.2.2.1 Quality Assurance/Quality Control Processes....125
5.2.2.2 Sampling Methods 126

5.2.3 Reporting Requirements 126

5.2.4 Evaluation and Evolution of Monitoring Network through Time 127

5.3 Waste Management....132

5.3.1 Waste Minimization....132

5.3.2 Potential Waste Streams 132

5.3.3 Fluid Management 133

5.3.4 Personal Protective Equipment/Equipment 133

5.3.5 Rinsate….....134

5.3.6 Soil 134

5.3.7 Investigation-Derived Waste Management....134

5.3.7.1 Sanitary Waste 135
5.3.7.2 Hydrocarbons....135
5.3.7.3 Hazardous Waste 135
5.3.7.4 Low-Level Waste....135
5.3.7.5 Mixed Wastes 136
5.3.7.6 PCB and Radioactive PCB Wastes....136

Table of Contents *(Continued)*

5.4 Required Authorizations, Notifications, and Permits 137

5.5 Proof-of-Concept 137

5.5.1 Strategy 139

5.5.1.1 Proposed Step-by-Step Procedure for Shoal Model Validation.....139

5.5.1.2 Implementation of Step 1 in the Procedure for Shoal Model Validation: Selection of Validation Targets.....144

5.5.1.3 Planned Implementation of Step 2 in the Procedure for Shoal Model Validation: Data Collection.....148

5.5.2 Evaluation Criteria 149

5.5.3 Reporting.....151

6.0 Schedule.....153

7.0 Post-Closure.....154

7.1 Inspections and Monitoring 154

7.2 Maintenance of Monitoring System.....155

7.3 Re-Evaluation of Model and Monitoring System.....155

8.0 References.....157

Appendix A – Proposed Engineering Specifications and Drawings

Appendix B – Deviation of Existing Boreholes and Depth Correction Procedure

Appendix C – Parametric Uncertainty Analysis for Validation Target Identification

Appendix D – Validation Metrics and Application to the Shoal Model

Appendix E – Nevada Environmental Restoration Project Document Review Sheet

List of Figures

Figure 1-1 CAU 447, Project Shoal Area location map 2

Figure 2-1 Exploratory boreholes and characterization wells at PSA 13

Figure 2-2 West-east profile through PSA showing the potentiometric surface 15

Figure 2-3 Histogram of hydraulic conductivity measurements in the granite aquifer at the PSA (Mihevc et al., 2000) 17

Figure 2-4 Numerically derived distribution of effective porosity and the associated lognormal distribution 18

Figure 2-5 West-east cross section through the northern Sand Springs Range and valleys on either side 26

Figure 2-6 3-D depiction of the PSA conceptual model 26

Figure 2-7 Conceptual model of the transport model source and processes considered 29

Figure 2-8 Three views of the model domain 33

Figure 2-9 Simulated and observed drawdown for HC-6 42

Figure 2-10 Simulated and observed drawdown for HC-7 43

Figure 2-11 Distributions of average velocities in the three coordinate directions for all realizations 49

Figure 2-12 Distribution of $\log_{10}$-transformed maximum velocity vectors for all realizations 50

Figure 2-13 Snapshots of the 3-D particle distribution 51

Figure 2-14 Projected maps of the maximum concentration distribution for tritium for the flow realization shown in Figure 2-13 52

Figure 2-15 Projected maps of the maximum concentration distribution for tritium for one flow realization 53

Figure 2-16 Contaminant boundary maps for tritium delineating the areas exceeding 20,000 pCi/L at the 50 percent confidence level for the 1,000-year simulation period 54

List of Figures *(Continued)*

Figure 2-17 Contaminant boundary maps for tritium delineating the areas exceeding 20,000 pCi/L at the 95 percent confidence level for the 1,000-year simulation period 55

Figure 2-18 Probability distribution function showing how typical confidence levels are determined 61

Figure 2-19 Probability distribution function showing how the concentration threshold is calculated for the contaminant boundary 62

Figure 2-20 An example of the probability distribution function and how the concentration threshold is calculated for the contaminant boundary....63

Figure 2-21 An example of a 3-D contaminant boundary and the associated mapping to an x-y plane (at top of figure) 64

Figure 2-22 Regulatory-based contaminant boundary for the Project Shoal Site 65

Figure 2-23 Compliance boundary 69

Figure 5-1 Conceptualization of the contamination source, plume migration, and siting horizons for locating monitoring wells 87

Figure 5-2 Selection of control plane locations and orientation normal to the mean flow direction 89

Figure 5-3 The model domain, the cavity, and the five CPs 91

Figure 5-4 Schematic diagram showing the location of contaminant plume, monitoring wells, and the distances and definitions used in Equations (5-2) through (5-4) 94

Figure 5-5 Location of the 15 potential wells and the five CPs 98

Figure 5-6 Map showing the well numbers used when applying tools 2 and 3 to the monitoring analysis....99

Figure 5-7 The *t*-*z* distribution of the resident mass in the vicinity of each of 20 potential well locations 101

Figure 5-8 Vertically-integrated resident mass in the vicinity of 20 potential well locations 102

Figure 5-9 Detection probability for the 20 potential wells at different times 103

Figure 5-10 Success probability of individual wells at different times for $\alpha = 1$ percent....105

List of Figures *(Continued)*

Figure 5-11 Number of detections by individual wells 106

Figure 5-12 Plume trajectories projected on a vertical section through the model domain.....108

Figure 5-13 Trajectories of detected plumes superimposed on the potential well locations for first configuration where well HC-1 is included 109

Figure 5-14 Trajectories of non-detected plumes superimposed on the potential well locations for first configuration where well HC-1 is included.....110

Figure 5-15 Trajectories of detected plumes superimposed on the potential well locations for second configuration where well HC-1 is excluded 111

Figure 5-16 Trajectories of non-detected plumes superimposed on the potential well locations for second configuration where well HC-1 is excluded 112

Figure 5-17 Detection efficiency for 76 three-well networks as computed by geometric considerations 114

Figure 5-18 Detection zones for networks 1 and 2 (a - to the left) and 36 and 37 (b - to the right) 115

Figure 5-19 Temporally integrated resident mass in the vicinity of 15 potential well locations as a function of elevation, z 119

Figure 5-20 Tested intervals and numbers of detected plume trajectories for each interval for wells 2, 4, and 6 120

Figure 5-21 Trajectories of plumes superimposed on the potential well locations 121

Figure 5-22 Proposed monitor well network relative to the test cavity and the computed MCL-based contaminant boundary.....122

Figure 5-23 Water levels measured in Shoal wells located west of the shear zone 129

Figure 5-24 Hydraulic head range predicted by the flow model for the proposed well locations 131

Figure 5-25 Detailed flowchart of the proposed model validation and postaudit processes for the Shoal model (from Hassan, 2005).....140

Figure 5-26 Validation decision tree chart 151

List of Figures *(Continued)*

Figure 6-1 Schedule 153

List of Tables

Table 2-1 Summary information for wells used in the Shoal investigation 14

Table 2-2 Fracture summary statistics (ND = not defined) 16

Table 2-3 Global prior probabilities for flow Categories 1 and 2 as determined from borehole fracture score analysis of video logs 16

Table 2-4 Summary of hydraulic test data for wells near the PSA (Mihevc et al., 2000) 17

Table 2-5 Selected static water level measurements from wells near the PSA. Summarized from Mihevc et al., 2000 18

Table 2-6 Linear and Freundlich isotherm parameters 20

Table 2-7 Chemical analyses of water samples collected from the HC wells at PSA, along with analyses of groundwater from other wells in the area of the Sand Springs Range (Chapman et al., 1994) 21

Table 2-8 Isotopic analyses for groundwater samples from PSA 21

Table 2-9 Summary statistics for the results of the PSA flow model 38

Table 2-10 Radionuclides used for the contaminant boundaries and related parameters (Pohll et al., 2003) 58

Table 3-1 Detailed evaluation of alternatives 76

Table 5-1 Parameters of Equation. (1), the resulting CP efficiency (Si/Wi), and the minimum number of wells, N_i, to span each CP at different times 92

Table 5-2 Well assignments in the evaluated monitoring networks 107

Table 5-3 Prediction quantiles for the plume height at different times and for the five CPs 117

Table 5-4 Prediction quantiles for the *z*-position of the plume c.o.m. at different times and for the five CPs 117

Table 5-5 Parameters of Equation (5-1) and the minimum number of intervals, N_i, to span each CP (or well) at different times 118

Table 5-6 Monitoring analytes and parameters 124

Table 5-7 Additional analytes 127

List of Tables

Table 5-8 Waste management regulations and requirements.....132

Table 5-9 Uncertainty cases for five flow parameters and four transport parameters. Two flow realizations are selected to run the transport parameter uncertainty analyses: a) one of the fastest realizations in the base case model, and b) the realization with the least RMSE in the base case model.....147

List of Acronyms and Abbreviations

AEC	U.S. Atomic Energy Commission
AMSL	Above mean sea level
ATV	Acoustic televiewer
ARAR	Applicable or relevant and appropriate requirement
BLM	U.S. Department of the Interior, Bureau of Land Management
^{o}C	Degrees Celsius
CADD	Corrective Action Decision Document
CADD/CAP	Corrective Action Decision Document/Corrective Action Plan
CAI	Corrective Action Investigation
CAIP	Corrective Action Investigation Plan
CAP	Corrective Action Plan
CAS	Corrective Action Site
CAU	Corrective Action Unit
CERCLA	*Comprehensive Environmental Response, Compensation, and Liability Act of 1980*
CFR	*Code of Federal Regulations*
cm	Centimeter
cm/yr	Centimeters per year
cm^3/g	Cubic centimeters per gram
COC	Contaminant of concern
c.o.m.	Center of mass
COPC	Contaminant of potential concern
CP	Control plane
DDA	Data Decision Analysis
DoD	U.S. Department of Defense
DOE	U.S. Department of Energy
DOE/NV	U.S. Department of Energy, Nevada Operations Office
DPM/gC	Disintegrations per minute per gram of carbon
DQO	Data Quality Objective
DRI	Desert Research Institute
EC	Electrical conductivity
EIS	Environmental Impact Statement
EPA	U.S. Environmental Protection Agency

List of Acronyms and Abbreviations *(Continued)*

FFACO	*Federal Facility Agreement and Consent Order*
ft	Foot
g	Gram
h_m	Measured head
h_s	Simulated head
HC	Hydrologic characterization
HWAAs	Hazardous waste accumulation areas
IDW	Investigation-derived waste
K	Hydraulic conductivity
km	Kilometer
LLW	Low-level radioactive waste
L/d	Liter per day
L/min	Liter per minute
m	Meter
m/d	Meter per day
m/yr	Meters per year
m^3	Cubic meter
m^2/g	Square meters per gram
m^3/d	Cubic meters per day
MCL	Maximum contaminant level
MEMO	Monitoring efficiency model
mg/kg	Milligrams per kilogram
mg/L	Milligrams per liter
μg/L	Micrograms per liter
mL	Milliliter
mrem/yr	Millirem per year
mSv/yr	Millisievert per year
NAC	*Nevada Administrative Code*
NMC	Number of Monte Carlo realizations

List of Acronyms and Abbreviations *(Continued)*

NNSA/NSO	U.S. Department of Energy, National Nuclear Security Administration/Nevada Site Office
NRS	*Nevada Revised Statutes*
NTS	Nevada Test Site
NTSWAC	*Nevada Test Site Waste Acceptance Criteria*
pCi/L	Picocuries per liter
PCB	Polychlorinated biphenyl
pdf	Probability distribution function
PLO	*Public Land Order*
PQ	Prediction quantile
PPE	Personal protective equipment
PSA	Project Shoal Area
PVC	Polyvinyl chloride
QAPP	Quality Assurance Project Plan
QA/QC	Quality Assurance/Quality Control
RadCon	Radiological Control
R_C	Cavity radius
RCRA	*Resource Conservation and Recovery Act*
RMSE	Root mean square error
RV	Reference value
RWPT	Random walk particle tracking
SAA	Satellite accumulation area
SDWA	*Safe Drinking Water Act*
UGTA	Underground Test Area
USGS	U.S. Geological Survey
UTM	Universal Transmercator
yr	Year
2-D	Two-dimensional
3-D	Three-dimensional

Radionuclides

^{14}C	Carbon-14
^{137}Cs	Cesium-137
^{129}I	Iodine-129
^{151}Sm	Samarium-151
^{90}Sr	Strontium-90
^{3}H	Tritium

Executive Summary

This Corrective Action Decision Document/Corrective Action Plan (CADD/CAP) has been prepared for Corrective Action Unit (CAU) 447, Project Shoal Area (PSA) - Subsurface, Nevada, in accordance with the *Federal Facility Agreement and Consent Order* (FFACO) (1996). Corrective Action Unit 447 is located in the Sand Springs Mountains in Churchill County, Nevada, approximately 48 kilometers (30 miles) southeast of Fallon, Nevada.

The CADD/CAP combines the decision document (CADD) with the Corrective Action Plan (CAP) and provides or references the specific information necessary to recommend corrective actions for CAU 447, as provided in the FFACO. Corrective Action Unit 447 consists of two corrective action sites (CASs): CAS 57-49-01, Emplacement Shaft, and CAS 57-57-001, Cavity. The emplacement shaft (CAS-57-49-01) was backfilled and plugged in 1996 and will not be evaluated further.

The purpose of the CADD portion of the document (Section 1.0 to Section 4.0) is to identify and provide a rationale for the selection of a recommended corrective action alternative for the subsurface at PSA. To achieve this, the following tasks were required:

- Develop corrective action objectives.
- Identify corrective action alternative screening criteria.
- Develop corrective action alternatives.
- Perform detailed and comparative evaluations of the corrective action alternatives in relation to the corrective action objectives and screening criteria.
- Recommend a preferred corrective action alternative for the subsurface at PSA.

The original Corrective Action Investigation Plan (CAIP) for the PSA was approved in September 1996 and described a plan to drill and test four characterization wells, followed by flow and transport modeling (DOE/NV, 1996). The resultant drilling is described in a data report (DOE/NV, 1998e) and the data analysis and modeling in an interim modeling report (Pohll et al., 1998). After considering the results of the modeling effort, the U.S. Department of Energy (DOE) determined that the degree of uncertainty in transport predictions for PSA remained unacceptably large. As a result, a second CAIP was developed by DOE and approved by the Nevada Division of Environmental Protection (NDEP) in December 1998 (DOE/NV, 1998a). This plan prescribed a rigorous analysis of uncertainty in the Shoal model and

quantification of methods of reducing uncertainty through data collection. This analysis is termed a Data Decision Analysis (Pohll et al., 1999a) and formed the basis for a second major characterization effort at PSA (Pohll et al., 1999b). The details for this second field effort are presented in an Addendum to the CAIP, which was approved by NDEP in April 1999 (DOE/NV, 1999a). Four additional characterization wells were drilled at PSA during summer and fall of 1999; details of the drilling and well installation are in IT Corporation (2000), with testing reported in Mihevc et al. (2000). A key component of the second field program was a tracer test between two of the new wells (Carroll et al., 2000; Reimus et al., 2003).

Based on the potential exposure pathways, two corrective action objectives were identified for CAU 447:

- Prevent or mitigate exposure to groundwater contaminants of concern at concentrations exceeding regulatory maximum contaminant levels or risk-based levels.
- Reduce the risk to human health and the environment to the extent practicable.

Based on the review of existing data, the results of the modeling, future use, and current operations at PSA, the following alternatives have been developed for consideration at CAU 447:

- Alternative 1 – No Further Action
- Alternative 2 – Proof-of-Concept and Monitoring with Institutional Controls
- Alternative 3 – Contaminant Control

The corrective action alternatives were evaluated based on the approach outlined in the *Focused Evaluation of Selected Remedial Alternatives for the Underground Test Area (*DOE/NV, 1998b). Each alternative was assessed against nine evaluation criteria. These criteria include overall protection of human health and the environment; compliance with appropriate requirements; long-term effectiveness; reduction of the toxicity, mobility, or volume of contamination; short-term effectiveness; implementability; cost; state acceptance; and community acceptance. Based on the results of this evaluation, the preferred alternative for CAU 447 is Alternative 2, Proof-of-Concept and Monitoring with Institutional Controls.

The preferred corrective action alternative was chosen for its technical implementability, focusing on performance, reliability, feasibility, safety, and cost. Alternative 2 was judged to meet all requirements for the technical components evaluated and will control inadvertent exposure to contaminated groundwater at CAU 447. Implementation of the corrective action and post-closure activities are described in the CAP portion of this document (Section 5.0 to Section 7.0).

1.0 INTRODUCTION

This Corrective Action Decision Document/Corrective Action Plan (CADD/CAP) has been prepared for Corrective Action Unit (CAU) 447, Project Shoal Area (PSA) - Subsurface, Nevada in accordance with the *Federal Facility Agreement and Consent Order* (FFACO) that was agreed to by the State of Nevada, the U.S. Department of Energy (DOE), and the U.S. Department of Defense (DoD) (FFACO, 1996). The CADD portion of the document (Section 1.0 to Section 4.0) provides or references the specific information necessary to recommend corrective actions for Corrective Action Site (CAS) 57-57-001, PSA Cavity, and CAS 57-49-01, Emplacement Shaft, at CAU 447. The emplacement shaft (CAU 57-49-01) was backfilled and plugged in 1996 and will not be evaluated further (DOE, NV, 1998a). The CAP portion of the document (Section 5.0 to Section 7.0) describes implementation of the corrective action and post-closure activities.

The PSA is located in the Sand Springs Mountains in Churchill County, Nevada, approximately 48 kilometers (km) (30 miles) southeast of Fallon, Nevada (Figure 1-1). The PSA was part of the Vela Uniform Program, which was conducted to improve the United States' ability to detect, identify, and locate underground nuclear detonations. The test consisted of detonating a 12-kiloton nuclear device deep underground in granitic rock to determine whether seismic waves produced by an underground nuclear test could be differentiated from seismic waves produced by a naturally occurring earthquake. The test was a joint effort conducted by the U.S. Atomic Energy Commission (AEC) and the DoD in October 1963 (AEC, 1964). The subsurface source of contamination is the PSA test cavity, and includes radioactive fission products, uranium, plutonium, and tritium (NNSA/NSO, 2004).

Corrective Action Unit 447 contains two subsurface CASs: CAS 57-49-01, Emplacement Shaft, and CAS 57-57-001, Cavity, which are collectively addressed by this document. In 1998, closure was completed for CAU 417, which contains three surface CASs. The Closure Report for the surface at PSA (DOE/NV, 1998c) was accepted without comment by the Nevada Division of Environmental Protection (NDEP).

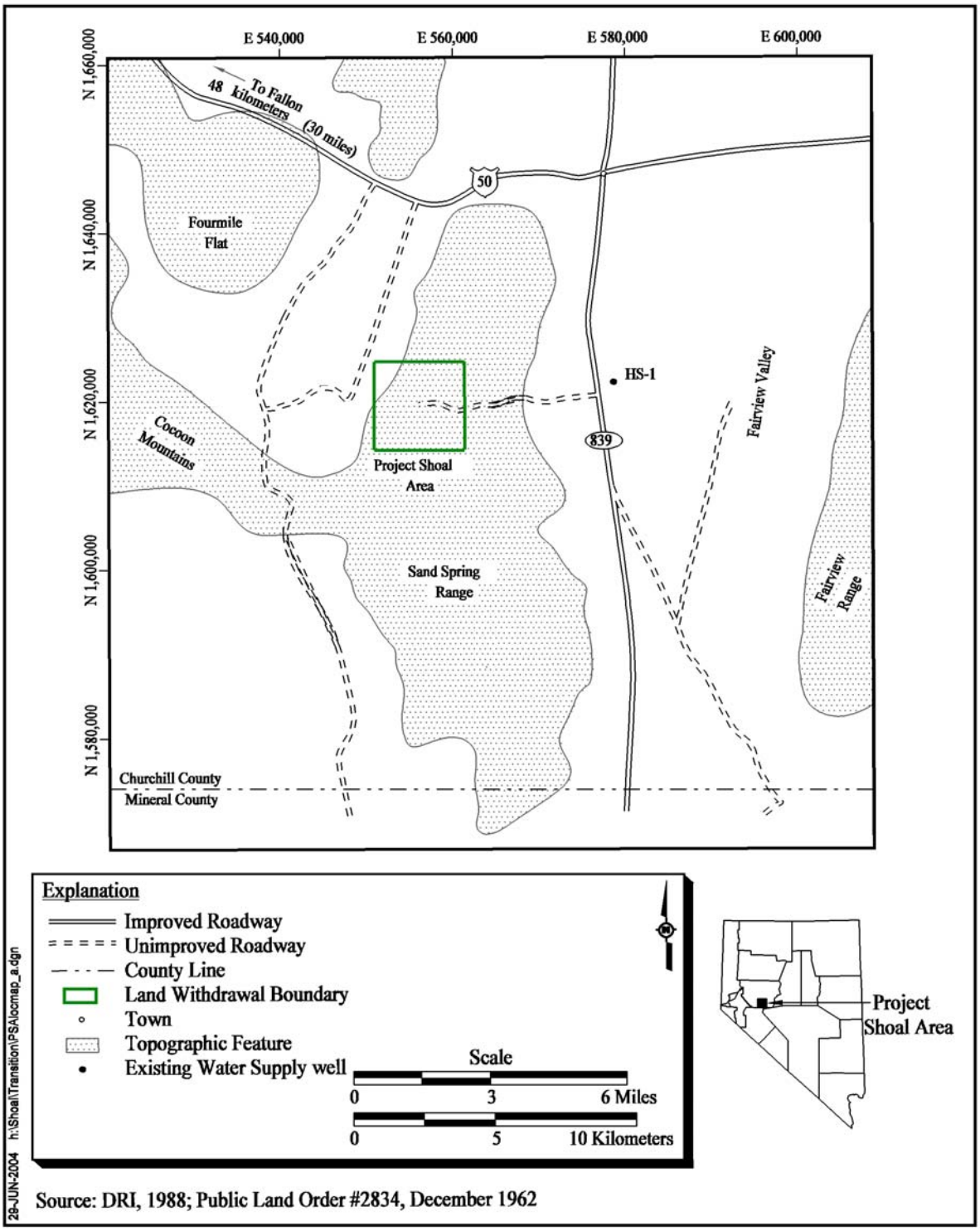

Figure 1-1
CAU 447, Project Shoal Area location map

1.1 Purpose

This CADD/CAP presents the results of two corrective action investigations (CAIs) conducted in 1996 and 1998 (DOE/NV, 1996; 1998a; and 1999a) and develops, evaluates, and recommends a corrective action alternative for CAU 447. Further, it describes implementation of the corrective action and post-closure monitoring strategy, the proof-of-concept strategy, and the reporting procedures for implementing the selected corrective action. The evaluation of corrective action alternatives is based on process knowledge and the results of investigative activities conducted in accordance with the two corrective action investigation plans (CAIPs) and one associated addendum (DOE/NV, 1996; 1998a; and 1999a).

1.2 Scope

The activities used to identify, evaluate, and recommend the proposed CAP alternative consisted of the following:

- Incorporate the results of the CAI and the groundwater modeling (Section 2.0).
- Develop a compliance boundary (Section 2.0).
- Develop corrective action objectives (Section 3.0).
- Identify corrective action alternative screening criteria (Section 3.0).
- Perform detailed and comparative evaluations of corrective action alternatives in relation to corrective action objectives and screening criteria (Section 3.0).
- Recommend and justify a preferred corrective action alternative for CAU 447 (Section 4.0).

Based on the results of the activities above, the preferred corrective action alternative for CAU 447 is Alternative 2, Proof-of-Concept and Monitoring with Institutional Controls. The proof-of-concept approach relies on the groundwater flow and transport model of the underground nuclear test at PSA. Monitoring will be accomplished by placing monitoring wells downgradient from the nuclear test emplacement point. Periodic water sampling and testing will confirm that contamination is confined within the compliance boundary. Finally, institutional controls will be put in place to restrict subsurface use in the vicinity of PSA.

Alternative 2 was judged to meet all requirements for the technical components evaluated, and will control inadvertent exposure to contaminated groundwater at CAU 447. Implementation of the corrective action and post-closure activities are described in the CAP portion of this document (Section 5.0 to Section 7.0).

1.3 CADD/CAP Contents

This CADD/CAP was developed in accordance with a standardized outline agreed to by the NDEP and DOE on August 26, 2003. The outline contains specific annotations prescribing the content of each section. Section 1.0 to Section 4.0 comprises the CADD portion of this document. The CAP portion is found in Section 5.0 to Section 7.0. The appendices are not specified in the FFACO. Each section is briefly summarized below:

Section 1.0 - Introduction: summarizes the purpose, scope, and contents of the CADD.

Section 2.0 - Corrective Action Investigation Summary: summarizes the investigation field activities, the results of the investigation, describes the contaminant and compliance boundaries, and the need for corrective action.

Section 3.0 - Evaluation of Alternatives: presents corrective action alternatives and documents the steps taken to determine a preferred corrective action alternative.

Section 4.0 - Recommended Alternative: presents the preferred corrective action alternative and the rationale for its selection based on the corrective action objectives and alternative screening criteria.

Section 5.0 - Implementation of the Corrective Action Plan: describes the proposed corrective action alternative and the key elements of its planned implementation.

Section 6.0 - Schedule: presents the schedule for major activities and milestones for implementing the approved corrective action.

Section 7.0 - Post-Closure: discusses DOE's commitment to and plans for post-closure inspection, monitoring, and long-term stewardship based on the CAP.

Section 8.0 - References: provides a list of all referenced documents.

Appendix A: Proposed Engineering Specifications and Drawings

Appendix B: Deviation of Existing Boreholes and Depth Correction Procedure

Appendix C: Parametric Uncertainty Analysis for Validation Target Identification

Appendix D: Validation Metrics and Application to the Shoal Model

All work was performed in accordance with the following documents:

- *Corrective Action Investigation Plan for Project Shoal Area CAU No. 416* (DOE/NV, 1996)
- *Corrective Action Investigation Plan for Corrective Action Unit 447: Project Shoal Area, Nevada Subsurface Site* (DOE/NV, 1998a)
- *Addendum to the Corrective Action Investigation Plan for Corrective Action Unit 447: Project Shoal Area, Nevada Subsurface Site* (DOE/NV, 1999a)
- *Focused Evaluation of Selected Remedial Alternatives for the Underground Test Area* (DOE/NV, 1998b)
- *Underground Test Area* (UGTA) *Quality Assurance Project Plan,*(QAPP) *Nevada Test Site, Nevada*, Rev. 2, and Rev. 3, DOE/NV--341 (DOE/NV, 1998d; 2000b)
- *Federal Facility Agreement and Consent Order* (1996)

2.0 CORRECTIVE ACTION INVESTIGATION SUMMARY

The CAI for CAU 447 focused on numerical modeling of groundwater flow and radionuclide transport. This is consistent with the strategy outlined in Appendix VI (Rev. 1, 2000) of the FFACO (1996). Investigation of the Shoal underground nuclear test was conducted under two CAIPs. The first of these (DOE/NV, 1996) was prepared for the combined surface and subsurface portions of the PSA under CAU 416. The second was prepared as a separate subsurface CAIP for CAU 447 (DOE/NV, 1998a). Both of these plans shared the common objective of evaluating groundwater flow and contaminant transport from the Shoal test cavity. Specific objectives described in the approved 1996 CAIP (DOE/NV, 1996) are as follows:

- Determine the groundwater gradient in the test area under undisturbed regions.
- Obtain information on the nature of permeability and porosity in the Sand Springs granite.
- Obtain information on recharge conditions.
- Obtain information on migration of contaminants from the nuclear test.
- Combine historic and newly acquired data to map aquifer properties and provide a framework for flow simulations to determine mean velocity, direction and spatial characteristics of the flow field.
- Predict solute migration to determine the boundary of specified contaminant concentrations in the aquifer.

The purpose of the state-approved 1998 CAIP (DOE/NV, 1998a) was to guide collection of additional hydrogeologic data in order to reduce uncertainties in model input parameters. It called for a Data Decision Analysis (DDA) (Pohll et al., 1999a) to determine which investigation and data collection methods would minimize model uncertainty. Specific objectives for the investigation, as determined from the DDA, can be found in the Addendum to the 1998 CAIP (DOE/NV, 1999a) and are as follows:

- Reduce uncertainty in groundwater recharge through vadose zone modeling.
- Reduce uncertainty in effective porosity by performing a two-well tracer test.
- Reduce uncertainty in the hydraulic properties of the saturated zone at depths greater than previously investigated at the site.

To ensure all project objectives, health and safety requirements, and quality control procedures were adhered to, all investigation activities were performed in accordance with the following documents:

- *Corrective Action Investigation Plan for Project Shoal Area, CAU No. 416* (DOE/NV, 1996)
- *Corrective Action Investigation Plan for Corrective Action Unit 447: Project Shoal Area, Nevada Subsurface Site* (DOE/NV, 1998a)
- *Addendum to the Corrective Action Investigation Plan for Corrective Action Unit 447: Project Shoal Area, Nevada Subsurface Site* (DOE/NV, 1999a)
- *Underground Test Area Quality Assurance Project Plan, Nevada Test Site, Nevada*, Rev. 2, and Rev. 3, DOE/NV--341 (DOE/NV, 1998d; and 2000b)
- *Federal Facility Agreement and Consent Order* (1996)

The following sections describe and summarize these activities, provide the investigation results, and identify the need for corrective action at CAU 447. The detailed investigation plan can be found in the CAIPs (DOE/NV, 1996;and 1998a).

CAI activities can be broadly grouped into two phases, consistent with the CAIPs. The first consisted of the drilling and testing of wells HC-1, -2, -3, and -4 in 1996 and 1997, followed by the first period of data analysis and modeling that was completed in 1998. The second encompassed the drilling and testing of wells HC-5, -6, -7, and -8, including the operation of a long-term tracer test that occurred from 1999 through 2000. This was followed by the second period of data analysis and modeling that culminated in the CAU model approved by NDEP in February 2004.

The reason for the two phases described above is as follows. At the conclusion of the 1998 modeling effort, DOE determined that the CAU model was unacceptable as a result of the remaining level of uncertainty. As the decision point in the FFACO process flow diagram requires concurrence from both DOE and NDEP on the model acceptability, the DOE decision alone forced the investigation to return to an earlier stage. The DOE and NDEP worked together and concluded that the subsurface strategy was achievable and that concerns regarding uncertainty could be addressed through additional data collection guided by a DDA. This agreement is documented through the submission of the CAIP for CAU 447 and its approval by NDEP on December 24, 1998. The field plan based on the DDA was presented by DOE to NDEP in an Addendum to the CAIP, and this addendum was approved by NDEP on April 20, 1999.

The model report developed under the CAIP for CAU 447 was presented to NDEP in January 2003. On March 20, 2003, DOE received NDEP's review of the modeling report in which they suggested that the document could be acceptable pending appropriate revisions per technical comments. Changes were made to the document, including additional modeling analysis, and the revised report was submitted to NDEP on January 13, 2004. The NDEP provided their concurrence with the PSA model by letter on February 18, 2004.

The approval of the model led to the next step in the CAI strategy, the calculation of a contaminant boundary. This boundary is presented in Section 2.2.

Each of the major elements of the investigation is described briefly below, with references to the detailed work.

2.1 Investigation Activities

The investigation activities are presented in three parts in this section. First, the data collection activities are described. Second, the modeling activities are presented. Third, the results of the investigations are summarized. Calculation of the contaminant boundary is presented in Section 2.2.

2.1.1 Data Collection

The Data Quality Objectives (DQOs) guiding data collection at PSA are presented in the original CAIP (DOE/NV, 1996). The DQOs focus on the data needed to support the development of the contaminant boundary. Data collection was implemented according to the FFACO (1996) and the *Underground Test Area Quality Assurance Project Plan* (DOE/NV, 1998d). The data collected under the 1996 CAIP were not sufficient to meet the DQOs, thus necessitating a second round of data collection in 1999. The combined data from both field campaigns, as well as supporting laboratory investigations, meets the DQO of developing a contaminant boundary for the PSA, as discussed below.

An overview of the two data collection periods and specific work is presented first, to help the reader understand the specific objectives guiding each data collection period and the work performed in response to those objectives. The data and interpretations themselves are then presented in a combined form, as the sequence of data collection is unimportant in terms of the overall objective of developing a contaminant boundary.

2.1.1.1 Data Collection from 1996 to 1998

The field characterization plan approved through the 1996 CAIP (DOE/NV, 1996) had the following objectives:

- Determine the groundwater gradient in the test area under undisturbed conditions.
- Obtain information on the nature of permeability and porosity in the Sand Springs granite.
- Obtain information on recharge conditions.
- Obtain information on migration of contaminants from the nuclear test.

These objectives were directed at refining how the conceptual model was developed during the 1960s for groundwater flow and transport at the site. For example, the presence of a hydrologic divide was well demonstrated by the 1960s data, but its location relative to the nuclear test was unclear. Thus the very basic information of the direction of flow from the nuclear test was a high priority objective. To meet the objectives, four Hydrologic Characterization (HC) wells were drilled in 1996. These wells were then subjected to a variety of well logging and aquifer testing activities. In addition, granite from the drilling muck pile was collected to characterize transport properties.

Data from HC-1, -2, -3, and -4 established that the groundwater divide was located west of the nuclear test. Given the distribution of head information and the conceptual model of groundwater flow from the mountain range to the valleys, this suggested flow from the nuclear test was essentially southeastward, perpendicular to the divide (see also Section 2.1.2.4). The nature of permeability and porosity was confirmed as confined to fractures in the granite. Bulk and discrete measurements of hydraulic conductivity were made, but no quantification of porosity was possible. Recharge was estimated using temperature profiles. The absence of radionuclides in the inferred downgradient well, HC-3, indicated lack of significant radionuclide transport, although low levels of test-derived nuclides were found in well HC-4, close to the test cavity. The equilibrium sorption experiments, conducted using granite from the site, evaluated retardation values of several cations and anions (Pohll et al, 1998).

The DOE/NV (1998e) document presents the drilling history for wells HC-1, -2, -3, and -4. Testing data can be found in the appendices to Pohll et al. (1998). Hydraulic head data from the wells provided information regarding the central question of the location of the groundwater divide relative to the nuclear test. Although information was gained in regard to all of the

objectives, the uncertainties remaining regarding porosity and recharge were primarily responsible for the second field campaign.

2.1.1.2 Data Collection from 1999 to 2003

The CAIP developed in 1998 called for a DDA to guide the choice of investigation and data collection methods for minimizing uncertainty in the groundwater flow and transport model predictions (Pohll et al., 1999a). A variety of parameters and data collection methods for the parameters were considered. The data collection activities selected were a two-well tracer test and an environmental tracer/deep-well hydraulic characterization well-nest.

The specific objectives for the two-well tracer test were to: (1) determine the effective porosity of the Shoal granite aquifer; (2) determine hydraulic properties of the aquifer; (3) quantify the dispersion coefficient at the 30-meter (m) scale (equivalent to the model grid block size); (4) quantify field-scale sorption for weakly sorbing solutes; (5) determine the significance of matrix diffusion; and (6) determine hydraulic properties of the fractures.

The objectives of the well-nest activity were to: (1) provide samples from several depths for groundwater velocity determination using environmental tracers (the primary flow direction in the upper saturated section at the site is downward); (2) provide measurement of hydraulic head variation with depth; (3) determine head in the first zone of saturation to address uncertainties raised by the water level history at HC-3; (4) document fracture frequency with depth and other characteristics (strike, dip, aperture) if possible; (5) determine fracture continuity between boreholes of the nest; and (6) measure hydraulic conductivity as a function of depth.

Plans for both the tracer test and the well-nest activity are presented in Pohll et al. (1999b). Data from the drilling activities can be found in IT Corporation (2000), and testing data are in Mihevc et al. (2000) and Lane et al. (2001). Additional specific data from the tracer test can be found in Carroll et al. (2000) and Reimus et al. (2003). All of the objectives for the tracer test were met, due in large part to a decision to extend the operation of the test from the planned four months to eleven months. The well-nest activity did not succeed in its goal of allowing a velocity determination using environmental tracers because the nested wells were located on different sides of a shear zone that was revealed as a major hydraulic barrier. Although that objective was not reached, the information gained regarding the character and impact of the shear zone proved invaluable. The environmental tracer data had been planned for use in the validation process, so that they were not critical for initial model development. The objectives related to determining fracture characteristics and hydraulic parameters at various depths, as well as addressing the uncertainty related to the low hydraulic head at HC-3, were met with the wells.

Given their importance, additional details regarding the tracer test and well-nest activities are given below.

2.1.1.3 Two-Well Tracer Test

The tracer test was conducted between wells HC-6 and HC-7, located approximately 30 m apart to reflect the scale of the numerical model. Pohll et al. (1999b) presents plans for the test in detail. Documentation of the conduct of the test and presentation of the data can be found in Carroll et al. (2000); and analysis of the test is presented by Reimus et al. (2003), as well as presented in the transport parameter section of the final modeling report (Pohlmann et al., 2004). The two wells were drilled approximately 350 m southeast of the Shoal cavity. They are approximately 375 m deep, with 35-m long sections of well screen beginning 40 to 75 m below the static water table (at a depth of 299 m). A submersible pump was set near the bottom of the well screen in HC-7. A temporary pump was used in HC-6 for recirculating the tracers during and immediately after injection to prevent density stratification. Before injecting tracers, a weak-dipole flow field was established by pumping HC-7 at approximately 11.3 liters per minute (L/min) while recirculating approximately 1.13 L/min of the produced water into HC-6 (the long term pumping rate was about 7.5 to 8.3 L/min, and even this reduced rate threatened to dewater HC-7 by the end of the test). After establishing a quasi-steady state flow field, injection occurred. An initial, smaller volume injection of sodium iodide was performed to evaluate the possibility of rapid transit times and identify any need to modify data collection during the main test. No tracer breakthrough occurred, so the larger injection occurred as planned. This consisted of a multiple tracer injection of bromide, pentafluorobenzoate, and lithium on November 10, 1999. Additional injections of cesium and microspheres occurred at later time, but neither cesium or microspheres were detected in the pumping well. Breakthrough of bromide began about one month into the test. The weak dipole was maintained until the last sample was collected from HC-7 on September 24, 2000. The tracer test was conducted for 319 days, or approximately 7,650 hours. Water levels in HC-7 slowly declined throughout the test and have been slowly recovering through 2004.

The multiple tracers allowed evaluation of flow porosity, dual-porosity transport involving matrix diffusion, and sorption. Results and interpretations of the tracer test indicate that a dual-porosity conceptual transport model should be used to describe dissolved radionuclide transport at the site. The results are consistent with stagnant water in the dual-porosity system being primarily in the matrix where there is plenty of surface area for radionuclide sorption, as opposed to free water in fractures. It was also found that lithium sorption in the field tracer test was considerably stronger than in batch laboratory sorption experiments, suggesting the use of

laboratory sorption data should be conservative for Shoal. Estimates were derived for effective fracture aperture, flow porosity, and longitudinal dispersivity. These estimates spanned ranges of an order of magnitude or more, but the uncertainty is less than would have occurred if only one tracer had been used.

2.1.1.4 Well Nest

The well cluster, or "nest" was planned to access three different depths in the hydrogeologic system. The shallowest well in the nest was to serve double-duty as one of the tracer test wells. The other two wells, HC-5 and HC-8, were completed at depths of 1,086.5 and 771.1 m, respectively. Each well was completed with a 36.6 m well screen at the bottom of the hole. Hydraulic testing was conducted with submersible pumps to measure aquifer characteristics at the different depths, while water levels were monitored in the other wells. Hydraulic head measurements continued after the tests to establish static levels. Groundwater samples were collected at the conclusion of aquifer testing. Fracture information was primarily obtained through logging operations. The following logs were run and data can be found in Mihevc et al. (2000): radar, acoustic televiewer, video, fracture interpretation, caliper, density, neutron, temperature, natural gamma, spectral gamma, deviation, and resistivity. Additional information for the borehole-radar reflection logs can be found in Lane et al. (2001).

While drilling the first well, HC-5, a large fault zone was penetrated. The zone was also penetrated by the intermediate depth well, HC-8. The fault zone is related to a naturally occurring shear zone expressed on the land surface. Due to its steep dip to the northwest, although the surface locations of HC-5 and HC-8 are located west of the shear zone, the wells penetrate the fault so that the screened intervals at the bottom are on the east side of the zone. As a result of the findings in HC-5, the tracer test wells (HC-6 and -7) were moved westward from their original planned locations so that the tracer test could take place on the same side of the shear zone as the Shoal nuclear test. The difference in water levels in HC-7 and HC-5, separated by only 50 m in a horizontal direction, is in excess of 100 m. Thus, the well-nest activity identified a major hydraulic barrier at the site and explained the lower hydraulic head observed at HC-3. However, with the fault between the completions of the tracer test wells and HC-5 and -8, there is no vertical flow path sampled through these wells to use for the velocity determination.

2.1.1.5 Summary of Data Collection Results

Eight wells were drilled during the PSA investigations, ranging in depth from 364.3 to 1,086.5 m. Their locations are shown on Figure 2-1, with coordinates and additional

specifications in Table 2-1. Projections of the wells onto a west-east profile through the site are shown in Figure 2-2, which portrays the impact of the shear zone on the potentiometric surface.

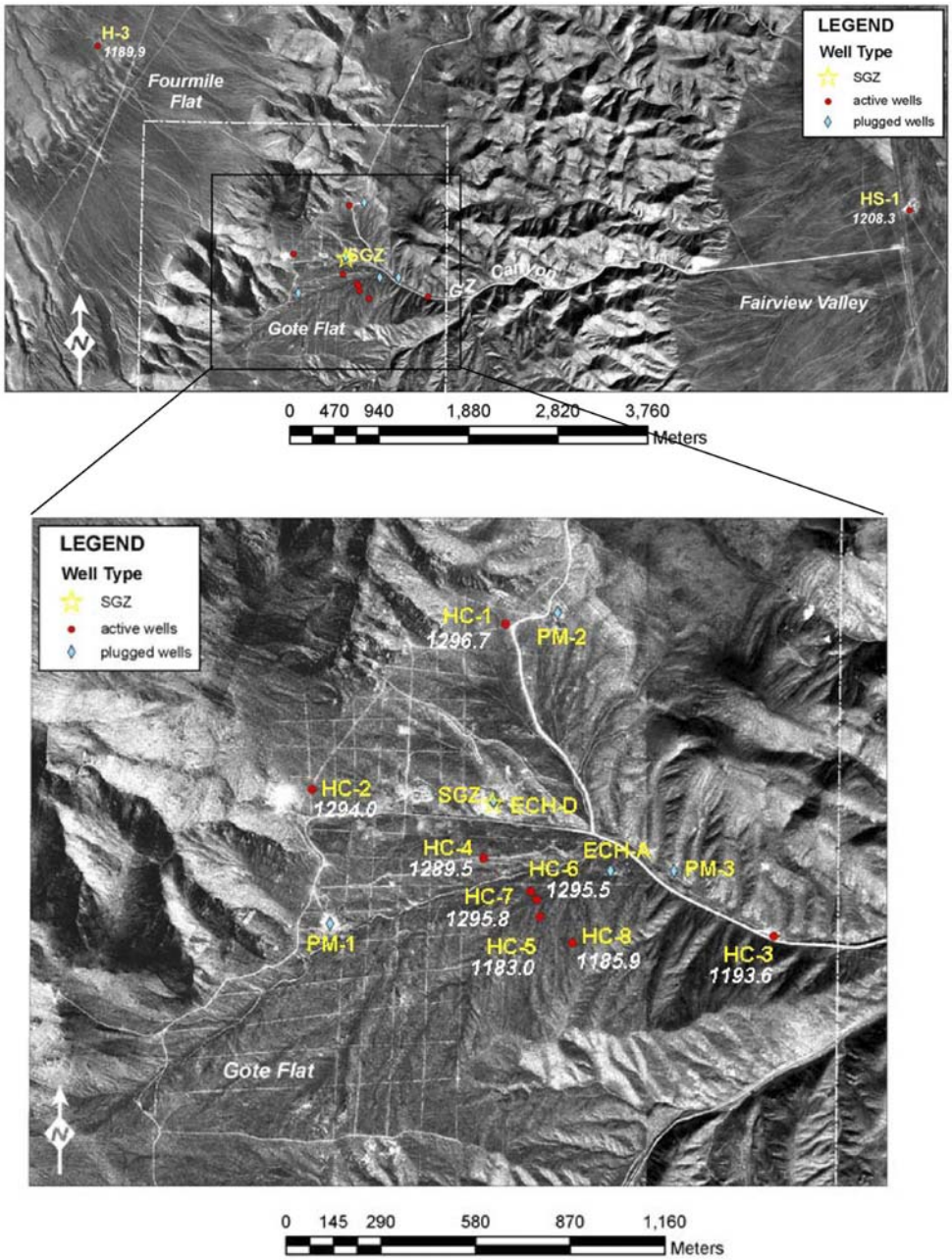

Note: View of the northeast corner of the land withdrawal area.

Figure 2-1
Exploratory boreholes and characterization wells at PSA

Table 2-1
Summary information for wells used in the Shoal investigation

Well ID	UTM Coordinates* East (m)	North (m)	Surface Elev. (m AMSL)	TD Elev. (m AMSL)	Open Interval Elevation Top (m)	Bottom (m)	Water Level** (m AMSL)	Source***
HC-1	380850.5	4340238.9	1618.3	1212.9	na	1212.9	1296.7	a
HC-2	380259.5	4339731.9	1629.8	1260.4	1338.7	1260.4	1294.0	a
HC-3	381669.5	4339282.9	1548.9	1184.6	1285.5	1184.6	1193.6	a
HC-4	380783.5	4339520.9	1603.5	1228.3	1294.7	1228.3	1289.5	a
HC-5	380954.5	4339341.9	1599.3	512.8	567.6	523.3	1183.0	a
HC-6	380926.5	4339418.9	1593.6	1215.7	1253.5	1218.0	1295.5	a
HC-7	380945.5	4339394.9	1593.9	1216.0	1256.7	1221.0	1295.8	a
HC-8	381054.5	4339261.9	1603.1	832.0	903.8	868.3	1185.9	a
PM-1	380315.5	4339320.9	1633.1	1225.0	na	1225.0	1299.5	a/d
PM-2	381010.5	4340273.9	1620.8	1226.1	na	1226.1	1356.3	a/d
PM-3	381365.5	4339482.9	1563.7	1229.3	na	1229.3	1237.2	a/d
ECH-A	381172.5	4339482.9	1572.4	993.3	nd	993.3	na	a/d
ECH-D	380814.1	4339693.7	1593.8	979.6	na	979.6	1300.0	b, e/d
USBM-1	381046.5	4339634.9	1588.6	1135.7	na	1135.7	1312.2	a/d
H-2	376481.1	4343246.3	1224.4	986.6	1029.4	986.7	1190.6	b
H-3	378211.4	4341919.7	1290.0	1143.7	1210.7	1143.7	1189.9	b
HS-1	386713.0	4340189.0	1293.2	1080.2	nd	nd	1208.3	b
US Navy EW Range	394532.8	4352932.6	1285.0	1120.4	1175.3	1123.5	1190.0	c
Frenchman's Station	390458.5	4348279.6	1265.9	1196.4	nd	nd	1197.0	d

* Zone 11, NAD27, meters

**Measurements do not represent one point in time, as noted by source date. Note that water levels in the PM, ECH and USBM wells may not be representative due to drilling effects.

***First letter denotes source of location information. A letter after a slash indicates a different source for the water level.

a = Mihevc et al. (2000) with GPS location survey conducted 2/2001
b = Mihevc et al. (2000)
c = Nevada Division of Water Resources, Well Log Database
d = University of Nevada (1965)
e = Coordinates reported in NVO-73 (Shoal Site Disposal Report)
Nd = no data
Na = not applicable, borehole uncased in saturated zone

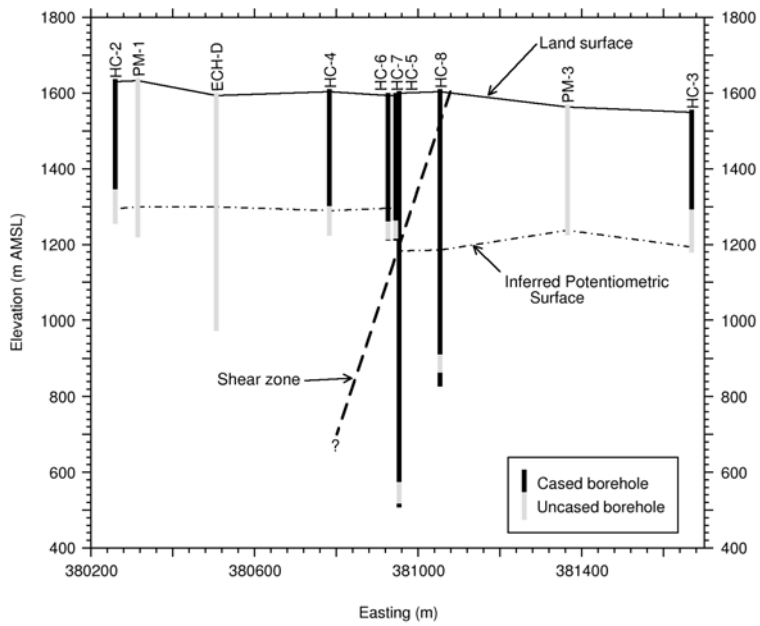

Note: Observe the large change in hydraulic head observed between HC-7 and HC-5. The wells are projected to the profile from their actual locations, which are shown in Figure 2-1.

Figure 2-2
West-east profile through PSA showing the potentiometric surface

Groundwater flow in the competent granite of the Sand Springs Range is confined to fractures and faults. These features were characterized in the boreholes using video logs, acoustic televiewer (ATV) logs, radar logs, and surface mapping. Summary statistics from analysis of the fracture data from ATV and radar logs are given in Table 2-2. Surface mapping was used to estimate the spatial persistence of fracture features. Group 1, with a strike of 0 to 70 and 130 to 180 east of north, has a mean length of 572 m using a log-normal distribution, and a natural log standard deviation of 0.86. Group 2, with a strike of 70 to 130 east of north, contained very few fractures and was assigned a uniform distribution with a range of 100 to 750 m. Video logs were used to assign fracture categories for developing prior probabilities of fracture-related flow categories. These assignments are shown in Table 2-3, with Category 1 relating to small or no fractures, Category 2 being medium-sized fractures, and Category 3 including large fractures.

Table 2-2
Fracture summary statistics (ND = not defined)

Fracture Set	Count of Fractures	Prior Probability (%)	Mean Strike	Mean Dip	κ
1	397	50.2	8.8°	62.2°	22.4
2	156	19.7	193.8°	61.8°	20.9
3	68	8.6	86.8°	65.7°	31.7
4	68	8.6	301.7°	63.8°	45.4
5	66	8.3	351.6°	60.9°	16.0
6	35	4.4	214.6°	60.8°	10.6
All	790	100.0	ND	ND	ND

Table 2-3
Global prior probabilities for flow Categories 1 and 2
as determined from borehole fracture score analysis of video logs

Fracture Score	1	2	3	0*
Prior Probability	0.64	0.28	0.05	0.03
Flow Category	1		2	
Prior Probability	0.64		0.36	

*Indicates no data.

Hydraulic conductivity data were obtained from pumping tests in seven of the wells and stressed thermal flow-meter tests in two of the wells. The pumping tests were all single-hole tests, with the exception of the cross-hole test conducted before the tracer test in wells HC-6 and HC-7. The mean of the tested interval lengths is 25 m. The 16 *K* values range from 8.3×10^{-4} to 1.7×10^{-1} meters per day (m/d). These data are presented in Table 2-4 and shown in Figure 2-3. The tracer test provides a data set representing long-term hydraulic stress on the system affecting a larger volume of the aquifer than the short-term pumping tests. Transient numerical simulations of the tracer test were performed in an inverse mode, using the time-drawdown and time-recovery data as the calibration data set to provide an independent estimate of *K*. The resulting *K* of 2.5×10^{-3} m/d falls near the median of the distribution from the individual single-well tests, providing confirmation of the range of *K* obtained in those tests.

Table 2-4
Summary of hydraulic test data for wells near the PSA (Mihevc et al., 2000)

Well ID	Test	Date	Tested Interval Top (m AMSL)	Tested Interval Base (m AMSL)	Tested Interval Length (m)	K (m/d)	$\log_{10}$ K ($\log_{10}$ m/d)
HC-1	Pumping[1]	02/20/1997	1,293.70	1,212.70	81.0	$1.8E^{-02}$	-1.8
HC-2	Pumping	02/24/1997	1,292.70	1,260.08	32.6	$2.3E^{-03}$	-2.6
HC-4	Pumping	02/23/1997	1,285.50	1,225.09	60.4	$3.5E^{-03}$	-2.5
HC-5	Pumping[1]	10/11/1999	568.58	532.00	36.6	$1.7E^{-01}$	-0.8
HC-6	Pumping	10/25/1999	1,292.26	1,255.68	36.6	$1.4E^{-02}$	-1.9
HC-7	Pumping	10/28/1999	1,292.26	1,221.00	36.6	$2.3E^{-02}$	-1.6
HC-8	Pumping	11/11/1999	903.84	868.33	36.6	$8.3E^{-04}$	-3.1
HC-7/HC-6	Pumping[2]	10/28/1999	1,292.26	1,255.68	36.6	$1.5E^{-01}$	-0.8
HC-1	TFM	07/09/1997	1,242.26	1,232.62	9.6	$4.6E^{-02}$	-1.3
HC-1	TFM	07/09/1997	1,232.62	1,225.86	6.8	$6.1E^{-02}$	-1.2
HC-4	TFM	08/07/1997	1,292.04	1,286.04	6.0	$8.6E^{-03}$	-2.1
HC-4	TFM	08/07/1997	1,286.04	1,274.04	12.0	$2.9E^{-03}$	-2.5
HC-4	TFM	08/07/1997	1,274.04	1,267.04	7.0	$2.0E^{-03}$	-2.7
HC-4	TFM	08/07/1997	1,267.04	1,255.04	12.0	$1.3E^{-03}$	-2.9
HC-4	TFM	08/07/1997	1,255.04	1,246.04	9.0	$3.1E^{-03}$	-2.5
HC-4	TFM	08/07/1997	1,246.04	1,236.04	10.0	$8.6E^{-04}$	-3.1
HC-4	TFM	08/07/1997	1,236.04	1,228.04	8.0	$3.8E^{-03}$	-2.4
Mean					25	$3.0E^{-02}$	-2.1
Variance					490	$2.6E^{-03}$	0.55

[1]Mean value of two tests
[2]Pumping in HC-7, observations in HC-6

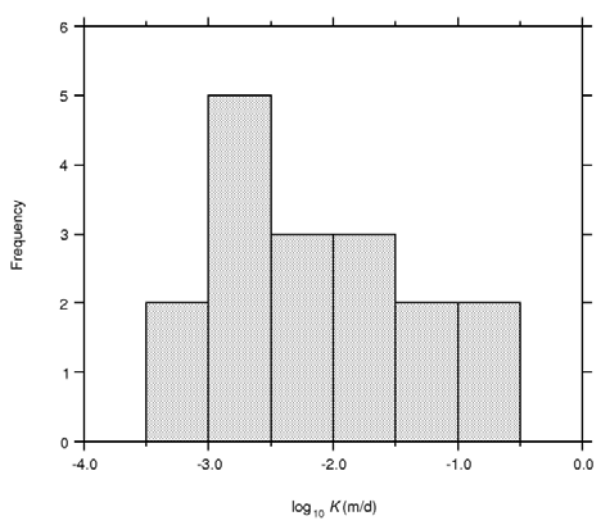

Figure 2-3
Histogram of hydraulic conductivity measurements in the granite aquifer at the PSA (Mihevc et al., 2000)

Hydraulic head measurements are available from the HC wells, and represent head over intervals ranging from 33 to 81 m. Static water levels are presented in Table 2-5 and range from 1,183.0 to 1,296.7 m AMSL.

Table 2-5
Selected static water level measurements from wells near the PSA. Summarized from Mihevc et al., 2000.

	Open Interval		
Well ID	**Top (m AMSL)**	**Base (m AMSL)**	**Water Level (m AMSL)**
HC-1	1,293.7	1,212.7	1,296.7
HC-2	1,292.7	1,260.1	1,294.0
HC-3	1,285.5	1,184.6	1,193.6
HC-4	1,285.5	1,228.3	1,289.5
HC-5	568.6	532.0	1,183.0
HC-6	1,292.3	1,255.7	1,295.5
HC-7	1,292.3	1,221.0	1,295.8
HC-8	903.8	868.3	1,185.9

Effective porosity is not measured directly, but rather is the result of interpretation of the results from the tracer test. Reimus et al. (2003) calculated a range in effective porosity of 0.027 to 0.054, but caution that the estimates may be high due to heterogeneity in the system. Additional analysis was performed to account for the uncertainties introduced by the calculations, and obtained a distribution of effective porosity (Figure 2-4). The geometric mean of the distribution is 0.019.

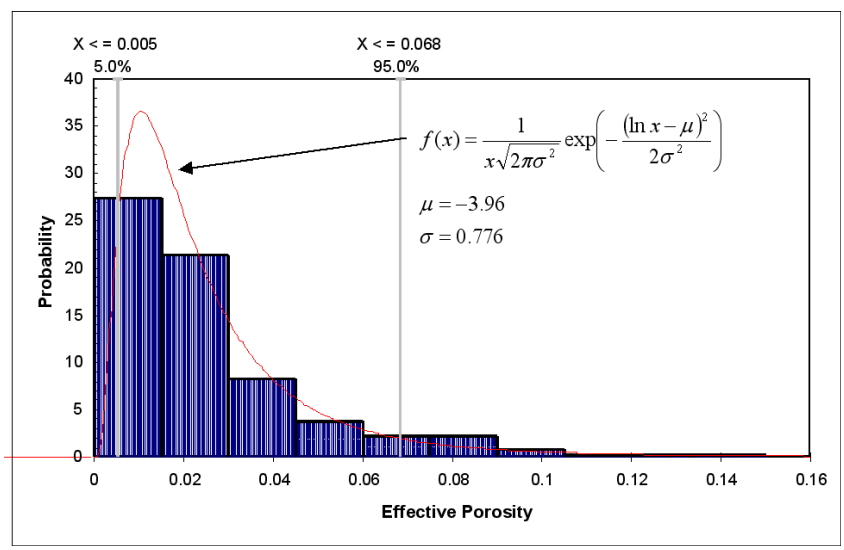

Figure 2-4
Numerically derived distribution of effective porosity and the associated lognormal distribution

Sorption data were obtained from batch sorption experiments conducted using granite collected from the Shoal muck pile (Pohll et al., 1998; Papelis, 2001; Reimus et al., 2003), and from retardation behavior observed during the tracer test (Reimus et al. 2003; Pohlmann et al., 2004). The batch experiments included parametric studies involving pH, sorbate concentration, ionic strength, and fluid composition. These were conducted using strongly, moderately, and weakly binding cations (lead, cesium, and strontium, respectively) and strongly and weakly binding anions (selenite and chromate, respectively). The results are summarized in Table 2-6. Additional laboratory investigation of lithium sorption was performed in connection with the tracer test (Reimus et al., 2003). It found a K_d value of 0.113 cubic centimeters per gram (cm^3/g), with a 95 percent confidence interval of 0.064 to 0.199 cm^3/g. The lithium K_d value derived from the field tracer test was in the range of 0.34 to 2.0 cm^3/g at the 95 percent confidence interval, indicating that lithium sorption in the field test was greater than in the laboratory tests.

Groundwater samples collected from the HC wells were analyzed for chemical and isotopic data to provide a means of evaluating the ability of the numerical models to represent the flow system. In addition, samples were collected and analyzed as part of the Fluid Management Plans (contained within the CAIP for CAU 416, and as a separate document for CAU 447 [DOE/NV, 1999b]). The results of the fluid management analyses are reported in DOE/NV (1998e) and IT Corporation (2000). Data from the chemical and isotopic characterization analyses are given in Table 2-7 and 2-8.

Table 2-6
Linear and Freundlich isotherm parameters

Ionic Strength (M) or Groundwater Type	pH	K_d (m^3/g)	K_F $(g/g)/(g/m^3)^{1/n}$	I/n (-)
Lead Sorption	4.0	1.78×10^{-5}	1.85×10^{-5}	0.94
I = 0.01 M	5.0	4.53×10^{-5}	2.05×10^{-5}	0.74
	6.0	3.56×10^{-4}	1.42×10^{-4}	0.81
	7.0	2.40×10^{-3}	5.44×10^{-4}	0.82
	8.0	9.99×10^{-2}	9.99×10^{-2}	1.00
	9.0	9.99×10^{-2}	9.99×10^{-2}	1.00
HS-1	4.0	4.08×10^{-5}	2.32×10^{-5}	0.87
	5.0	4.49×10^{-5}	1.10×10^{-5}	0.67
	6.0	1.33×10^{-3}	4.67×10^{-4}	0.84
	7.0	9.99×10^{-2}	9.99×10^{-2}	1.00
	8.0	9.99×10^{-2}	9.99×10^{-2}	1.00
	9.0	9.99×10^{-2}	9.99×10^{-2}	1.00
HC-4	6.0	7.33×10^{-4}	2.11×10^{-4}	0.79
	7.0	1.90×10^{-3}	9.30×10^{-3}	0.90
	8.0	4.90×10^{-3}	4.90×10^{-3}	1.00
Chromate Sorption	4.0	1.00×10^{-4}	2.16×10^{-6}	0.46
I = 0.01 M	5.0	1.00×10^{-4}	3.96×10^{-6}	0.48
	6.0	9.96×10^{-6}	6.12×10^{-7}	0.35
	7.0	8.89×10^{-6}	4.38×10^{-7}	0.34
	8.0	6.65×10^{-6}	2.53×10^{-7}	0.32
	9.0	5.44×10^{-6}	1.25×10^{-7}	0.28
HS-1	5.0	4.00×10^{-4}	9.53×10^{-6}	0.46
	7.0	1.23×10^{-4}	4.60×10^{-6}	0.46
	8.0	1.79×10^{-5}	2.06×10^{-7}	0.18
	9.0	1.65×10^{-5}	2.15×10^{-7}	0.20
HC-4	9.0	4.25×10^{-6}	2.49×10^{-7}	0.47
Selenite Sorption	4.0	2.20×10^{-5}	1.46×10^{-5}	0.94
I = 0.01 M	5.0	3.91×10^{-5}	7.69×10^{-6}	0.78
	6.0	8.20×10^{-5}	4.28×10^{-5}	0.92
	7.0	5.41×10^{-5}	7.06×10^{-6}	0.73
	8.0	2.53×10^{-5}	5.85×10^{-8}	0.25
	9.0	1.39×10^{-5}	1.86×10^{-7}	0.41
HS-1	4.0	2.07×10^{-5}	7.10×10^{-8}	0.23
	5.0	5.38×10^{-5}	8.15×10^{-8}	0.14
	6.0	1.64×10^{-4}	2.31×10^{-6}	0.47
	7.0	1.00×10^{-4}	1.52×10^{-6}	0.46
	8.0	5.66×10^{-5}	5.05×10^{-6}	0.68
	9.0	2.07×10^{-5}	1.27×10^{-6}	0.62
HC-4	4.0	1.51×10^{-5}	6.32×10^{-7}	0.57
	5.0	4.12×10^{-5}	6.17×10^{-7}	0.44
	6.0	2.13×10^{-4}	1.80×10^{-4}	0.98
	7.0	1.00×10^{-4}	2.84×10^{-5}	0.84
	8.0	4.32×10^{-5}	1.89×10^{-6}	0.58
	9.0	2.08×10^{-5}	1.66×10^{-7}	0.34
Cesium Sorption	5.0	3.07×10^{-5}	4.56×10^{-5}	0.85
HC-4	6.0	2.75×10^{-5}	3.88×10^{-5}	0.88
	7.0	3.11×10^{-5}	3.62×10^{-5}	0.98
	8.0	4.30×10^{-5}	3.88×10^{-5}	1.07
	9.0	5.46×10^{-5}	4.14×10^{-5}	1.13

Table 2-7
Chemical analyses of water samples collected from the HC wells at PSA, along with analyses of groundwater from other wells in the area of the Sand Springs Range (Chapman et al., 1994)

Well	Depth (m)	Date	T (°C)	pH[1] (S.U.)	EC[1] (µS/cm)	SiO_2 (mg/L)	Ca (mg/L)	Mg (mg/L)	Na (mg/L)	K (mg/L)	Cl (mg/L)	SO_4 (mg/L)	HCO_3 (mg/L)	CO_3 (mg/L)	NO_3 (mg/L)	Br (mg/L)
HC-1	336	02-21-1997	13.6	8.00/8.01	423/467	19.8	45.7	6.01	38.7	2.79	47.7	52.2	116	na	11.1	0.7
HC-2	347	03-19-1997	na	na/8.03	na/670	20.8	58.1	7.87	64.8	3.48	80.8	108.0	118	na	0.44	0.59
HC-4	327	02-24-1997	13.7	7.20/8.04	658/727	22.7	66.4	9.87	63.7	3.67	101.0	90.3	113	na	26.8	1.67
HC-5	476	01-12-2000	31.5	8.26	948	32.2	31.6	0.20	170	2.24	92.1	228	83.5	na	0.31	0.23
HC-6	371	10-06-1999	24.0	7.72	1,060	26.1	139	19.6	58.5	4.43	126	235	133	na	16.7	0.4
HC-7	371	11-03-1999	20.5	7.75	1,380	24.4	178	26.4	77	5.18	189	329	165	na	0.58	0.6
HC-8	610	10-29-1999	26.6	8.16	799	30.0	37.6	0.44	130	3.12	120	133	91.5	na	0.04	0.3
HS-1	92	03-30-1992	na	7.72/8.14	428/438	68.7	31.5	5.37	47.2	7.11	29.3	51.5	110/140	na	3.99	<0.1

[1]First number is a measurement in the field at the time of sample collection. Second number is a laboratory measurement. If there is only one number, it is a laboratory measurement.
[*]Based on TDS measurements

Table 2-8
Isotopic analyses for groundwater samples from PSA

Well	^{14}C Percent Modern Carbon	δD (‰)	$\delta^{13}C$ (‰)	$\delta^{18}O$ (‰)	Tritium (pCi/L)
HC-1	48.68 ± 0.83	-114	-10.8	-14.5	<5
HC-2	22.13 ± 0.51	-115	-10.4	-14.5	<5
HC-4	5,408 ± 51.9[++]	-113	-11.2	-14.2	1,130±15
HC-5	6.47 ± 0.24	-122	-8.5	-14.9	<2.6
HC-6	12.26 ± .18	-113	-9.9	-13.8	<2.6
HC-7	7.45 ± .15	-115	-9.2	-13.9	<2.6
HC-8	9.61 ± .15	-117	-9.7	-14.4	<2.6
HS-1	8.3 ± 0.9	-123	-9.9	-16.3	<10

[++]Percent modern carbon affected by nuclear device

2.1.2 Groundwater Flow and Contaminant Transport Modeling

The objective of the overall FFACO strategy for underground nuclear test sites is to define boundaries around each CAU that establish areas containing water that may be unsafe for domestic and municipal use. Given that this boundary must predict contaminant extent one thousand years into the future, as well as considering the limitations on the ability to observe the deep subsurface, modeling is the primary tool.

The modeling approach, as specified in the CAIP, called for a three-dimensional (3-D) model that incorporates subsurface heterogeneity. Calibration to observed hydraulic head values was suggested. A random walk particle tracking (RWPT) method is specified for transport. A deterministic modeling approach would be inadequate to express the uncertainty in the contaminant boundary, and to incorporate the presence of substantial uncertainty in parameter values. Therefore, a multi-parameter stochastic approach was followed, through which the uncertainty in the model conceptualization and parameterization could be included in the model results. The approach acknowledges the uncertainties in parameters and includes it in the analysis. This allows the contaminant boundary maps to contain this uncertainty, expressed as a confidence level.

There were three phases of modeling for the PSA. The first included the assimilation of historic data with the data collected during 1996 and 1997 into a 3-D numerical model of flow produced in 1998. Output of the flow model formed the basis for a transport model of radionuclide release and migration behavior. The results of this first model were deemed too uncertain by DOE and precipitated the second CAIP. The second phase of modeling occurred after NDEP approval of the CAIP for CAU 447, and was the DDA. The DDA was conducted using the 3-D model developed in phase 1, and examined the model uncertainty and effectiveness of possible data collection activities at reducing that uncertainty. The outcome of the DDA formed the plan presented in the Addendum to the CAIP for CAU 447 and guided the data collection efforts in 1999 and 2000. The final, and largest, modeling effort was conducted using the data from all the preceding field and laboratory studies. The centerpiece of this third phase is the PSA flow and transport model. It is supported by several larger size flow models that evaluate regional and subregional features, and smaller-scale models of the vadose zone, recharge, shear zone hydraulic properties, and the tracer test.

Limited discussion of the first two phases of modeling for PSA is presented here as the work was superceded by the third modeling effort. A brief description of the first PSA model and of the DDA is provided, and then a more detailed description of the third modeling phase is presented

using the sequence of steps defined for the ten-step modeling protocol prescribed in the dictionary section of Rev. 1, 2000 of the FFACO.

The details of the original flow and transport model can be found in Pohll et al. (1998), and in the peer-reviewed scientific literature in Pohll et al. (1999c). Pohll et al. (1999a) presents the DDA. The final PSA flow and transport model is described in detail in Pohlmann et al. (2004). Additional supporting modeling efforts are also presented in Pohlmann et al. (2004), with details for some of these given in Pohll (1999), Reimus et al. (2003), and Carroll et al. (2001).

2.1.2.1 The 1998 PSA Groundwater Model

The first-phase PSA numerical model was oriented northwest to southeast (along the inferred principal flow direction), with an upgradient no-flow boundary at the approximate location of the groundwater flow divide, no-flow boundaries on the lateral sides (parallel to the direction of flow), and a specified head boundary at the downgradient edge. Recharge entered the model through the upper-modeled surface. The fractured rock aquifer was treated as an equivalent porous medium. The field data were used to divide the system into three fracture classes (large, medium, and no/small fractures), and hydraulic conductivities were assigned based on the field data. Fracture orientation and persistence were based on downhole logs and surface mapping, and were treated as uncertain in the model. The flow model was calibrated to hydraulic heads. Transport of radionuclides assumed sorption only occurred on fracture surfaces and neglected the process of diffusion into matrix blocks from the fractures.

The numerical model could not be reconciled with three pieces of information from the field program. First, the hydraulic head at HC-3, in the downgradient direction of the model, could not be replicated. The measured head is significantly lower than that predicted by the model. Due to completion difficulties in HC-3, it was unclear whether the difference was due to a data quality problem or a model issue. Second, chemical and stable isotopic data from the wells on the Sand Springs Range are inconsistent with the range being a major supply for groundwater sampled at well HS-1 in Fairview Valley, east of the site. Understanding the significance of this finding was complicated by the unknown hydraulic role of the range bounding fault and the recharge contribution of the Fairview Range (on the east side of the valley) relative to the Sand Springs Range. Finally, groundwater velocities predicted in the model were too high to be consistent with the general groundwater ages and flow conditions inferred from the isotopic data, which suggested residence times on the order of thousands of years for groundwater in the model domain and thus velocities at least an order of magnitude lower than simulated.

2.1.2.2 The Data Decision Analysis

The DDA was performed to guide the choice of investigation and data collection methods for minimizing uncertainty in groundwater flow and transport model predictions. The uncertain parameters specified by the CAIP for consideration included effective porosity, hydraulic head at the downgradient boundary, recharge, hydraulic conductivity, fracture connectivity, fracture orientations, fracture dip, glass dissolution rate, and retardation. Field activities that could provide additional information were also identified.

The DDA assigned prior distributions for the parameters identified in the CAIP, then used the first-phase model to calculate the full uncertainty of the model predictions. Then it was assumed individual parameter values were known perfectly, and the resulting reduction in uncertainty was calculated. These uncertainty reductions reflect the contribution of each parameter to model uncertainty. It was found that effective porosity and recharge contributed the largest amount of uncertainty to the model results. Posterior distributions for each parameter were also estimated, based on an evaluation of the effectiveness of possible field activities at providing data on the parameter. These posterior distributions were then used in the model to calculate the reduction in model uncertainty that would be gained by performing each field activity.

By combining the uncertainty reduction estimates for the field activities with preliminary cost estimates, a cost-benefit analysis was performed. Activities that provided the highest uncertainty reduction for the lowest cost were identified. The relationship between optimal activities and the parameter uncertainty analysis was clear in the results; the large uncertainty presented by effective porosity and recharge led to the greatest gains in uncertainty reduction for field activities that reduced uncertainty in those parameters.

The DOE used the results of the DDA to propose three activities (vadose zone modeling, a two-well tracer test, and an environmental tracer/deep-well hydraulic characterization nest [well-nest]) in the addendum to the CAIP (DOE, 1999a).

2.1.2.3 Model Purpose

As stated in the CAIP for CAU 447, the overall modeling objective for the PSA is to predict an acceptable contaminant boundary, achieved through flow and transport modeling of contaminants from the underground test through the fractured granite aquifer. Specific objectives of the modeling, also presented in the same document are as follows:

- Integrate a wide a variety of data into a mass conservative description of contaminant migration in groundwater from the PSA underground nuclear test.

- Simulate the concentration of individual contaminants downgradient of the underground test location over a time period of 1,000 years.
- Serve as a tool to evaluate impacts of future flow system changes on the migration of contaminants in the CAU.

2.1.2.4 Conceptual Model

The conceptual model for groundwater flow is presented first, followed by the conceptual model for transport."

2.1.2.4.1 Conceptual Flow Model

The PSA is located in north-central Nevada along the crest of the Sand Springs Range. The Shoal nuclear test was conducted at a depth of 367 m below land surface. The Sand Springs Range is comprised of fractured granite and is bounded on the east and west by alluvium-filled valleys. Faulting is present in the range, with a prominent shear zone and other major faults striking southwest to northeast across the site. Groundwater recharge occurs by infiltration of precipitation on the mountain range, with regional discharge occurring in the valleys. A groundwater divide occurs below the upland area of the range, separating flow to the east and west. The nuclear test is located on the eastern side of the divide such that groundwater from the nuclear test area moves toward Fairview Valley.

The conceptual flow model for the site considers groundwater flow through the fractured granite aquifer comprising the Sand Springs Range. Its fundamental components can be seen in the cross sectional view presented in Figure 2-5 and in a 3-D depiction of the model domain in Figure 2-6. Water enters the system by the infiltration of precipitation directly on the surface of the mountain range. Because the model does not extend in an upgradient direction to a natural boundary, there is lateral flux into the southern face that originates as recharge through the ground surface upgradient of the model area. Groundwater leaves the granite aquifer by flowing into alluvial deposits in the adjacent basins of Fourmile Flat and Fairview Valley. A groundwater divide runs along the western portion of the Sand Springs Range, west of the underground nuclear test, directing flow from the test to Fairview Valley. This divide was first recognized by the University of Nevada (1965) and is consistent with basin-and-range hydrogeologic principles (Maxey, 1968). Its location west of the test was demonstrated by hydraulic heads measured in wells at the site (Figure 2-1 and Table 2-1), though evaluation of the regional hydrogeology indicates that the divide may not be a prominent, easily detectable feature (Pohlmann et al., 2004). This is due to the very low relief in the water table below Gote Flat, as a result of barriers to flow formed by a shear zone on the east and the range-front fault on

the west. The groundwater divide forms a no-flow boundary on the western side of the model. A very low conductivity shear zone roughly parallels the divide, east of the nuclear test, and creates another no-flow boundary on the eastern edge. The presence of these lateral boundaries causes groundwater from the site to flow in a northeastward direction on its way to Fairview Valley.

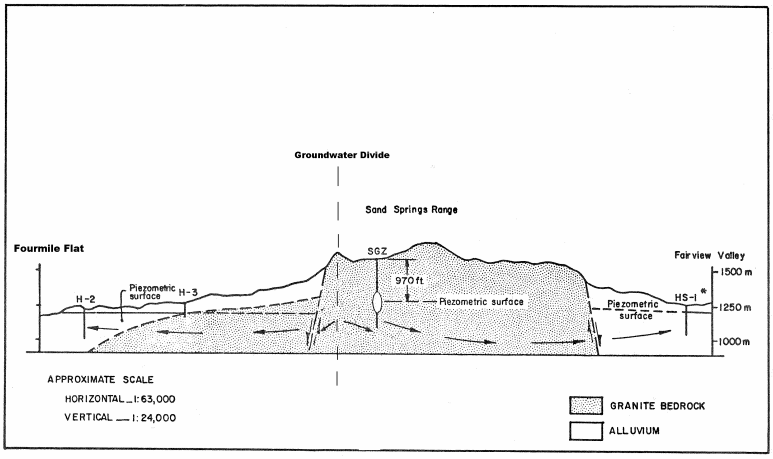

Figure 2-5
West-east cross section through the northern Sand Springs Range and valleys on either side

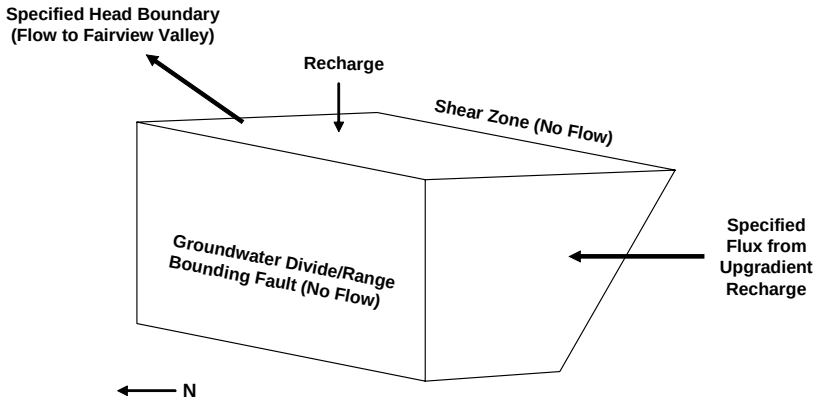

Figure 2-6
3-D depiction of the PSA conceptual model

Essential components of the Shoal conceptual flow model can be summarized as follows:

- Steady-state conditions.
- Isothermal conditions.
- Recharge distributed uniformly across the surface of the Sand Springs Range.
- A hydrologic divide located along the western portion of the range, forming a no-flow boundary on the west side of the domain.
- A low-conductivity, thick shear zone creating an impermeable no-flow boundary along the east side of the domain, dipping to the west at depth (causing the model to pinch in lateral extent with depth).
- The southern model boundary is assigned specified flux corresponding to flow into the domain from the region between the model boundary and the hydrologic divide in that direction; this flux is estimated from the regional models and the surface recharge rate.
- Flow exits the model through the northern boundary, directed across the site by the shear zone; this flow is assumed to eventually move to basin fill in Fairview Valley, outside of this model domain.
- Flow is simulated using a stochastic continuum approximation comprised of large, oriented fracture zones and intervening zones of granite with random, small fractures; these zones are referred to herein as Flow Category 2 and Flow Category 1, respectively.
- A region of higher hydraulic conductivity and higher porosity is located around the cavity and chimney to represent the impact of the Shoal test on the flow field.
- Uncertainty is included for fracture geometry, hydraulic conductivity, surface recharge, and flux through the southern boundary.

As compared to environments with complex hydrostratigraphy, the single aquifer of the Shoal fractured granite, situated on the crest of a mountain range, simplifies some model decisions. For example, the site presents no alternate model to that of flow through fractured granite fed by infiltration of precipitation through the surface of the range and directed toward the adjacent valleys. Vertical recharge from precipitation is the only source of groundwater; there are essentially no sources of lateral flow because the site is located at the crest of the Sand Springs Range.

Alternate conceptual models for the behavior of the shear zone, flow conditions on the west side of the range, and for other aspects of the boundary conditions and parameters, are evaluated using models designed expressly for this purpose. A model of Fairview Basin is used to

establish recharge and discharge relationships and general hydrologic properties, and ensure consistency with properties demanded by the natural basin boundaries. A model of the northern Sand Springs Range is used to evaluate alternate models for hydrologic behavior of the shear zone, based on observed hydraulic heads and hydraulic tests in nearby wells. The shear zone was determined to be a very low permeability barrier. Alternate models for hydraulic parameters and boundary conditions are examined with a model of the vicinity of the Shoal site. The results from these tests of alternate models were used to construct the PSA flow and transport model.

2.1.2.4.2 Conceptual Transport Model

The conceptual transport model describes the source of contaminants, how the contaminants are released, and the processes that control their migration through the groundwater system (Figure 2-7). It is based on site-specific data, as well as information gained by decades of research into underground nuclear tests at the Nevada Test Site (NTS).

Contaminants of potential concern (COPCs) are the radionuclides produced by or left over from the Shoal test and the daughters created by radioactive decay. The test design was relatively simple, with sand stemming in much of the void space of the drift and shaft rather than metals, such that nonradioactive species are not a concern (Pohll et al., 1998). Most of the radionuclide mass is assumed to be located within the cavity; however, a small portion is distributed throughout a wider fractured region around the cavity. Nuclides are not placed into the unsaturated zone in the model, although it is possible that some were forced upward by the explosion. Neglecting possible contaminant movement in the unsaturated zone is consistent with the eventual return of most volatile nuclides back to the water table by downward movement of recharge water, and as such, conservatively overpredicts initial nuclide masses dissolved in the groundwater.

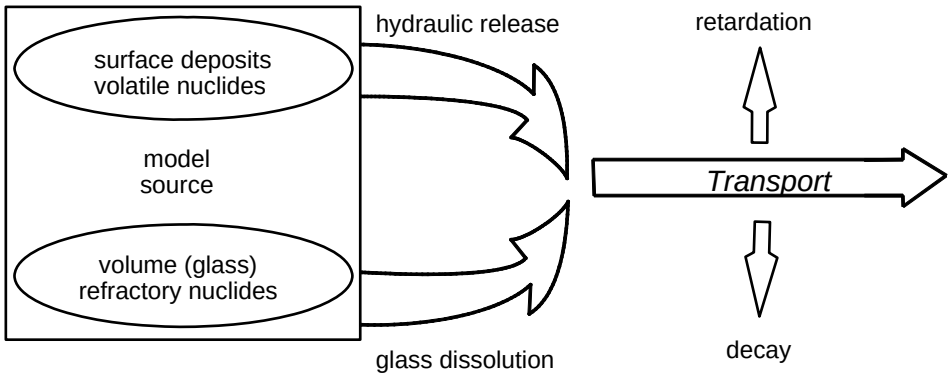

Figure 2-7
Conceptual model of the transport model source and processes considered

Radionuclides are initially apportioned according to their volatility among surface deposits and volume deposits in nuclear melt glass. Volatile and surface-deposited nuclides are assumed to migrate once hydraulic equilibrium conditions are reached. Nuclides within the glass are released according to glass dissolution rates calculated based on glass dissolution behavior and radionuclide melt glass characteristics.

It is assumed that no migration of radionuclides occurs until the cavity has infilled with groundwater, following the dewatering caused by the thermal and compressional forces of the nuclear test. This assumption neglects any molecular diffusion that occurs during the infill period, presuming that the flow of low-contaminant-concentration groundwater toward the hydraulic sink is much larger than the movement of contaminants away from the sink driven by concentration gradients.

Once released, the radionuclides are subject to retardation processes. Diffusion of contaminants from fractures into surrounding matrix blocks is included, because the tracer test demonstrated that diffusion of solutes from the fracture flow system into the granite matrix blocks is a significant process at Shoal. Parameters for simulating retardation and diffusion processes are estimated from laboratory and field-scale experimental results. Nuclides are grouped according to general sorptive behavior and each group is assigned a retardation factor.

2.1.2.5 Computer Code Selection and Verification

The criteria used to evaluate computer codes for meeting the flow modeling objectives for the Shoal CAI are defined in the 1998 CAIP (DOE/NV, 1998a) as follows:

- Fully 3-D processes
- Heterogeneous and anisotropic subsurface hydrogeologic properties
- Flexible boundary conditions
- Ability to handle unconfined aquifer conditions
- Steady-state and/or transient conditions
- Hydrologic sources and sinks (e.g., surface recharge)
- Capability for Monte Carlo simulations
- Access to source code

Additional computational considerations, also outlined in the CAIP, included data formats, efficient data handling, pre- and post-processors, efficient numerical solvers, and compatibility with existing hardware and software. By representing the PSA fractured flow system as a stochastic continuum, virtually any finite element or finite difference flow code can be used to solve the groundwater flow problem. MODFLOW-2000 (Harbaugh et al., 2000) was chosen for its public domain source, straightforward compilation on a variety of computational platforms, the ability to scale the code to the complexity of the modeling problem through the code's modular design, and its widespread acceptance in the hydrogeologic community. MODFLOW-2000 is the latest version of the code that was originally documented by McDonald and Harbaugh (1984) and received significant updates in 1988 (McDonald and Harbaugh, 1988) and in 1996 (Harbaugh and McDonald, 1996a, b).

The PEST software package (Doherty, 2000) is used to automatically calibrate each flow realization. PEST is a non-linear, model-independent parameter estimation software package. For each Monte Carlo realization, a value of recharge, R, is chosen from the distribution suggested by PSA field data and site-specific modeling. PEST and MODFLOW-2000 are used to determine the value of hydraulic conductivity, K_1, for zones of small random fractures (Flow Category 1) and to ensure that the flow model provides a reasonable agreement to observed hydraulic heads. Thus, this process provides for the internal calibration of each flow realization. The error between simulated and observed heads for each realization is then saved for post-processing so that each transport realization can be weighted according to its goodness of fit to the field data.

The simulation program FRACK was developed to generate 3-D distributions of fracture zones mapped to a finite difference grid. The method used to generate the fracture zones is an

extension of the method used by Long et al. (1982), but extended to 3-D space as is available in the FRACMAN code (Dershowitz et al., 1993). The spatial distribution and geometry of the simulated fracture zones honor the statistics of the observed fracture orientation and length. The FRACK code also conditions the fracture zones according to fractures observed in PSA boreholes. The generation of the fracture zones is analogous to methods of Long et al., (1982) and Dershowitz et al. (1993). Although these methods use the fracture simulators to generate fracture networks for discrete fracture models, FRACK generates a fracture network that is then mapped to a finite difference grid for flow simulation using a continuum approach.

A series of deterministic groundwater flow models was developed to investigate alternate models for various aspects of groundwater flow in the Sand Springs Range and Fairview Valley in preparation for the stochastic simulations of groundwater flow and radionuclide transport. The deterministic flow models were developed using the FEFLOW code (Diersch, 1998), a finite-element simulation package for two and three dimensions that is available from the WASY Institute for Water Resources Planning and Systems Research, Ltd. FEFLOW uses a Galerkin-based, finite-element method for solving the advection-dispersion balance equations on unstructured meshes. Although FEFLOW is designed for flow and transport problems involving density-dependent flow, mass, and heat transport processes, the models described here do not include these effects. However, the high-level graphical interface, the Geographic Information System capabilities, and the capacity for detailed mesh generation built into FEFLOW are important features that allowed the rapid development and testing of models. Furthermore, the code can account for free surfaces using moving meshes to model 3-D, regional unconfined aquifers, an important capability for modeling the unconfined system of the Sand Springs Range. The code and the results of benchmarking studies are fully described by Diersch (1998).

Criteria for the transport code are specified in the CAIP as follows:

- Transport via advection, dispersion, adsorption, and matrix diffusion
- Radioactive decay, daughter products
- Minimal numerical dispersion
- Capability for Monte Carlo simulations
- Access to source code

The RWPT method was selected to solve the transport equation. Although other numerical approaches are available (e.g., finite differences and finite elements), these can demand very fine grids and can introduce numerical dispersion. Moltyaner et al. (1993) have shown that the RWPT method completely eliminates numerical dispersion as compared to finite differences and finite elements solutions. The RWPT code used for radionuclide transport underwent a rigorous

comparative study with other transport codes, and was then verified through independent peer-reviewed publication (Hassan and Mohamed, 2003). A particle transfer probability approach was used to express the diffusion of particles into the matrix and back into the fractures, as first introduced by Liu et al. (2000) and discussed by Hassan et al. (2002). The matrix diffusion enhancement was also verified by comparative study with other transport codes such as the analytical solution of fracture transport of Sudicky and Frind (1982) and the TOUGH2 numerical code (Pruess, 1991) as documented in Liu et al. (2000).

2.1.2.6 Model Design

The numerical PSA model is oriented southwest to northeast, with a no-flow boundary paralleling the groundwater divide to the west, a no-flow boundary along the shear zone to the east, specified flux through the southwestern face to account for recharge upgradient of the model domain, and specified head where groundwater flow exits the model on the northeastern face. Recharge is also applied evenly over the upper model surface, and specified flux is set at the lower surface to account for groundwater exiting the domain vertically under the force of the downward-directed gradient. The model is roughly rectangular in plan view, measuring 1,588 m wide from northwest to southeast on the upgradient edge, and 1,900 m long from southwest to northeast (Figure 2-8). It is 1,300 m thick, from the water table downward. Cell size in the model is approximately 20 m on a side to be consistent with the scales of geophysical and hydraulic measurements at the site, to approximate the estimated volume of the cavity, and to satisfy computational considerations.

Uncertainty is incorporated in the important flow parameters. Several independent methods of estimating recharge resulted in a potential range of recharge over the PSA of 0.05 to 0.7 centimeters per year (cm/yr). The recharge rate and the incoming flux from the southwest (from recharge upgradient of the model) are selected using Monte Carlo techniques to sample from this distribution.

The flow system is conceptualized as a stochastic continuum with hydraulic conductivity treated as a random variable. The fractured granite is divided into two flow categories: large, oriented fractures and small, random fractures. Embedded within this natural flow field is a region of higher K and higher porosity representing the nuclear cavity, chimney, and surrounding disturbed zone. The large, oriented fractures represent the high-hydraulic conductivity fracture flow system developed by the anisotropic structural grain of the range. The small, random fractures provide flow conduits through otherwise impermeable matrix blocks. The distribution and orientation of the two flow categories is allowed to vary through 1,000 realizations, adhering to spatial statistics derived from fracture observations from boreholes. The hydraulic conductivity

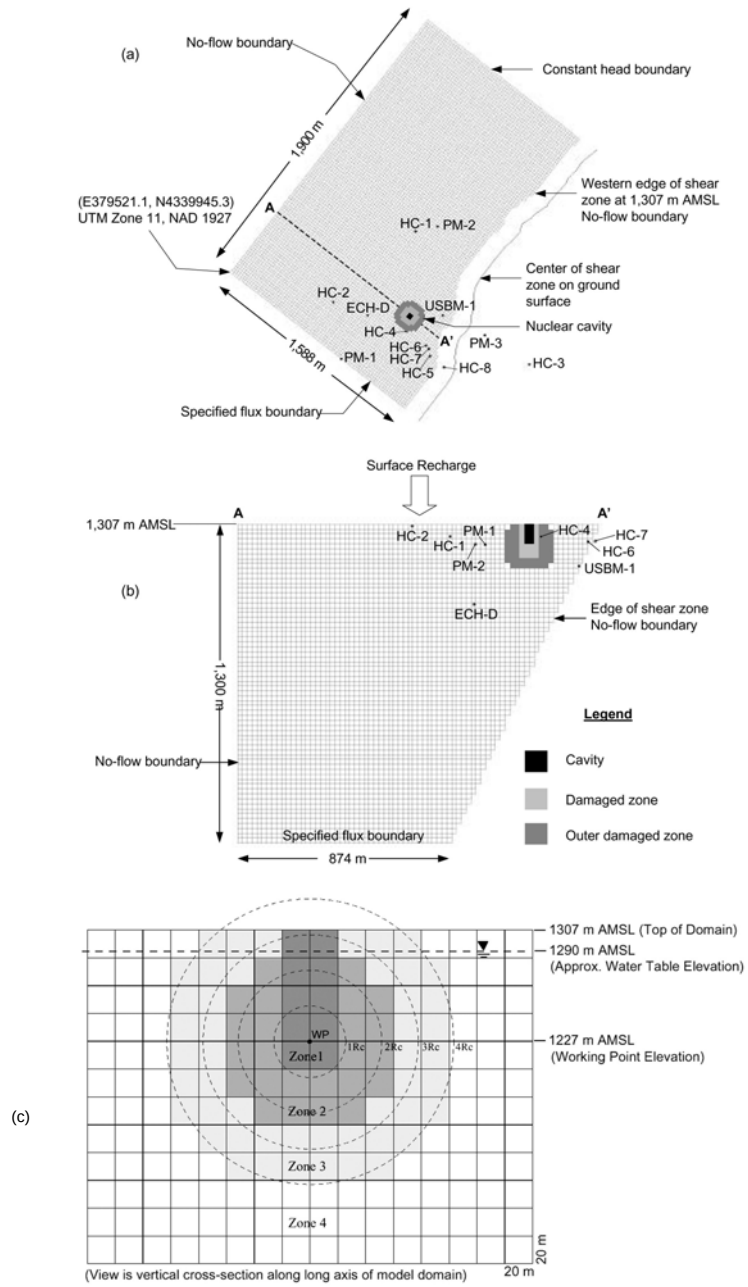

Note: View (a) shows the model domain in plan view, (b) a cross-sectional view through line A-A', and (c) detail of the near-cavity properties. Observation wells, boundary conditions, and regions associated with the nuclear cavity are indicated, with wells projected onto the section.

Figure 2-8
Three views of the model domain

(*K*) of the large-fracture category is randomly selected from a distribution of 1.0 x 10^{-5} to 1.0 m/d, based on hydrologic testing. The conductivity of the small-fracture category is also variable from the range of field data, but is selected during calibration of each flow realization to observed head values. The *K* value of the small-fracture category thus depends on the *K* of the large-fracture category, the recharge value, and the spatial distribution of fractures in the realization. Individual calibration ensures the integrity of each realization relative to known characteristics of the flow system (measured heads). Each realization is weighted based on goodness of fit to the observed head data and these weights are used later to calculate the level of confidence for the contaminant boundary.

The test cavity and surrounding damaged zone are represented by three zones that together radially span across five model cells from the simulated working point (Figure 2-8[c]). The configuration and properties of these zones are based on the performance of the Shoal test and relationships observed in granite at various distances from the working points of French nuclear tests conducted in granite in the Sahara (Borg, 1975). Porosity in the nuclear cavity is chosen from a uniform range between 18 and 35 percent (the estimated bulking porosity is 30 percent based on geometric considerations), and assigned a *K* from a distribution with a mean of 43 m/d. The damaged zone around the cavity is represented as a spherical zone with a porosity range of 7 to 18 percent and a distribution of *K* with a mean of 8.6 m/d. This is surrounded by a transition zone from the damaged area to native fractured granite where the porosity is selected from the porosity range for the natural granite, but the mean *K* of the distribution is set at the high end of the natural *K* range, 0.86 m/d.

The cavity region is the source of the contaminants in the transport model. The radionuclides resulting from the Shoal test are grouped into transport classes corresponding to their release behavior and transport characteristics. Two release modes are simulated: (1) hydraulic release, where radionuclides are free to migrate in the flow field immediately after the test; and (2) glass dissolution release, whereby nuclides included in the nuclear melt glass are released as the glass dissolves. The glass dissolution rate is treated as a random variable, controlled by a range of reactive surface area of 0.001 to 0.01 square meters per gram (m^2/g). At the low end of the range, just over three percent of the glass dissolves in 1,000 years; at the high end, almost 30 percent dissolves. All radionuclides have at least five percent of their mass released immediately after the nuclear test, to account for any small portion not incorporated into the puddle glass. To simulate potential dispersion of radionuclides in fractures and/or prompt injection away from the cavity, 90 percent of the contaminant source is uniformly distributed in a sphere of radius 20 m, with the remaining 10 percent distributed from 20 m to 100 m in exponentially decreasing amounts.

Once released, contaminant migration is simulated using the RWPT method. The retardation processes of sorption and matrix diffusion are included in the transport analysis. Sorption behavior is based on the results of both laboratory and field experiments. Lithium sorption in the field tracer experiment was considerably stronger than in the laboratory batch sorption experiments, suggesting that applying laboratory values for other cation-exchanging radionuclides should be conservative. The lithium breakthrough curve from the two-well tracer test indicated that sorption occurs both in the matrix and on fracture surfaces, although sorption in the matrix is much greater. The tracer test also clearly revealed the importance of matrix diffusion during transport processes in the Sand Springs granite. This was observed in the test by comparing the breakthrough of bromide with that of pentafluorobenzoate, a large molecule with a smaller free-diffusion rate than bromide. The dual-porosity conceptual transport model is implemented in the RWPT method using a particle transfer approach. A Markov chain model is used to simulate the particle transfer between the mobile and immobile waters. It was calibrated for the Shoal site using the tracer test results. Porosity is another critical transport parameter derived from the tracer test. It is also treated as uncertain in the transport model, with the mean (0.025) and standard deviation (0.023) determined by analysis of the tracer breakthrough behavior. The 90 percent confidence interval for effective porosity ranges between 0.005 and 0.07.

2.1.2.7 Model Calibration

Calibration is conducted to ensure that the model adequately represents the flow system. The modeling approach for Shoal integrated calibration into the selection of parameters for each individual realization. The flow modeling was conducted using MODFLOW-2000 (Harbaugh et al., 2000) to solve the groundwater flow equations and the PEST software package (Doherty, 2000) to automatically calibrate each realization. MODFLOW-2000 is a finite difference flow solver, which uses the hydraulic conductivity distributions and boundary conditions to calculate the 3-D hydraulic head field. PEST is a nonlinear, model-independent parameter estimation software package. For each Monte Carlo realization, a value of recharge (R) is chosen from the distribution suggested by PSA field data and site-specific modeling. PEST and MODFLOW-2000 are used to determine the value of hydraulic conductivity, K_1, for zones of small random fractures (Flow Category 1) and to ensure that the flow model provides reasonable agreement to observed hydraulic heads. Thus, this process provides for the internal calibration of each flow realization.

The Monte Carlo simulations are performed by a PERL script that executes FRACK (a simulation program to generate 3-D distributions of fracture zones mapped to a finite

difference grid), MODFLOW and the associated supporting codes, in addition to managing all the input and output files. For each realization, the script generates the following information:

- A fracture map using observed conditioning data and the FRACK program.
- Boundary conditions via the MODFLOW recharge, well and constant head packages. Note that the flux boundaries are determined from a randomly selected recharge value and the head boundaries are constant for each realization.
- A hydraulic conductivity field based on the fracture map and random samples for each cell in Flow Category 2. An initial guess for the hydraulic conductivity for Flow Category 1 is also provided to PEST. The hydraulic conductivity values for the cavity region and the related surrounding zones are selected from the appropriate distributions and assigned at this stage.
- MODFLOW and PEST are executed and the hydraulic conductivity value for Flow Category 1 is automatically calibrated.
- Upon successful calibration, the simulated hydraulic head, conductivity, fracture code, and recharge data are saved for use in the transport calculations. Summary statistics such as the root-mean-squared error (RMSE) between simulated and observed hydraulic head, and effective conductivities along the three axes, are saved.

The inverse method performed by PEST is central processing unit-intensive, but greatly increases the accuracy of each realization, as the hydraulic conductivity for Flow Category 1 is determined such that heads are in agreement with measured values. In this study, measured water levels at wells PM-1, PM-2, ECH-D, HC-1, HC-2, HC-4, HC-6 and HC-7 are used as observation values. It is important to note that data obtained from PM-1, PM-2 and ECH-D are considered questionable; therefore, are weighted arbitrarily one-hundredth less in sensitivity and error calculations. Many difficulties were experienced in measuring water levels in the early (1960s) wells due to lack of equilibrium head conditions following drilling (University of Nevada, 1965). In contrast, head measurements in the HC wells were collected over discrete intervals and great care was used during drilling and testing to minimize perturbations to the aquifer. PEST uses a nonlinear regression algorithm to minimize the weighted sum-of-squared error between simulated and observed hydraulic heads to determine the optimum value for the hydraulic conductivity of Flow Category 1 (Doherty, 2000).

The inversion algorithm used in PEST is essentially the same as UCODE (Poeter and Hill, 1998), and MODFLOW, but numerical testing showed that PEST tended to be a more efficient and stable algorithm for groundwater flow model inversion. Likewise, other inverse codes provide a similar approach and similar calibration estimates, but with a larger computational demand, so little would be gained by choosing a different algorithm.

In a traditional stochastic numerical flow and transport model using Monte Carlo techniques, each flow realization receives equal weight in the transport analysis. However, it is clear from the range of simulated results that some realizations fit field data better than others. In an effort to honor site-specific data throughout the modeling process, those realizations that are in good agreement with the field data are given a greater relative weight in the transport modeling than those that are in poor agreement.

The weighting procedure used is the Generalized Likelihood Uncertainty Estimator (Beven and Binley, 1992) that extends Monte Carlo random sampling to incorporate the goodness-of-fit of each realization. The goodness-of-fit is quantified by the likelihood measure

$$L(\vec{Y} \mid \vec{\Theta}) = \left[\sum (\varepsilon)^2\right]^{-N} \tag{2-1}$$

where

$$\varepsilon = (h_s - h_m)_i \tag{2-2}$$

and $L(\vec{Y} \mid \vec{\Theta})$ is the likelihood of the vector of outputs, $\vec{Y}$ given $\vec{\Theta}$ is the vector of random inputs, h_s is the simulated head at the point i, h_m is the observed head at that point, and N is a likelihood shape factor. Although the choice of N is subjective, its value defines its relative function. As N approaches zero, the likelihood approaches unity and each simulation receives equal weight, as in the traditional Monte Carlo analysis. As N approaches infinity, the simulations with the lowest sum of squares error (the simulations that best fit the field data) receive essentially all of the weight, which is analogous to an inverse solution. In this study, the value of N is assumed to be unity, which is a value typically used for this type of analysis (Beven and Binley, 1992; Freer et al., 1996; Franks and Beven, 1997; Morse et al., 2003).

Each realization from the model is weighted based on an application of the Bayes equation of the form:

$$P(\vec{\Theta} \mid \vec{Y}) = \frac{L(\vec{Y} \mid \vec{\Theta}) P(\vec{\Theta})}{C} \tag{2-3}$$

where $P(\vec{\Theta})$ is the prior probability of the input parameters produced by the Monte Carlo simulation, $L(\vec{Y} \mid \vec{\Theta})$ is the likelihood measure from Equation (2-1), C is a normalization constant, and $P(\vec{\Theta} \mid \vec{Y})$ is the posterior density. The posterior density is the probability of the input parameters occurring after taking into account the likelihood measure and is used to calculate the contaminant boundary as described in Section 2.2. The weights for individual realizations are

determined by Equation (2-3), which is simply a normalization of the likelihood such that the sum of the weights for all realizations is unity. In this way, each transport realization is appropriately weighted according to the goodness-of-fit of its hydraulic head distribution to the available field measurements.

A total of 1,000 Monte Carlo realizations of the flow field were produced using the procedure described above. Table 2-9 presents summary statistics of recharge rates, calibrated K_1 values, RMSE values at well locations, and the percent discrepancy in mass-balance calculations.

Table 2-9
Summary statistics for the results of the PSA flow model

		Minimum	Mean	Maximum
R (cm/yr)		0.05	0.27	0.68
K_1 (m/d)		5.79×10^{-9}	8.67×10^{-3}	1.00
Ke,x (m/d)		5.85×10^{-4}	3.01×10^{-3}	1.48×10^{-2}
Ke,y (m/d)		8.93×10^{-4}	3.77×10^{-3}	1.41×10^{-2}
Ke,z (m/d)		1.28×10^{-3}	5.29×10^{-3}	3.44×10^{-2}
Residual (Obs - Pred) (m)	PM-1	-98.46	-0.88	19.54
	PM-2	-123.38	68.77	76.82
	ECH-D	-7.70	10.41	20.44
	HC-1	-11.37	8.51	17.25
	HC-2	-14.42	0.41	13.48
	HC-4	-18.51	-1.11	9.71
	HC-6	-15.49	4.03	15.56
	HC-7	-15.12	3.91	15.79
RMSE (m)		0.01	3.75	7.56
Vertical Gradient (layers 24-40)		2.2×10^{-6}	2.7×10^{-3}	2.2×10^{-1}
Mass Balance Error (%)		0.00	0.05	2.97

In the NDEP acceptance letter for the Shoal model, concern was expressed about the size of the residuals for wells PM-2 and HC-1 ("The model calibration, based on hydraulic conductivity, for these wells showed higher mean deviations than wells closer to ground zero [e.g., HC-6 and HC-7]. Based on the calibration error shown in Table 2-9, it would appear that some model parameters [e.g., western or northern boundary conditions] may not have the appropriate quantity or quality of input data" [Maize, 2004]). Of the new wells, HC-1 does have the highest mean residual (8.5 m). However, the 95 percent confidence interval of the range of the residuals (16.1 m) is comparable to the ranges of the other wells (13.5 to 16.1 m, not including PM-2). It can also be seen from these results that the mean residual of HC-1 is approximately half of the range of heads (accounting for uncertainty) simulated at that location in the stochastic model. Considering the fractured nature of the aquifer, the wide range in hydraulic conductivity

observed during the hydraulic testing, the necessarily imperfect knowledge of subsurface conditions, and that the stochastic model incorporates all of these sources of uncertainty, the head residual at HC-1 is considered entirely reasonable.

2.1.2.8 Sensitivity and Uncertainty Analysis

A multi-parameter stochastic approach is used for the Shoal model, through which the uncertainty in the model conceptualization and parameterization is included in the model results. The approach acknowledges the uncertainty in the parameters and includes it in the analysis. This allows the simulated maps of contaminant boundaries to contain this uncertainty, expressed as a confidence level in simulated concentrations falling below given threshold concentrations.

The NDEP (Maize, 2004) specifically requested that the effects of remaining uncertainty in input parameters and in the location of the predicted contaminant boundaries be quantified. This quantification is inherent in the modeling of the Shoal site. Uncertainty in the input parameters is directly accounted for in the multi-parameter stochastic approach and presented through the confidence interval in the contaminant boundary.

The numerical model of groundwater flow at the PSA requires quantitative descriptions of several aspects of the conceptual model including shear zone geometry and hydraulic properties, fracture geometry and hydraulic properties, and groundwater recharge. All of these components of the model contribute to the transport predictions as they determine the pattern and magnitude of groundwater velocities and, as a consequence, influence the travel times of radionuclides from the cavity. Large-scale flow and transport models have shown that the results of radionuclide transport calculations are most profoundly impacted by parameters that affect travel time (Pohll et al., 1999a; Pohlmann et al., 1999; Hassan et al., 2002).

The uncertain components of the PSA groundwater flow model are:

- The orientation and spatial continuity of large fractures.
- The hydraulic conductivity of zones of large, oriented fractures.
- The hydraulic conductivity of intervening zones of small, random fractures.
- The recharge from precipitation entering the top surface of the model.
- The flux originating from upland recharge that enters the upgradient vertical face of the model.

Several independent methods of estimating recharge resulted in a potential range of recharge over the PSA of 0.05 to 0.7 cm/yr. Methods used include a numerical vadose zone model (Pohll, 1999), borehole temperature profiles at Shoal (Pohll et al, 1998), an analysis based on the Maxey-Eakin method (Pohlmann et al., 2004), and a revised recharge model (Polhmann et al., 2004), all of which are summarized in Pohlmann et al., 2004. The recharge rate and the incoming flux from the southwest (from recharge upgradient of the model) are selected using Monte Carlo techniques to sample from this distribution (Pohlmann et al., 2004). The distribution and orientation of the two fracture-flow categories is allowed to vary through 1,000 realizations, adhering to spatial statistics derived from fracture observations from boreholes. The hydraulic conductivity (*K*) of the large-fracture category is randomly selected from a distribution of 1.0×10^{-5} to 1.0 m/d, based on hydrologic testing. The conductivity of the small-fracture category is also variable from te range of field data, but is selected during calibration of each flow realization to observed head values. The *K* value of the small-fracture category thus depends on the *K* of the large-fracture category, the recharge value, and the spatial distribution of fractures in the realization. Individual calibration ensures the integrity of each realization relative to known characteristics of the flow system (measured heads). Each realization is weighted based on goodness of fit to the observed head data and these weights are used later to calculate the level of confidence for the contaminant boundary.

The shear zone and hydraulic divide are considered to be no-flow boundaries with known geometry. These were handled deterministically after testing alternate conceptual models of the shear zone and performing sensitivity analyses for the western boundary location.

Alternate conceptual models for the behavior of the shear zone, flow conditions on the west side of the range, and for other aspects of the boundary conditions and parameters, were evaluated using models designed expressly for this purpose. These alternative models are described in detail in Pohlmann et al., 2004. A model of Fairview Basin was used to establish recharge and discharge relationships and general hydrologic properties, and ensure consistency with properties demanded by the natural basin boundaries. A model of the northern Sand Springs Range was used to evaluate alternate models for hydrologic behavior of the shear zone, based on observed hydraulic heads and hydraulic tests in nearby wells. From the model results based on these data, the shear zone was determined to be a very low permeability barrier. Alternate models for hydraulic parameters and boundary conditions (including sensitivity to the location of the hydraulic divide) were examined with a model of the vicinity of the Shoal site. The results from these tests of alternate models were used to construct the PSA flow and transport model.

In addition to uncertainty in flow parameters, uncertainty was also incorporated in parameters governing transport of radionuclides. The uncertain components of the PSA transport model are as follows:

- Nuclear melt glass dissolution rate
- Effective porosity

Porosity is another critical transport parameter derived from the tracer test. It is also treated as uncertain in the transport model, with the mean (0.025) and standard deviation (0.023) determined by analysis of the tracer breakthrough behavior. The 95 percent confidence interval for effective porosity at PSA ranges between 0.004 and 0.088.

2.1.2.9 Model Verification

Verification of the PSA model follows two approaches. First, the numerical model was quantitatively verified by using the calibrated model to reproduce an independent data set. Second, aspects of the conceptual model were verified using interpretations of hydrochemical analyses.

The tracer test experiment conducted at PSA provided an excellent data set for flow model verification. The tracer test is essentially a long-term pumping test that was used to evaluate how well the model simulates the groundwater flow conditions observed in the field. The tracer test was conducted between wells located 30 m apart. Numerical modeling suggests that the zone of influence of the year-long test was approximately 100-150 m. The verification exercise is performed by using the hydrogeologic parameters and stresses used in the steady-state model, but with the inclusion of the pumping and injection stresses applied during the tracer experiment. This transient modeling is performed in a Monte Carlo framework in a manner that is essentially identical to the methods used for the steady-state flow model. Therefore, all 1,000 realizations obtained from the steady-state analysis were used in the verification exercise. The hydraulic conductivity field and boundary conditions are used directly from the steady-state model. The pumping and injection rates are specified from measured rates taken during the tracer test experiment.

The simulated and observed drawdowns are shown in Figures 2-9 and 2-10 for HC-6 and HC-7, respectively. The median prediction from both HC-6 and HC-7 are in excellent agreement with the observed data. The RMSE between the median prediction and observed data is 1.2 and 3.5 m, for HC-6 and HC-7, respectively. These errors are of the same magnitude as the errors in the steady-state model. The larger errors associated with HC-7 are attributed to the smoothing

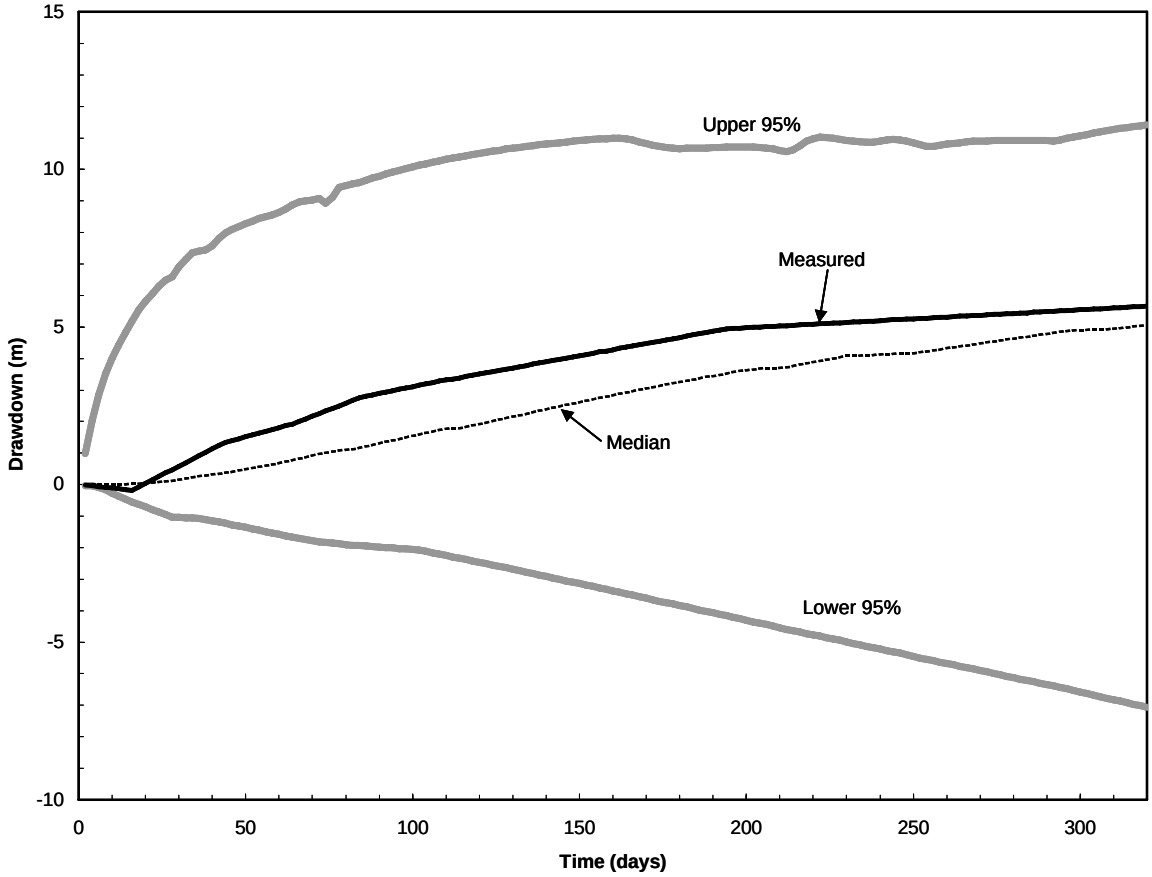

Figure 2-9
Simulated and observed drawdown for HC-6

created by the median calculation. The median represents the 50th percentile as derived from 1,000 realizations, and as such, the median for each time step is not necessarily from the same realization, thereby causing a smoothing effect.

The verification analysis shows that the modeling errors associated with the verification simulations are less than or equal to the errors produced by the calibrated steady-state model. Therefore, one can deem the flow model as successfully verified (Pohlmann et al., 2004).

Chemical and isotopic data from groundwater collected in the Sand Springs Range and Fairview Valley were not used for development of the numerical flow model. Evaluating these data in the context of the model results thereby provides a means of evaluating the consistency of the numerical model with the conceptual model.

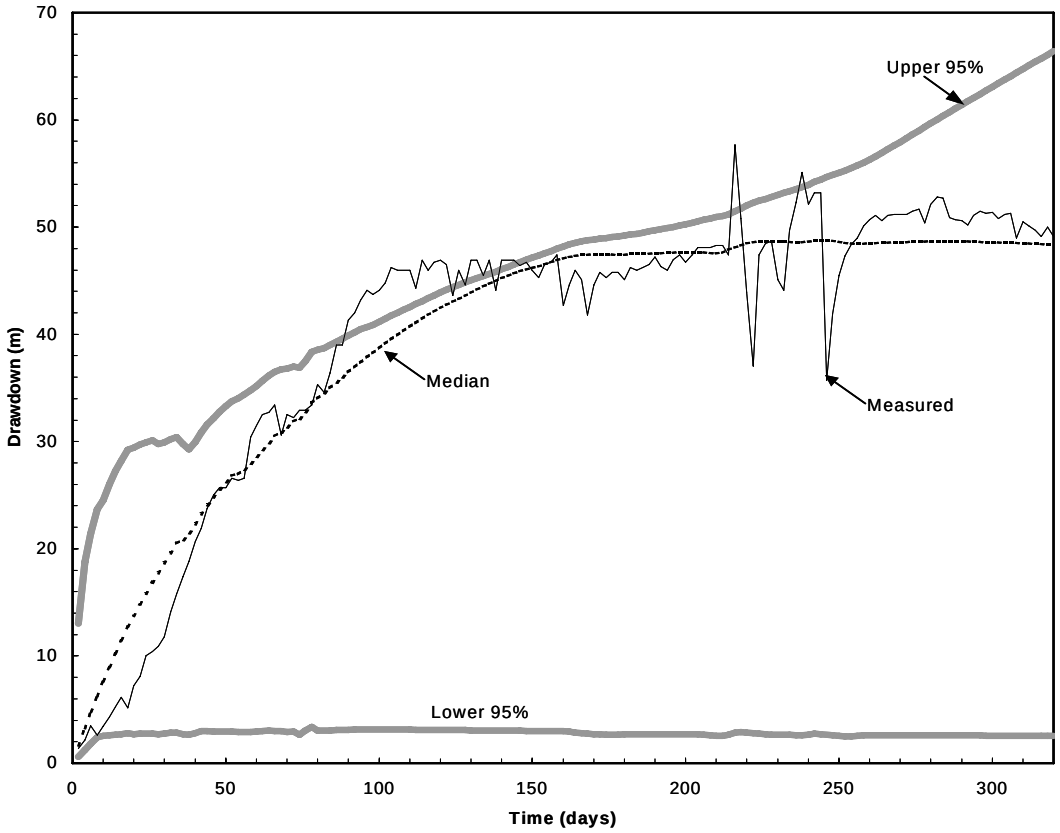

Figure 2-10
Simulated and observed drawdown for HC-7

The high degree of chemical variability observed for groundwater at PSA supports the conceptual view of a fracture flow system. The degree of chemical homogeneity in a fracture system is dependent upon the degree of interconnection between the fracture sets and exchange rates with intervening matrix blocks. The observed variability, even between wells distant from the shear zone (e.g., HC-1 and HC-2), is consistent with a relatively disconnected fracture system with large matrix blocks.

Significant chemical and isotopic differences exist between groundwater at Shoal and groundwater from well HS-1 in Fairview Valley. In particular, HS-1 has a more depleted (lighter) stable isotopic composition and lower dissolved solids content than groundwater sampled beneath the Sand Springs Range (Pohll et al., 1998). The data indicate little contribution to Fairview Valley groundwater from groundwater beneath PSA, supporting the hydrologic interpretation of the shear zone as a barrier to flow. In addition, the chemical and isotopic content of groundwater in the Fourmile Basin west of Shoal show the influence of residual brines, indicating a low contribution of flow from the Sand Springs westward. This

supports the low recharge rates identified for the site, in addition to the behavior of the western range-bounding fault as a hydraulic barrier.

Both the stable isotopes and naturally occurring radioactive carbon-14 (^{14}C) indicate long residence times for groundwater sampled from the Sand Springs Range at the Shoal site. Apparent ^{14}C ages range from 6,000 to more than 21,000 years before present. The stable isotopes reflect a contribution of post-pluvial recharge. These findings are consistent with the slow groundwater velocities in the model, and with the process of matrix diffusion, which can increase the residence time of dissolved constituents such as ^{14}C relative to the residence time of groundwater in fractures.

2.1.2.10 Predictive Simulations

Predictive simulations of radionuclide transport from the Shoal test were conducted with an emphasis on defining contaminant boundaries. The procedure for boundary calculation is presented in detail by Pohll et al. (2003) and in Section 2.2.

2.1.2.11 Presentation of Model Results

Per this step in the FFACO ten-step validation process, the results of the CAI modeling were presented in the interim modeling report (Pohll et al., 1998), in the DDA report (Pohll et al., 1999a), in the final modeling report (Pohlmann et al., 2004), and in the contaminant boundary letter report (Pohll and Pohlmann, 2004). Findings of these reports were also provided to NDEP through presentation at technical meetings. The results are summarized here in Section 2.1.3.

2.1.2.12 Post-Audit

Rev. 1, 2000 of the FFACO (1996) states: "The five-year proof of concept is the model post-audit to establish, within a longer time frame, that the model is capable of producing meaningful results with an acceptable degree of uncertainty." The model validation and monitoring processes that will occur during this post-audit phase are described in detail in the CAP portion of this document. They involve obtaining new data from PSA to compare with the model, as well as monitoring of the groundwater system based on contaminant transport predictions.

2.1.2.13 Quality Assurance/Quality Control (QA/QC)

The work carried out under the CAIP for CAUs 416 and 447 was designed and implemented in accordance with the FFACO (1996) and the UGTA QAPP (DOE/NV, 1998d; and 2000b). As

stated in the UGTA QAPP, three fundamental types of activities are necessary to accomplish project objectives. These are data collection, assessment of new and existing data, and flow and transport modeling.

Field activities at PSA were accomplished using approved plans and contractor-specific procedures and instructions. Personnel were qualified for their work and used appropriate tools and calibrated equipment. Plans included the CAIPs for CAUs 416 and 447 (DOE/NV, 1996; 1998a), the addendum to the CAIP for CAU 447 (DOE/NV, 1999a), related fluid management plans (DOE/NV, 1999b), and field instructions (IT Corporation, 1996; Pohll et al., 1999b).

Data were evaluated against their intended use. This analysis consisted of screening, checking, verifying, and reviewing the data. Some of these data were decades old and their quality was assessed by review of the testing and analysis methods presented in published reports, and assessment of the data in the context of regional and general hydrogeologic knowledge.

Quality assurance of the numerical modeling work relied on several overlapping efforts. These are:

- Project control procedures
- Personnel qualifications
- Technical control procedures
- Peer review

2.1.2.13.1 Evaluation

Code developed external to the Desert Research Institute (DRI) originates from commercial software firms and nonprofit organizations (e.g., the MODFLOW code from the U.S. Geological Survey). External code is selected based on its technical capabilities to meet project needs and acceptance in the wider groundwater modeling community. Before selecting externally developed code for a particular modeling purpose, a rigorous review and comparison is conducted of the available pertinent codes. Internal modeling programs are developed when external programs are not available to meet project needs and/or when additional flexibility or new algorithms are required for the task at hand (e.g., the RWPT code used for radionuclide transport modeling).

2.1.2.13.2 Code Verification/Validation

Software verification and validation activities are intended to provide confidence that the software adequately and correctly performs all intended functions. Significant portions of the Shoal modeling were performed using externally developed software (e.g., SIS, SGS,

MODFLOW). These software packages are subjected to rigorous test-case analyses, per the software's documentation, to ensure proper operation. Externally developed modeling programs are not, to the extent practicable, modified in any way. In some cases, modifications are not possible because the source code is proprietary and not available; however, even in the case of open-source software such as MODFLOW, internal modifications can prevent the application of the code to other modeling scenarios without further modifications and may increase uncertainty in the results. For these reasons, the modeling team prefers to develop input and output routines that provide the input data and accept the results in the default format of the codes. In addition, it is unlikely that internal changes would be required to, for example, improve performance or integrate additional functionality, as these factors would have been evaluated during code evaluation. Additional functionality is generally provided only by development and integration of auxiliary codes in the modeling system.

Individuals knowledgeable in the area of code development review all newly developed DRI computer codes. These reviews consider whether the assumptions are reasonable and valid, the correctness of the mathematical models, conformance of methods to accepted and published concepts, consistency of results with known data, reasonable and prudent use of data and analysis tools, and appropriateness for the intended purpose. Where appropriate, solutions are compared to analytically derived solutions to check the theory and application represented by the codes. In the case of the RWPT code used for radionuclide transport, additional quality assurance was provided through independent peer-reviewed publication of a rigorous comparative study with other transport codes (Hassan and Mohamed, 2003).

2.1.2.13.3 Documentation

Continual evaluation and record keeping are conducted during the modeling phases of the project to ensure that the work is internally consistent, well-documented, and readily repeatable for the purposes of technical review and future model refinements. All developed and procured computer codes are uniquely identified and internally documented so that it is obvious to the user of the version they are implementing. Unique run identifiers are used to link model output with the corresponding model input; and the associated documentation identifies the specific input files, versions of the codes, and other related information so that the output for any run can be readily regenerated. This procedure is followed even during initial testing of model parameterization and boundary conditions, in order to track sensitivity to these fundamental aspects of the model. Computer software code documentation is maintained in project files.

2.1.2.13.4 Peer Review

Peer review is an assessment of the assumptions, calculations, extrapolations, alternate interpretations, methodology, acceptance criteria, and conclusions pertaining to interpretative work products generated through the use of computer software. Peer review is performed to ensure that interpretative work products are technically adequate, are properly documented, and satisfy technical and quality requirements. Peer reviewers shall possess the appropriate subject matter/technical expertise and not have participated in preparing the original work.

Internal peer review was routinely conducted during the modeling effort. External peer review occurred at the conclusion of the draft model report and used the Modeling Subcommittee of the UGTA Technical Working Group. The review committee consisted of:

- Andrew F.B. Tompson (Chair), Lawrence Livermore National Laboratory
- David E. Prudic, U.S. Geological Survey
- Richard Waddell, HSI Geotrans
- Andrew Wolfsberg, Los Alamos National Laboratory
- Vefa Yucel, Bechtel Nevada

The draft report was sent to the committee on October 4, 2001. Committee comments were received on April 16, 2002 and incorporated into the model and model report before submission to NDEP. The model report was delivered to NDEP for review on January 21, 2003. The regulatory review conducted by NDEP also serves as a peer review. Technical comments were received from NDEP by letter dated March 20, 2003. The report underwent additional revision in response to the NDEP comments and was resubmitted on January 13, 2004. Concurrence with the PSA model was received from NDEP by letter dated February 18, 2004.

Rigorous peer review also occurred through the process of publication in the open scientific literature. Pohll et al. (1999c) presented the results of the interim Shoal model. Papelis (2001) discusses the sorption experiments and results. Pohlmann et al. (2002) presented the modeling process in relation to the data collection efforts. Reimus et al. (2003) presented the tracer test and its analysis.

2.1.3 Modeling Results

The primary result of the PSA modeling is the calculation of the contaminant boundary maps. These are presented in Section 2.2. The following describes the general hydrogeologic results of the flow model and the contaminant transport behavior.

Groundwater flow in the PSA model basically moves toward the northeast, paralleling the structural grain of the Sand Springs Range. There is a dominant component of vertical flow in the model, driven by the surface recharge. The relative proportion of lateral to vertical flow varies from one realization to the next, driven by the *K* values assigned to the two flow categories. Embedded within this natural flow field is a region of higher *K* and higher porosity representing the nuclear cavity, chimney, and surrounding disturbed zone.

The mean value of groundwater velocity is 2.3×10^{-5} m/d, with a distribution between log-normal and normal. As expected from the configuration of the flux boundaries and the principal direction of fracture strikes in the flow model, the highest mean velocities are in the *y* and *z* directions (Figure 2-11), parallel to the long axis of the model and the trend of the shear zone. The fracture zones dip at about 60 to 65 degrees, so velocities downward along the fracture zones are actually higher than those in Figure 2-11 by about 10 to 20 percent. The small range of mean velocities in the *x* direction (perpendicular to the long axis of the model) reflect movement along dipping fracture planes and fractures oriented off-axis to the principal fracture strike. The average maximum groundwater velocity for all realizations is 2.6×10^{-3} m/d, while all maximum velocities fall below 1.5×10^{-2} m/d. The maximum groundwater velocities are roughly log-normally distributed (Figure 2-12), reflecting the log-normal distributions of hydraulic conductivity, fracture length, and porosity.

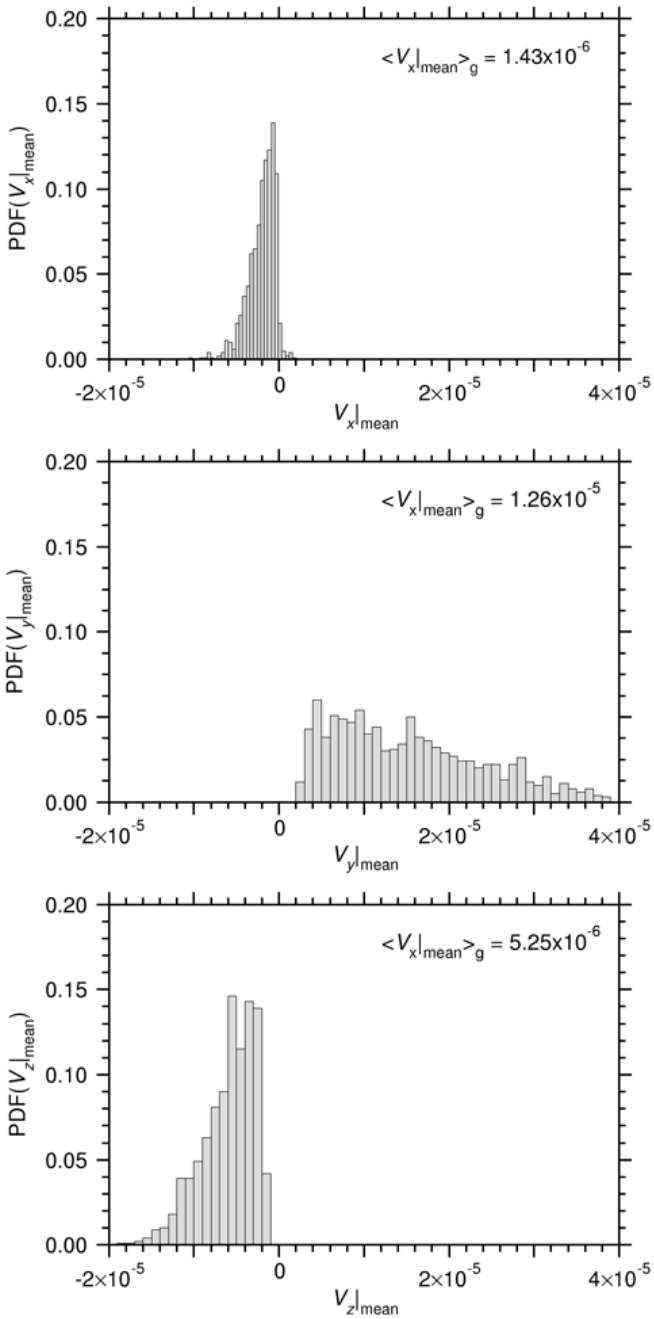

Note: The geometric means of each distribution are also shown on each plot.

Figure 2-11
Distributions of average velocities in the three coordinate directions for all realizations

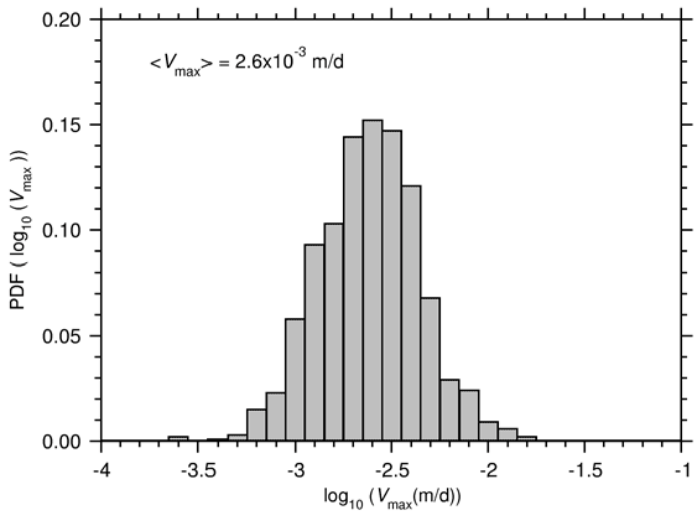

Figure 2-12
Distribution of log$_{10}$-transformed maximum velocity vectors for all realizations

The velocity fields from the flow realizations form the foundation for particle-tracking transport calculations. Figure 2-13 displays three snapshots of the particle distribution in the simulation domain at 100, 500, and 1,000 years for a single realization. The three plots on the left represent vertical (y-z) views at the three times with z representing the elevation AMSL in m, and the right plots represent plan (x-y) views of the 3-D plume (particle) distribution. Particle movement reflects the patterns of flow simulated in the flow model. Particles move vertically downward, accompanied by lateral movement in a northeasterly direction. The downward movement is due to the surface recharge, and the northeastern trend is oriented with the major fracture trend, N 20°E. For the one realization shown in the figure, particles move at most 500 m laterally and about 300 m vertically downward after 500 years. In 1,000 years, two particles out of 40,000 reach the boundary of the simulation domain for that particular realization (note that the particles undergo advection, dispersion, and matrix diffusion, but not radioactive decay in this figure). The figure displays the flow pattern that is repeated in many realizations: vertical downward movement accompanied by lateral movement in a northeasterly direction. How far the particles travel in different realizations is dependent on the location and hydraulic conductivity of the fractures, the fracture porosity, surface recharge, and value of flux at the southern inflow boundary, all of which are spatially variable and/or uncertain parameters.

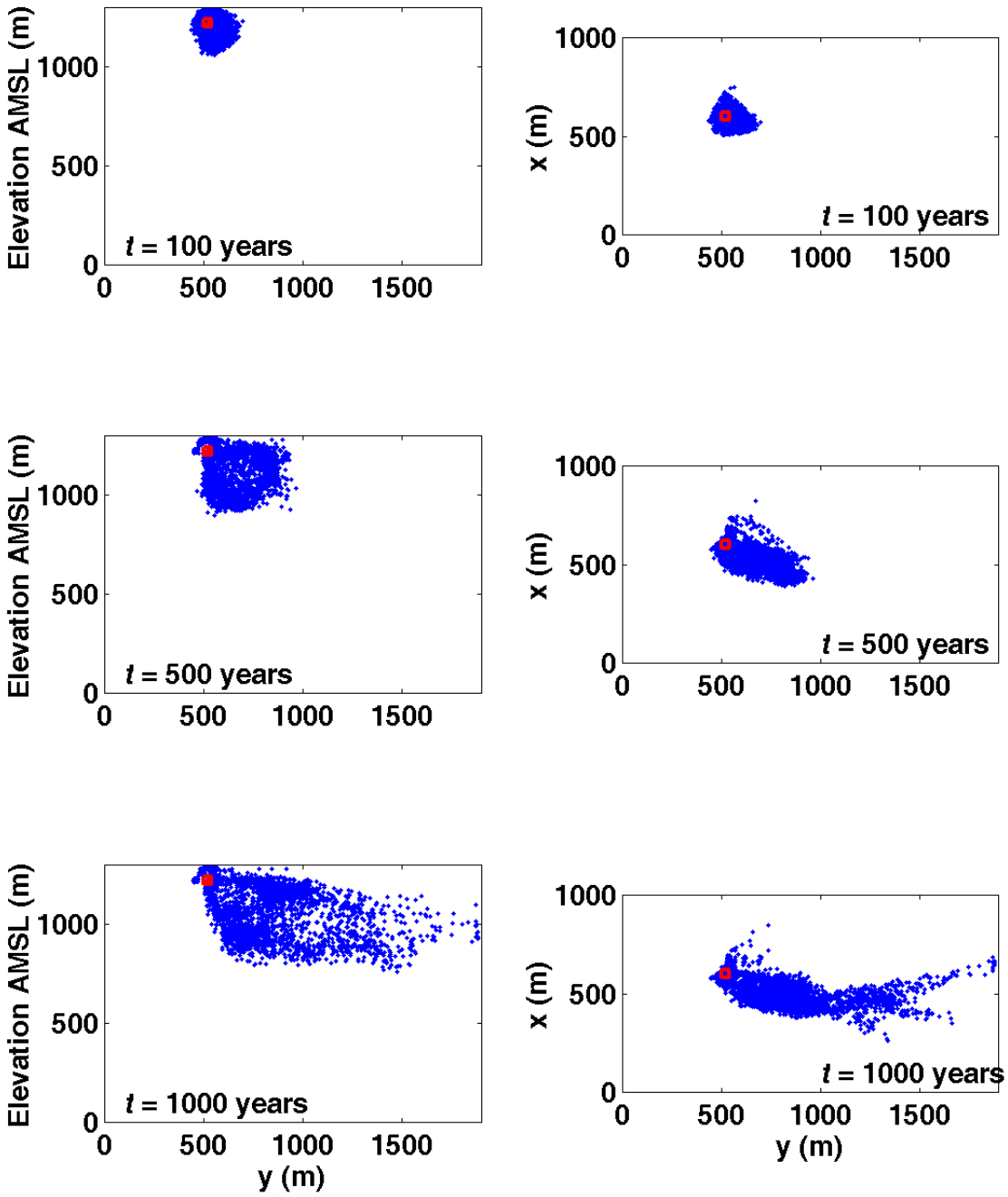

Note: The left side shows vertical views and the right shows plan views, exhibiting the extent and pattern of movement in a single flow realization. These particles represent no sorption, no effect of nuclear melt glass dissolution, and no radioactive decay.

Figure 2-13
Snapshots of the 3-D particle distribution

Using an unclassified estimate of the tritium source term (Hazelton-Nuclear Science, 1965), a map of tritium concentration can be created for each of the 1,000 realizations. Figure 2-14 shows two-dimensional (2-D) projected maps (*x*-*y*, *x*-*z*, and *y*-*z*) for the maximum tritium concentration for the same flow realization as shown in Figure 2-13. Note that the concentrations shown in Figure 2-14 account for tritium radioactive decay, whereas Figure 2-13 represents only particle positions prior to decay. A high concentration can be seen around the cavity and extends for about 200 m in the *y* direction and for a similar distance in the vertical *z* direction. Beyond about 300 m, the maximum concentration values for tritium are below the maximum contaminant level (MCL) and they quickly fall below the detection limit. Figure 2-15 is similar to Figure 2-14, but is produced using a different flow realization. This realization exhibits less longitudinal (*y*-direction) movement as compared to Figure 2-14, but again concentrations above the MCL are localized around the cavity. Most of the 1,000 realizations exhibit similar patterns to these two realizations, with sometimes faster longitudinal or vertical transport.

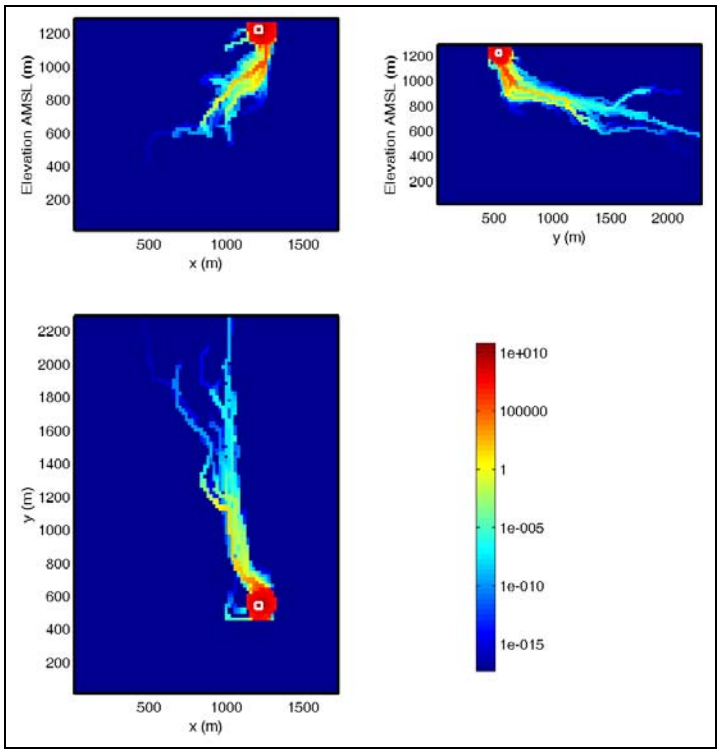

Note: Color bar is tritium concentration in picocuries per liter (pCi/L), based on an unclassified source estimate.

Figure 2-14
Projected maps of the maximum concentration distribution for tritium for the flow realization shown in Figure 2-13

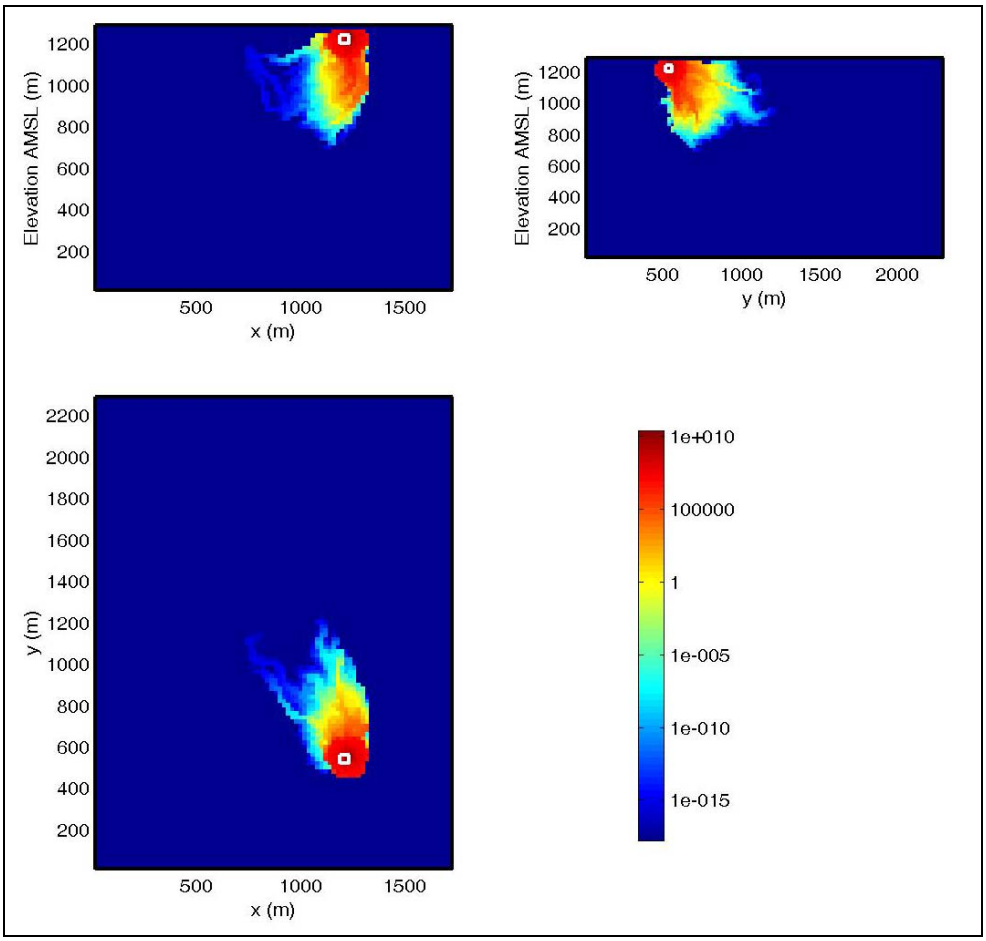

Note: This flow realization is different from that in Figure 2-14. Color bar is tritium concentration in pCi/L, based on an unclassified source estimate

Figure 2-15
Projected maps of the maximum concentration distribution for tritium for one flow realization

With the uncertainty of the flow and transport parameters, many flow scenarios are possible, as demonstrated by comparing Figures 2-14 and 2-15. Combining the different flow scenarios with the different possible values for the transport parameters, a spectrum of possible transport regimes results. These are statistically analyzed to obtain maps of the contaminant boundaries, using the goodness-of-fit weights obtained during calibration of the flow realizations.

Individual contaminant boundary maps were calculated for unclassified estimates of tritium, strontium-90 (^{90}Sr), cesium-137 (^{137}Cs), and samarium-151 (^{151}Sm). At a 50 percent confidence interval, tritium concentrations above the MCLs of the *Safe Drinking Water Act* (SDWA) barely exist beyond the initial source location through a 1,000-year period (Figure 2-16). At a 95 percent confidence level for the tritium class, there is a lateral extent of about 180 m in the *y*

direction downstream of the cavity, and a vertical extent of about 160 m below the cavity (Figure 2-17). Based on these results, the tritium-contaminated area will be localized in the vicinity of the source. The other nuclides examined have smaller boundaries than tritium, due primarily to their retardation properties.

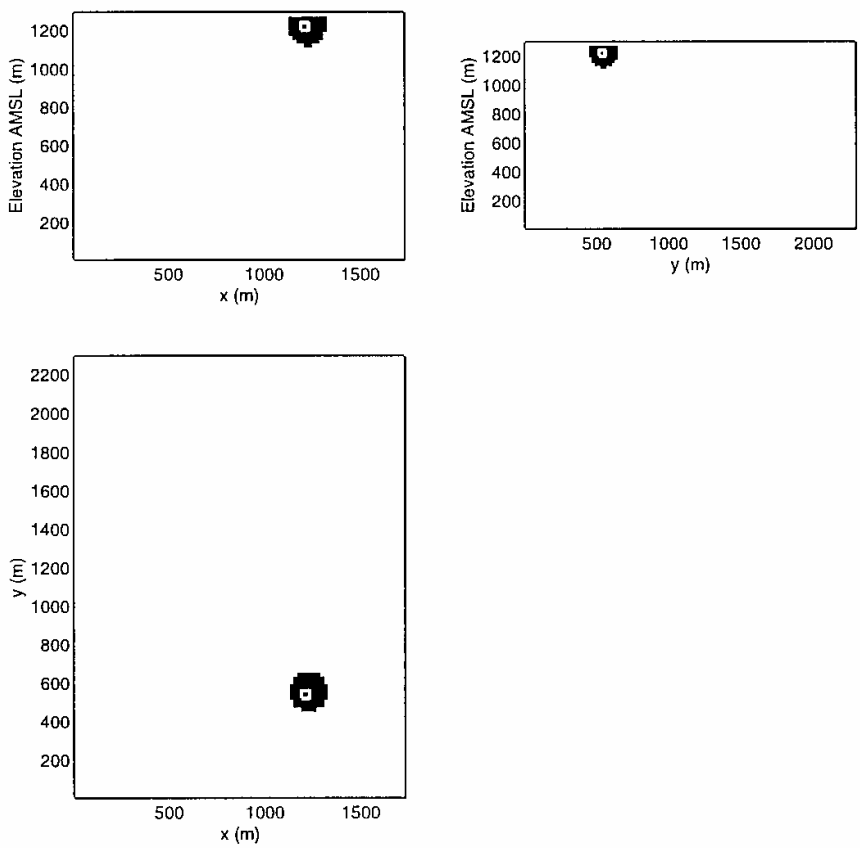

Note: An unclassified estimate of initial tritium mass was used.

Figure 2-16
Contaminant boundary maps for tritium delineating the areas exceeding 20,000 pCi/L at the 50 percent confidence level for the 1,000-year simulation period

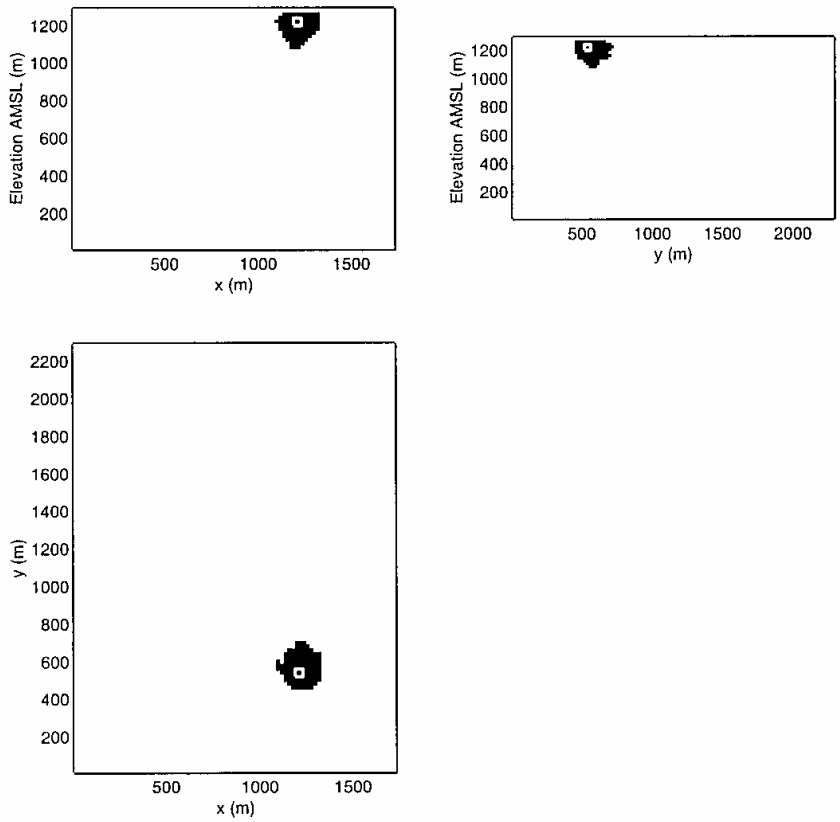

Note: An unclassified estimate of initial tritium mass was used.

Figure 2-17
Contaminant boundary maps for tritium delineating the areas exceeding 20,000 pCi/L at the 95 percent confidence level for the 1,000-year simulation period

The final result of the modeling is the contaminant boundary produced using the full radionuclide source. That boundary, as well as the methodology used to calculate it, is presented in Section 2.2.

2.2 Contaminant Boundary Determination

The purpose of the contaminant boundary calculation is to provide "the model-predicted perimeter which defines the extent of radionuclide-contaminated groundwater above background conditions exceeding the SDWA standards" (FFACO, 1996). From the contaminant boundary predicted by the computer model, the compliance boundary is negotiated between NDEP and DOE (Section 2.3). Thus, the contaminant and compliance boundaries are the final product of the CAI.

The contaminant boundary for the Shoal underground nuclear test was calculated using the groundwater flow and transport model of Pohlmann et al. (2004). There are two differences between the preliminary transport results in Pohlmann et al. (2004) and the contaminant boundary presented here. One is the radionuclide mass data. Pohlmann et al. (2004) use unclassified source-term data from Hazelton-Nuclear Science (1965), while the contaminant boundary uses the classified radionuclide mass data presented by Goishi et al. (1995). Second is the manner of presenting the results. Pohlmann et al. (2004) present boundaries for the transport of a single radionuclide. The contaminant boundaries presented here combine the transport results for all of the significant radionuclides in the source term, as discussed below.

The methodology used to calculate the contaminant boundary is summarized below. A detailed presentation of the approach is in Pohll et al. (2003).

2.2.1 Land Use and the Contaminant Boundary

The PSA is surrounded by open terrain that is managed by the U.S. Department of the Interior, Bureau of Land Management (BLM), which has historically been used for ranching and mining. The area is also used for public recreation including hunting, camping, and off-road driving. The site is part of a much larger area that was withdrawn by the U.S. Navy in 1999. Under the DOE land withdrawal agreement and military land withdrawal criteria, this land has been withdrawn from all forms of appropriation under the public land laws. The DOE will maintain the existing land withdrawal and establish use restrictions using the FFACO process. The U.S. Navy withdrawal should help maintain government oversight and control of the subsurface resources at PSA, although it does not currently prevent public access to the site. Future land use for the site and surrounding area is expected to remain the same; however, the DoD will determine the future use of the surface area.

There is no human population within four miles of PSA; however, several ranches are in the vicinity. There are two mines in the southern part of the Sand Springs Range, but no oil or gas leases. Fallon is the largest town in the region and it lies 30 miles northwest of the site. The Nevada Scheelite Mine and the Kennecott Rawhide Mine are within 20 miles of the site, at the southern end of the Sand Springs Range.

The contaminant boundary is based on these current conditions of no groundwater development, per agreement between NDEP and DOE. It is important to note that the groundwater flow and transport simulations provide predictions of radionuclide transport under ambient conditions and that those predictions could change with the addition of pumping stress to the aquifer.

2.2.2 Relationship Between Risk and Safe Drinking Water Act Requirements

The FFACO specifies that the SDWA standards are the metric of concern for the boundary. The National Primary Drinking Water Regulations for radionuclides (EPA, 2000a and b) identify 0.04 millisievert per year (mSv/yr) (4 millirem per year [mrem/yr]) as the total annual dose equivalent to an organ or the whole body that cannot be exceeded from internal exposure to beta particle and photon radioactivity. For beta/photon emitters the 4 mrem/yr equates approximately to a 50 picocuries per liter (pCi/L) screening level. This annual dose equivalent, along with a 2 liters per day (L/d) consumption rate, is used as a basis for setting annual average activity-concentration limits for drinking water intake for beta particle and photon-emitting radionuclides (EPA, 1976). This method is best described as the "critical-organ dose-limit approach" because it involves using an acceptable dose limit for a critical organ as a fundamental parameter for setting a concentration limit. In addition, the regulations require that the sum of the activity concentrations of alpha-emitting radionuclides must not exceed 15 pCi/L, and the sum of mass concentrations of uranium isotopes must not exceed 30 micrograms per liter (μg/L). The beta/photon MCL is 50 pCi/L and it is a screening level. The MCLs are given in Table 2-10.

Lifetime excess cancer risk is calculated using radionuclide-specific cancer-risk coefficients applied to drinking water activity concentrations predicted for specific radionuclides, and estimating lifetime exposure to drinking water. Certain combinations of radionuclides in groundwater might yield estimates of lifetime excess cancer risk that could exceed a risk of 10^{-6}, even though a categorical MCL may not be exceeded. Details regarding the risk and MCL approaches are presented in Pohll et al., 2003.

Table 2-10
Radionuclides used for the contaminant boundaries and related parameters (Pohll et al., 2003)

Isotope	Half life ($t_{1/2}$; yr)	Used in MCL Boundary	MCL Standard	Emission Type
Tritium	1.23E+01	x	20000 pCi/L	Beta
Carbon-14	5.73E+03	x	2000 pCi/L	Beta
Aluminum-26	7.30E+05		*n/a*	Beta
Chlorine-36	3.01E+05	x	700 pCi/L	Beta
Calcium-41	1.03E+05		*n/a*	Beta
Nickel-59	7.60E+04	x	300 pCi/L	Beta
Nickel-63	1.00E+02	x	50 pCi/L	Beta
Strontium-90	2.91E+01	x	8 pCi/L	Beta
Zirconium-93	1.50E+06	x	2000 pCi/L	Beta
Niobium-94	2.00E+04		*n/a*	Beta
Technetium-99	2.13E+05	x	900 pCi/L	Beta
Paladium-107	6.50E+06		*n/a*	Beta
Cadmium-113m	1.41E+01		*n/a*	Beta
Tin-121m	5.50E+01		*n/a*	Beta
Tin-126	1.00E+05		*n/a*	Beta
Iodine-129	1.57E+07	x	1 pCi/L	Beta
Cesium-135	2.30E+06	x	900 pCi/L	Beta
Cesium-137	3.02E+01	x	200 pCi/L	Beta
Samarium-151	9.00E+01	x	1000 pCi/L	Beta
Europium-150	3.60E+01		*n/a*	Beta
Europium-152	1.35E+01	x	200 pCi/L	Beta
Europium-154	8.59E+00	x	60 pCi/L	Beta
Holmium-166m	1.20E+03	x	90 pCi/L	Beta
Thorium-232	1.40E+10	x	15 pCi/L	Alpha
Uranium-232	7.00E+01	x	30 mg/L	Uranium & Alpha
Uranium-233	1.59E+05	x	30 mg/L	Uranium & Alpha
Uranium-234	2.46E+05	x	30 mg/L	Uranium & Alpha
Uranium-235	7.04E+08	x	30 mg/L	Uranium & Alpha
Uranium-236	2.34E+07	x	30 mg/L	Uranium & Alpha
Uranium-238	4.47E+09	x	30 mg/L	Uranium & Alpha
Neptunium-237	2.14E+06	x	15 pCi/L	Alpha
Plutonium-238	8.77E+01	x	15 pCi/L	Alpha
Plutonium-239	2.41E+04	x	15 pCi/L	Alpha
Plutonium-240	6.56E+03	x	15 pCi/L	Alpha
Plutonium-241	1.44E+01	x	300 pCi/L	Beta
Plutonium-242	3.75E+05	x	15 pCi/L	Alpha
Americium-241	4.33E+02	x	15 pCi/L	Alpha
Curium-244	1.81E+01	x	15 pCi/L	Alpha

2.2.3 Model Uncertainty and Boundary Calculation Process

If there were no uncertainty in the solute transport model, the risk-based or regulatory-based analysis would provide explicit definition of the boundary maps. In reality, the groundwater models contain a certain degree of uncertainty, which needs to be represented in an analysis of the boundary delineation. This was recognized in the FFACO and expressed as a requirement that the contaminant boundary be predicted at a 95 percent level of confidence. This requirement can actually be interpreted in two different, but complementary, ways to map the 3-D extent where groundwater has been contaminated and the associated uncertainty. One approach is to identify the region in which there is a 95 percent certainty that contaminants exist and exceed the health risk or regulatory threshold. The boundary will then encircle the region that meets this criterion. The alternative approach is to identify the region where there is a 95 percent certainty that contaminants do not pose a health risk; therefore, encompasses the region that fails to meet the boundary criterion. In other words, the water that does not pose a health risk is external to the region enclosed by the boundary. The description of the boundary in Rev. 1, 2000 of the FFACO is ambiguous as to which of these two perspectives should be used for the contaminant boundary. The approach presented here follows the second alternative, identifying the region where it is 95 percent certain that contaminants do not pose a health risk.

Uncertainty in the groundwater flow and transport model is handled directly within a Monte Carlo type approach. Monte Carlo methods describe the uncertainty in model predictions based upon an analysis of the uncertainty in model input parameters. Bayesian methods are used in combination with Monte Carlo techniques to weight each Monte Carlo realization based on its ability to reproduce observed system behavior. The Bayesian methods (see Section 2.1.2.7) allow one to “calibrate” the stochastic model within the framework of the uncertainty analysis.

The general approach to quantify the model uncertainty is described by the following steps:

1. Determine all model parameters that are considered uncertain. It is important to note that uncertainty is derived from parameter measurement errors, spatial heterogeneity, and errors in model conceptualization, each of which can be included in the uncertainty analysis.

2. Quantify the distributions of all uncertain parameters. This is typically done via a specification of a probability distribution function (pdf) for each parameter.

3. Perform numerical simulation of groundwater flow and transport with randomly sampled parameter distributions.

4. Calculate the likelihood function (e.g., weights) for each realization. The likelihood function is a measure of the "fit" between simulated and observed system behavior. Hydraulic heads are used as the basis for calculating the likelihood measure.

5. Quantify the pdf for the simulated solute transport. In the context of calculating boundary maps, a pdf is created for each cell within the solute transport model that specifies the probability that radionuclide concentrations will exceed the MCL over a 1,000-year period.

6. Determine the 95 percent confidence threshold for the contaminant boundary.

The quantification of the pdf uses the results of the solute transport model and the source mass for individual radionuclides to determine if a fluid parcel exceeds the MCL with the inclusion of model uncertainty. A continuous pdf is generated for each spatial position at 70-year intervals.

A confidence interval defines a range of concentrations for a given significance level (e.g., 95 percent), which describes the magnitude of the uncertainty inherent in the numerical model. A typical confidence region as defined by statisticians is given by:

$$\int_a^b f(x) = \gamma \qquad (2\text{-}4)$$

where f(x) is the pdf (in this case of simulated radionuclide concentrations), γ is the significance level and *a* and *b* are the lower and upper bounds of the confidence region (i.e., confidence levels). Figure 2-18 is a graphical representation of this type of definition. The shaded region represents an area equal to γ. This type of definition captures the central portion of the pdf, which is not appropriate for the definition of boundary maps, as the tails represent very high concentrations and very low concentrations.

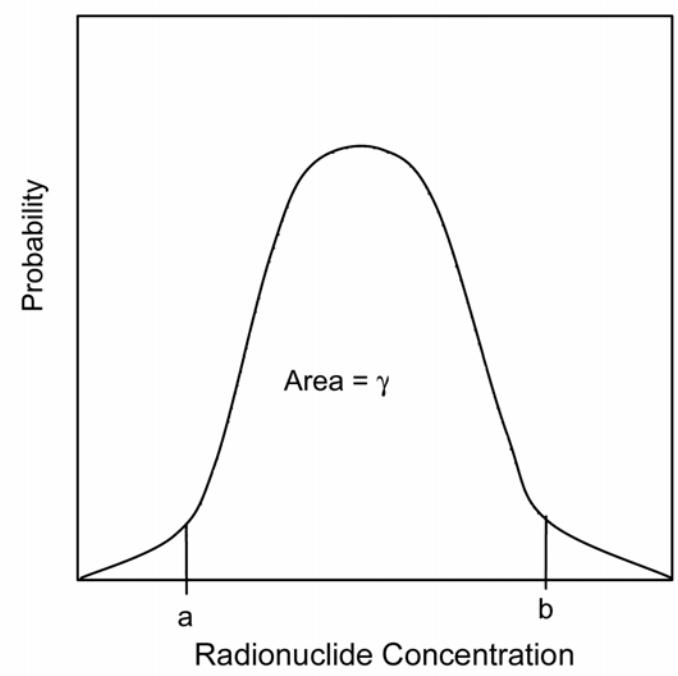

Figure 2-18
Probability distribution function showing how typical confidence levels are determined

For the purposes of contaminant boundaries, the choice is made to focus on the region of "clean" water and as such, the lower end (i.e., uncontaminated region) of the pdf is used in the determination of the confidence threshold:

$$\int_{o}^{a_1} f(x) = \gamma \qquad (2\text{-}5)$$

where a_1 is the threshold concentration value that captures an area of size γ. Figure 2-19 shows a graphical representation of the proposed contaminant boundary confidence threshold. The contaminant definition captures all transport realizations with concentrations greater than a_1 and determines the threshold concentration that captures our knowledge to a level equal to γ. If, for example, a γ was chosen at a 95 percent level, then the threshold value represents a concentration in which there is 95 percent confidence that the concentration is less than or equal to a_1.

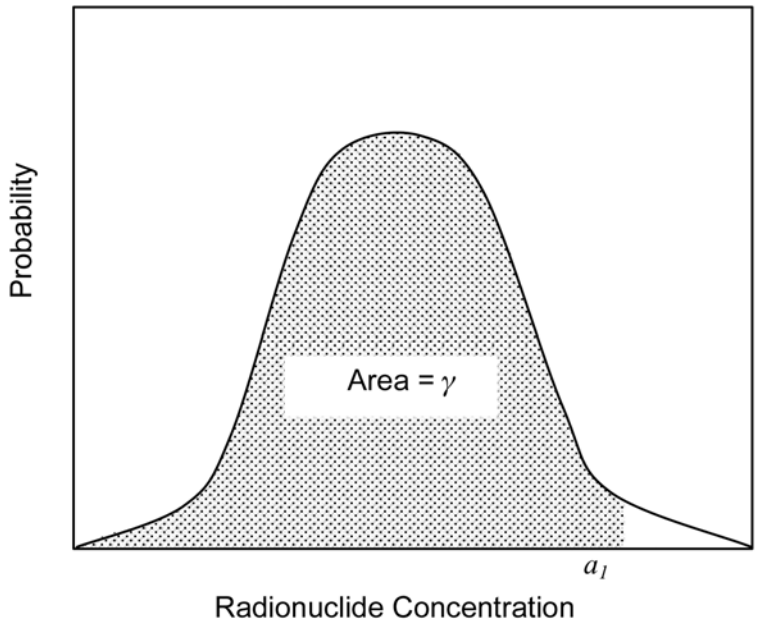

Figure 2-19
Probability distribution function showing how the concentration threshold is calculated for the contaminant boundary

The boundary maps are created by determining the threshold concentration for individual locations at 70-year intervals. The weighted concentrations (i.e., the probabilities incorporate the Bayesian likelihoods) are used to create a pdf of concentration. The threshold concentration is determined as shown in Figure 2-20. If the MCL of any category is not exceeded at the 95 percent level, then the location is considered to be external to the contaminant boundary. This process is repeated for all locations within the model domain. All cells that did not meet the above criterion define the contaminant boundary region. Therefore, the contaminant boundary is a 3-D surface that encloses all cells that violate the MCL. The boundary maps are presented in three 2-D sections representing the x-y, x-z, and y-z Cartesian planes. The boundary sections are 2-D projections of the 3-D boundary surface. For example, the aerial view (x-y plane) represents the maximum extent of the 3-D boundary or volume as projected to the surface as shown in Figure 2-21. A location is considered to be within the boundary if at any x-y location there is at least one vertical position that is found to be within the boundary. Similar projections are made for the x-z and y-z planes.

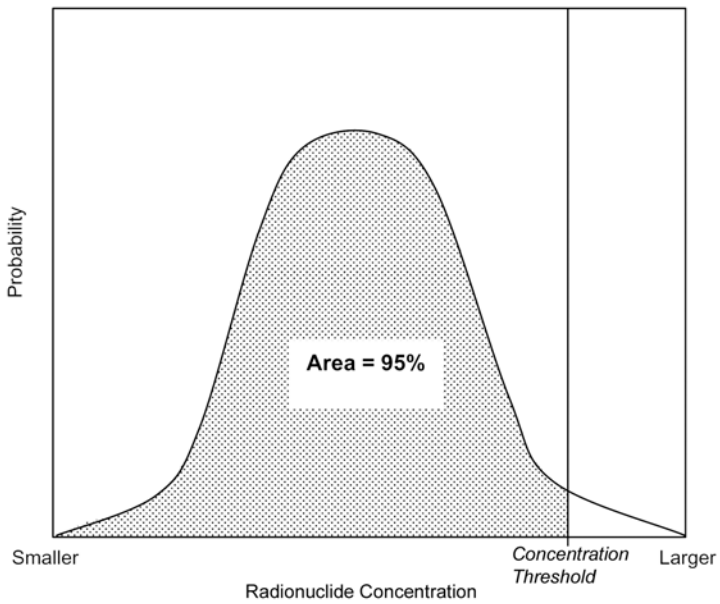

Figure 2-20
An example of the probability distribution function and how the concentration threshold is calculated for the contaminant boundary

2.2.4 Shoal Contaminant Boundary

A regulatory-based approach was used to calculate a contaminant boundary for the Shoal underground nuclear test. The methodology used for the calculation focuses on identifying the region where there is a 95 percent certainty that water is "clean" based on the MCL standard. This region is external to (outside) the boundary. The region internal to this boundary is 5 percent certain to contain water exceeding the MCL standard.

The source term used to scale the transport results from the model is the classified radionuclide source presented in Goishi et al. (1995). The types of radionuclides present in underground nuclear tests and their relative importance based on production, risk factor and MCLs can be discerned by examining the unclassified source term mass from the average of nuclear tests conducted in Areas 19 and 20 at the NTS (Smith, 2001). The exact source values used for the Shoal contaminant boundary are presented in Pohll (2004).

The contaminant boundary using the regulatory-based calculation at a significance level of 95 percent for the cumulative 1,000-year period after the detonation is presented in Figure 2-22. The MCL-based boundary encompasses an area of 1.34×10^5 m^2).

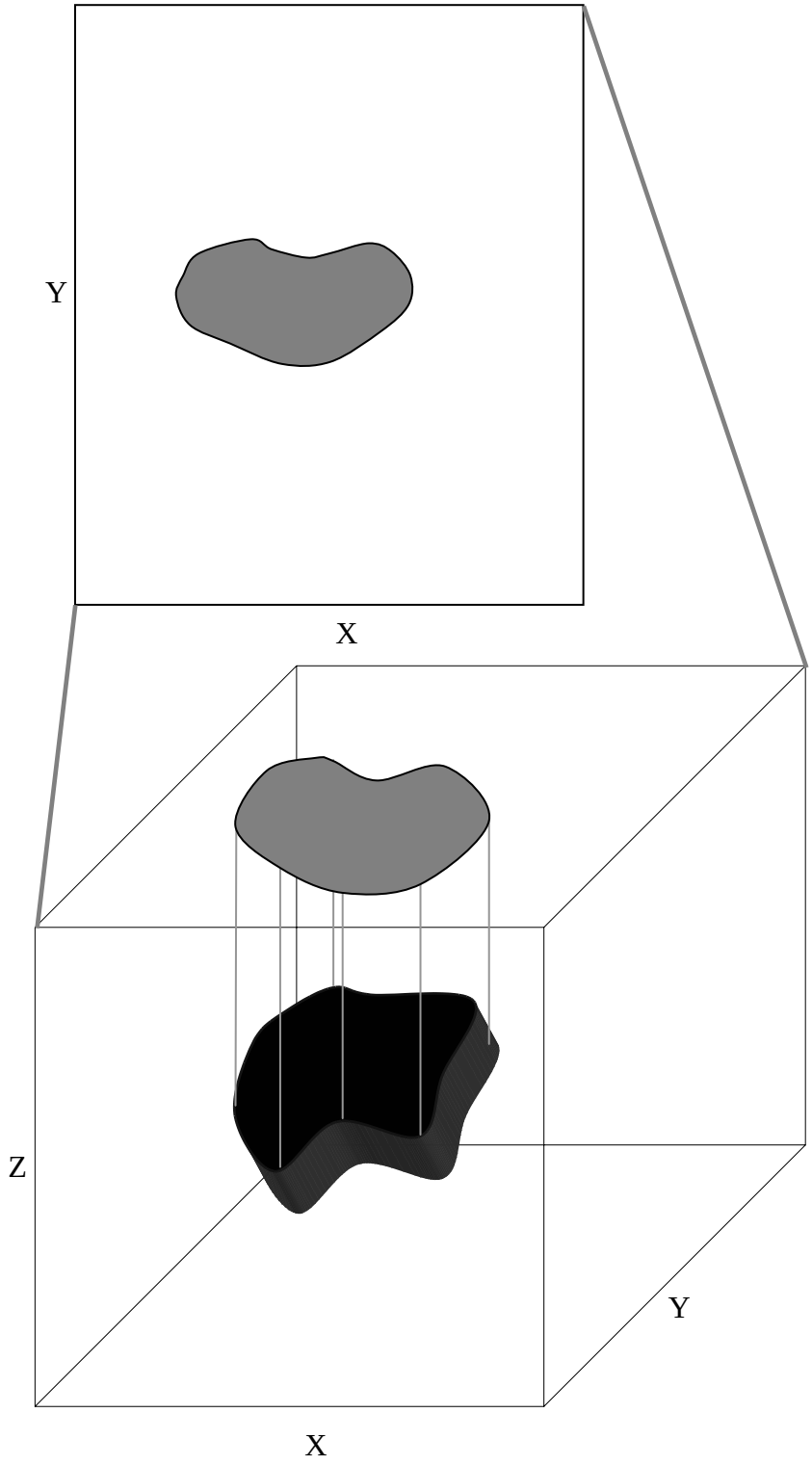

Figure 2-21
An example of a 3-D contaminant boundary and the associated mapping to an x-y plane (at top of figure)

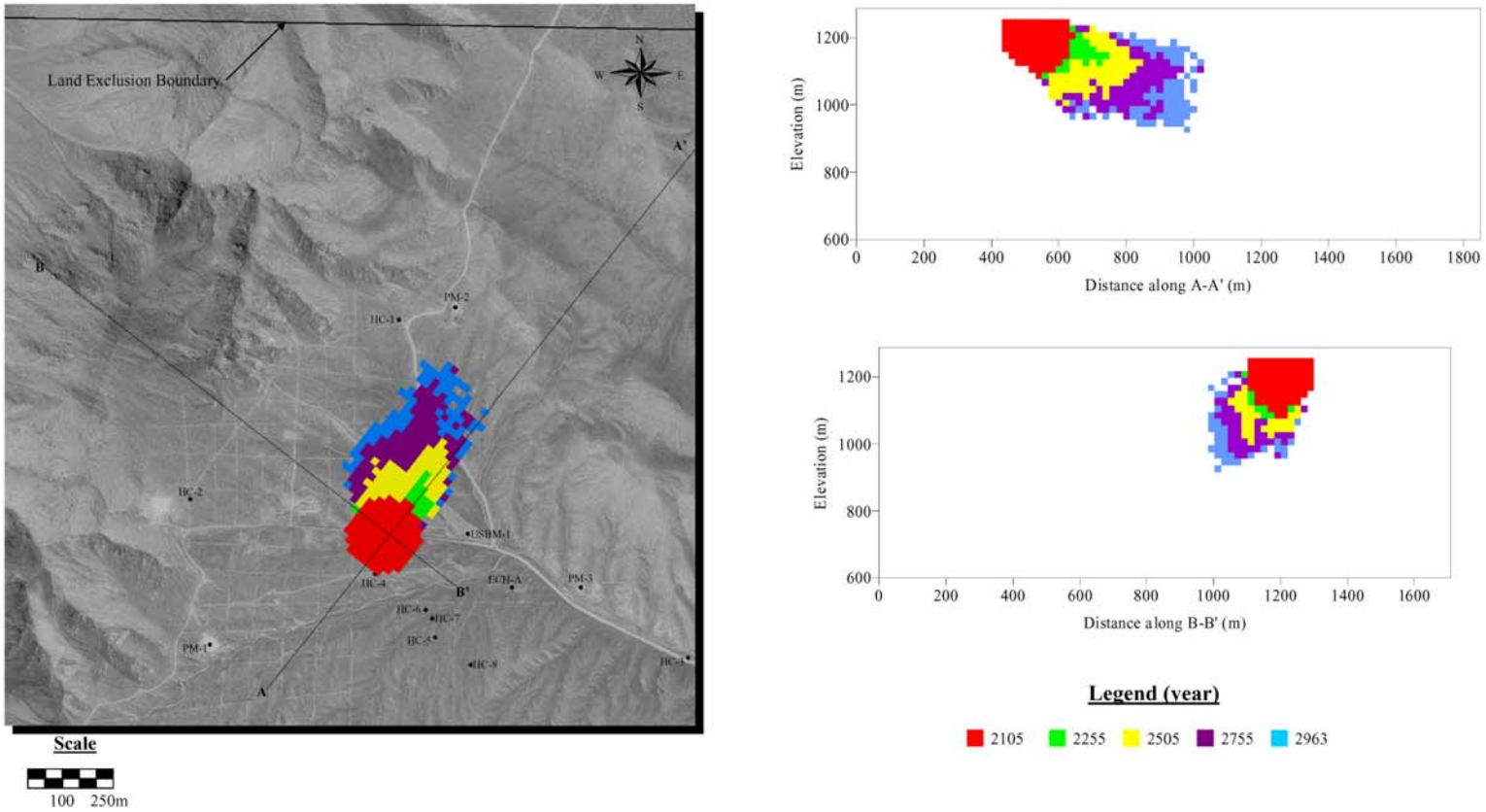

Figure 1. Regulatory-based contaminant boundary for the Project Shoal Site.

Figure 2-22
Regulatory-based contaminant boundary for the Project Shoal Site

2.2.5 Boundary Through Time

Two options are available to present the temporal history of the contaminant boundary maps. One option is to produce maps that represent an instantaneous view of the boundaries for a given 70-year time interval and the other option is to present the cumulative boundary from time zero to a given time period. The latter option is used here, as it represents the maximum extent of the boundary at any given time within 1,000 years and is consistent with Rev. 1, 2000 of the FFACO (1996).

The boundary shown in Figure 2-22 is presented for five different time periods. These represent the years 2105, 2255, 2505, 2755, and 2963. The year 2963 is 1,000 years after the nuclear test and is the contaminant boundary as defined in the FFACO. As shown in the plot, for the first several hundred years, the contaminant boundary is centered on the cavity region while exhibiting some downward migration. Recall that the model simulates not only a cavity, but also a high conductivity zone around it to account for fracturing related to the nuclear test. This higher *K* zone has a radius of 100 m, and the initial positions of the radioactive particles in the model are distributed through that entire sphere. The downward growth in the boundary (driven by recharge) continues through the later time periods, but the boundary also incrementally extends laterally, to the northeast.

The similarity in the tritium-only boundary shown in Figure 2-17 and the early-time boundary in Figure 2-22 (year 2105) is the result of the relatively short tritium half-life. After the first couple of hundred years, the tritium has decayed away to nonradioactive helium. The boundary at later times, and the outer boundary defining the FFACO contaminant boundary at 1,000 years, is the result of longer-lived radionuclides. Pohll et al. (2003) identify carbon-14 (^{14}C) and iodine-129 (^{129}I) as contributors to the areal extent over the 1,000-year time frame.

2.3 Compliance Boundary

The objective of the CAI process is to define boundaries around each CAU to establish areas that contain water that may be unsafe for domestic and municipal use. These are the "contaminant boundaries" defined by the FFACO (1996). The FFACO corrective action strategy (Appendix VI; Rev. 1, 2000) requires the following to define the compliance boundary:

> "From the contaminant boundary predicted by the computer model, a compliance boundary will be negotiated between NDEP and DOE. The compliance boundary will define the area within which the radiological contaminants above the SDWA standards relative to background are to remain. DOE will be responsible for

ensuring compliance with this boundary. The compliance boundary may or may not coincide with the contaminant boundary. If the predicted location of the contaminant boundary cannot be accepted as the compliance boundary, an alternate compliance boundary will be negotiated by both parties."

Monitoring compliance with the CAU boundaries will be accomplished by measuring appropriate physical and chemical parameters in wells within the modeled region.

A CAU flow and contaminant transport model was used to estimate the Shoal contaminant boundary. The boundary is composed of a perimeter and lower boundary. The accepted contaminant boundary and other considerations formed the basis for the negotiated compliance boundary, as required per the dictionary for the UGTA process flow diagram in the FFACO. No spatial definition of the compliance boundary is provided in the FFACO, but the compliance boundary should have definition similar to that for the contaminant boundary. That is, the compliance boundary will be a defined perimeter and lower boundary. However, the compliance boundary provides the opportunity for consideration of factors not quantified in the calculation of the contaminant boundary.

As noted in Section 2.2.1, the contaminant boundary calculation is based on ambient conditions, without groundwater withdrawals in the area. Pumping to extract groundwater may impact the rate and direction of contaminant migration. Control of groundwater use in a larger region than that encompassed by the contaminant boundary is necessary to protect against potential human exposure.

The following factors were considered in the development of the compliance boundary at Shoal:

1. The SDWA regulations guiding the metric for the FFACO contaminant boundary.
2. Extraction of subsurface materials is restricted within a 3,300-ft radius of surface ground zero in the area of Shoal, for national security and public safety concerns (details of this restriction are given below).
3. There is no land buffer surrounding Shoal, such as is found for CAUs on the NTS, although there is currently a withdrawal for military use surrounding the site.

Future land use for the site and the surrounding area is expected to remain the same; however, the DoD will determine the future use of the surface area. Current restrictions on subsurface intrusion (drilling) around the Project Shoal Site ground zero, are listed in Public Land Order (PLO) 2771 and PLO 2834 as follows (*Federal Register*, 1962a; *Federal Register*, 1962b):

> "No excavation, drilling, and/or removal of materials is permitted between a level of plus 5,050 feet above mean sea level and plus 3,530 feet and out to a horizontal distance of 3,300 feet from this surface ground zero location (Nevada State Coordinates N 1,620,170 E 557,544) in sections 33 and 34, T16N, R32E, and sections 4 and 5, T15N, R23E, Churchill County, Nevada. Any reentry into drill holes or the shaft within this horizontal restricted area is prohibited."

Given the above, the compliance boundary for Shoal is defined as the outer perimeter of the regulatory-based boundary shown in Figure 2-23. The compliance region fits within the current exclusion zone maintained by the DOE, so that no additional restriction of groundwater resources results from the designation.

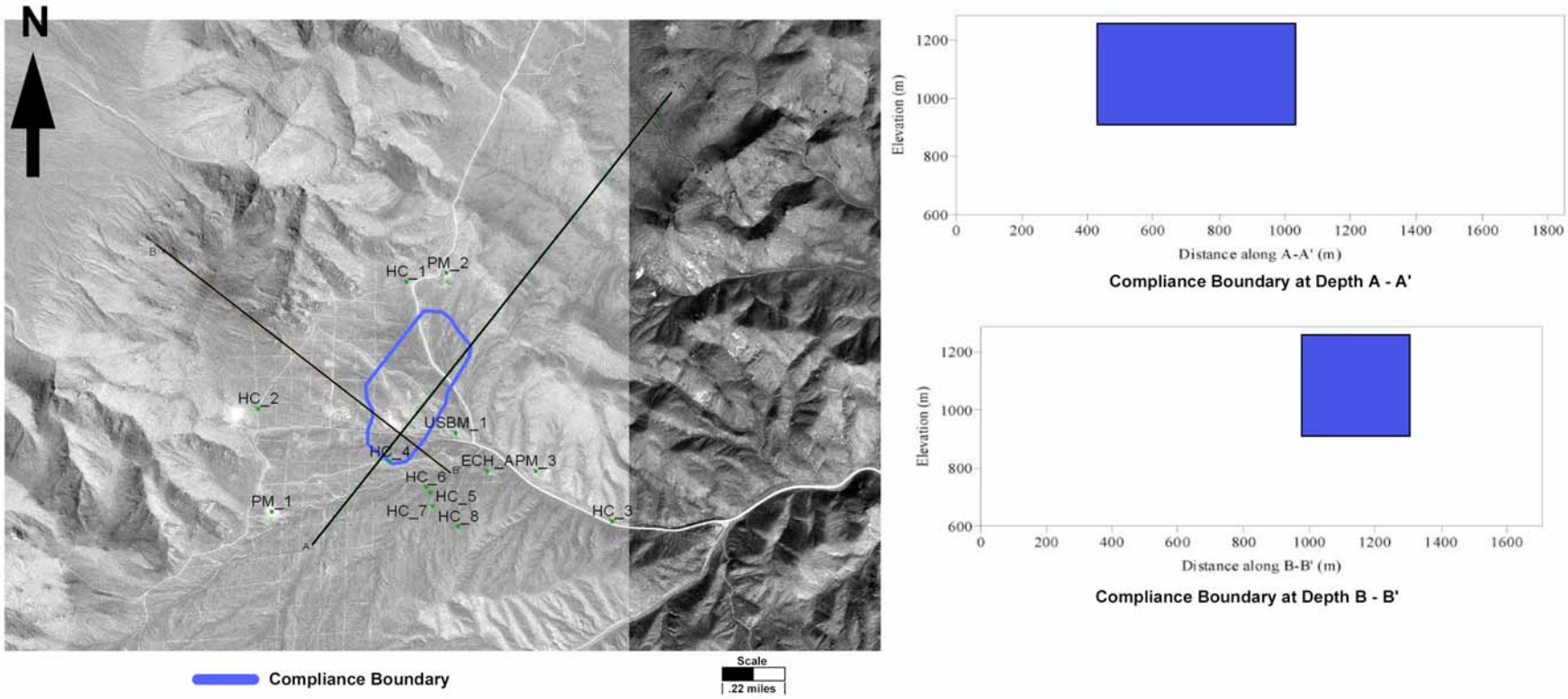

Figure 2-23
Compliance boundary

3.0 EVALUATION OF ALTERNATIVES

This section presents the corrective action objectives for CAU 447, describes the general standards and decision factors used to screen the corrective action alternatives, and develops and evaluates a set of corrective action alternatives that could be used to meet the corrective action objectives.

3.1 Corrective Action Objectives

The corrective action objectives are media-specific goals for protecting human health and the environment. Based on potential exposure pathways, the following corrective action objectives have been identified for CAU 447:

- Prevent or mitigate exposure to groundwater contaminants of concern at concentrations exceeding MCLs
- Reduce the risk to human health and the environment to the extent practicable

3.2 Screening Criteria

The corrective action alternatives are evaluated based on the approach outlined in *Focused Evaluation of Selected Remedial Alternatives for the Underground Test Area (*DOE/NV, 1998b). Although the site is not regulated under the *Comprehensive Environmental Response, Compensation, and Liability Act* (CERCLA), a CERCLA-style alternative (threshold criteria, primary balancing criteria, and modifying criteria) evaluation was performed. Each alternative is assessed against the following evaluation criteria developed to address the CERCLA requirements as mandated by the National Oil and Hazardous Substances Pollution Contingency Plan (40 CFR 300.430[e][9][CFR, 2003b]):

- Overall protection of human health and the environment
- Compliance with applicable or relevant and appropriate requirement(s) (ARARs)
- Long-term effectiveness and permanence
- Reduction of toxicity, mobility, or volume
- Short-term effectiveness
- Implementability
- Cost
- State acceptance
- Community acceptance

3.2.1 Evaluation Criteria

The following text describes the criteria used to evaluate the corrective action alternatives:

Overall Protection of Human Health and the Environment

Protection of human health and the environment is a threshold requirement under CERCLA (CFR, 2003b). This mandate requires that the corrective action include any protective measures that are needed to mitigate cancer risks and non-cancer toxicity. These measures may or may not be directly related to media cleanup, source control, or management of waste. The corrective action alternatives are evaluated for the ability to meet corrective action objectives as defined in Section 3.1.

Compliance with Applicable or Relevant and Appropriate Requirement(s) (ARARs)

Compliance with ARARs is a threshold requirement under CERCLA (CFR, 2003b). Each corrective action alternative must meet the proposed media cleanup standards as set forth in applicable state and federal regulations and as specified in the CAIPs (DOE/NV, 1996; DOE/NV 1998a).

Long-Term Effectiveness and Permanence

Long-term effectiveness and permanence is a primary balancing criterion under CERCLA (CFR, 2003b). Each corrective action alternative must be evaluated in terms of risk remaining at the CAU after the corrective action alternative has been implemented. The primary focus of this evaluation is on the extent and effectiveness of the controls that may be required to manage risk posed by treatment residuals and/or untreated waste.

Reduction of Toxicity, Mobility, and/or Volume (Through Treatment)

Reduction of toxicity, mobility, and/or volume is a primary balancing criterion under CERCLA (CFR, 2003b). Each corrective action alternative must be evaluated for its ability to reduce the toxicity, mobility, and/or volume of the contaminated media. Reduction in toxicity, mobility, and/or volume refers to changes in one or more characteristics of the contaminated media by the use of corrective measures that decrease the inherent threats associated with that media. In regards to certain radiogenic nuclides that are included as COPCs in subsurface rock and groundwater, natural radioactive decay is the only way that toxicity of these substances is reduced. However, removal of radiogenic nuclides from subsurface rock and/or groundwater remains an alternative to reduce toxicity of the contaminated media.

Short-Term Effectiveness

Short-term effectiveness is a primary balancing criterion under CERCLA (CFR, 2003b). Each corrective action alternative must be evaluated with respect to its effect on human health and the environment during implementation of the corrective action. The following factors will be addressed for each alternative:

- Protection of the community from potential risks associated with implementation such as fugitive dusts, transportation of hazardous materials, and explosion
- Protection of remediation workers during implementation
- Environmental impacts that may result from implementation
- The amount of time until the corrective action objectives are achieved

Implementability

Implementability is a primary balancing criterion under CERCLA (CFR, 2003b). Implementability addresses the technical and administrative feasibility of implementing a corrective action alternative and the availability of services and materials needed during implementation. Each corrective action alternative must be evaluated for the following criteria:

- **Construction and Operation -** refers to the feasibility of implementing a corrective action alternative given the existing set of waste and site-specific conditions.
- **Administrative Feasibility -** refers to the administrative activities needed to implement the corrective action alternative (e.g., permits, public acceptance, rights-of-way, off-site approval).
- **Availability of Services and Materials -** refers to the availability of adequate off-site and on-site treatment, storage capacity, disposal services, necessary technical services and materials, and prospective technologies for each corrective action alternative.

Cost

Cost is a primary balancing criterion under CERCLA (CFR, 2003b). Costs for each alternative are estimated for comparison purposes only. The cost estimate for each corrective action alternative includes both capital and operation and maintenance costs, as applicable.

The following is a brief description of each component:

- **Capital Costs -** include both direct and indirect costs. Direct costs may consist of materials, labor, mobilization, demobilization, site preparation, construction materials, equipment purchase and rental, sampling and analysis, waste disposal, and health and safety measures. Indirect costs include such items as engineering design, permits and/or fees, start-up costs, and any contingency allowances.

- **Operation and Maintenance -** include labor, training, sampling and analysis, maintenance materials, utilities, and health and safety measures.

State Acceptance

State acceptance is a modifying criterion under CERCLA (CFR, 2003b). Each corrective action alternative must be evaluated with respect to the potential for acceptance by NDEP. Such acceptance may be affected by prior agreements between DOE and state regulatory agencies concerning previous surface corrective actions, interim groundwater modeling results, contaminant flow and transport modeling results, or model validation results. State acceptance of the alternatives set forth here can more accurately be gauged subsequent to submission of this document.

Community Acceptance

Community acceptance is a modifying criterion under CERCLA (CFR, 2003b). However, the requirement for community acceptance as it applies to PSA is governed by the *National Environmental Policy Act* (NEPA), and was addressed to a certain extent by the NTS Environmental Impact Statement (EIS). Each corrective action must be evaluated with respect to community acceptance and community perception of potential risk. Community acceptance of alternatives could potentially rely on the quality of public outreach and public education efforts as much as on the intrinsic risks or benefits associated with each alternative. The NTS EIS addressed public comment and acceptance for environmental remediation activities, although that document did not address the massive excavation activities discussed in Table 3-1 as part of Alternative 3b. Community acceptance of such a massive reclamation project would require additional public comment and acceptance.

3.3 Development of Corrective Action Alternatives

This section identifies and briefly describes the viable corrective action alternative technologies and the corrective action alternatives considered for the affected media. Based on the review of

existing data, future use, and current operations at the PSA, the following alternatives have been developed for consideration at CAU 447:

- Alternative 1 – No Further Action
- Alternative 2 – Proof of Concept and Monitoring with Institutional Controls
- Alternative 3 – Contaminant Control

3.3.1 Alternative 1 - No Further Action (Without Institutional Controls)

Under the No Further Action alternative, no activities would be implemented and current institutional and land-use controls would be discontinued. This alternative is a baseline case with which to compare and assess the other corrective action alternatives and their ability to meet corrective action standards. The preliminary risk assessment (DOE/NV, 2000c) evaluates the potential threat to human health and the environment in the absence of any remedial action or degradation of the contaminant source. This alternative does not meet the corrective action objectives because it does not protect human health and the environment. Under the No Further Action alternative, people could be exposed to the COPCs at unacceptably high levels through intrusion into the subsurface environment or drilling of water supply wells. This alternative will be compared to the other alternatives using the selection decision factors for the CAU.

3.3.2 Alternative 2 – Proof-of-Concept and Monitoring with Institutional Controls

Under Alternative 2, a model-directed network of monitoring and validation wells would be installed in the vicinity of ground zero to monitor the CAU compliance boundary and to measure parameters necessary to determine that the model prepared in the CAIs (Section 2.0) makes reasonable predictions with an acceptable level of confidence.

The corrective action strategy relies on the groundwater flow and transport model of the Shoal site to determine the compliance boundary. A proof-of-concept period would be used as a post-audit of the model and would test the model over a five-year time frame. During this period, it would be determined if the model produces meaningful results with acceptable uncertainty. Periodic water sampling for radionuclides and water level measurements in the wells would confirm that contamination is not crossing the compliance boundary and that actual hydrologic conditions at the CAU have not evolved away from the conditions predicted by the model. Institutional controls would include restrictions on subsurface intrusion within the compliance boundary to protect the environment and the public from inadvertent release of contaminants.

3.3.3 Alternative 3 – Contaminant Control

As stated by Appendix VI (Rev. 1, 2000) of the FFACO (1996), the corrective action strategy for groundwater at the PSA will incorporate (on a limited scale) concepts being developed for the UGTA CAUs at NTS. Several alternatives for removing or controlling contaminant sources were analyzed for UGTA, and are presented in detail in the *Focused Evaluation of Selected Remedial Alternatives for the Underground Test Area* (DOE/NV, 1998b). These same alternatives could also be used for CAU 447 at PSA.

Therefore, as presented in the *Focused Evaluation of Selected Remedial Alternatives for the Underground Test Area* (DOE/NV, 1998b), the following two alternatives for contaminant source control that were analyzed for UGTA sites were considered for active remediation at PSA:

- 3a - Pump and treat (with institutional controls)
- 3b - Excavation and disposal

3.4 Evaluation of Alternatives

The evaluation criteria described in Section 3.2 were used to conduct detailed and comparative analyses of each corrective action alternative. The advantages and disadvantages of each alternative were assessed to select a preferred alternative for CAU 447. Table 3-1 summarizes the detailed analysis of the alternatives.

Table 3-1
Detailed evaluation of alternatives
(Page 1 of 5)

Evaluation Criteria	Alternative 1 No Further Action	Alternative 2 Proof of Concept and Monitoring with Institutional Controls	Alternative 3 Contaminant Control
Overall Protection of Human Health and the Environment	Does not meet corrective action objective of preventing or mitigating exposure to subsurface groundwater containing COPCs. Does not prevent exposure to contaminated groundwater. Does not prevent spread of COPCs in the groundwater. No worker exposure associated with implementation. Low risk to public due to remote location and controlled access to the subsurface and groundwater at the CAU.	Meets corrective action objectives. Prevents inadvertent intrusion into the contaminated zone. Prevents exposure to subsurface contamination. Prevents exposure to contaminated groundwater. Does not prevent spread of COPCs in the groundwater. Minimal risk to workers associated with contact with heavy equipment during well installation, and also with periodic maintenance of pumps. Low risk to public due to remote location and controlled access to the subsurface and groundwater at the CAU.	3a: Pump and treat (with institutional controls): Potentially meets corrective action objectives if appropriate technology is found to mitigate tritium and other contaminants in the groundwater. Prevents inadvertent intrusion into the contaminated zone. Prevents exposure to subsurface. Prevents exposure to contaminated groundwater. Workers potentially exposed to radioactive contaminants in treatment residues. 3b: Excavation and disposal: Potentially meets corrective action objectives, although significant surface impact likely would require additional corrective action. Prevents spread of COPCs. High potential for worker exposure associated with implementation.
Compliance with ARARs	Does not comply with ARARs because COPCs remain exposed to dissolution and migration in the groundwater, and pathways remain for human exposure.	COPCs remain exposed to dissolution and migration in the groundwater. However, compliance with ARARs is achieved because exposure pathways are eliminated through land-use restrictions.	3a: Complies with ARARs because potentially mobile COPCs are removed from the groundwater, and exposure to immobile COPCs in the subsurface environment is eliminated by land-use restrictions.

Table 3-1
Detailed evaluation of alternatives
(Page 2 of 5)

Evaluation Criteria	Alternative 1 No Further Action	Alternative 2 Proof of Concept and Monitoring with Institutional Controls	Alternative 3 Contaminant Control
Compliance with ARARs (Continued)			3b: Complies with ARARs by removing soil containing COPCs, but could create different pathways by creating dust contaminated with COPCs, and by relocating rock contaminated with COPCs from the subsurface to the surface, and increasing long-term stewardship responsibilities. Potential pathways to the accessible environment are not necessarily diminished by removing them from the deep subsurface environment.
Long-Term Effectiveness and Permanence	Long-term risk to public mitigated by slow contaminant migration rates. Potentially ineffective in isolating COPCs from the accessible environment due to lack of access controls, allowing potential inadvertent exposure to contaminated groundwater. Long-term effectiveness is enhanced with the passage of time as the most mobile COPCs manifest relatively short radioactive half-lives.	Long-term risk to public mitigated by slow contaminant migration rates. Institutional controls prevent inadvertent intrusion into, and exposure to remaining COPCs. Administrative controls must be maintained. Long-term effectiveness is enhanced with the passage of time as the most mobile COPCs manifest relatively short radioactive half-lives..	3a: Long-term risk to public eliminated by removal of mobile COPCs from groundwater and isolation of immobile COPCs by land-use restrictions. Long-term effectiveness is enhanced with the passage of time as the most mobile COPCs manifest relatively short radioactive half-lives. 3b: Moving contaminated bedrock from the subsurface environment to an appropriate on-site disposal facility compounds the problem of long-term isolation of long-lived radionuclides from the environment. The potential impact to surface environment from excavating the contaminated bedrock is enormous.

Table 3-1
Detailed evaluation of alternatives
(Page 3 of 5)

Evaluation Criteria	Alternative 1 No Further Action	Alternative 2 Proof of Concept and Monitoring with Institutional Controls	Alternative 3 Contaminant Control
Reduction of Toxicity, Mobility, or Volume	Reduction in toxicity by natural radioactive decay only. Reduction in mobility by sorption of naturally occurring minerals only. No known volume reduction. Mobility of COPCs is limited due to groundwater velocity and retardation processes and the resultant low migration rates. However, enhanced mobility due to inadvertent intrusion is not prevented.	Reduction in toxicity by natural radioactive decay only. Reduction in mobility by sorption of naturally occurring minerals only. No known volume reduction. However, the mobility of COPCs is limited due to groundwater velocity and retardation processes and the resultant low migration rates. Enhanced mobility due to inadvertent intrusion prevented by administrative controls.	3a: Reduction in toxicity by radioactive decay only. Reduction in mobility and volume achieved by removal of mobile COPCs from groundwater. 3b: Reduction in toxicity by radioactive decay only. Mobility reduction by removing COPCs from subsurface environment, but surface isolation compounded by the need for active long-term stewardship. Volume increase in contaminated rock upon excavation.
Short-Term Effectiveness	Effective in isolating COPCs from the accessible environment in the short term because of the remote location and low migration rate. Workers not exposed to radioactive contaminants.	Effective in isolating COPCs from the accessible environment in the short term because of low migration rate. Public protected by remote location, low migration rate, and site access controls. Workers not exposed to radioactive contaminants. Environmental impacts limited to a few drill pads that would have to be reclaimed.	3a: Effective in isolating COPCs from accessible environment by removing mobile COPCs from the groundwater, assuming that an effective way of treating tritiated water is employed during the initial 30 years of treatment.

Table 3-1
Detailed evaluation of alternatives
(Page 4 of 5)

Evaluation Criteria	Alternative 1 No Further Action	Alternative 2 Proof of Concept and Monitoring with Institutional Controls	Alternative 3 Contaminant Control
Short-Term Effectiveness (Continued)		Implementation would not require an extended period of time, but monitoring and institutional controls would be in effect for an extended period of time.	3b: Not effective in isolating COPCs from accessible environment in the short-term because COPCs are removed from inaccessible subsurface environment and moved to more accessible surface environment. High risk to workers associated with potential contact with impacted media during excavation activities as well as the physical hazards of open pit mining. Serious environmental impacts are anticipated due to implementation. Implementation would require an extended period of time. Short-term risks to the community would be high because of the dangers associated with dust control in excavating large volumes of contaminated rock and soil. Environmental impacts would be high.
Implementability	Easily implemented. Technical feasibility is high. Administrative feasibility is high. All of the services and materials are readily available.	Easily implemented. Coordination of all entities is necessary to ensure compliance with administrative controls to prevent intrusion into, and exposure to contaminated soil and groundwater. Technical feasibility is high. Administrative feasibility is high. All of the services and materials are readily available.	3a: Difficult to implement due to a number of deep extraction wells that need to be drilled, the treatment of tritiated water, and the handling of water and treatment residues after treatment. Technical feasibility is low and services are not readily available for the treatment of tritium in the water. 3b: Extremely difficult to implement due to the enormous volume of overburden to be removed, the large volume of contaminated bedrock to be excavated and isolated, the volume of contaminated groundwater to be pumped from the excavation and treated, and the long-term stewardship of the contaminated material. Technical feasibility is low and the availability of services is inadequate. Workers likely to be exposed to high radiation doses.

Table 3-1
Detailed evaluation of alternatives
(Page 5 of 5)

Evaluation Criteria	Alternative 1 No Further Action	Alternative 2 Proof of Concept and Monitoring with Institutional Controls	Alternative 3 Contaminant Control
Cost	$0	Estimated cost ranges from $1,500,000 to $5,000,000 for monitoring well installation, plus additional cost for long-term monitoring.	3a: Estimated cost ranges in the tens of millions of dollars if tritium is allowed to naturally decay in the groundwater. Cost likely to be in the hundreds of millions of dollars if tritium must be removed from the groundwater. 3b: Estimated cost ranges from many hundreds of millions of dollars to billions of dollars.
State Acceptance	State acceptance is unlikely and can be gauged better following submission of CADD/CAP	State acceptance is likely and can be gauged better following submission of CADD/CAP.	3a: State acceptance unknown but likely and can be gauged better following submission of CADD/CAP. 3b: State acceptance unknown, but unlikely because of the massive impact to the surface environment. Acceptance can be gauged better following submission of CADD/CAP
Community Acceptance	Community acceptance is unlikely, although acceptance would probably be related to the perceived community threat.	Community acceptance is likely, although acceptance would probably be related to perceived community safety.	3a: Community acceptance is likely because of the perceived public health safety in removing contaminated groundwater, and in the future lack of access restrictions for this parcel of public land. However, additional public involvement activities are likely necessary to support this option. 3b: Community acceptance is very unlikely because of the massive impact to the surface environment resulting from excavation of COPCs from a depth of 1,200 m.

4.0 RECOMMENDED ALTERNATIVE

Based on the results of the CAIs discussed in Section 2.0 and the detailed and comparative analysis of the potential corrective action alternatives presented in Section 3.0, the preferred corrective action alternative selected for implementation at CAU 447 is Alternative 2, Proof-of-Concept and Monitoring with Institutional Controls. This alternative (along with Alternative 3a) meets the requirement of Protection of Human Health and the Environment. Alternative 2 was superior to Alternative 3a in Implementability and Cost. The rationale for selecting Alternative 2 is described below:

- Health risks are minimized by preventing worker exposure and public access to the contaminated groundwater by administrative controls.
- Only minimal waste from drilling and sampling will be generated. If groundwater in the monitoring wells is not contaminated, almost all of these wastes will be neither hazardous nor radioactive.
- It is easily implemented, although coordination of all entities is necessary to ensure compliance with administrative controls. The required services and materials are readily available.
- It provides a cost-effective method to achieve protection of human health and the environment and to meet closure requirements.

4.1 Proof-of-Concept

The proof-of-concept approach relies on the groundwater flow and transport model of the nuclear test at PSA. The model was developed to predict groundwater flow in the granite aquifer in the vicinity of the nuclear test, and radionuclide transport by groundwater away from the test cavity. Numerical flow and transport models are effective tools for predicting migration of contaminants through the subsurface, where lithologic and hydrologic data are sparse relative to the natural heterogeneity of the systems. The variability in hydrologic characteristics can be simulated through numerous model runs. These results define a range of predicted values for the variables that control the fate and transport of contaminants in the groundwater, and provide statistically testable results for contaminant plume migration. Model validation entails placing wells at locations within the modeled volume at PSA and confirming the distribution of hydraulic conductivity values, hydraulic head, fracture size and frequency, and contaminant transport predictions.

4.2 Monitoring

Monitoring wells will be placed downgradient from the test cavity to monitor the compliance boundary. The distance between the monitoring wells and the compliance boundary considers the need to provide adequate early warning to allow time for reaction in the event of unanticipated contaminant migration. Periodic water sampling and testing of the monitoring wells will confirm that contamination is confined to within the compliance boundary.

4.3 Institutional Controls

The DOE has a land withdrawal for PSA. This withdrawal is within a much larger area that is withdrawn by the U.S. Navy. Under both the DOE and military land withdrawal criteria, this land has been withdrawn from all forms of appropriation under the public land laws. The DOE will maintain the existing land withdrawal and establish use restrictions using the FFACO process. The Navy withdrawal should help maintain government oversight and control of the subsurface resources at PSA, although it does not currently prevent public access to the site.

Future land use for the site and the surrounding area is expected to remain the same; however, the DoD will determine the future use of the surface area. Current restrictions on subsurface intrusion (drilling) around the Project Shoal Site ground zero, are listed in PLO 2771 and PLO 2834 as follows (*Federal Register*, 1962a; *Federal Register*, 1962b):

> "No excavation, drilling, and/or removal of materials is permitted between a level of plus 5,050 feet above mean sea level and plus 3,530 feet and out to a horizontal distance of 3,300 feet from this surface ground zero location (Nevada State Coordinates N 1,620,170 E 557,544) in sections 33 and 34, T16N, R32E, and sections 4 and 5, T15N, R23E, Churchill County, Nevada. Any reentry into drill holes or the shaft within this horizontal restricted area is prohibited."

5.0 IMPLEMENTATION OF THE CORRECTIVE ACTION PLAN

The preferred corrective action alternative for the Shoal site is to leave the Shoal test cavity in place, monitor groundwater conditions, and control activities impacting the subsurface in the area through long-term stewardship (including use restrictions). The strategy for the Shoal monitoring network is presented in the following sections. The framework for forming the post closure stewardship activities is presented in Section 7.0.

With a large radionuclide source being left in place, and given the uncertainties inherent in modeling the behavior of groundwater systems, monitoring of the Shoal site is an important component of ensuring the effectiveness of the corrective action. Monitoring can be viewed as the final step in addressing the uncertainty present in the Shoal closure. Groundwater monitoring not only builds confidence that the system is performing as predicted, it acknowledges the uncertainties inherent in the modeling process and the possibility, however remote, of unexpected outcomes.

Monitoring of groundwater conditions is one of two major actions recommended in this alternative. The second action is long-term site stewardship. The need for effective stewardship of the site is dictated by the dynamic groundwater system containing the contaminants. The contaminant boundary calculated to preserve public health and the environment is based on current hydrologic conditions. The extent of harmful contaminants migrating from the Shoal test could be dramatically changed by certain resource extraction activities, principally large-scale groundwater pumping. As a result, effective controls on activities involving the subsurface will be needed in the region outside the contaminant boundary. Stewardship of the site will also entail evaluating natural changes in the hydrologic system that could affect the closure decision, and protecting the national security aspects of the site from willful or inadvertent intrusion.

5.1 Monitoring Objectives

The objectives of groundwater quality monitoring are generally divided into four categories: (1) ambient monitoring; (2) detection monitoring; (3) compliance monitoring; and (4) research monitoring (Todd et al., 1976). Long-term monitoring for PSA combines the second and third objectives. Detection monitoring provides early indication of the migration of radionuclides from the test cavity to the downgradient direction. At the same time, these data also fall under the requirement for compliance monitoring in the FFACO.

Appendix VI (Rev. 1, 2000) of the FFACO (1996) specifies a five-year proof of concept monitoring network during the corrective action phase. “This phase of monitoring will use groundwater wells in a monitoring network to determine if the monitoring network design will

provide adequate CAU surveillance. Measurements of field parameters will be used to demonstrate that the model is capable of making reasonable predictions that fall within an acceptable level of confidence" (FFACO, 1996). Using the results of the proof-of-concept monitoring and model validation, the long-term monitoring requirements for the CAU are developed in the Closure Report (FFACO, 1996).

The objectives of the PSA proof-of-concept monitoring network are to: (1) provide a means to evaluate the groundwater transport model and its predictions through the validation process; (2) provide a system with high detection probability that takes into account uncertainty in the migration pathways; (3) provide a system for early detection of radionuclide migration rates in excess of what has been predicted by the model; (4) assure the public and the regulators that public health is not compromised; (5) provide compliance monitoring of physical parameters to demonstrate that groundwater conditions have not significantly changed from those simulated in the model; (6) achieve site closure and minimize long-term risk of public exposure to contaminated groundwater; and (7) achieve all of these objectives while providing the best value to the taxpayers.

The validation process is necessary for developing an effective detection monitoring system. The detection system is based on the model results. Validation of the model, and reduction of uncertainty in the model predictions in the process, is a priority for detection monitoring. In addition, validation also meets FFACO requirements regarding proof-of-concept monitoring. Details regarding the proposed validation process are given in Section 5.5.

When a monitoring program has multiple objectives, it is possible the objectives can be conflicting. For example, objectives such as low cost, high detection probability, and early detection can be conflicting. These objectives conflict because an increase in the detection probability is accomplished by either installing more wells (increasing cost) or by placing the wells further from the source, thereby increasing time to detection (Storck et al., 1997). Because of this conflict, one optimal solution does not exist, and the trade-offs among these objectives must be considered.

5.2 Monitoring Network

The proposed monitoring program is comprised of the physical network and the operations conducted with that network. The design of the network of wells is first described. Then the operational aspects of the monitoring frequency, analytes and parameters, reporting requirements, and evaluation and evolution of the network through time are presented.

5.2.0 Network Design

Approaches used to design detection-based compliance monitoring systems can be classified as statistical simulation or qualitative. Statistical simulation approaches use transport models to simulate the evolution of contaminants in groundwater (e.g., Massmann and Freeze, 1987; Meyer and Brill, 1988; Ahlfeld and Pinder, 1988; Meyer et al., 1989). Each contaminant distribution is obtained from realizations of flow and transport parameters that are drawn from assumed statistical distributions. The results are used with an optimization model, which determines a monitoring well configuration from a distribution of candidate monitoring sites. The procedure is computationally intensive because groundwater flow and transport models must be used to generate hundreds of contaminant distributions. Qualitative approaches are based on judgments made without the use of quantitative mathematical methods (Everett, 1980; Loaiciga et al., 1992). Sampling locations are determined by the hydrogeologic conditions near the source of contamination. As indicated by Hudak (1994), *Resource Conservation and Recovery Act* (RCRA) guidelines for groundwater monitoring (EPA, 1986) use qualitative means to specify the placement of downgradient monitoring wells. Relative to statistical simulation methods, qualitative approaches are easy to implement for field applications; however, they are highly subjective and are not well defined.

Development of the Shoal monitoring network relies on statistical simulation approaches. Three statistical tools using the PSA model simulations are used to locate monitoring wells around the site. Using results from several design approaches builds confidence that selected locations are optimal. The purpose is to place wells such that they will identify groundwater contamination before a plume traverses a regulatory boundary. The first tool identifies and analyzes siting horizons for potential monitoring wells and determines the number of wells needed to span each horizon. The second tool uses a simulation-probablistic approach to analyze the success probability of individual well locations on the siting horizons. The third tool also analyzes the detection efficiency of individual well locations as well as combinations of the wells, using a monitoring efficiency model.

Details of each approach and its application are presented in Hassan (2005). Summaries of each application and findings are presented below, followed by the recommended network design.

5.2.0.1 Monitoring Design Tool #1

The first tool is applied to select a number of potential siting horizons to which monitoring wells could be allocated. Hudak (1994) developed an approach for designing detection-based compliance groundwater quality monitoring networks that integrates numerical simulation of

contaminant transport and mathematical programming. His approach is adapted and applied to Shoal as the first tool for selecting the number and location of detection monitoring wells. Based on plume geometry, this tool is used to determine the efficiency of each siting horizon and the minimum number of wells needed to span each horizon for detection monitoring.

Hudak (1994) considers the hypothetical problem layout depicted in Figure 5-1. The objective is to detect groundwater contamination emanating from a contaminant source before it migrates to a boundary of concern. A plume can be detected by one or more monitoring wells located along various siting horizons (or control planes as employed here) oriented perpendicular to the main direction of groundwater flow. In effect, each horizon offers a potential line of defense against plume migration to a boundary (Hudak, 1994). For the purpose of detection monitoring, the perpendicular orientation of siting horizons (relative to the prevailing direction of groundwater flow) is more effective than an oblique configuration.

In the context of detection monitoring networks for waste disposal facilities such as landfills, Hudak (1994) defines the parameters in Figure 5-1 as follows. A plume originating at the downgradient corner of the landfill defines a maximum well spacing, S_i, for each siting horizon, i. If a horizon is used as a line of defense against contaminant migration to the compliance boundary, the spacing between adjacent wells should not exceed S_i. Hudak's (1994) analysis considered a deterministic problem where the geometry of the zone of potential contaminant migration is defined by simulating the migration of plumes originating from various points along the perimeter of the landfill. The width of this zone, W_i, is defined by the intersection of the siting horizon and this migration zone as shown in Figure 5-1. Different siting horizons can thus be ranked for detection efficiency by evaluating, for each horizon i, the ratio of the maximum well spacing, S_i, to the width of the potential zone of contaminant migration, W_i. A high S_i/W_i value indicates an effective horizon because the migration zone can be traversed with fewer wells (Hudak, 1994).

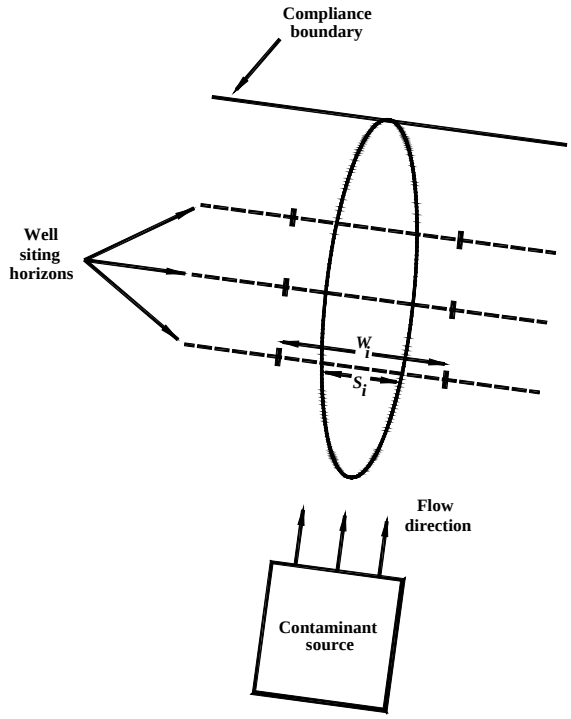

Note: Schematic diagram, modified from Hudak, 1994

Figure 5-1
Conceptualization of the contamination source, plume migration, and siting horizons for locating monitoring wells

The approach discussed above was developed and applied to fairly simplistic and deterministic problems (e.g., Hudak, 1994, 1996, 2001). Here it is extended to the stochastic Shoal model with some modifications. The maximum well spacing, S_i, in the deterministic case is determined by the plume width in such a way that the plume cannot migrate between two wells without being detected. This can be replaced by the mean, mode, or another representative statistical quantity derived from the distribution of the width of the stochastic plumes simulated at Shoal. The quantity needed for analysis of deterministic problems is the maximum plume width when the plume crosses a particular CP. For the stochastic Shoal model, this quantity is obtained for each realization and then the average of these plume widths are obtained and used to determine maximum well spacing. For the deterministic problem, the actual plume width (in the field) may be larger or smaller than what is used in the analysis. Thus there is a 50 percent probability that the selected plume width in the monitoring design is smaller than the actual plume, and thus there is a 50 percent chance that the resulting well spacing is less than the actual plume width. To be consistent with these probabilities, the mean plume width of the stochastic model was chosen, which would mean that the resulting well spacing has a 50 percent probability to be less than the plume width (because the selected plume width is less than the plume width in

50 percent of the realizations). The other quantity, W_i, can be obtained for each siting horizon by, for example, computing the distance between the center of mass (c.o.m.) of the two plumes that are farthest apart. This distance represents the width of the zone of potential plume migration at the particular siting horizon.

Given values for S_i and W_i, the minimum number of monitoring wells, N_i, needed to span a horizon to ensure a well spacing that is equal to or less than S_i is given as (Hudak, 1994)

$$N_i = \lceil (W_i - 2S_i)/S_i \rceil + 1 \qquad (5\text{-}1)$$

where $\lceil \ \rceil$ is the ceiling function that yields the least integer that is greater than or equal to the quantity it operates on. Details of the derivation of Equation (5-1) can be found in Hudak (1994).

Five siting horizons, or control planes (CPs) were selected for analysis. The CPs are oriented perpendicular to the mean flow direction because this is more effective than an oblique configuration (Hudak, 1994). This is not parallel to any of the Shoal model axes, so a rotated coordinate system (*x'*,*y'*) is used in the monitoring well analyses. The locations of the CPs along the mean flow direction were selected to evaluate monitoring along the compliance boundary and at interior distances that would provide a reaction time of 50 years before the compliance boundary is reached. It is assumed that a reaction time of 50 years is sufficient to take an action in case a monitoring well detects contaminants approaching the compliance boundary. The average velocity of the c.o.m. of particles tracked by the Shoal transport model, computed at hundred-year increments throughout 1,000 years, was used to determine the distance that would provide a reaction time of 50 years. The highest velocity (97.5th percentile, occurring at 400 years) is about 0.00321 m/day, requiring a traveling distance of about 60 m to provide a 50-year reaction window.

The selected CPs are shown in Figure 5-2. Due to the irregular shape of the compliance boundary and the uncertainty in plume trajectory, the CPs are located relative to three different points on the downgradient edge of the boundary: the farthest (central) downgradient point, the farthest downgradient point on the western edge, and the farthest downgradient point on the eastern edge. CP #5 passes through the farthest western point, and CP #2 passes through the farthest eastern point. No plane is placed at the farthest central point because the line would pass entirely outside the compliance boundary. By taking a 50-year reaction time from CP #2, CP #5, and the farthest central point, a safeguard is provided against contaminants crossing the

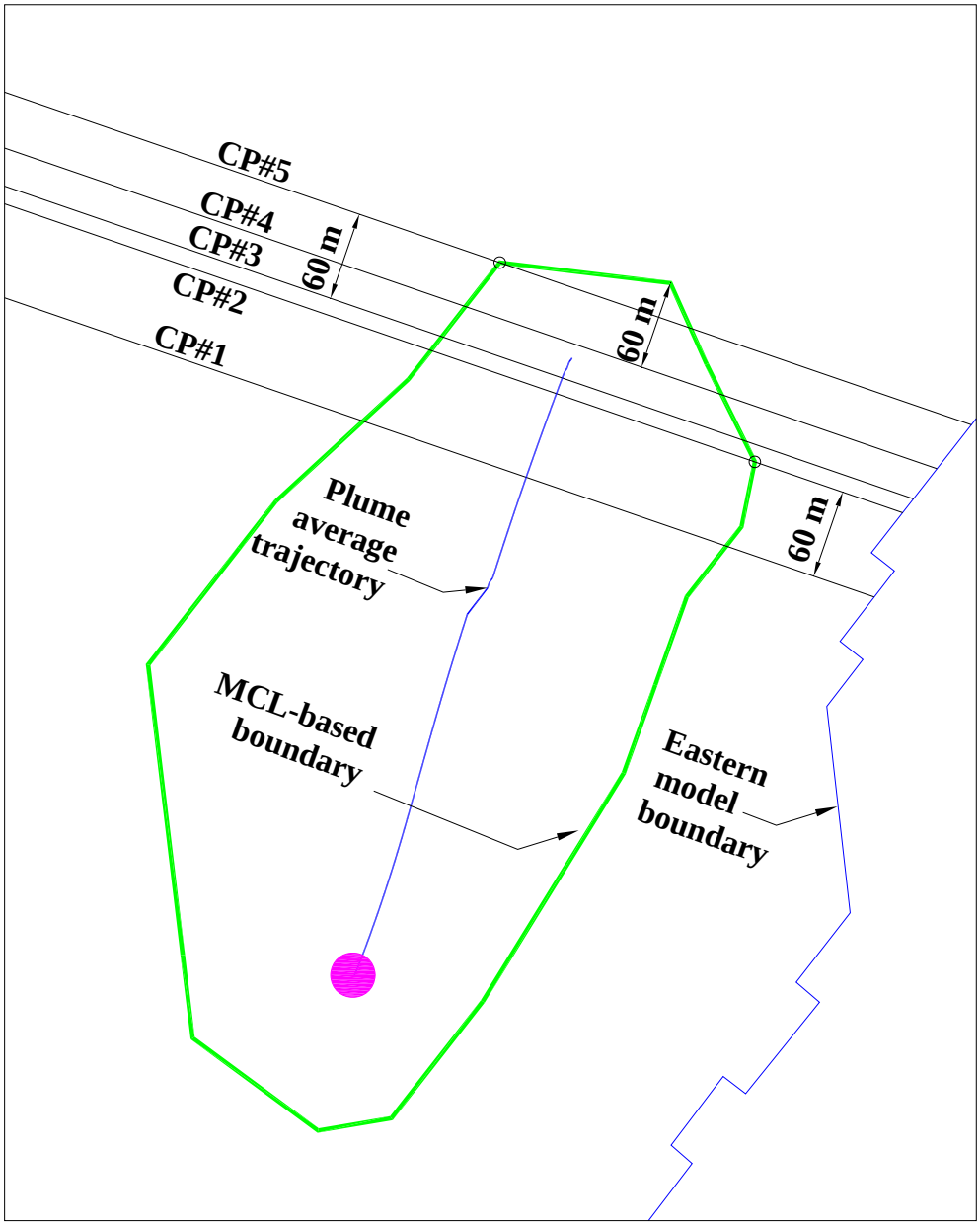

Note: See text for discussion of the plane locations

Figure 5-2
Selection of control plane locations and orientation normal to the mean flow direction

compliance boundary along the mean flow direction and from either side of the mean trajectory as bounded by the northwestern and northeastern points on the boundary. These "reaction time" planes are provided by CP#3 (60-m upgradient of CP#5), CP#4 (60-m upgradient of the farthest central point), and CP#1 (60-m upgradient of CP #2).

Transport analysis for the selected CPs is performed using the simulation layout shown schematically in Figure 5-3. This figure shows a 3-D view of the simulation domain, the cavity location and five CPs located as described above. The figure also shows a zoom-in view showing the source and the five CPs, with the *y'*-axis scale exaggerated to clearly show the five CPs. A plan view is also presented to show the numbering sequence of the CPs, which will help in tying the results to this schematic picture.

The transport calculations are conducted using the RWPT method and employing the same grid discretization and domain size as the groundwater flow model (Pohlmann et al., 2004). A large number of particles is used to represent the radionuclide source. These particles are tracked in the space-time domain for the regulatory time frame of 1,000 years. Matrix diffusion and radioactive decay are ignored in these calculations because it is plume location, not contaminant concentrations, that is of interest for locating the monitoring wells. At every time step and for each CP, the dimensions of the plume as it crosses a particular CP are obtained and recorded. This output is subsequently analyzed at 100, 200, 500, and 1,000 years after detonation.

Histograms displaying the distributions of plume width, height, horizontal location, and vertical location, for the different control planes and for all 1,000 model realizations are presented in Hassan (2005). Also shown, in tables, are the prediction quantiles for the plume width and c.o.m. for different control planes. The histograms and tables show that the c.o.m. in many realizations is around x=1,200 m from the domain origin with some skewness in the distribution of x toward smaller values (closer to the domain origin). In the z direction, the plume c.o.m. is skewed toward lower elevations with a maximum of about 1,200 m, coinciding with the bottom edge of the cavity.

The average plume width of plumes traveling at least as far as the CPs, barely exceeded 400 m at 1,000 years. At 100 years, the plume width is about 120 m on average. The parameter S_i is obtained for each CP using the plume width statistics for that plane. The zone of potential contaminant migration, W_i, is obtained for each CP by analyzing the distribution of the *x'*-coordinate of the plume c.o.m. as it crosses the given plane.

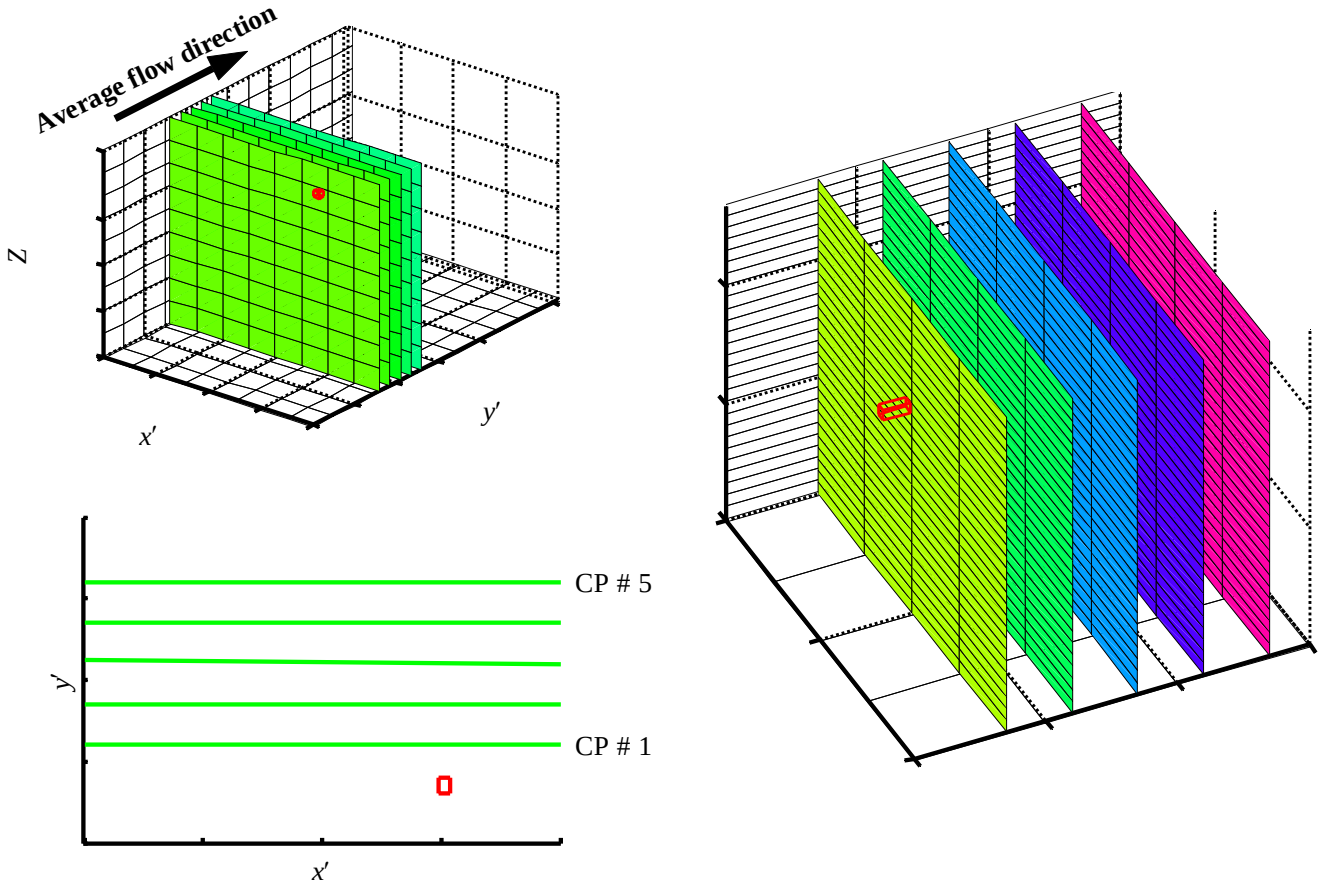

Note: The top shows a schematic 3-D view, while the right presents a zoom-in view of the cavity and CPs (exaggerated scale in the y'- direction to allow distinction between control planes). A 2-D plan view showing the location of the five CPs relative to the cavity is on the bottom left.

Figure 5-3
The model domain, the cavity, and the five CPs

After determining the two parameters S_i and W_i for all CPs, the CP detection efficiency, S_i/W_i is determined and Equation (1) is used to obtain the minimum number of wells needed for each CP. Table 5-1 shows the values of S_i, W_i, S_i/W_i, and N_i for each CP and all times considered. In general, CP #5 tends to have the lowest efficiency (smallest S_i/W_i ratio) and CP #1 tends to have the highest efficiency, but this is not consistent through time and the efficiencies of the various CPs are often very similar. From Table 5-1, it seems that CP #1 is slightly favored, though wells on the other CPs (particularly CP #2 and #4) offer similar efficiency.

Table 5-1
Parameters of Equation. (1), the resulting CP efficiency (Si/Wi), and the minimum number of wells, N_i, to span each CP at different times

S_i, W_i, siting horizon efficiency (S_i / W_i), and N_i for the five CPs and the different times																
Control	t = 100 years				t = 200 years				t = 500 years				t = 1,000 years			
Plane	S_i	W_i	S_i/W_i	N_i	S_i	W_i	S_i/W_i	N_i	S_i	W_i	S_i/W_i	N_i	S_i	W_i	S_i/W_i	N_i
CP #1	114.5	379.1	0.30	3	174.2	440.8	0.40	2	288.8	446.4	0.65	1	402.0	514.8	0.78	1
CP #2	137.8	403.9	0.34	2	172.3	470.1	0.37	2	287.7	488.4	0.59	1	400.8	514.3	0.78	1
CP #3	127.9	412.6	0.31	3	165.5	482.4	0.34	2	293.5	500.6	0.59	1	402.4	511.1	0.79	1
CP #4	129.5	420.5	0.31	3	178.2	483.2	0.37	2	290.4	499.9	0.58	1	408.2	504.9	0.81	1
CP #5	104.5	494.0	0.21	4	179.0	494.8	0.36	2	287.1	527.5	0.54	1	406.9	547.7	0.74	1

It can also be seen from Table 5-1 that the required number of wells is generally between one and two. Only at t = 100 years does the analysis suggest a need for 3 or 4 wells, and this is a result of very narrow plumes (e.g., few fast particles) reaching control planes and leading to a small S_i value and in turn a large number N_i of required wells. Based on these results, it is reasonable to assume that two wells at any single siting horizon or control plane will have a high likelihood chance of detecting the plume migration if it reaches that particular CP. Therefore, in all subsequent analysis, it is assumed that the monitoring network at Shoal will not have more than two wells along any single siting horizon or CP.

5.2.0.2 Monitoring Design Tool #2

The second set of analyses performed for designing the long-term monitoring network at Shoal relies on the simulation approach (using the existing Shoal model) combined with hydrogeologic expertise and probabilistic design methodology to analyze the success probability of individual well locations on the siting horizons. Details of the simulation-probabilistic approach are presented in Hassan (2003b) along with a detailed description of the application to Shoal in Hassan (2005).

For illustration purposes, the problem of the monitoring network design (selection of the well locations for the first stage) was hypothesized as shown in Figure 5-4. The radionuclide plume emanating from the source migrates to the north and one would normally place the monitoring

wells to intercept the plume. The distance along the flow direction between the working point (center of the cavity) and the CP passing through each monitoring well is denoted as x_k. Massmann and Freeze (1987) and Meyer and Brill (1988) consider the failure of a monitoring network to occur when the monitoring network does not detect the contaminant before it reaches a compliance boundary. In fact, the probability of failure in year t, $P_f(t)$, is simply the probability that the time until breach of the containment plus the travel time of the plume through the hydrogeological environment lies within year t (Massmann and Freeze, 1987). If these components of failure are independent, Massmann and Freeze (1987) write

$$P_f(t) = \sum_{t^l=0}^{t-t_{op}} \left\{ P(t' = t^l)\, P(t'' = t - t_{op} - t^l) \right\} \tag{5-2}$$

where t is the time for which the calculations are carried out (year), t_{op} is the time at which the facility is put into operation (year), t' is the time until containment is breached (year), and t'' is the time of travel for the contaminant plume to migrate from the containment structure to the compliance surface (year). Massmann and Freeze (1987) define the probability in Equation (5-2) as the failure probability of the unmonitored facility. For the monitored facility, they define the failure probability as

$$P_f^m(t) = P_f(t)\,(1 - P_d) \tag{5-3}$$

where $P_f^m(t)$ is the failure probability of the monitored facility at year t (*i.e.*, the probability that containment is breached and contaminants travel through the system to the compliance boundary within year t without detection), and P_d is the probability of detection by the monitoring network.

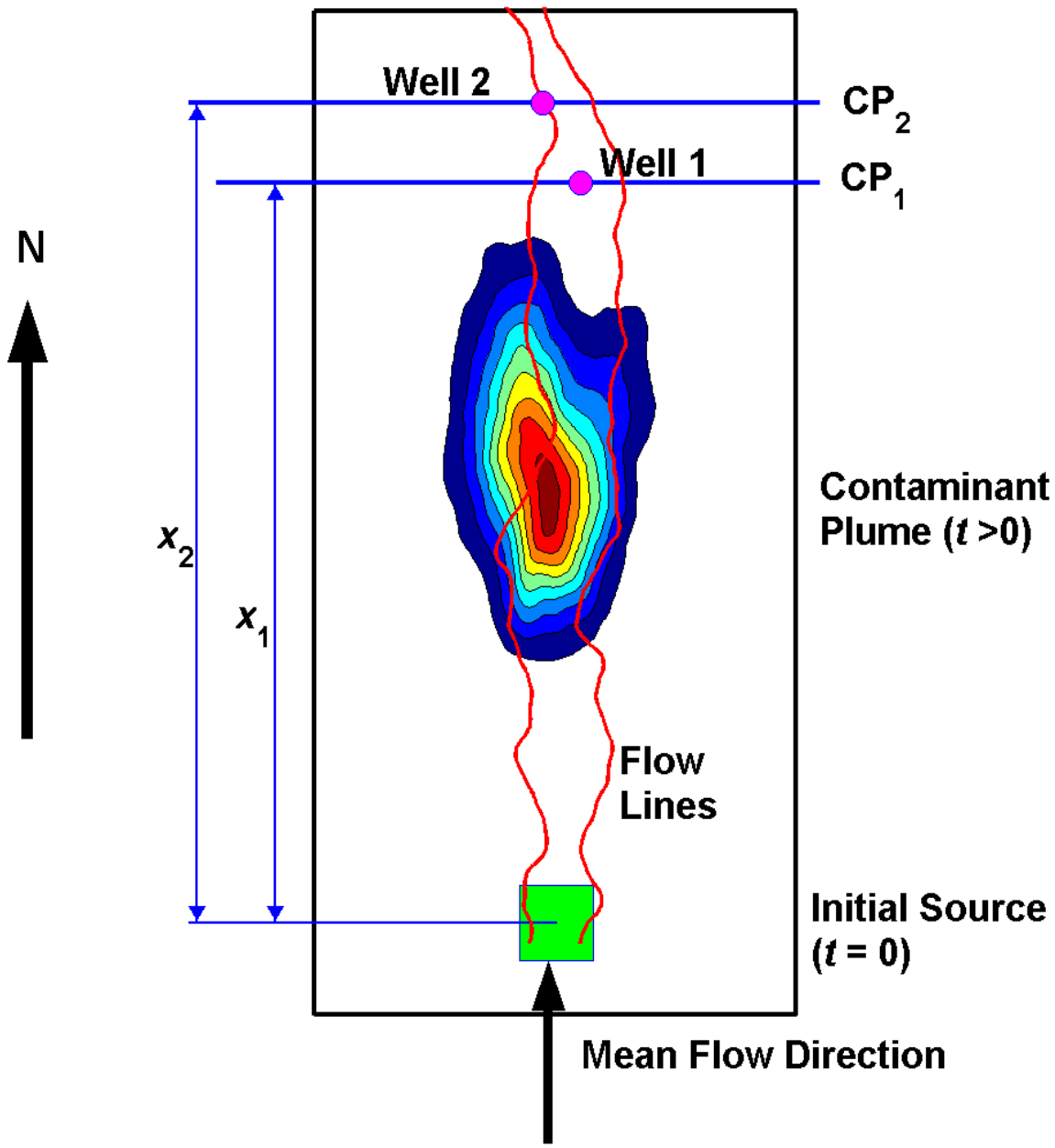

Figure 5-4
Schematic diagram showing the location of contaminant plume, monitoring wells, and the distances and definitions used in Equations (5-2) through (5-4)

For the Shoal case, one can assume that a monitoring well fails if 1) an arbitrary percentage (e.g., 20 percent) of the plume mass crosses the CP normal to the mean flow direction and passing through the well, and 2) the well does not detect the presence of contaminants. Because these two events are independent of one another, one can define the probability of failure in year t for a monitoring well located at $\mathbf{x}_j = (x_j, y_j, z_j)$, as

$$P_f(t; \mathbf{x}_{jk}) = P\left(\frac{1}{M_{total}}\int_0^t Q(\tau; x_k)\, d\tau \geq \alpha\right)\left(1 - P_{dj}\right) \tag{5-4}$$

where $P_f(t; \mathbf{x}_{jk})$ is probability that the well located at $\mathbf{x}_j$ will not detect the plume when α percent of its mass crosses the CP located at distance x_k from the center of the source along the mean flow direction (to the northeast for the Shoal model) in a time frame less than or equal to t years, $\int_0^t Q(\tau; x_k)\, d\tau$ is the cumulative mass arrival to the CP located at x_k, M_{total} is the total mass of contaminant available in the aqueous phase, and P_{dj} is the probability of detection by the monitoring well located at $\mathbf{x}_j$. For example, if the schematic plume shown in Figure 5-4 splits along the two flowpaths shown, Well 1 may not detect the plume, giving a false negative. This will give a zero value for P_{d1}, which in turn leads to a high failure probability as shown from Equation (5-4). Analogously, define

$$P_s(t; \mathbf{x}_{jk}) = P\left(\frac{1}{M_{total}}\int_0^t Q(\tau; x_k)\, d\tau \leq \alpha\right) P_{dj} \tag{5-5}$$

where $P_s(t; \mathbf{x}_{jk})$ is the success probability, that is, the probability that the monitoring well will detect the plume in year t if α percent of its total mass or less arrives at the CP of the monitoring well by year t. It can be seen that for individual wells, the time-dependent probability of failure and probability of success are zero at early times and then they both start to increase when the plume reaches the CP where the well is located. If a certain percentage of the plume mass crosses the CP before the monitoring well detects any contaminants, P_{dj} is zero and the success probability is zero. If the well detects contaminants before α percent of the mass crosses the CP, then P_{dj} is 1.0 and the failure probability becomes zero. This binary decision point provides a tangible measure of success, which can be expanded to multiple wells.

The value of P_{dj} can be determined from the plume migration analysis. A plume will be detected by a monitoring system only if the groundwater flow lines passing through the cavity also pass through the monitoring well (Massmann and Freeze, 1987a). Plume intersection along the well

sampling interval will lead to contaminant detection. This probability of detection by a monitoring well can be determined from Monte Carlo simulations used to predict plume migration. The detection occurs when particles representing the contaminant mass (using a particle tracking approach for modeling the transport processes) pass through any of the vertical cells where the well is located. However, to account for the temporal aspect, to overcome the issue of the classified initial source mass, and to allow for comparing different well locations, the area of the *t-z* distribution of the normalized masses (particle masses) for a monitoring well is used as an indicator of the likelihood of detection. Thus the detection probability for a monitoring well *j* can be obtained using Monte Carlo simulation as

$$P_{dj} = \sum_{i=1}^{NMC} \frac{W_{ji}}{NMC} \tag{5-6}$$

where *NMC* is the number of Monte Carlo realizations used in the analysis and W_{ji} can be obtained as

$$W_{ji} = \int_0^t \int_{z=z_b}^{z=z_t} M_{ji}(\tau, z)\, dz\, d\tau \tag{5-7}$$

$M_{ji}(\tau, z)$ is the resident mass in the monitoring well cell located at elevation *z* and time τ, z_b is the bottom elevation of the lowest cell that can be sampled by the well, and z_t is the top elevation of the uppermost cell that can be sampled.

The implementation of the above analysis is done through the following steps. The first step is to identify the possible candidate locations, *J*, for the monitoring wells. The exact location will be determined with this analysis where the different candidate locations of different wells are compared and the optimal location with highest success probability (lowest failure probability) is chosen. The second step is to select a time frame for the analysis, which is represented by the simulation time scale, *T*, and the time, *t*, at which probabilities are to be obtained.

The third step is to run Monte Carlo simulations and record for each realization the *t-z* distribution of the resident mass ($M_{ji}(\tau, z)$ in Equation (5-7)) within the cells occupied by each monitoring well. The integration of this mass distribution gives W_{ji} for each realization $i = 1$ to *NMC* and each well *j*. The fourth step is to compute for each candidate well location the probability that α percent of the total plume mass crosses the CP, *k*, passing through that location in time *t* or less. This can simply be obtained by integrating the total mass flux breakthrough curve for each CP ($k = 1, \ldots K$ with $K \leq J$) from time zero to time *t*. The fifth step is to use

Equation (5-5) to compute the success probability for each candidate well location (due to the computational burden, only a finite number of candidate locations will be evaluated). The locations with the highest success probability will then be selected as potential well locations.

Fifteen candidate locations are selected along the five CPs (CP #1 through CP #5) with three potential well locations assigned to each CP. The central well coincides with the average plume trajectory. The edge wells are located such that they enclose 50 percent of the plume trajectories at each CP. The locations of these edge wells are determined from the analysis of histograms of the plume c.o.m. position, x', as it crosses each CP. The locations of the resulting 15 wells are shown in Figure 5-5. These 15 wells in addition to HC-1 and HC-4 will be analyzed as potential monitoring wells for the purpose of selecting a three-well network with high detection efficiency (using Design Tool #3).

One additional three-well network will be analyzed and compared to the results of the individual networks formed from the 17 wells mentioned above. This network is obtained by drawing a new boundary inside the MCL-based contaminant boundary at a perpendicular distance (an offset) of about 60 m (i.e., equivalent to a 50-year reaction time) and locating three wells at the eastern, northeastern, and western edges of this new boundary. These wells are denoted as NW1, NW2, and NW3. The numbers assigned to each well are shown on Figure 5-6, with the three NW wells in red circles.

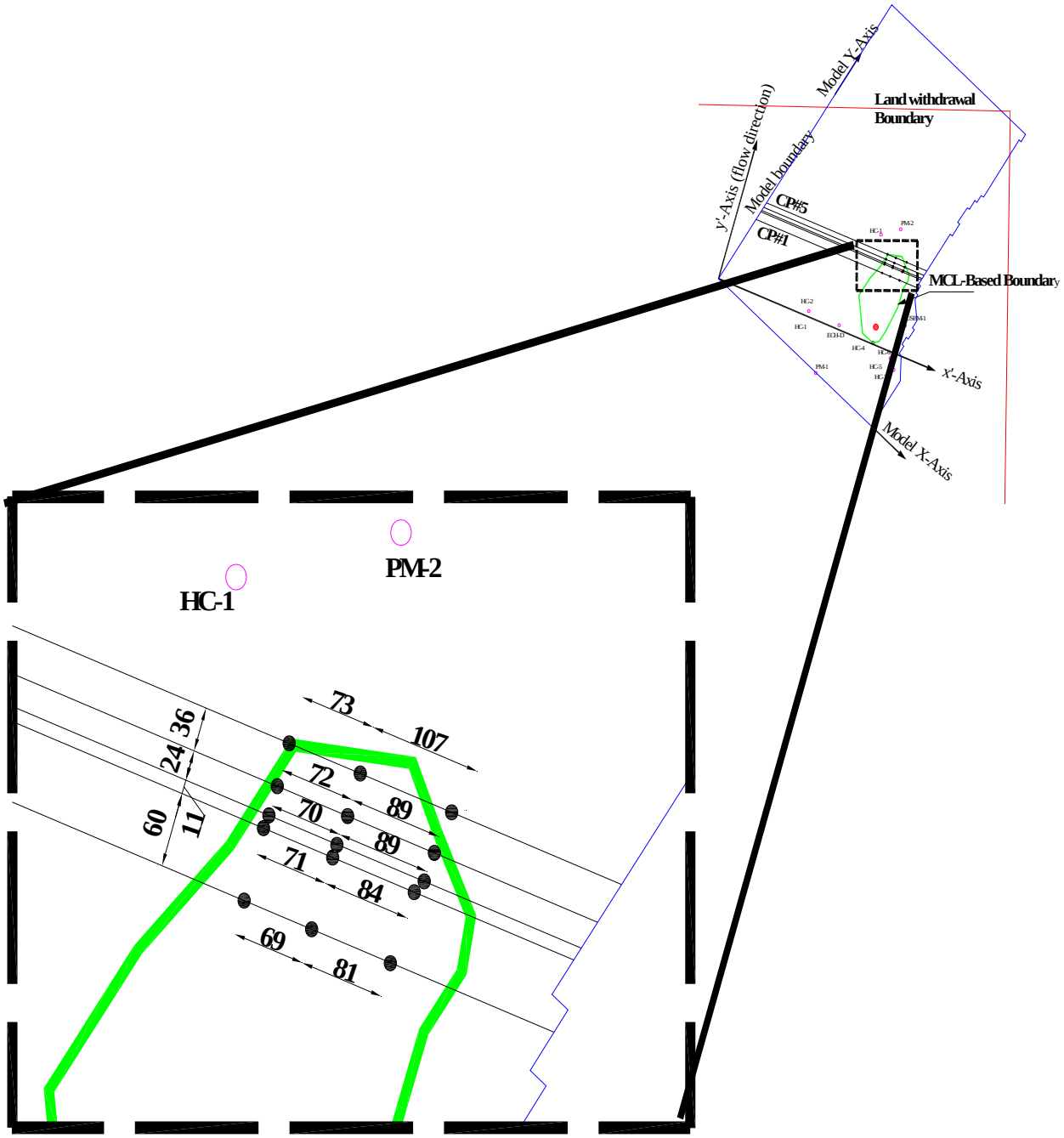

Note: A plan view shows the wells and CPs relative to the boundary. The red-filled circle in the inset map represents the Shoal cavity.

Figure 5-5
Location of the 15 potential wells and the five CPs

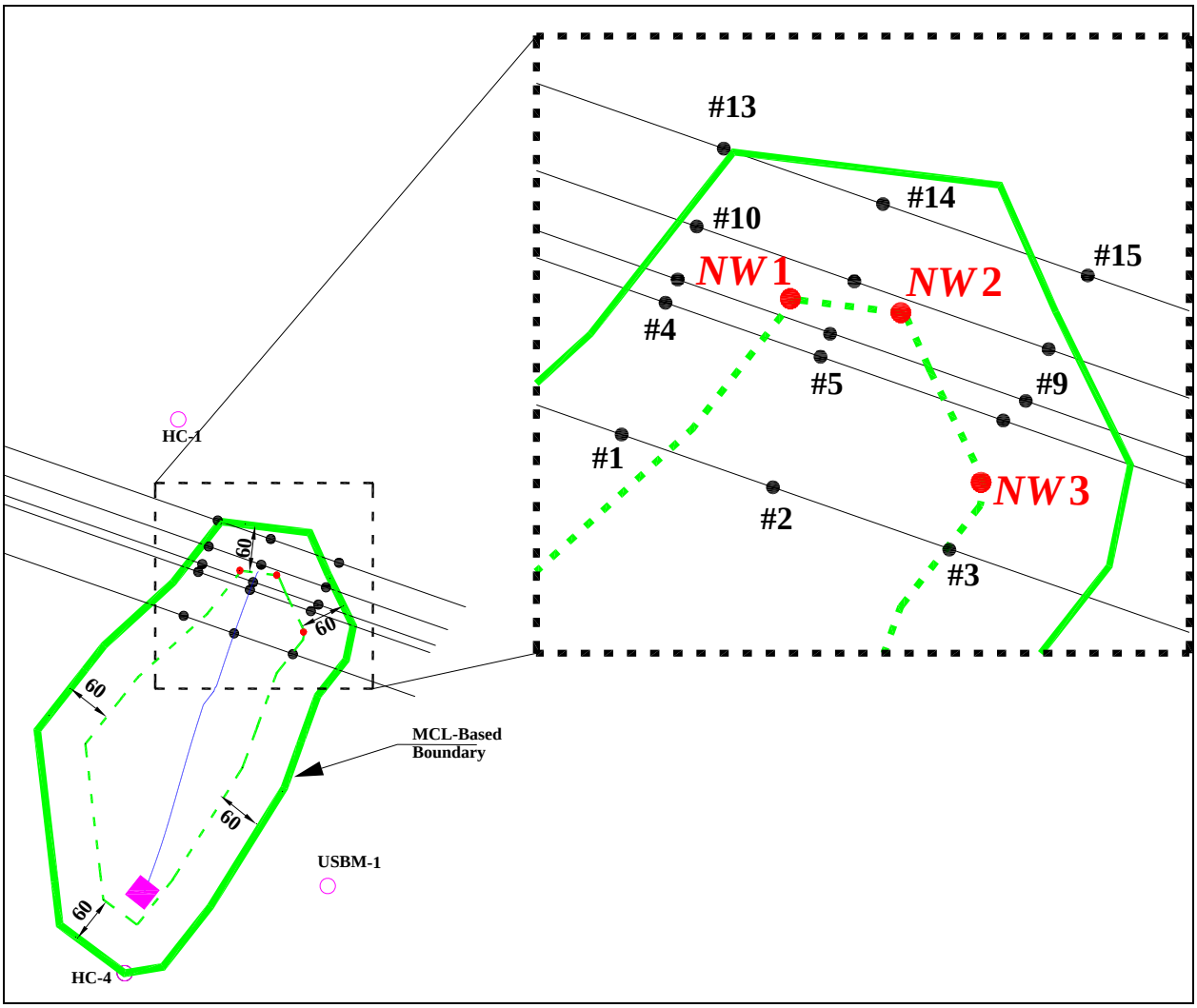

Figure 5-6
Map showing the well numbers used when applying tools 2 and 3 to the monitoring analysis

The total simulation time is selected as the regulatory time frame of 1,000 years and the time for computing probabilities is selected at the same four times analyzed earlier (100, 200, 500, and 1,000 years). The parameter α is varied between 0.5 and 4 percent of the total initial source mass with increments of 0.5 percent. Recall that for a well to be successful in detecting a plume, it has to detect the presence of contaminants when or before a percentage mass of value α crosses the control plane. Since this value is somewhat arbitrary, the analysis was conducted for the above- mentioned eight α values. Under these parameter values, the transport simulations are conducted for 1,000 years and total mass flux breakthrough, $Q(t, x_k)$, are computed for each CP (k = 1, …, 5). In addition, at each potential well location the resident mass, $M_{ji}(t, z)$, that

exists within a certain vicinity of the well ($\Delta x \times \Delta y$) is monitored and saved for each time step and at all elevations.

As an example, Figure 5-7 shows the t-z distributions of the $\log_{10}$ of the resident mass for each of the 20 potential well locations (wells 1 through 15, HC-1, HC-4, NW1, NW2, and NW3). It is important to note the different color bars and different peak values on these bars. If one integrates these masses along the vertical z direction, the results can be plotted as in Figure 5-8. This figure shows the mean value (across all realizations) of this vertically-integrated resident mass as a function of time. As can be seen from the figure, the average resident mass does not exhibit any particular pattern. This is because the amount of mass approaching a certain well location depends on the heterogeneity of fractures and how many realizations have fractures intersecting a well.

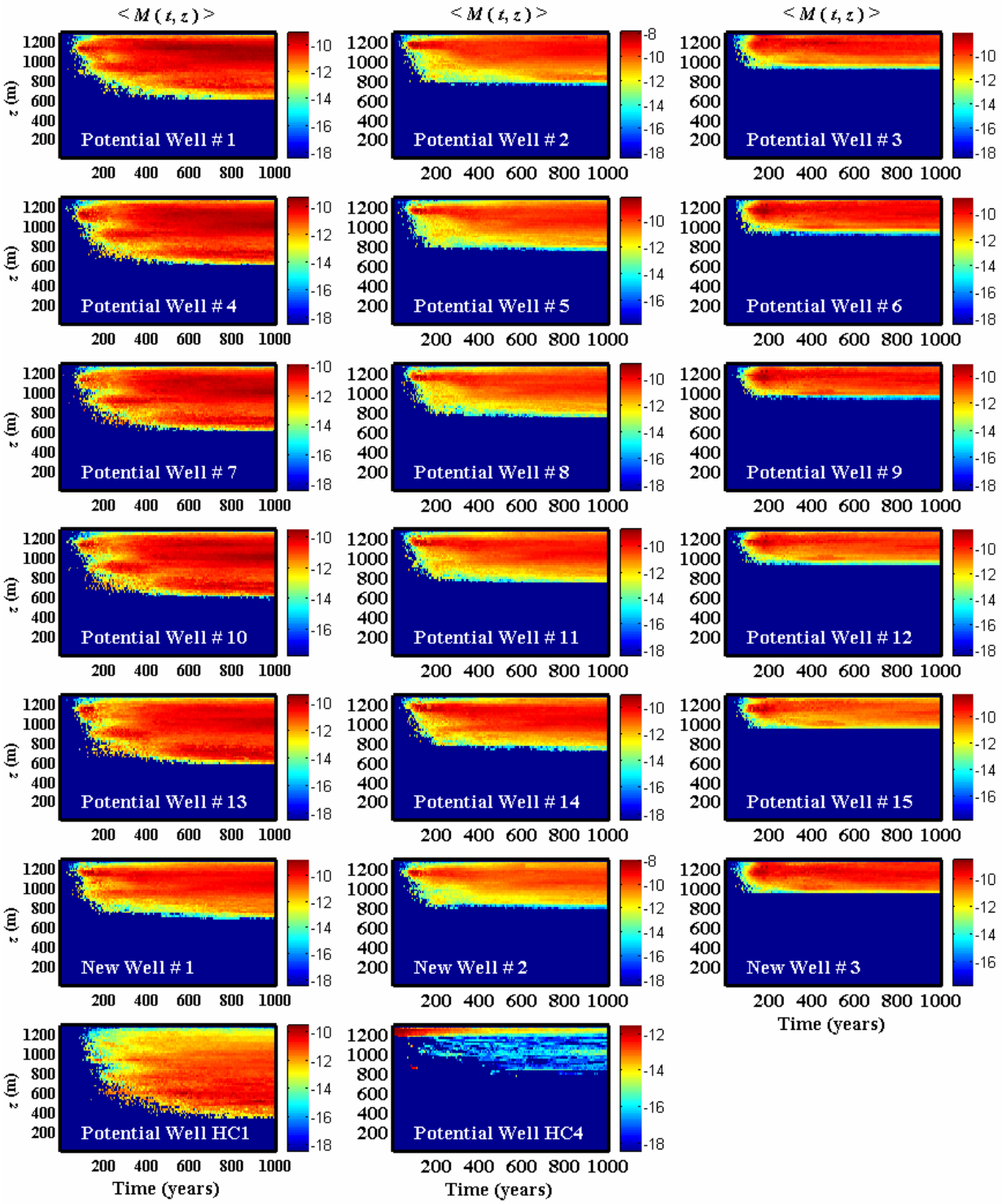

Figure 5-7
The *t-z* distribution of the resident mass in the vicinity of each of 20 potential well locations

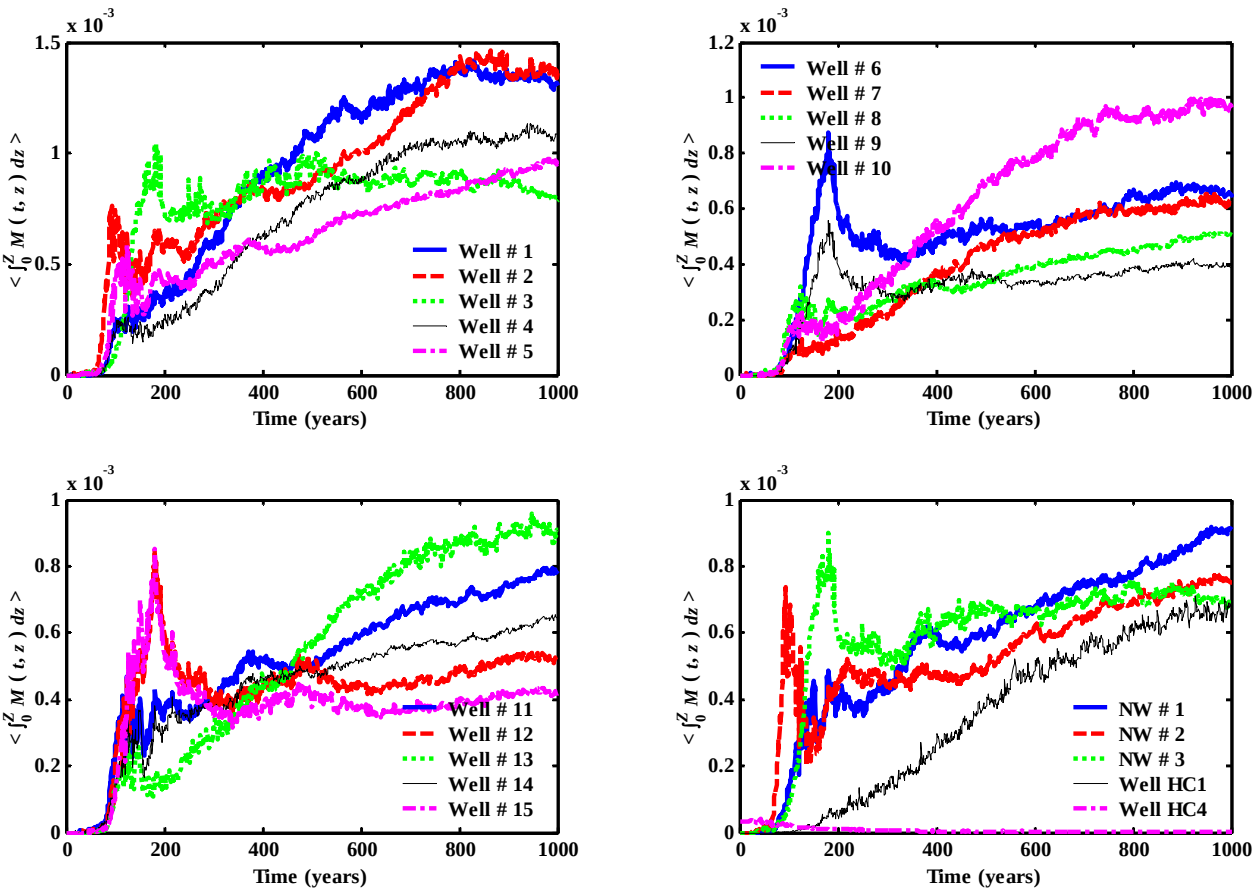

Figure 5-8
Vertically-integrated resident mass in the vicinity of 20 potential well locations

The next step in the analysis is to compute the weights, W_{ij}, for each well j. These weights represent vertical and temporal integration (from time zero to t) of the resident mass. These steps are then repeated for each of the 1,000 realizations considered for the Shoal model. The next step is to compute P_{dj} for each of the potential well locations, with P_{dj} representing the probability that well j detects the plume. Whether this detection is successful or not is computed by a different term (P_s in Equation 5-2). In other words, if the well detects a plume but after a large portion of the plume has crossed the CP, that well will have a low success probability.

Figure 5-9 shows different patterns for the detection probability, P_{dj}, at different times. At 100 years, the central wells on the different CPs attain higher detection probability than the edge wells. However, for t = 200, and 500 years, detection probability increases from the western edge well to the eastern edge well. At 1,000 years, the trend is reversed and detection probability decreases from the western edge well to the eastern edge well. Two factors affect the results, the

time at which detection probability is computed and the velocity encountered by each plume (thus residence time within well vicinity). At 100 years, only a few realizations traveled far from the cavity and are located along the mean flow direction thereby hitting the central wells. At intermediate times, fast realizations (mostly to the eastern side of the cavity and the eastern side of the mean plume trajectory) contribute to the eastern edge wells and lead to the increase in detection probability from west to east. At late times (t = 1,000 years), the slower western realizations arrive to the different CPs and as they are migrating slowly, the particles reside for a long time within the well vicinity thereby contributing to higher M(t, z), W_{ji}, and P_{dj} at the western edge wells compared to the eastern edge wells.

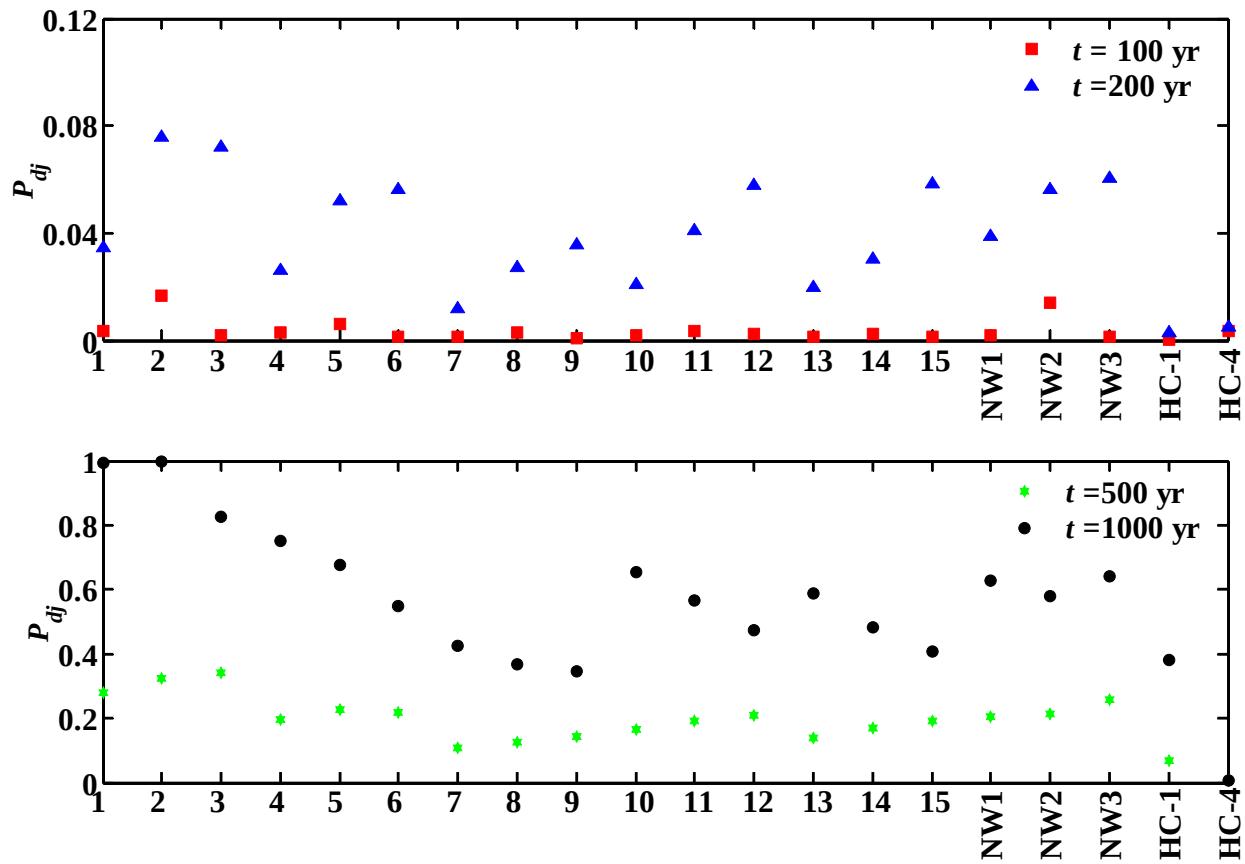

Figure 5-9
Detection probability for the 20 potential wells at different times

The last step in this analysis is to compute the success probability for each well according to Equation (5-2). This success probability is the result of multiplying the probability that a contaminant percentage of α or less crosses the CP passing through the well by the particular well's detection probability. Since this probability term requires the probability that a mass of α or less crosses the CP passing through the well, it is not computed for wells HC-1, HC-4, NW1,

NW2, and NW3 as no control planes are analyzed for these wells. Figure 5-10 shows the success probability for the potential wells at a value of α of 0.01.

Consistent with the previous set of analyses, wells 1, 2, and 3 located at CP #1 have the highest potential for success in detecting the plume. As one moves away from the cavity, success potential decreases as the variability in plume trajectory dictated by the fractured system at Shoal decreases the chance of a well to intercept a large number of the stochastic plumes. However, wells on CPs #4 and #5 exhibit better success probability than wells at CP #3 at 500 and 1,000 years. This is attributed to the interplay between fast moving realizations and short residence time for particles around different wells and the opposite interplay between slow moving realizations and longer residence time for particles. Also, the fractured system may cause some of the wells to be always located along a fracture or in a matrix block (based on fracture network and conditioning data). Thus the success probability exhibits different patterns at different times. This is explained earlier in discussing the patterns of the detection probability P_{dj} at different times, which dictates the patterns of the success probability, P_s.

From this analysis, it can be concluded that a well located on CP #1 is a good choice. As mentioned earlier, the wells contributing to the long-term monitoring network at Shoal need to be reasonably spaced to meet the monitoring objectives as well as be placed with regard to practical issues such as drill-rig access. Therefore, if a well on CP #1 is selected as part of the monitoring network, wells on the other CPs should be considered for additions to the network. It can be seen from Figure 5-10 that many of the other wells have generally equivalent success probabilities, with the exception that wells on CP #3 (wells 7,8,9) tend to be lower. Therefore, there are a number of other wells that represent good choices to augment a well on CP #1 and form a three-well monitoring network.

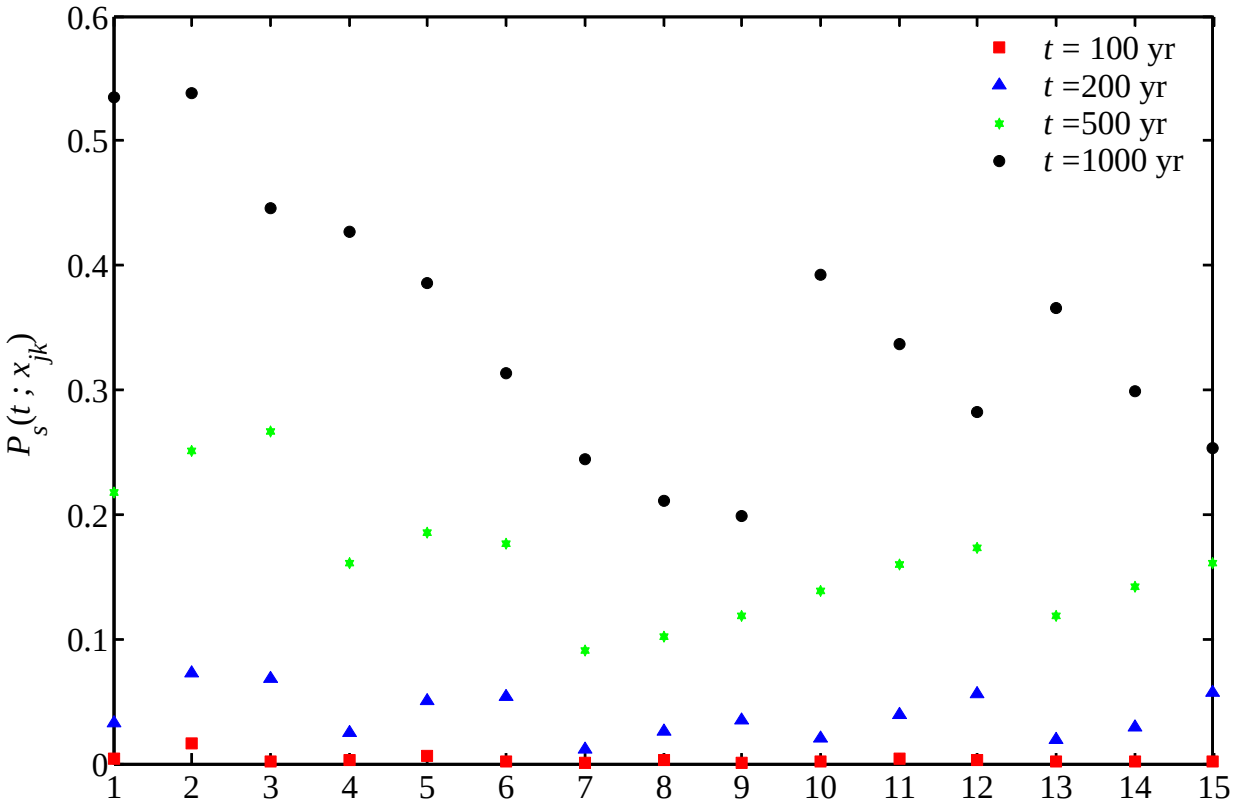

Figure 5-10
Success probability of individual wells at different times for α = 1 percent.

5.2.0.3 Monitoring Design Tool #3

The success probabilities from Tool #2 alone cannot maximize the benefit from more than one well. For example, if one selects the two wells with the highest success probability, they may be successful at detecting the same set of stochastic plumes leaving a large number of equally likely plumes undetected. This, therefore, necessitates the use of another tool to evaluate the efficiency or success probability of the designed network.

The third tool is an extension to a monitoring efficiency model (MEMO) that was developed by Wilson et al. (1992). The purpose of MEMO was to assist in the design of monitoring well networks. Their model quantifies the monitoring efficiency of a given monitoring well network by determining the areas within a potential contaminant source area where a release of that contaminant would or would not be detected by the monitoring well network. Monitoring efficiency is defined as the ratio of the area of detection to the total area of the source. For example, a detection efficiency of 90 percent in Wilson et al.'s (1992) model means that releases occurring over 90 percent of the source area would be detected by the monitoring wells, and releases occurring over the remaining 10 percent of the area would not be detected.

The analytic model developed by Wilson et al. (1992) for deterministic problems is modified and extended to stochastic plumes for Shoal as described by Hassan (2005). The detection efficiency for individual wells is first analyzed, setting the criterion that a plume is considered detected by a well if the vertically-integrated resident mass within the well vicinity attains a percentage mass of 0.5 percent when or before an equivalent percentage reaches the compliance boundary (Figure 5-11). This percentage is arbitrary and other values are used and discussed in Hassan (2005). The figure shows in general that eastern wells have larger numbers of detections than western wells. This is attributed to faster plumes migrating to the eastern side of the cavity.

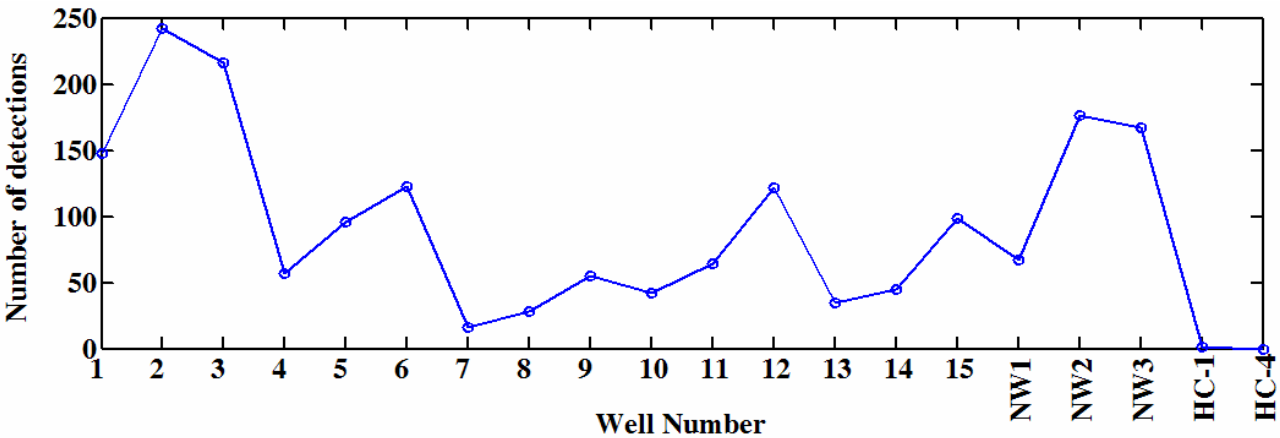

Note: Detections are shown where the criterion is that the resident mass within the well vicinity reaches a value (alpha) of 0.5 percent before an equivalent mass crosses the compliance boundary.

Figure 5-11
Number of detections by individual wells

MEMO was then used to determine the detection efficiency of 76 different three-well networks. The wells comprising each network are listed in Table 5-2. A rectangular detection box encompassing the three wells is used to count the number of plume trajectories that pass through and thus are likely to be detected by any of the three wells forming the evaluated network. The sides of this rectangle are specified by subtracting half a grid cell ($0.5\ \Delta x$) from the smallest x-coordinate among the wells and adding $0.5\ \Delta x$ to the largest x-coordinate and doing the same in the y-direction. Then a plume is considered to be detected if its c.o.m. trajectory passes inside this detection zone before reaching the land withdrawal boundary. The ratio of this number to the total number of realizations is used as a measure of the network's detection efficiency.

Table 5-2
Well assignments in the evaluated monitoring networks

Network #	First Well	Second Well	Third Well	Network #	First Well	Second Well	Third Well
1	1	4	5	39	4	7	9
2	1	5	6	40	5	7	8
3	1	4	6	41	5	8	9
4	2	4	5	42	5	7	9
5	2	5	6	43	6	7	8
6	2	4	6	44	6	8	9
7	3	4	5	45	6	7	9
8	3	5	6	46	4	10	11
9	3	4	6	47	4	11	12
10	1	7	8	48	4	10	12
11	1	8	9	49	5	10	11
12	1	7	9	50	5	11	12
13	2	7	8	51	5	10	12
14	2	8	9	52	6	10	11
15	2	7	9	53	6	11	12
16	3	7	8	54	6	10	12
17	3	8	9	55	4	13	14
18	3	7	9	56	4	14	15
19	1	10	11	57	4	13	15
20	1	11	12	58	5	13	14
21	1	10	12	59	5	14	15
22	2	10	11	60	5	13	15
23	2	11	12	61	6	13	14
24	2	10	12	62	6	14	15
25	3	10	11	63	6	13	15
26	3	11	12	64	1	HC-1	11
27	3	10	12	65	1	HC-1	12
28	1	13	14	66	2	HC-1	11
29	1	14	15	67	2	HC-1	12
30	1	13	15	68	3	HC-1	11
31	2	13	14	69	3	HC-1	12
32	2	14	15	70	4	HC-1	11
33	2	13	15	71	4	HC-1	12
34	3	13	14	72	5	HC-1	11
35	3	14	15	73	5	HC-1	12
36	3	13	15	74	6	HC-1	11
37	4	7	8	75	6	HC-1	12
38	4	8	9	76	NW1	NW2	NW3

Well HC-1 is one of the three wells in twelve of the networks. Including HC-1 leads to a larger detection box, encompassing more plumes on the western side, and thus higher network efficiency. Although HC-1 seems to enhance the overall efficiency in the MEMO analysis, its actual effect would be much diminished because the majority of modeled plumes are at depths much greater than the well by the time they have traversed the distance from the cavity to HC-1 (Figure 5-12), and because the well spacing in that larger box is unlikely to intercept all the plumes passing through it (compare Figures 5-13 and 5-14 with Figures 5-15 and 5-16). Note that in either well configuration (with or without HC-1), there are a large number of plumes that do not travel very far laterally from the cavity. Only about 180 plume centers-of-mass travel past the *y'* location of the detection box, out of 1,000 realizations in 1,000 years. The location of HC-1 outside the compliance boundary and its own very small detection probability (see Figure 5-9) minimize the benefit of including it in the long-term monitoring network, at least at the expense of another well location.

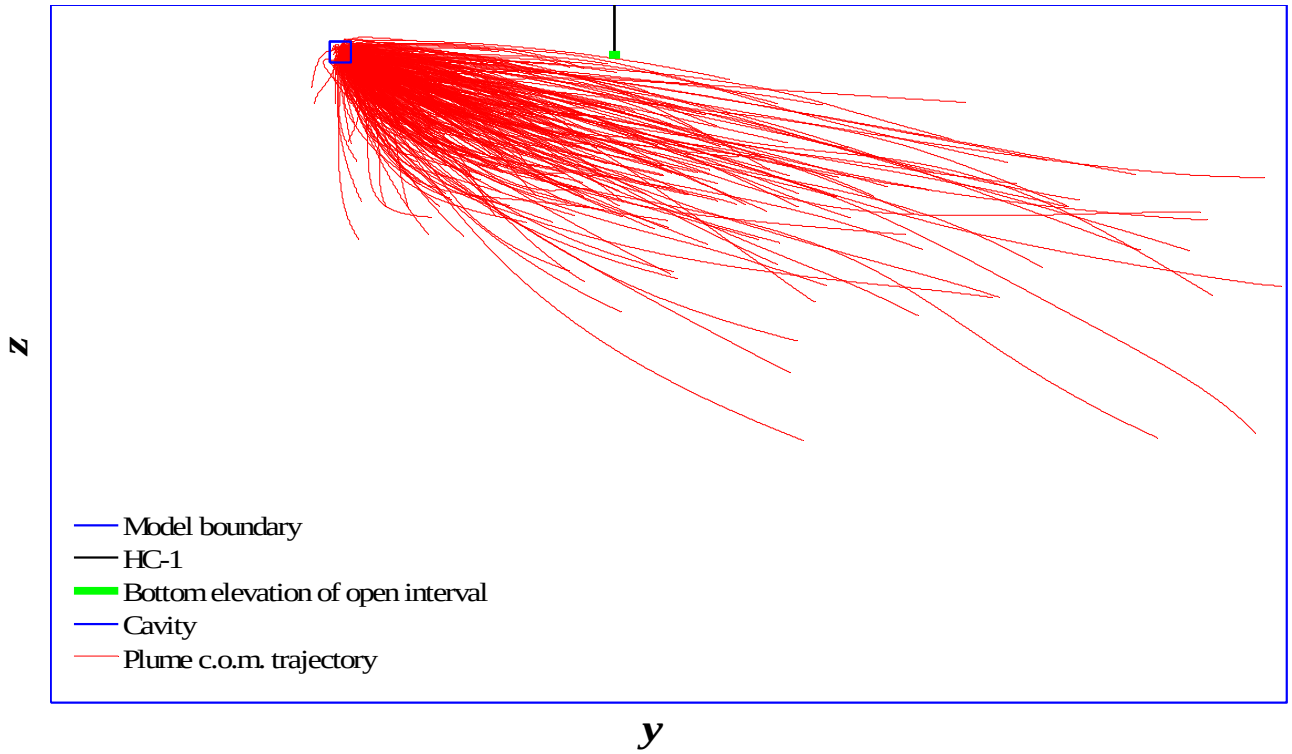

Note: The trajectories pass below the elevation of the open interval in well HC-1 and, though not visible on this vertical section, many of the plumes are also not coincident with the *x-y* location of the well.

Figure 5-12
Plume trajectories projected on a vertical section through the model domain

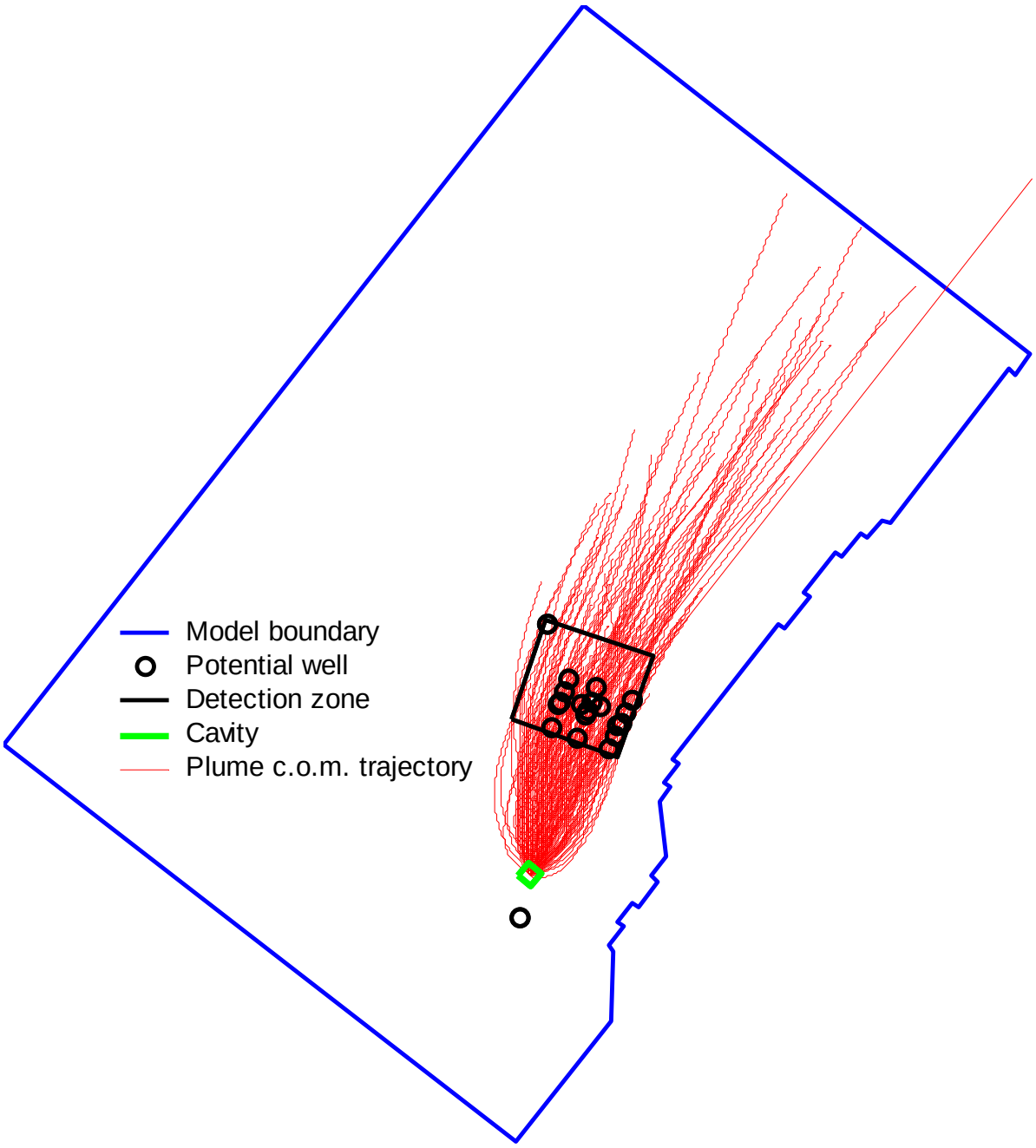

Note: Rectangular detection zone and the test cavity are also shown.

Figure 5-13
Trajectories of detected plumes superimposed on the potential well locations for first configuration where well HC-1 is included

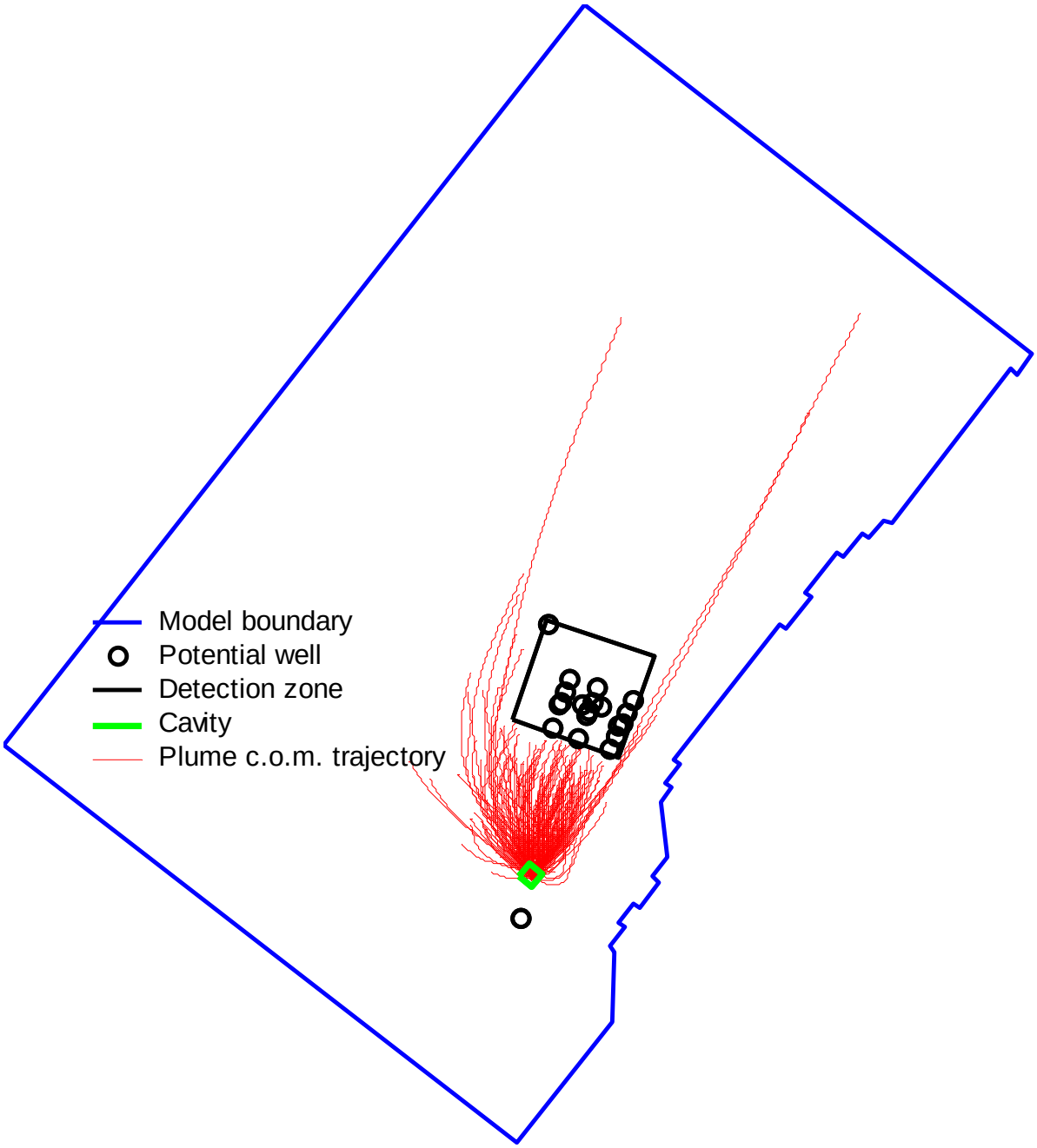

Note: Rectangular detection zone and the test cavity are also shown.

Figure 5-14
Trajectories of non-detected plumes superimposed on the potential well locations for first configuration where well HC-1 is included

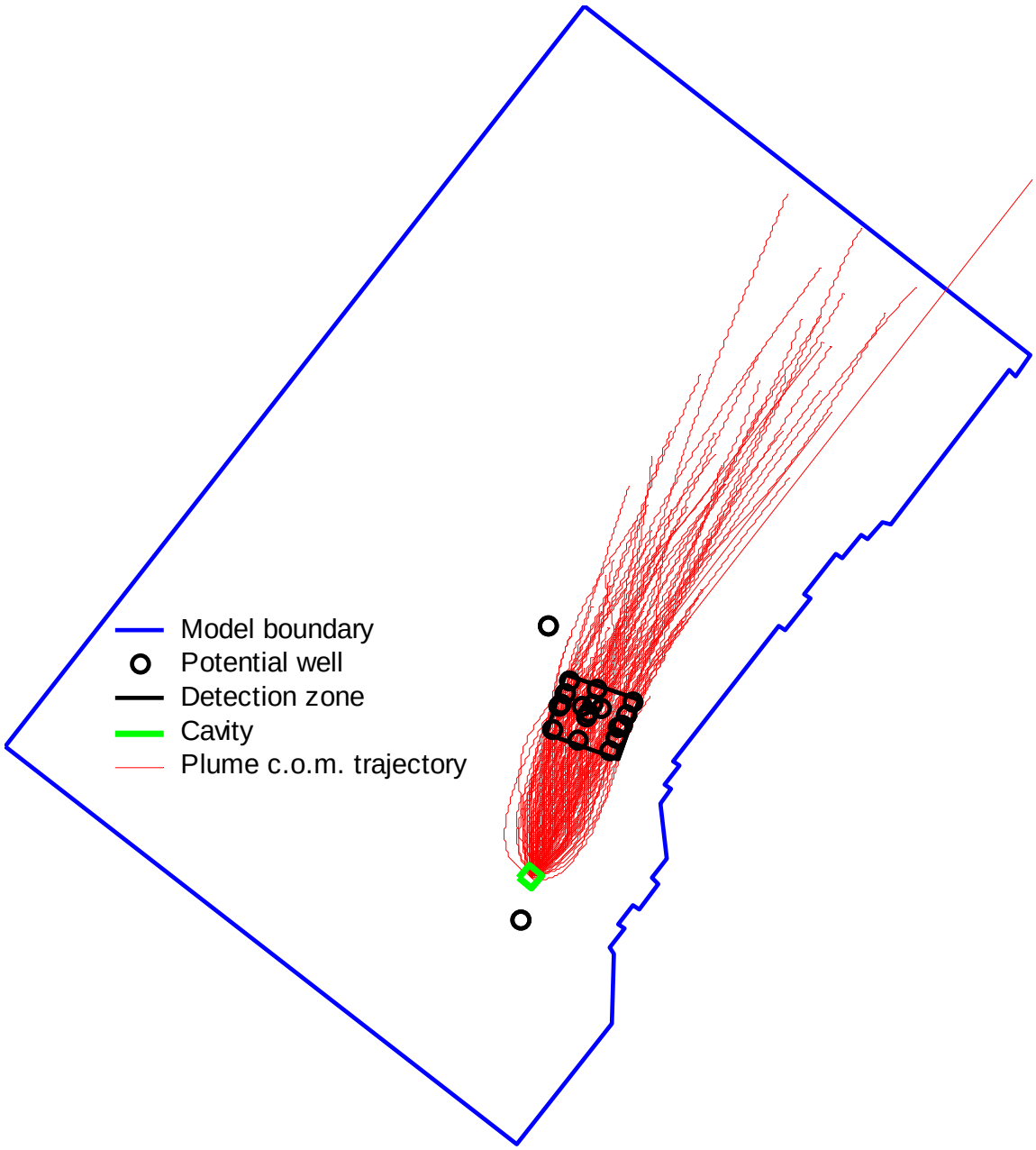

Note: Rectangular detection zone and the test cavity are also shown.

Figure 5-15
Trajectories of detected plumes superimposed on the potential well locations for second configuration where well HC-1 is excluded

Note: Rectangular detection zone and the test cavity are also shown.

Figure 5-16
Trajectories of non-detected plumes superimposed on the potential well locations for second configuration where well HC-1 is excluded

The detection efficiency for the 76 networks is shown in Figure 5-17. It is important to remember that the c.o.m. of about 820 trajectories (out of 1,000) do not travel the distance to CP #1 in 1,000 years. The efficiencies reported are the percentage of realizations detected among the ones where the c.o.m. makes it to the compliance boundary in 1,000 years. For example, an efficiency of 70 percent means that 126 plumes were detected of the 180 traveling to the boundary. Adding these to the plumes with limited travel distance (820), means that only five percent of the realizations would travel past the monitoring well undetected. The figure reveals a number of interesting results. The first network composed of wells 1, 4, and 5 has a low detection efficiency of about 40 percent, whereas network 2 composed of wells 1, 5, and 6 has a higher efficiency of about 70 percent. Similarly, networks 36 and 37 exhibit the same pattern. These findings can be understood in Figure 5-18(a) where the well locations and detection zones relative to the plume trajectories (only a small number of trajectories is plotted for clarity) for networks 1 and 2 (superimposed) and for networks 36 and 37 (Figure 5-18[b]) are plotted. A larger number of trajectories pass outside the right edge of the detection zone in network 1 whereas the larger detection zone of network 2 captures these trajectories. The same is true for the comparison between networks 36 and 37, and for other, unplotted network comparisons. In each case, one detection box is much larger than the other resulting in higher detection efficiency.

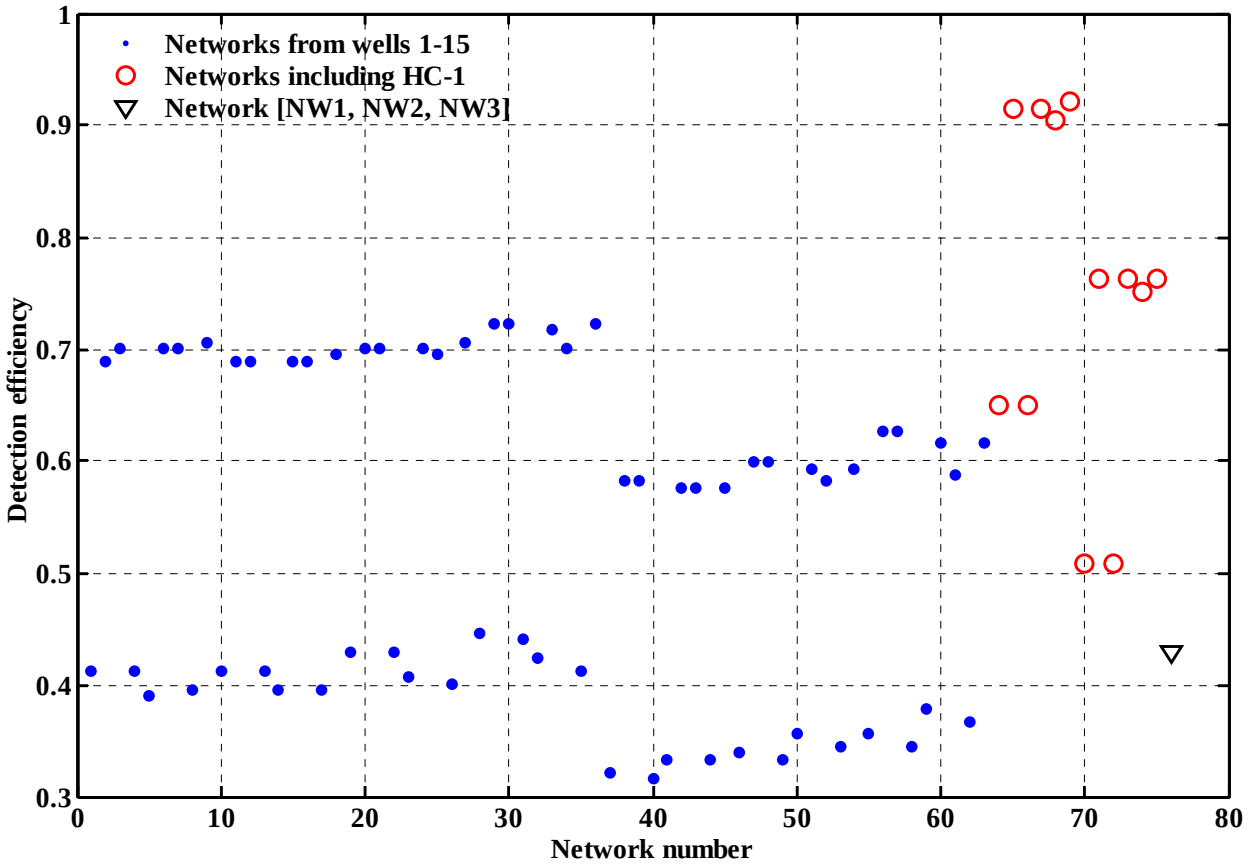

Note: Detection efficiency shows where a network detects a plume when its trajectory passes within the network's rectangular detection zone.

Figure 5-17
Detection efficiency for 76 three-well networks as computed by geometric considerations

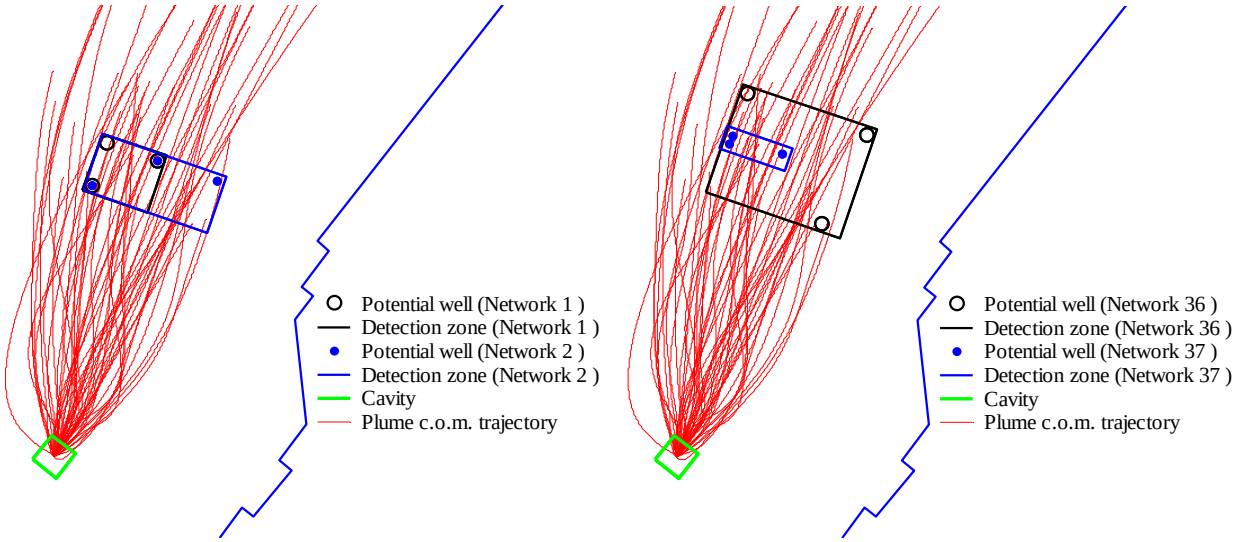

Figure 5-18
Detection zones for networks 1 and 2
(a - to the left) and 36 and 37 (b - to the right)

It can also be seen from Figure 5-17 that the network composed of wells NW1, NW2, and NW3 has a low detection efficiency compared to other networks. This is because these three wells are close to each other and the detection box enclosing them is small compared to other networks which leads to a smaller number of trajectories crossing this small box. It is also clear that many of the networks that include well HC-1 have better detection efficiency than most of the tested networks. This is because of the location of HC-1 which allows the detection box to be very large leading to this high detection efficiency. However, as mentioned earlier, well HC-1 has a very low detection probability and is located outside the compliance boundary and thus is not a good choice for the long term monitoring network from the detection efficiency perspective.

Figure 5-17 shows four bands of networks with similar efficiencies (neglecting the networks that include HC-1). Twenty well combinations achieve detection efficiencies around 70 percent. Of these, networks 29, 30, 33, and 36 attain the highest efficiency. Each of these includes one well on CP #1 and two on CP #5, such that two network wells would monitor the compliance boundary but not provide as much reaction time as wells on other CPs in the event of contaminant detection.

Well Selection

Selection of the optimum monitoring network combines the findings of the three design tools. First, only networks comprised of three new wells, as compared to HC-1, are considered. This is further limited to networks in the highest tier of detection efficiency, as computed using Tool #3.

Preference is then given to networks with wells that provide the 50-yr reaction time (part of the analysis of Tool #1). Finally, selection among the essentially equivalent networks remaining is based on the results of the individual well performance measures given by Tool #2. The best individual well performance was attained by Well 2. It is on the first CP (best performing in Tool #1) and also on the mean trajectory of the c.o.m. The high efficiency networks including Well 2 that also meet the other criteria are networks 6, 15, and 24. Network 6 is selected as the optimum due to the poorer performance of wells 7 and 9 (and CP#3 in general) in Network 15, and the possible absence of reaction time for wells 10 and 12, depending on plume trajectory, of Network 24. Network 6 is comprised of wells 2, 4, and 6.

5.2.0.4 Monitoring Well Completion Interval

Having determined the three wells to be used for detection monitoring and validation purposes, the first tool (Hudak, 1994) can be used to provide some guidance into the completion or sampling interval for each well. Similar to the analysis performed using the plume width and the *x'* location of the plume c.o.m. for the purpose of determining the minimum number of wells, N_i, needed to span a siting horizon, we analyze the plume height and the *z* location of the c.o.m. to obtain N_i in the vertical direction. To first obtain the maximum interval spacing, S_i, we analyze the simulation results for the five CPs where the plume height at each CP is reported for each realization of the stochastic flow and transport model at Shoal. To summarize the results for the different times, different CPs, and different realizations, Table 5-3 presents the prediction quantiles (PQ) obtained from the 1,000 realizations of plume heights. These are obtained in a similar manner to the analysis reported earlier in Section 5.2.0.1. It can be seen that on average the plume height slightly exceeded 400 m at 1,000 years. At 100 years though, the plume height is about 125 m on average. For each CP and for each time considered, the parameter S_i is obtained as the 50 percent PQ of the plume height as it crosses the CPs.

Table 5-3
Prediction quantiles for the plume height at different times and for the five CPs

Plume height when crossing the CP (m)												
Control	t = 100 years			t = 200 years			t = 500 years			t = 1,000 years		
Plane	2.5% PQ	50% PQ	97.5% PQ	2.5% PQ	50% PQ	97.5% PQ	2.5% PQ	50% PQ	97.5% PQ	2.5% PQ	50% PQ	97.5% PQ
CP #1	5.4	120.2	444.5	13.9	185.1	631.3	38.0	287.1	979.9	46.9	401.4	1102.0
CP #2	5.2	137.3	396.4	9.0	169.6	552.5	27.3	282.3	953.7	34.6	404.0	1095.4
CP #3	13.1	123.7	475.9	3.8	158.3	594.5	22.2	278.6	962.1	40.4	403.9	1100.3
CP #4	25.2	123.5	545.4	9.3	161.5	568.6	22.9	280.9	935.4	41.8	403.3	1097.1
CP #5	9.1	100.5	489.5	13.5	174.5	532.4	21.6	280.2	866.3	36.3	404.3	1049.4

For each CP and at each time considered, the zone of potential contaminant migration, W_i, in the vertical direction is obtained by analyzing the distribution of the z-coordinate of the plume c.o.m. as it crosses the CPs. Table 5-4 displays the PQs for the z position of the c.o.m. of the plume. To obtain the parameter W_i, the difference between the 97.5 percent PQ (representing the upper bound or the uppermost plume) and the 2.5 percent PQ (representing the lower bound or the lowermost plume) is computed and taken as a representation of the zone of potential migration in the vertical direction.

Table 5-4
Prediction quantiles for the *z*-position of the plume c.o.m. at different times and for the five CPs

Vertical coordinate z of the plume center of mass when crossing the CP (m)												
Control	t = 100 years			t = 200 years			t = 500 years			t = 1,000 years		
Plane	2.5% PQ	50% PQ	97.5% PQ	2.5% PQ	50% PQ	97.5% PQ	2.5% PQ	50% PQ	97.5% PQ	2.5% PQ	50% PQ	97.5% PQ
CP #1	924.1	1157.2	1226.9	841.8	1121.2	1227.7	844.8	1090	1218	806.7	1077	1211.3
CP #2	918.1	1153.9	1219.1	875	1116.7	1224.2	799.2	1074.8	1215	773.9	1059.9	1211
CP #3	831.9	1156.1	1215.9	863.9	1117.5	1228.2	776.6	1074.3	1214.9	779.8	1057.5	1210
CP #4	698.6	1133.5	1217.3	854	1111.9	1221	779.4	1068.7	1216.5	751.8	1047.9	1212.5
CP #5	692.7	1136.9	1219.9	798.8	1102.9	1221.1	758.7	1057.5	1213.6	738.7	1036.5	1208.6

After determining the two parameters S_i and W_i for all CPs, Equation (5-1) is used to obtain the minimum number of sampling intervals needed for well 2 (at CP#1 and wells 4 and 6 (at CP#2). Table 5-5 shows the values of S_i, W_i, S_i/W_i, and N_i for each CP and all times considered. It can be seen from Table 5-5 that the required number of sampling intervals in the vertical direction is generally between one and two. Only at t = 100 years are 5 sampling intervals required. However, this is a result of very thin plumes (e.g., few fast particles) reaching CP#5 at 100 years leading to a small S_i value and in turn a large number N_i of required intervals. Based on these results, and the fact that a single completion zone prevents the possibility of cross-flow, mixing and dilution in the well bore, a single interval is recommended for each well.

Table 5-5
Parameters of Equation (5-1) and the minimum number of intervals, N_i, to span each CP (or well) at different times

S_i, W_i, siting horizon efficiency (S_i / W_i), and N_i for the five CPs and the different times																
Control	t = 100 years				t = 200 years				t = 500 years				t = 1,000 years			
Plane	S_i	W_i	S_i/W_i	N_i	S_i	W_i	S_i/W_i	N_i	S_i	W_i	S_i/W_i	N_i	S_i	W_i	S_i/W_i	N_i
CP #1	120.2	302.8	0.40	2	185.1	385.9	0.48	2	287.1	373.2	0.77	1	401.4	404.6	0.99	1
CP #2	137.3	301.0	0.46	2	169.6	349.2	0.49	2	282.3	415.8	0.68	1	404.0	437.1	0.92	1
CP #3	123.7	384.0	0.32	3	158.3	364.3	0.43	2	278.6	438.3	0.64	1	403.9	430.2	0.94	1
CP #4	123.5	518.7	0.24	4	161.5	367.0	0.44	2	280.9	437.1	0.64	1	403.3	460.7	0.88	1
CP #5	100.5	527.2	0.19	5	174.5	422.3	0.41	2	280.2	454.9	0.62	1	404.3	469.9	0.86	1

The above analysis indicates that one sampling interval per well should be sufficient for detection monitoring. However, the analysis does not provide guidance on where to place this sampling interval for each well. The other tools provide some guidance in this regard. By integrating the resident mass for each well in the time domain, one obtains a vertical profile for mass distribution in each well's vicinity, which provides some guidance on the selection of the sampling interval location. Figure 5-19 displays the temporally-integrated resident mass (averaged over all realizations) in the vicinity of the 15 potential well locations. Again the vicinity of the wells is defined by the grid cell ($\Delta x \times \Delta y$) where the well is located. It can be seen that for well #2, a high value of resident mass exists at an elevation of about 1,150 m. For well 4, the peak value is at approximately 1,100 m, and at well 6, the high value of the resident mass exists at an elevation of about 1,175 m.

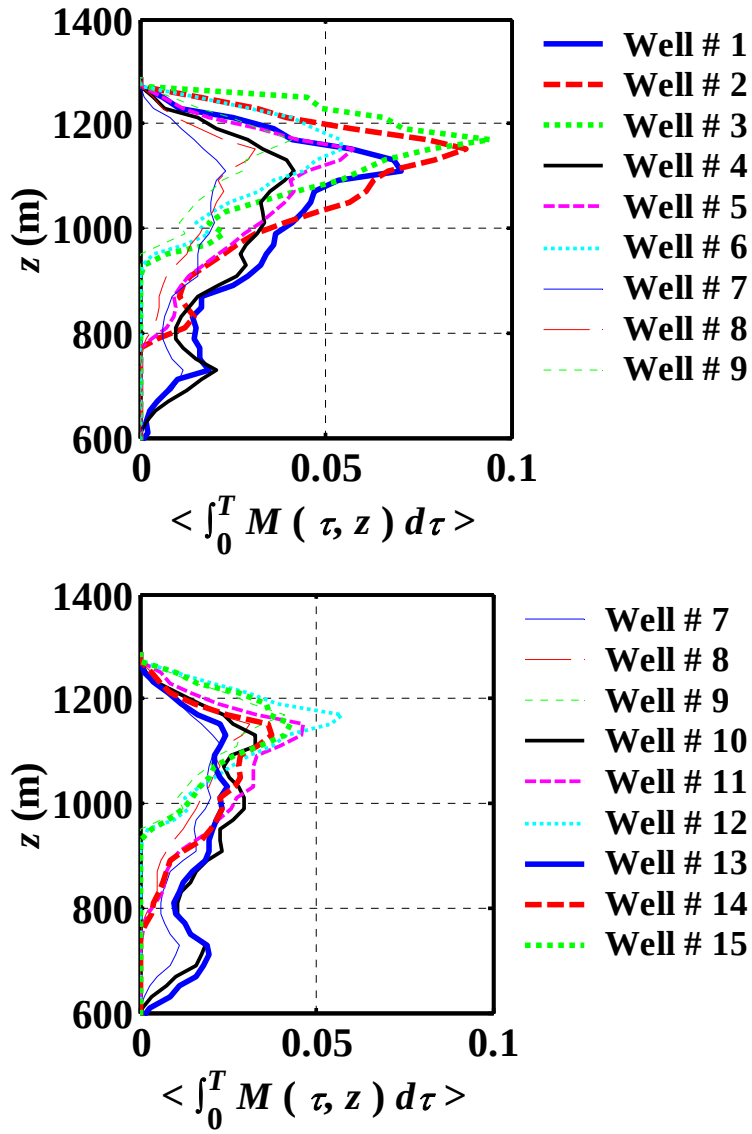

Figure 5-19
Temporally integrated resident mass in the vicinity of 15 potential well locations as a function of elevation, z

Given this guidance, 15 intervals at different elevations are tested for each selected well with the interval being 50 m long. The elevations of these intervals for each well are shown in Figure 5-20. Then a detection zone of size ([50 + Δz] × Δx × Δy) centered on the interval center is used to determine the number of plume trajectories that pass through it (i.e., detected by this sampling interval). The number of detections obtained for each interval at each of the three wells is shown in Figure 5-20. The interval with maximum detection efficiency is shown in red in these figures. It should be remembered that these trajectories are the plume c.o.m. trajectories and thus plumes that are wide can be detected by the different intervals even if the c.o.m. trajectory does not cross the detecting zone of these intervals. In other words, the different wells

can detect portions of dispersed plumes where the plume c.o.m. trajectory does not cross the grid cells where these wells are located.

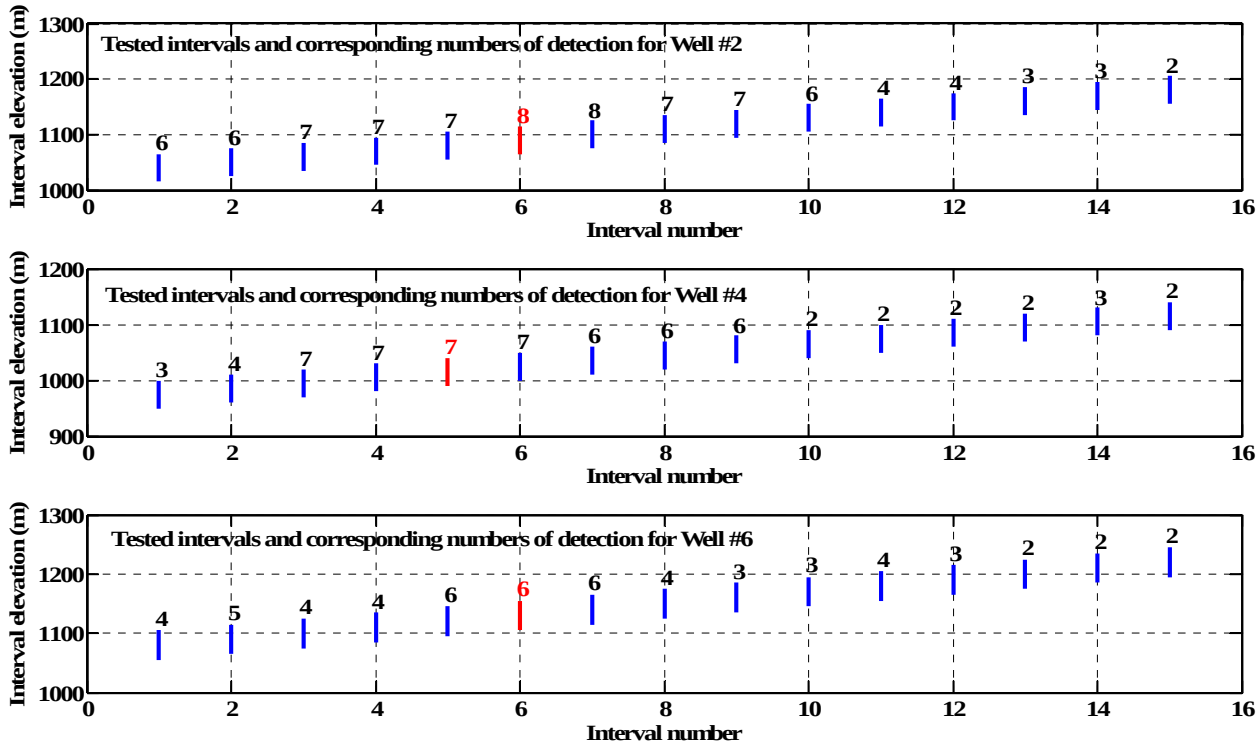

Figure 5-20
Tested intervals and numbers of detected plume trajectories for each interval for wells 2, 4, and 6

To confirm that the selected intervals are reasonable, the plume trajectories in the *y-z* plane are plotted with the selected wells and sampling intervals superimposed in Figure 5-21. The interval for well #2 spanning the elevations 1,065 and 1,115 m and for well #4 spanning elevations 1,000 and 1,050 m capture many of the trajectories shown in Figure 5-21. Based on Figure 5-19, these intervals are close to the peak of the resident mass in the vicinity of each of the three wells indicating that these intervals would have a high chance of detecting contaminant mass if plumes arrive close to the wells.

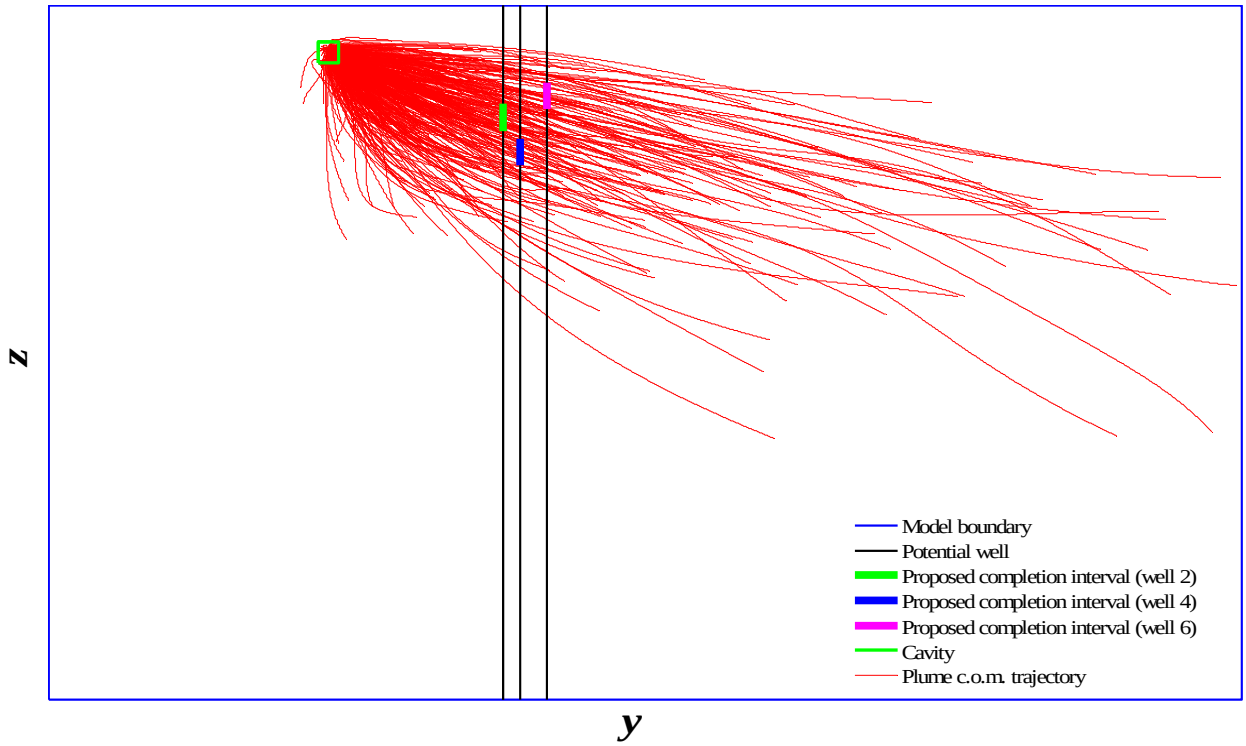

Note: Proposed sampling intervals for wells 2, 4, and 6 are shown.

Figure 5-21
Trajectories of plumes superimposed on the potential well locations

5.2.0.5 Monitoring Design Summary

Using three different quantitative approaches and the numerical groundwater flow and transport model developed for Shoal, three new monitoring well locations have been identified from 76 different networks. The selected wells are assigned names MV-1 (well #2 in the previous analysis), MV-2 (well #4), and MV-3 (well #6), designating their purpose for monitoring and validation, as compared to the HC wells. Figure 5-21 shows the locations of the proposed new wells relative to the Shoal cavity and the MCL-based boundary (Pohll and Pohlmann, 2004). The proposed three wells are reasonably located relative to the cavity from a qualitative inspection of Figure 5-22. These locations may be slightly modified to avoid practical limitations encountered when selecting drill sites. In addition to the proposed new wells, existing wells HC-1 and HC-4 are proposed for inclusion in the network. Neither had good individual well performance, but they are low cost additions that will provide additional areal coverage.

In addition to the quantitative analyses using the numerical model, the development of the monitoring network for Shoal will also be subject to qualitative hydrogeologic interpretation

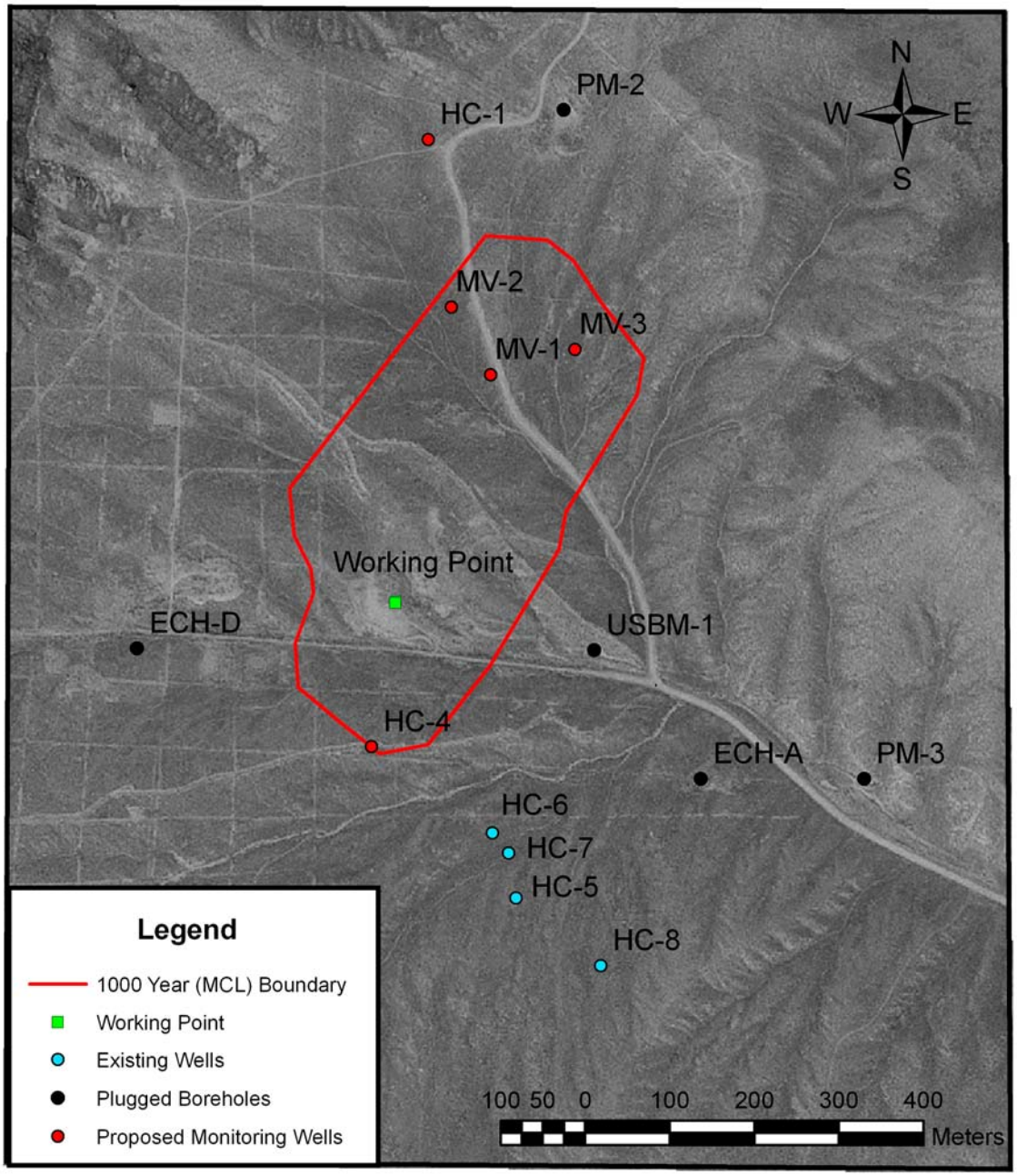

Figure 5-22
Proposed monitor well network relative to the test cavity and the computed MCL-based contaminant boundary

during implementation. Insight developed from knowledge of the hydrogeologic environment will directly affect the final well completions. For example, transport through fractures is the pathway of concern through the granite. Although the simulation and probability-based approaches indicate that the best vertical location to screen the monitoring wells spans intervals from elevations of 1,000 to 1,155 m, any large fracture zone encountered during drilling will be carefully evaluated as a potential screen location, whether or not it is at that exact vertical horizon predicted by the model. Other factors that will be considered during drilling and testing the monitoring wells are the hydraulic heads encountered and the identification of faults or other significant hydrogeologic features. As this information will only be available during the fieldwork, it will be incorporated in the monitoring well design at the time of well installation.

5.2.1 Monitoring Frequency

Monitoring will occur annually during the five-year proof-of-concept period. The frequency of data collection should correspond to contaminant transport times as predicted by the flow and transport models. The expected value of groundwater velocity at Shoal is approximately 8.2×10^{-3} meters per year (m/yr) (see Section 2.0 for more discussion), with the velocity of even non-sorbing radionuclides slower due to the process of matrix diffusion. Although monitoring at decadal timescales would provide adequate data for such slow migration, long monitoring intervals contrast with practical needs. These needs include maintaining active knowledge of the monitoring system, surveillance of activities in the region around the site, and generation of data to support the proof of concept determination. These needs are best met with a monitoring interval of once a year. The monitoring of some system parameters, such as hydraulic head, may need to occur more frequently than once a year, depending on whether equilibrium conditions are regained rapidly after well installation. These conditions will be reported to NDEP as specified in Section 5.2.2.

5.2.2 Monitoring Analytes and Parameters

The monitoring analytes and parameters include tritium, ^{14}C, ^{129}I, and hydraulic head, as summarized in Table 5-6. Tritium will be the primary radiochemical analyte. This selection is based on the mobility of tritium, its abundance in the source term for the first hundred years, and the low detection limits available. Due to the relatively short half-life of tritium, longer-lived radionuclides will gain in importance during post-closure monitoring. Carbon-14 and ^{129}I are selected as long-lived radionuclides for the monitoring program because of their importance in defining the contaminant boundary (Pohll et al., 2003). Although ^{14}C and ^{129}I are selected to address post-closure monitoring, data collected preclosure will be used to establish background conditions.

Table 5-6
Monitoring analytes and parameters

Analyte	Measurement Method	Container Type	Preservative	Filtration	Holding time	Required Detection Limit
Tritium	Scintillation counting	1-liter glass	None	Nonfiltered	180 days	300 pCi/L
Carbon-14	Accelerator mass spectrometry	2-liters glass	None	Nonfiltered	180 days	5 pCi/L
Iodine-129	Accelerator mass spectrometry	1 liter amber glass	None	Nonfiltered	180 days	0.1 pCi/L
Uranium (isotopic)	EPA 908.0 Comparable HASL-300	1-liter polyethylene	HnO_3 ph<2	Filtered and unfiltered	180 days	0.1pCi/L (each isotope)
Gross Alpha	EPA 900.0/9310	1-liter polyethylene	HnO_3 ph<2	Filtered and unfiltered	180 days	4 pCi/L
Uranium	SW846-6010B	1-liter polyethylene	HnO_3 ph<2	Filtered and unfiltered	180 days	0.05mg/L
Hydraulic Head	Wireline, transducer, electric tape	NA	NA	NA	NA	± 0.1 ft

*Monitoring of hydraulic head may need to be more frequent than annually at the beginning of the proof-of-concept period until post-drilling equilibration is reached.

Elevated gross alpha (ranging from 3.9 pCi/L in HC-5 to 121.2 pCi/L in HC-4) has been found in many of the Shoal HC wells. The gross alpha MCL is 15 pCi/L, but this is exclusive of uranium and radon. Data on radon and uranium, including isotopic uranium analysis are needed to demonstrate that the elevated gross alpha at PSA is from natural sources.

Although gross alpha is not expected to be part of the long-term analytical suite, documentation of the conditions is needed to prevent confusion and concern when/if alpha analyses are performed in the future.

The system parameter selected for proof-of-concept monitoring is hydraulic head. It is selected based on the sensitivity of hydraulic head to changes in a hydrologic system. Due to the current pump column configuration in well HC-4, there is no access for water level measurements. It will be excluded from the hydraulic head monitoring until future well maintenance activities allow an access tube to be installed.

5.2.2.1 Quality Assurance/Quality Control Processes

The quality of the monitoring results depends on establishment and implementation of effective sampling, analysis, and support processes. Plans and procedures governing data collection are developed in accordance with the UGTA QAPP (NNSA/NSO, 2003a). The fundamental aspects of this plan are presented below.

Collecting the water samples in accordance with established processes will ensure sample quality. Plans and procedures are developed to ensure that appropriate sampling controls are planned and implemented. Representative samples are achieved by pumping the well and purging to the point of collecting representative groundwater. Groundwater will be considered representative only after at least one well volume has been purged and the field-measured parameters of temperature, electrical conductivity (EC) and pH have stabilized. Electrical conductivity and pH are measured to establish the representative nature of the groundwater sample, and not as empirical parameters within the monitoring program.

Analytical quality will be ensured through laboratory and field QA/QC systems to include the use of established processes and standards for calibration. Trip blanks, laboratory blanks, field blanks, and duplicate samples will be included in the routine monitoring to determine the effectiveness and precision of sampling processes. Although the contaminant boundary is based on SDWA levels that equate to 20,000 pCi/L for tritium, 2,000 pCi/L for ^{14}C, and 1 pCi/L for ^{129}I, the quality requirement for the monitoring will be the detection levels as given in Table 5-6. The detection requirements for ^{14}C and ^{129}I, in particular, are low because these analyses will be used to establish background conditions for comparison during post-closure monitoring.

Comparison of hydraulic head between the flow model and field measurements is complicated by issues of scale. The model simulates head values at the cell scale of 20x20x20 m, whereas a well provides access to a very limited portion of the aquifer directly adjoining the screen and filter pack. Thus, field measurements of heads in a fractured aquifer are much more highly resolved than model-simulated heads, and their high precision does not provide additional information for proof-of-concept when comparing them to simulated heads that can be considered averages over relatively large blocks of the aquifer. (The issue of different scales of measurement in the validation process is discussed in Appendix E of Hassan, 2003.) Nonetheless, subtle variations in hydraulic head may be useful indicators of change in the overall hydrologic system in response to climatic or anthropogenic causes. Thus, the ability to detect trends with a precision of plus or minus a tenth of a foot (3 centimeters [cm]) is the quality requirement for the hydraulic head measurements. Absolute accuracy of the measurement is

dependent on well deviation and not necessary for monitoring trends in head within a single well. Data quality will be obtained through the use of calibrated field equipment (wirelines, transducers or water level probes), and a standard operating procedure requiring three repetitive measurements within the acceptable precision.

5.2.2.2 Sampling Methods

Groundwater samples will be obtained using submersible pumps installed in the new wells and will be used for model validation and proof-of-concept analysis, as well as monitoring. It is also possible that samples will be collected with a wireline and discrete sampler, or a submersible pump, from existing site wells and piezometers in the new wells, as part of the validation and proof-of-concept analysis.

Samples from the new wells will be collected with a submersible pump. The drilling contractor will develop the wells before the first sample collection. An aquifer test will then be conducted on each well to obtain hydraulic parameters, but also to purge the borehole of drilling fluid so that representative samples can be obtained. This initial purging will be conducted until pH, EC, and temperature stabilize, and any chemical tags added to drilling fluids are reduced to acceptable levels. Subsequent sample collection from the new wells and any other well sampled using a pump, will be conducted after one well volume is purged and pH, EC, and temperature stabilize.

Conditions that require validation or proof-of-concept samples to be collected with a discrete sampler are likely to prohibit purging. In these cases, it is proximity of the sampler to the screened horizon that is relied on for providing representative groundwater, but these samples will be designated of lower reliability than those collected after purging.

Table 5-7 lists additional analytes that may be used for the validation and proof-of-concept analysis.

5.2.3 Reporting Requirements

Reporting frequency for results from the Shoal monitoring program will vary during the initial stages of the program. It is envisioned that the reporting frequency will eventually stabilize to match the annual frequency of actual monitoring events. An initial report will be completed and submitted to NDEP after completion of the monitoring wells and will discuss findings that resulted from drilling, well completion, and well development. Hydraulic head measurements initially will likely occur more frequently than once a year, as discussed in Section 5.2.1. However, two or more episodes of hydraulic head measurement will be necessary to establish

Table 5-7
Additional analytes

Analyte	Analytical Method	Container Type	Preservative	Filtration	Holding Time	Required Detection Limit
Cations						
Calcium Magnesium Potassium Sodium	SW-846 6010B	1 liter[a], amber glass or polyethylene	HNO_3 to pH<2[a], Cool/Ice to 4°C	Filtered	6 months[a]	1,000 (µg/L)[b]
Anions						
Bicarbonate Carbonate	EPA 310.1[d]	1 liter[a] polyethylene	Cool/Ice to 4°C	Nonfiltered	14 days[a, d]	1,000 (µg/L)[c]
Chloride	EPA 300.1[e]			Filtered	28 days[a, e]	250 (µg/L)[c]
Sulfate	EPA 300.1[d]					1,000 (µg/L)[c]
Age and Migration Parameters						
$^{18/16}$Oxygen	Mass spectrometry	125-mL glass	None	Nonfiltered	180 days	+/- 0.2 per mil (precision)
Deuterium/ Hydrogen	Mass spectrometry	10-mL glass Polyseal lids	None	Nonfiltered	Indefinitely	+/- 1.0 per mil (precision)

[a]USEPA Test Methods for Evaluating Solid Waste, 3rd Edition, Parts 1-4 (EPA, 1996)
[b]USEPA Contract Laboratory Program Statement of Work for Inorganic Analysis, Multi-Media, Multi-Concentration, ILM04.0, EPA/540/R-95/121. Washington, DC. (EPA, 1995)
[c]Laboratory-specified detection limit
[d]Methods for Chemical Analysis of Water and Waste, EPA/600/4-79/020. 1983. Washington, DC. (EPA, 1983)
[e]Determination of Inorganic Anions in Drinking Water by Ion Chromatography, EPA/600/R-98/118. 1997. Cincinnati, Ohio. (EPA, 1997a)
µg/L = Micrograms per liter
mL = Milliliter

post-development trends in the immediate vicinity of the new monitoring wells, so an annual reporting frequency will suffice to provide NDEP with useful data within the local and regional context of Shoal. If noteworthy or unexpected results are discovered during the period of time that the new monitoring wells are equilibrating with local hydrologic conditions, these would be reported to NDEP as special reports. Once the monitoring wells are completed, developed, and have achieved equilibration within the context of the local hydrology, an annual reporting frequency in conjunction with the annual testing frequency will be observed. These data will be reported to NDEP in the form of a letter report, and will include any charts and/or data tables necessary to accurately represent monitoring results.

5.2.4 Evaluation and Evolution of Monitoring Network through Time

Data collected from the monitoring network will be used to determine compliance with the CAU compliance boundary in terms of contaminant concentrations, and to monitor the hydraulic system relative to the steady-state assumption. Analysis of the data relative to the range of

values used in the groundwater modeling is part of the validation and proof-of-concept work, described in detail in Section 5.5.

The data evaluation for monitoring the compliance boundary will entail comparison of radionuclide concentrations measured in groundwater samples from the wells to regulatory limits. The range of values expected for each analyte from the numerical modeling are all below the MCL for the next 100 years. Well HC-4 has detectable tritium and ^{14}C (no ^{129}I analysis has been performed). Values of tritium have ranged from 220 +/- 139 pCi/L (in 2001) to 863 +/- 158 pCi/L (in 1997), as reported by the USEPA's Long Term Hydrologic Monitoring Program (EPA, 1997b; 2001). Sampling during site characterization indicates a ^{14}C concentration of approximately 7 pCi/L, based on an activity of 733 disintegrations per minute per gram of carbon (DPM/gC). Water produced during drilling, development, and hydraulic testing will be monitored and reported as part of the Fluid Management Plan. Trends will be tracked in the long-term monitoring data to reveal systematic changes in radionuclide concentration in the monitoring wells, in addition to comparison to regulatory limits.

Hydraulic head will be used to monitor the quasi steady-state condition of the groundwater system (i.e., to determine if mean hydraulic head values remain constant through time, given fluctuations caused by natural temporal stresses and stresses related to well drilling, construction, and testing). This requires first determining when heads have stabilized following drilling and testing activities, then quantifying the natural mean and temporal variation in hydraulic head, and finally comparing subsequent monitoring measurements to that range. The frequency of measurement will be dictated by the recovery behavior. As recovery progresses, the stabilized hydraulic head in the wells will be estimated using methods described in ASTM D 4750. Determining the mean and variation will encompass data collection during and after recovery from the drilling and testing operations and evaluation of well efficiency at responding to the periodic stresses of earth tides and barometric pressure fluctuations over a period of at least one year. Once the data indicate that heads have reached quasi steady-state and the range of head variation is determined, the third phase will begin and entail comparison of subsequently collected head data to the range identified in the second step.

Gaining stabilized heads may be a long-term process. Monitoring water levels in the HC wells has demonstrated continued recovery from drilling and testing activities (Figure 5-23). As of June 11, 2004, the water level in HC-1 was at an elevation of 1,298.7 m AMSL. Note that this elevation includes a substantial correction for borehole deviation; the raw elevation is 1,292 m AMSL. Borehole deviation for the existing wells, and the procedure for correcting water levels to true elevation, is documented in Appendix B. The pump configuration in HC-4 prevents

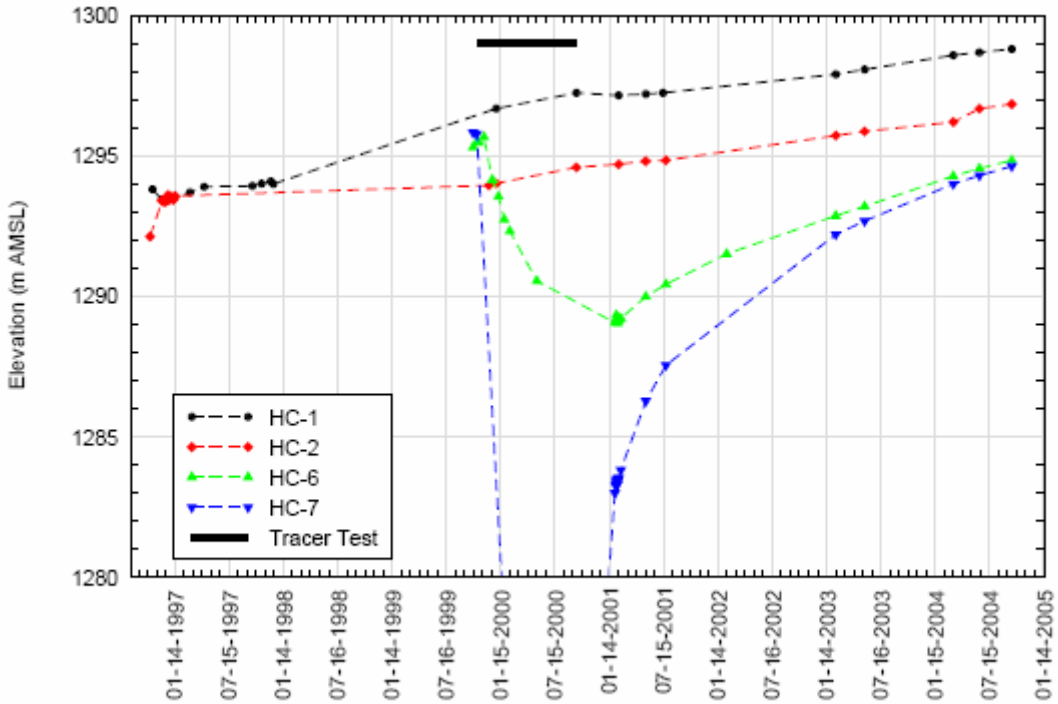

Figure 5-23
Water levels measured in Shoal wells located west of the shear zone

routine water level measurements. The head at HC-4 was at an elevation of 1,289.5 m AMSL before the year 2000. The range of hydraulic head predicted by the model at the new well locations is shown in Figure 5-24. The mean head predicted at the planned completion elevation of the new monitoring wells is approximately 1,288.2 m AMSL for MV-1; 1,287.7 m AMSL for MV-2; and 1,287.9 m AMSL for MV-3. The 95 percent confidence interval around these mean values is shown in Figure 5-24. Evaluation of the measurements relative to these distributions is part of the model validation process and is described in detail in Section 5.5.

The fluctuations encountered in a well while the groundwater system is at quasi steady-state are distinct from the range in hydraulic head predicted by the model, with the model range resulting from heterogeneity and uncertainty in the modeling process. From July 2002 to July 2004, the maximum water level change was about 2.5 m and the rate of water level recovery is decreasing over time as shown in Figure 5-23. Given that the uncertainty range predicted by the model is about 15 m (Figure 5-24), the use of the quasi-steady state head during the 5-year proof-of-concept period and the incremental change in heads are much smaller than this uncertainty range and thus are not expected to significantly influence the results of the validation analysis.

The periodic fluctuations relevant for defining quasi steady-state are due to earth tides and barometric pressure changes, with measurement precision also playing a role. In addition, there are sporadic impacts from seismic events. As defined in Table 5-6, a precision of ± a tenth of a foot (3 cm) will be achieved for the hydraulic head measurements. Water wells in Frenchman Flat at NTS experienced hydraulic head fluctuations on the order of 0.4 feet (ft) due to earth tides and 1 ft due to barometric effects (Bright et al., 2001). Barometric effects can be larger in response to especially strong storms. The range in periodic fluctuation will be reported to NDEP with the quasi steady-state mean value for each well, based on observations during the first year (assuming steady-state is obtained in a year). Future monitoring data outside of that range will trigger investigation of external causes (e.g., earthquakes) and trend analysis.

Because the monitoring network is based on the groundwater model, evaluating the network through time involves continued validation of the model. This post-closure validation will be provided by the hydraulic head measurements. Evolution of the monitoring network through time is expected in terms of the analytical suite. Once baseline values for ^{14}C and ^{129}I are established, analysis of these nuclides may be deferred for several decades. In later time, tritium with its short half-life will cease to be a useful target and monitoring will shift to the longer-lived nuclides of ^{14}C and ^{129}I. Significant changes to the monitoring system will be presented for NDEP concurrence.

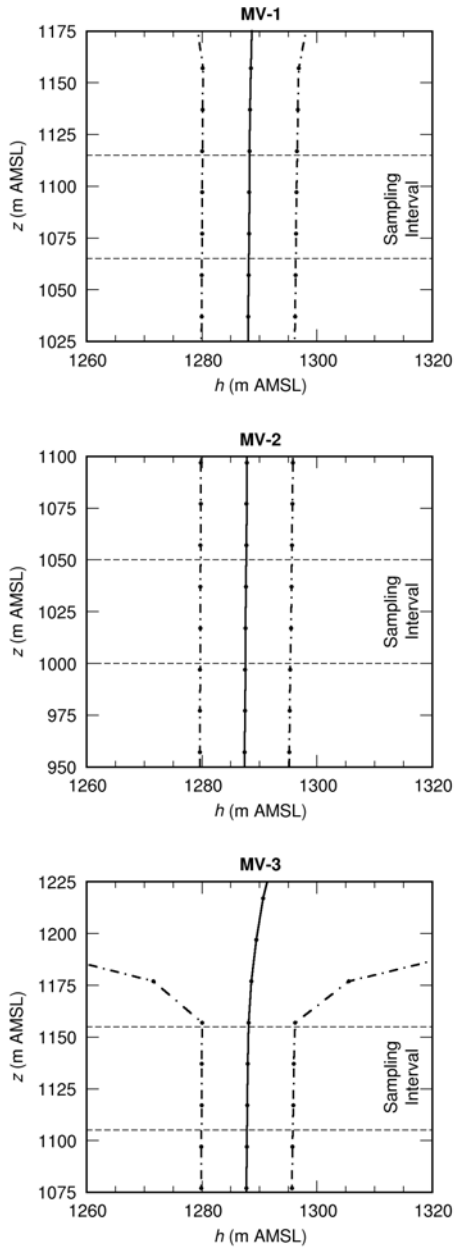

Note: Head values represent hydraulic head for a 20 m^3 cell of the model. Dashed lines show the 95 percent confidence interval.

Figure 5-24
Hydraulic head range predicted by the flow model for the proposed well locations

5.3 Waste Management

Activities that may generate investigation-derived waste (IDW) include the drilling and construction of new wells, sampling and monitoring of new and existing wells, well development, geophysical logging, and hydrologic/aquifer testing. Management of IDW will be based on regulatory requirements, field observations, process knowledge, and the results of laboratory analysis of PSA investigation samples. Sanitary, hazardous, radioactive, and/or mixed waste, if generated, will be managed and disposed of according to DOE Orders, U.S. Department of Transportation regulations, RCRA regulations, state and federal waste regulations, and agreements and permits between the DOE and NDEP. Applicable waste management regulations and requirements are listed in Table 5-8.

Table 5-8
Waste management regulations and requirements

Waste Type	Federal Regulation	Additional Requirements
Solid (nonhazardous)	N/A	NRS 444.440 – 444.645[a] NAC 444.570 – 444.7499[b]
Hazardous	RCRA[c]	NRS 459.400 – 459.600[a] NAC 444.850 – 444.8746[b] POC[d]
Low-Level Radioactive	N/A	DOE Orders and NTSWAC[e]
Mixed	RCRA[c]	NTSWAC[e] POC[d]
Hydrocarbon	N/A	NAC 445A.2272(b)[b]

[a]*Nevada Revised Statutes* (NRS, 2003a and b)
[b]*Nevada Administrative Code* (NAC, 2004a and b)
[c]*Resource Conservation and Recovery Act* (CFR, 2003a)
[d]*Performance Objective for the Certification of Nonradioactive Hazardous Waste* (BN, 1995)
[e]*Nevada Test Site Waste Acceptance Criteria* (NTSWAC), Revision 5 (NNSA/NSO, 2003b)

N/A=Not Applicable

5.3.1 Waste Minimization

Corrective action investigation activities have been planned to minimize IDW generation. All IDW will be segregated to the greatest extent possible. Use of hazardous materials will be minimized to limit unnecessary generation of hazardous and/or mixed wastes. Decontamination activities will be planned and executed to minimize the volume of rinsate.

5.3.2 Potential Waste Streams

Depending on COPCs, the types of IDW that may be generated include low-level radioactive waste (LLW), mixed wastes (LLW and hazardous waste), hydrocarbon waste, hazardous waste,

and sanitary waste. IDW typically generated during investigation activities may include one or more of the following:

- Environmental media (e.g., groundwater, drilling fluids and cuttings, soil)
- Decontamination rinsate
- Development and sample purge water
- Personal Protective Equipment (PPE) and disposable sampling equipment (e.g., plastic, paper, sample containers, aluminum foil, spoons, bowls)
- Field-screening waste (e.g., groundwater, rinsate, spent solvent, disposable sampling equipment, and PPE contaminated by field-screening activities)

All waste from PSA investigative areas will be evaluated against radiological standards as no RCRA constituents have been identified. However, should hazardous waste be generated from field sample kits, fuel spills, or waste brought onto the site, it will be managed according to RCRA, NDEP, and internal procedures. Each waste stream generated will be segregated to the greatest extent possible.

5.3.3 Fluid Management

Fluids will be managed according to a PSA Fluid Management Plan that is approved by NDEP. Fluids found to meet fluid management criteria (i.e., less than or equal to five times the SDWA MCLs) may be released to the ground surface. Fluids that do not meet fluid management criteria will be managed according to applicable regulatory requirements and DOE Orders. If fluid is encountered that contains radionuclides approaching established health and safety or air quality limits (such as those listed in the National Emissions Standards for Hazardous Air Pollutants), drilling will stop until a management strategy is developed.

5.3.4 Personal Protective Equipment/Equipment

Disposable sampling equipment, PPE, and rinsate are considered potentially contaminated waste only by virtue of contact with potentially contaminated media (e.g., drill cuttings) or potentially contaminated water. PPE, disposable sampling equipment, and debris will be visually inspected for gross contamination (e.g., clumps of soil/sludge) and will be segregated as it is generated. Grossly contaminated PPE/equipment that comes in contact with hazardous waste, should any be encountered, will be managed as potentially “characteristic” hazardous waste. This segregated waste will either (1) be assigned the characterization of the contaminated material that was sampled, (2) be sampled directly, or (3) undergo further evaluation using the contaminated media

sample results to determine how much contaminated media would need to be present in the waste to exceed regulatory levels. The PPE/equipment that is not visibly stained, discolored, or grossly contaminated will be managed as it is generated as nonhazardous waste and disposed of as sanitary or LLW depending on the concentration of radioactive contamination, if present.

5.3.5 Rinsate

Decontamination activities will be performed according to approved contractor procedures specified in the contractor field instructions and as appropriate for the COPCs at PSA. Decontamination rinsate will initially be evaluated using analytical results for samples associated with the rinsate (i.e., soil sample results from borehole or sampling activities associated with the generation of rinsate). Decontamination rinsate at this site will not be considered hazardous waste unless there is evidence that it may exhibit a RCRA characteristic. Evidence may include such things as hazardous constituents in associated samples, the presence of a visible sheen, pH, or association with equipment/materials used to respond to a release/spill of a hazardous waste/substance. If determined to be hazardous, the rinsate will be managed and disposed of according to the requirements of RCRA.

5.3.6 Soil

This waste stream consists of cuttings produced during drilling. This waste stream is considered to have the same COPCs as the material remaining in the ground. Regardless of the COPCs at the site, the preferred method for managing this waste form is to place the material back into the borehole or excavation, berming, and covering the material next to the excavation pending contouring and/or revegetation, or by placement in a container(s). Containerized soil will be characterized, managed, and disposed of according to federal and state requirements.

5.3.7 Investigation-Derived Waste Management

Process knowledge indicates that the drilling locations within the PSA investigative area may (but are not expected to) be contaminated with radioactive constituents. To allow for the segregation of radioactive and “nonradioactive” waste and materials, radiological swipe and/or direct surveys may be conducted on reusable sampling equipment, PPE, and disposable sampling equipment waste streams exiting from within the controlled area. Removable contamination limits, as defined in Table 4-2 of the current *NV/YMP Radiological Control* (RadCon) *Manual* (DOE/NV, 2000a), shall be used to determine if such materials may be declared “nonradioactive.” Management requirements for sanitary, low-level, hazardous, or mixed wastes are discussed further in the following sections.

5.3.7.1 Sanitary Waste

Sanitary waste will be packaged in plastic bags or an appropriate receptacle and will be transported to a solid waste management unit. The IDW generated within a radioactive controlled area will be swiped and/or surveyed as appropriate, to determine if the removable contamination is under the limits defined in Table 4-2 of the current NV/YMP RadCon Manual (DOE/NV, 2000a). The IDW will be characterized as radioactive or nonradioactive based on these results.

5.3.7.2 Hydrocarbons

The action level for soil contaminated with hydrocarbons is 100 milligrams per kilogram (mg/kg) in the State of Nevada, as specified in *Nevada Administrative Code* (NAC) 445A.2272 (NAC, 2003). Soils and associated IDW with hydrocarbon levels above 100 mg/kg, provided other regulated constituents are below regulatory limits, shall be managed as hydrocarbon waste and disposed of in accordance with all applicable regulations.

5.3.7.3 Hazardous Waste

Hazardous waste accumulation areas (HWAAs) and/or satellite accumulation areas (SAAs) will be established to accumulate waste that may be hazardous. The HWAAs will be properly controlled for access and will be equipped with spill kits and appropriate spill containment. All containers in HWAAs will be managed consistent with the requirements of 40 CFR 265 Subpart I (CFR, 2003a). A “Hazardous Waste Pending Analysis” marking will be placed on the waste containers until waste characterization is complete. Once the waste is characterized, containers of waste determined to be hazardous will be clearly marked or labeled as “Hazardous Waste.” The HWAAs will be inspected weekly and will be covered under a site-specific emergency response plan until the waste is determined to be nonhazardous or all containers of hazardous waste have been removed from the accumulation area. The SAAs, if established, will be managed in accordance with 40 CFR 262.34(c) (CFR, 2003a). The SAAs may be employed to temporarily accumulate waste associated with field-screening methods (e.g., field test kits) or for IDW pending characterization. These waste management methods will be appropriate for the amount of waste being accumulated.

5.3.7.4 Low-Level Waste

The IDW may be characterized incorporating the use of process knowledge, analytical results of direct or associated samples, visual examination, radiological surveys, and swipe results. Radiological swipe surveys and/or direct scan surveys may be conducted on reusable sampling equipment and the PPE and disposable sampling equipment waste streams exiting a

radiologically controlled area. This allows for the immediate segregation of radioactive waste from waste that may be unrestricted regarding radiological release. Removable contamination limits, as defined in Table 4-2 of the current version of the NV/YMP RadCon Manual (DOE/NV, 2000a), may be used to determine if such waste may be declared unrestricted regarding radiological release versus being declared radioactive waste. Direct sampling of the waste may be conducted to help determine if a particular waste unit (e.g., drum of soil) contains LLW, as necessary. Waste that is determined to be below the values of the RadCon Manual, Table 4-2, by either direct radiological survey/swipe results or through process knowledge will not be managed as potential radioactive waste, but will be managed in accordance with the appropriate section of the site-specific documents. Waste in excess of NV/YMP RadCon Manual, Table 4-2 values (DOE/NV, 2000a), will be managed as a potential radioactive waste. Suspected LLW will be managed in accordance with the contractor-specific waste certification program, contractor-specific procedures, and the Nevada Test Site Waste Acceptance Criteria (NTSWAC) (NNSA/NSO, 2003b). The IDW will be staged at a designated Radiological Controlled Area or Radioactive Materials Area pending certification and disposal under NTSWAC requirements (NNSA/NSO, 2003b). Waste drums will be labeled “Radioactive Material Pending Analysis.”

5.3.7.5 Mixed Wastes

Mixed waste, if generated, shall be managed in accordance with RCRA (CFR, 2003a) and State of Nevada requirements. These regulations, as well as DOE requirements for radioactive waste, are interpreted as follows. Where there is a conflict in regulations or requirements, the most stringent shall apply. For example, weekly inspections per RCRA regulations will be applied to mixed waste even although it is not required for radioactive waste. In general, mixed waste shall be managed in the same manner as hazardous waste, with additional mandatory radioactive waste management program requirements. Mixed waste shall be transported via an approved waste transporter to the NTS transuranic waste storage pad for storage pending treatment or disposal.

5.3.7.6 PCB and Radioactive PCB Wastes

Polychlorinated biphenyls (PCBs) are governed by the *Toxic Substances Control Act* and its implementing regulations in 40 CFR 761 (CFR, 2003c). No PCB contaminated waste is anticipated during this project. If any type of PCB waste is generated, it will be managed according to 40 CFR 761, or subject to agreements between U.S. Department of Energy, National Nuclear Security Administration Nevada Site Office (NNSA/NSO) and NDEP.

5.4 Required Authorizations, Notifications, and Permits

Several State of Nevada and Federal permits and studies must be completed before drilling begins at PSA. The surface activities in different parts of PSA are administered by the BLM and the U.S. Navy, which are required to administer the *Endangered Species Act* and the *National Antiquities Act*. These acts, and NEPA, require that a biological surface survey and an archeological surface survey respectively be completed before any surface disturbing activities, such as the construction of the access roads, drill pads, and containment ponds that will be necessary for installing monitoring wells. The State of Nevada Division of Water Resources requires a "Request for Waiver to Drill Observation or Monitoring Well" to be completed before drilling any water quality monitoring well. The Water Resources Board also requires an "Affidavit of Intent to Abandon a Monitoring Well" to be completed and submitted with each waiver for a monitoring well. Any well that is abandoned must be plugged and abandoned in accordance with NAC 534.4365 (NAC, 1998). If a public water source, such as a well located on or near PSA, is intended to be used for either drilling purposes or for dust abatement measures, then a temporary water use application form must also be completed. Before initiating surface construction activities (i.e., building access roads, well pads, and fluid sumps), NNSA/NSO will obtain a Surface Area Disturbance Air Quality Operating Permit in accordance with NAC 445B.22037 (NAC, 2005).

5.5 Proof-of-Concept

The recommended corrective action for the Shoal site is based in large part on the results of numerical models of groundwater flow and radionuclide transport. Many uncertainties are inherent in these models, and most stem from the inability to precisely know the conditions everywhere in the subsurface. In response to these uncertainties, the FFACO prescribes a validation and proof-of-concept period for groundwater models used in closing underground nuclear test sites.

The description of the proof of concept process is given in Rev. 1, 2000 of the FFACO in the process flow diagram dictionary for the UGTA CAUs. It is as follows:

> A five-year proof of concept monitoring network will be developed in accordance with the CAP. This phase of monitoring will use groundwater wells in a monitoring network to determine if the monitoring network design will provide adequate CAU surveillance. Measurements of field parameters will be used to demonstrate that the model is capable of making reasonable predictions that fall with an acceptable level of confidence.

> Model validation, to ensure fidelity of the model to the physical system, will use a ten-step protocol to demonstrate that a model has been developed that meets user needs. These ten steps are: (1) establishment of model purpose, (2) development of conceptual model, (3) selection of a computer code and verification of code, (4) model design, (5) model calibration, (6) sensitivity and uncertainty analysis, (7) model verification, (8) predictive simulations, (9) presentation of model results, and (10) postaudit.
>
> The validation postaudit step tests whether the model can predict future system behavior. The five-year proof-of-concept is the model postaudit to establish, within a longer time frame, that the model is capable of producing meaningful results with an acceptable degree of uncertainty. Model validation is substantiated once all ten steps are shown to have been acceptably completed.

In their acceptance of the CAU model, NDEP expressed concern regarding uncertainty in the input data. Explicit concern is expressed regarding the absence of verification data in the direction of flow (the model was verified using data from wells HC-6 and HC-7). In addition, NDEP states that future documents need to quantify the reduction in model uncertainty achieved through the prior field investigations and to quantify the effects of remaining uncertainty in the input parameters and in the location of the predicted contaminant boundary (Maize, 2004).

As described in Section 2.2, the confidence level calculated for the contaminant boundary quantifies the effect of uncertainty in the input parameters on the location of the contaminant boundary. This reflects the total, combined, uncertainty. A substantially different modeling approach (incorporating more uncertainty and performing realization-specific calibration) was employed for the approved model, so there is no consistent basis for quantifying the reduction in model uncertainty resulting from the fieldwork. As no value is obvious from such an analysis in terms of defining site closure, it is interpreted that the underlying motivation of the request by Maize (2004) is an evaluation of the contributions of individual parameters to the remaining uncertainty in an effort to evaluate the sufficiency of the characterization. This evaluation forms the basis here for determining which parameters are optimum model validation targets. The NDEP's concern regarding the spatial distribution of verification data, as well as monitoring needs, are used to guide the location for validation investigations.

The proof-of-concept phase for Shoal focuses on model validation. This is consistent with the post-audit specified in the FFACO, which is to establish, within a longer time frame, that the model is capable of producing meaningful results with an acceptable degree of uncertainty. Given the steady-state nature of the flow model and the relatively slow transport predicted for

the site, the model's ability to predict future system behavior must be tested based on its ability to represent the subsurface. The requirement to present mechanisms for revisiting the model is also consistent with the validation strategy presented in the FFACO, which is based on the iterative approach to developing and improving models recommended by Anderson and Woessner (1992).

5.5.1 Strategy

The proposed approach to validate the Shoal model relies on using both multi-response data and diverse statistical tests to evaluate model performance. The approach follows a systematic step-by-step adaptive strategy and is aimed at building confidence in the model predictions (Hassan, 2004a and b). Even the simplest deterministic subsurface model is very difficult to evaluate. The proposed plan accounts for the stochastic nature of the Shoal model and aims to reduce the uncertainty inherent in the large number of realizations considered in the Monte Carlo analysis (Hassan, 2004c).

The focus of the proposed validation methodology is centered around the following three main themes: (1) testing how predictions of numerical groundwater flow and transport models of Shoal and the underlying conceptual models and assumptions are robust and consistent with regulatory purposes, and (2) reevaluating and refining model predictions and reducing the uncertainty level based on data collected in the proposed field activities for model validation.

5.5.1.1 Proposed Step-by-Step Procedure for Shoal Model Validation

Figure 5-25 displays the step-by-step approach for performing the validation and postaudit processes for the Shoal model. There is one clearly defined point in the validation process where a significant revision of the model can be triggered. This trigger point occurs at Step 6, where the results may be determined to not meet regulatory objectives. All of the validation steps are described below.

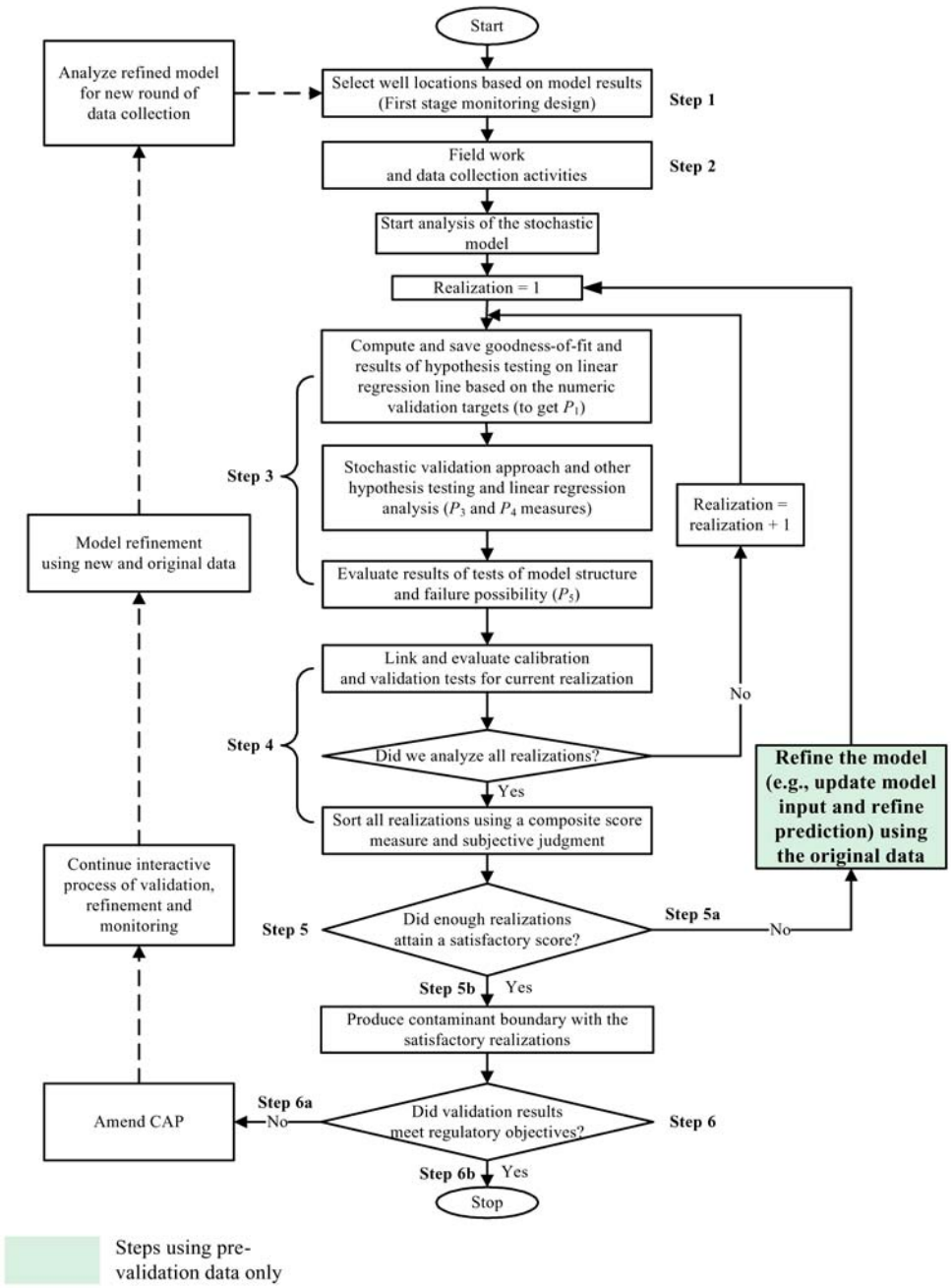

Note: Selection criteria measures (P_1 through P_5) are explained in Section 5.3.

Figure 5-25
Detailed flowchart of the proposed model validation and postaudit processes for the Shoal model (from Hassan, 2005)

Step 1: Identify the data needed for validation, the number and location of the wells, and the type of laboratory or field experiments needed. Well locations can be determined based on the existing model and should favor locations likely to encounter fast migration pathways. The

monitoring design process helps select these locations, as well as the concern by NDEP for verification data in the direction of flow (Maize, 2004). Other factors such as the location of the contaminant and compliance boundaries, and the cost of drilling and collecting data have to be considered. Sequencing of data collection is also important, as is the ability to adjust the plan as information is gathered.

Step 2: Carry out the fieldwork to install the wells and obtain the largest amount of data possible from the wells. The data should include geophysical logging, head measurements, conductivity measurements, concentrations (e.g., checking for tritium or ^{14}C), and any other information (e.g., temperature logs, fracture information) that could be used to test the model structure, input, or output.

Step 3: Perform the different validation tests that will help evaluate the different submodels and components of the model. The stochastic validation approach proposed by Luis and McLaughlin (1992) can be adapted and used to test the flow model output (heads) under saturated conditions. Other objective tests (e.g., goodness-of-fit tests) can be used for the heads to complement this stochastic approach that is based on hypothesis testing. Some data will be used to check the occurrence or lack thereof of failure scenarios (e.g., whether tritium or ^{14}C exists much farther from the cavity than is predicted by any realization of the stochastic Shoal model). The philosophy here is to test each individual realization with as many diverse tests (in terms of the statistical nature of the test and the tested aspect of the model) as possible and have a quantitative measure of the adequacy of each realization in capturing the main features of the modeled system. It is important to note that goodness-of-fit results and other statistical results for the current realization will be used after analyzing all realizations to obtain some of the acceptance criteria measures, P_1 through P_5, which are discussed in detail in Section 5.3.

Step 4: Link the results of the calibration accuracy evaluations performed during the model building stage and the validation tests (Step 3) for all realizations and sort the realizations in terms of their adequacy and closeness to the field data. A subjective element may be invoked in this sorting based on expert judgment and hydrogeologic understanding. The objective here is to filter out the realizations that show a major deviation or inadequacy in many of the tested aspects and focus on those that “passed” the majority of the tests and evaluations. By doing so, the range of output uncertainty is reduced and the subsequent effort can be focused on the most representative realizations/scenarios. To continue reducing the uncertainty level, a refinement of the conductivity or other input distribution can be made based on information collected from the validation wells. More details about the acceptance criteria for individual realizations and for the conceptual model are presented in Appendix D.

Step 5: Step 4 results will determine the forward path and guide the decision as to whether there is a sufficient number of realizations that attained a satisfactory high score (thus building confidence in the original model) and are considered sufficient for further analysis or whether this number of realizations is not sufficient in comparison to the realizations with low scores indicating that the original flow and transport models or their input parameter distributions need adjustment.

5a. If the number of realizations with low scores is very large compared to the total number of model realizations (The P_1 measure discussed in Section 5.3), it could be an indication that the model has a major deficiency or conceptual problem or it could be that the input is not correct. In the latter case, it may be that the model is conceptually good, but the input parameter distributions may be skewed one way or another. Generating more realizations and keeping those that fit the validation criteria can shift the distribution to the proper position. This can be done using the existing model without conditioning or using any of the new validation data. If the model has a major deficiency or conceptual problem, generating additional realizations will not correct it and continued failure per the validation criteria (see Section 5.3) will be obvious. Bredehoeft (2003) discusses the importance of the distinction between conceptualization problems and inappropriate input distributions. He states that one should carefully ask the question of whether the mismatch between the model and the field observations is a result of poor parameter adjustments or whether the conceptual model needs to be rethought. The use of different metrics such as P_1 and P_2 discussed in Section 5.3 provides a tool for making this distinction.

5b**.** If the number of realizations with high scores is found sufficient, this indicates that the model does not have any major deficiencies or conceptual problems. This determination will be made according to a number of metrics as detailed in the validation criteria section. These metrics are tested and supported by statistical hypothesis testing and provide good evaluation criteria for the model realizations. Based on the realizations retained in the analysis and deemed acceptable, a contaminant boundary will be calculated and compared to the original contaminant boundary. Decision makers will present this comparison for reference in Step 6.

Step 6: Once the model performance has been evaluated per the acceptance criteria, the model sponsors and regulators have to answer the last question in Figure 5-25. This question will determine whether the validation results meet the regulatory objectives or not. This is the trigger point that could lead to significant revision of the original model.

6a. If the answer to the question posed is no, then the left-hand side path in Figure 5-25 begins with an evaluation of the investigation strategy, consistent with the process flow diagram in Rev. 1, 2000 of the FFACO. If the original strategy is deemed sound, a new iteration of model development will begin, using the data originally collected for validation, and steps 1 to 6 will be eventually repeated. Whatever strategy is selected, the CADD/CAP will be amended before execution.

6b. If the answer to the question posed is yes, validation is deemed sufficient and the model is considered adequate or robust.

Numerical groundwater models, and in particular stochastic models, are very complex and modifying or changing any aspect of the model may produce unanticipated consequences in a different aspect of the model. To get the best outcome of the validation process, one needs to both consider the different details separately and take the broader view of the entire model while working step-by-step through the different decisions and trade-offs.

It can be seen and expected that the process of validating a site-specific groundwater model is not an easy one. Throughout the structured process described above, there may be a desire to confirm that the work is on the right track. The way to this confirmation is the cumulative knowledge gained from the different stages of the validation process. That is, a set of independent tests and evaluations will provide knowledge about the model performance, and the test results will provide some incremental, but additive, pieces of information that will be of importance. While there are no guarantees of success (attaining a conclusive outcome about model performance), the combined presence of these different results and evaluations sharply improves the odds that one can make a good decision about the model performance.

Two aspects of the validation process are explained in the following subsections. These are the validation targets for the Shoal model, and the acceptance criteria for determining the sufficiency of the number of acceptable realizations. It should be emphasized here that the proposed validation targets and the acceptance criteria depend on the type of data that can be obtained and the practicality of collecting certain types of information. In other words, from a statistical point of view, one would desire to obtain a large number of head measurements for example, but the practical limitations may render this desire unrealistic. Therefore, the tools and tests to be used and the targets to be analyzed must consider the role they play in the model as well as practical considerations.

5.5.1.2 Implementation of Step 1 in the Procedure for Shoal Model Validation: Selection of Validation Targets

To select the validation targets at Shoal, and to respond to the NDEP request for additional quantification of input parameter uncertainty (Maize, 2004), a multi-parameter uncertainty analysis was performed to identify the sensitivity of contaminant boundaries to various parameters. One should distinguish between sensitivity analysis and uncertainty analysis. Sensitivity analysis is the systematic investigation of the model responses to extreme values of the model input or to drastic changes in the model structure (Kleijnen, 1999). Sensitivity analysis can support validation: such analysis shows whether factors have effects that agree with the modeler's prior qualitative knowledge (for example, faster transport rates result from lower fracture porosity). Unfortunately, not all subsurface processes have effects with known signs; yet, many do have factors with known signs. Sensitivity analysis further shows which factors are important.

Related to sensitivity analysis is uncertainty analysis. Uncertainty analysis also runs a simulation model for various combinations of input parameter values. Uncertainty analysis is performed when the input parameter values of the simulation model are not accurately known, and thus uncertainty analysis samples from a pre-specified probability distribution for these parameters. The simulation results for uncertainty analysis are commonly presented as ranges of values with associated probabilities or confidence intervals. Uncertainty analysis can be performed for individual parameters and for combinations of parameters. When it is desired to determine the impact of uncertainty in an individual parameter on the model output, the input values for that parameter are generated from its respective probability distribution while keeping all other model parameters at fixed values. In a combined parametric uncertainty analysis, all uncertain model parameters are simultaneously sampled from their respective probability distributions.

The numerical model of groundwater flow and transport at Shoal requires quantitative descriptions of numerous aspects of the conceptual model including fracture geometry and hydraulic properties, groundwater recharge, matrix diffusion, and rates of radionuclide release from glass puddles in the cavity. All of these components contribute to the transport predictions, but the most critical are those that determine the pattern and magnitude of groundwater velocities and, as a consequence, influence the travel times of radionuclides away from the cavity. Large-scale flow and transport models have shown that the results of radionuclide transport calculations are most profoundly impacted by parameters that affect travel time (Pohll et al., 1999a; Pohlmann et al., 1999; Hassan et al., 2002). Naturally, all of the flow and transport parameters are subject to the uncertainties that are always present when representing subsurface conditions. These parametric uncertainties are incorporated and carried through the

Shoal numerical modeling process, and are therefore ultimately included in predictions of the contaminant boundaries.

Although the Shoal model presented by Pohlmann et al. (2004) analyzed combined parametric uncertainty, sensitivity of the transport predictions to individual parameter uncertainties was not assessed. Thus, the following analysis presents the results of individual parametric uncertainty analysis and the impact on an estimated contaminant boundary for ^{14}C. Carbon-14 is selected because of the long half-life (thus minimum decay in the 1,000 year regulatory time frame) and because it does not adsorb onto the solid matrix thereby representing one of the main elements determining the shape and extent of a contaminant boundary (Pohll et al., 2003). The use of ^{14}C in this analysis will yield contaminant boundaries that are similar to, but not identical, to the contaminant boundary calculated using the entire test inventory by Pohll and Pohlmann (2004). Note that the ^{14}C boundary analysis presented here is based on the regulatory MCL of 2,000 pCi/L.

The components of the Shoal groundwater flow and transport model that incorporate uncertainty are listed below. It should be noted that the shear zone and hydraulic divide are considered to be no-flow boundaries with known geometry and are therefore treated as deterministic aspects of the model (Pohlmann et al., 2004).

- Orientation of fracture zones
- Spatial continuity of fracture zones
- Hydraulic conductivity of fracture zones
- Hydraulic conductivity of intervening zones of small random fractures
- Hydraulic conductivity of the cavity and damaged zone
- Recharge from precipitation entering the top surface of the model
- Flux originating from upland recharge that enters the up-gradient vertical face of the model
- Porosity of fracture zones
- Porosity of the cavity
- Porosity of the damaged zone around the cavity

- Rate of nuclear glass dissolution in the cavity
- Diffusion of radionuclides between fractures and matrix

All these parameters were explicitly considered uncertain in the Shoal model analysis except the hydraulic conductivity of intervening zones of small random fractures that was considered as a calibration parameter and the matrix diffusion parameter that was spatially and temporally varying (Pohlmann et al., 2004). Although a statistical distribution for the hydraulic conductivity of the intervening small fractures is not directly specified, it is indirectly handled as an uncertain parameter via the automated calibration process. Similarly, the matrix diffusion parameter was varying in space and in time based on the spatial variability of the velocity field and the residence time of each particle in the fractures (implicitly uncertain). However, it was based on deterministic values of the fracture spacing, the fracture retardation, the matrix retardation, fracture porosity, matrix porosity, and molecular diffusion coefficient. These values were obtained by calibrating the transport model to the Shoal tracer test data (see Appendix D in Pohlmann et al. [2004] for more details.)

Hereafter, Pohlmann et al.'s (2004) model is referred to as the base case model. Not all of the model parameters listed above are included in the individual parametric uncertainty analysis. The flux from the upgradient face, the nuclear melt glass dissolution rate, and the calibration parameter of hydraulic conductivity of small fracture zones all have limited usefulness as model validation targets because they would be difficult to quantify even with further fieldwork. Other parameters included in the individual uncertainty analysis that are similarly ill-suited for validation are the conductivity of the cavity and damaged zone, porosity of the cavity and damaged zone, and length of fracture zones. For example, the lengths of fracture zones have been extensively studied through geologic mapping of the land surface at Shoal. It is therefore unlikely that further data collection would provide information that differs from the model because virtually all of the visible fractures have been mapped. Therefore, five flow parameters and four transport parameters are selected to perform the individual parametric uncertainty analysis. Table 5-9 shows the nine cases and the notation used in the results discussion presented in Appendix C.

Table 5-9
Uncertainty cases for five flow parameters and four transport parameters. Two flow realizations are selected to run the transport parameter uncertainty analyses: a) one of the fastest realizations in the base case model, and b) the realization with the least RMSE in the base case model.

	Parameters									
Case	**Fracture Orientation (both orientations)**	**Fracture Length (both orientations)**	**Cavity *K* (all 3 zones)**	**Fracture *K***	**Recharge**	**Fracture Porosity**	**Cavity Porosity**	**Damage Zone Porposity**	**Matrix Diffusion**	**Comments**
1	**Uncertain**	Fixed	Fixed	Fixed	Fixed	Fixed	Fixed	Fixed	Fixed	Uncertain flow parameters that require generating 500 flow realizations each
2	Fixed	**Uncertain**	Fixed	Fixed	Fixed	Fixed	Fixed	Fixed	Fixed	
3	Fixed	Fixed	**Uncertain**	Fixed	Fixed	Fixed	Fixed	Fixed	Fixed	
4	Fixed	Fixed	Fixed	**Uncertain**	Fixed	Fixed	Fixed	Fixed	Fixed	
5	Fixed	Fixed	Fixed	Fixed	**Uncertain**	Fixed	Fixed	Fixed	Fixed	
6a	Fixed	Fixed	Fixed	Fixed	Fixed	**Uncertain**	Fixed	Fixed	Fixed	Uncertain transport parameters using one of the fastest flow realizations in the base case model
7a	Fixed	Fixed	Fixed	Fixed	Fixed	Fixed	**Uncertain**	Fixed	Fixed	
8a	Fixed	Fixed	Fixed	Fixed	Fixed	Fixed	Fixed	**Uncertain**	Fixed	
9a	Fixed	Fixed	Fixed	Fixed	Fixed	Fixed	Fixed	Fixed	**Uncertain**	
6b	Fixed	Fixed	Fixed	Fixed	Fixed	**Uncertain**	Fixed	Fixed	Fixed	Uncertain transport parameters using the flow realization with the smallest RMSE in the base case model
7b	Fixed	Fixed	Fixed	Fixed	Fixed	Fixed	**Uncertain**	Fixed	Fixed	
8b	Fixed	Fixed	Fixed	Fixed	Fixed	Fixed	Fixed	**Uncertain**	Fixed	
9b	Fixed	Fixed	Fixed	Fixed	Fixed	Fixed	Fixed	Fixed	**Uncertain**	
Base Case	**Uncertain**								**Spatially and temporally varying**	

The analysis of parametric uncertainty independently evaluates the selected uncertain components of the model, producing a comparison of the relative contribution of each to the overall output uncertainty. The output uncertainty for the base case and for all the uncertainty cases is obtained in terms of an estimated ^{14}C contaminant boundary. Appendix C presents the results of the uncertainty analysis for the five flow cases and the four transport cases, analyzing their relative impact on the overall uncertainty in the size of the ^{14}C contaminant boundary.

Tsang (1987) highlights the importance of the choice of measurable quantities used for validation purposes, as there are measurable quantities that are almost impossible to use for model validation (e.g., point and instantaneous concentration data). The averaged solute concentration over a large region and over a period of time is a more relevant quantity for purposes such as determining the effectiveness of geological isolation of nuclear or toxic waste (Tsang, 1987).

Most of the model components (conceptual model, mathematical model, computer code, and input data) contain some degree of uncertainty due to lack of perfect knowledge about the

subsurface conditions no matter how well the system is characterized. Furthermore, experimental results (e.g., field measurements) that are designed for model validation studies contain some errors or uncertainty. The validation tests must consider these sources of uncertainty because they make it difficult to ascertain whether or not the model results agree with the experimental data; the more uncertain the data are, the more difficult it is to conclude that the model is acceptable (Davis et al., 1991). However, these uncertainty effects should be viewed in terms of whether or not they affect the quantity of regulatory interest. In some cases, input uncertainty may have minor impact on the resulting regulatory quantity (Pohll and Mihevc 2000). These effects were the subject of the parametric uncertainty analysis.

Based on the results of the individual parametric uncertainty analysis presented in Appendix C, hydraulic conductivity is the most viable validation target on the input side of the model. Fracture porosity is a similarly sensitive target, but obtaining porosity data is quite difficult and the data remain subject to large uncertainties due to both test constraints and complexity of interpretation. On the output side, the hydraulic head as well as the head gradient are viable validation targets. In addition, presence or absence of certain radionuclides at the locations of the validation wells will be used as validation targets. However, point concentration measurements may not be helpful for the validation as much as the determination of the presence or absence of radionuclides (i.e., the binary aspect of radionuclide presence as opposed to the value of their concentration). Also, if geophysical logging or other information could be gathered about the fracture sizes and intensity as a function of depth in each of the new validation wells, this can be used as validation targets for the purpose of conditioning the model and reducing the uncertainty built into the fracture characteristics in the model.

5.5.1.3 Planned Implementation of Step 2 in the Procedure for Shoal Model Validation: Data Collection

The approach proposed for each validation target is as follows:

1. Hydraulic conductivity: Perform aquifer tests to validate the mean and distribution of conductivity assigned to flow category 2 in the model. Single-hole aquifer tests will be performed in the new wells to obtain K values from the new locations. Packer tests and stressed flowlogging tests may also be conducted in the new wells and in HC-1 and HC-2 to match the 20-m scale of conductivity assigned to the model cells.

2. Hydraulic head: Measure hydraulic head, particularly in the downgradient direction, to confirm lateral and vertical flow directions. These measurements will be performed in the well bore and in piezometers installed in the annular space of the new monitoring wells.

3. Contaminant transport: Collect and analyze groundwater samples for tritium, as an indicator of Shoal-related contaminants. These samples will be collected from the well bore following purging. General hydrochemical components will also be determined to confirm conceptual model characteristics. These will include major ions, silica, pH, EC, temperature, and stable isotopes of oxygen and hydrogen.

4. Fracture size and frequency: Perform geophysical logging, video logging, and geologic logging to determine the frequency and character of fractures with depth in the new monitoring wells. These data will be analyzed in combination with existing fracture data to determine if the combined data result in a significant shift of the mean or distribution used in the model.

Each of the new monitoring wells will be able to provide information on the validation targets. Hydraulic tests will be attempted in wells HC-1 and HC-2 to provide additional data for target 1.

The monitoring analysis determined the optimum location of wells to serve the long-term monitoring need. The well locations and completion intervals are summarized in Section 5.2.0.5. The validation requirements are not spatially sensitive as long as data are provided that were not used in the original model construction. Indeed, it is logically preferable for validation data to derive from locations in the undersampled downgradient direction, which coincides with the proposed monitoring locations. Thus, no competing objectives for the well locations are presented by the validation targets and dual-purpose wells (model validation and long-term monitoring) can be constructed, as encouraged by NDEP for the Faultless nuclear test (Liebendorfer, 2000).

Note that both tritium and hydraulic head are monitoring parameters, as well as validation targets. As a monitoring parameter, tritium concentrations will be compared to regulatory limits and trends tracked to reveal systematic changes. For validation, a binary measure of presence or absence of tritium will be used, given the scaling incompatibility between resident concentrations predicted for 20 m^3 blocks versus point measurements from a well. Hydraulic head provides a system measurement for proof-of-concept. Once the wells reach quasi steady-state after drilling and testing, they will be monitored routinely for indications of perturbations to the system by either natural or man-made forces. Unfortunately, as water level records from the PSA wells show, equilibration after testing can take many years. Prior to determination of quasi steady-state, the gradient in hydraulic head (the relative values of head) between wells will be used for proof-of-concept monitoring.

5.5.2 Evaluation Criteria

According to the validation plan shown in Figure 5-25, the first set of analyses using the field data collected for validation purposes will yield results that will be evaluated to determine the

path forward. The first "if" statement in the validation approach pertains to whether a sufficient number of realizations attained satisfactory scores on how they represent the field data used for calibration (old) and used for validation (new). The determination of whether a sufficient number exists will be based on five criteria with the decision made in a hierarchical manner as will be discussed later. The five criteria are summarized below.

- Individual realization scores (S_j, j = 1, …, number of realizations) obtained based on how well each realization fits the validation data will be evaluated. The first criterion then becomes the percentage of these scores (P_1) which exceeds a certain reference value.
- The number of validation targets where field data fits within the inner 95 percent of the pdf of these targets as used in the model (P_2) is the second criterion.
- The results of hypothesis testing to be conducted using the stochastic perturbation approach of Luis and McLaughlin (1992) that decomposes the differences between measured and observed heads, identifies those attributed to the model, and statistically evaluates the hypothesis that those differences are negligible (i.e., the model is valid) (P_3). This approach is described in detail in the validation report of Hassan (2003a).
- The results of linear regression analysis and other hypothesis testing (e.g., testing error variance based on calibration data and based on validation data) that could be feasible (depending on the size of data set obtained in the field) (P_4).
- The results of the correlation analysis where the log-conductivity variance is plotted against the head variance for the targeted locations and the resulting plot for the model is compared against the field validation data (P_5).

The hierarchical approach to make the above determination is described by a decision tree. This decision tree for the acceptance of the realizations and for passing the first decision point on the validation approach is shown in Figure 5-26. The process starts with evaluating S_j and determining whether the percentage of realizations with scores above the reference value (RV), P_1, is more than 40 percent, between 30 and 40 percent, or less than 30 percent. If the number is more than 40 percent, it is deemed sufficient. If it is between 30 and 40 percent or less than 30 percent, then the second criterion, P_2, is used as shown in Figure 5-26.

The second criterion represents the number of validation targets where the field data point lies within the inner 95 percent of the pdf for that target as used in (input) or produced by the Shoal model. Then if P_1 is between 30 and 40 percent and P_2 is between 40 and 50 percent or if P_1 is less than 30 percent but P_2 is greater than 50 percent, the number of realizations is deemed sufficient. If P_1 is less than 30 percent and P_2 is less than 40 percent, then the remaining three measures, P_3, P_4, and P_5, are used to determine whether the model needs revision or whether more realizations can be generated to replace some of the current realizations. In this latter case,

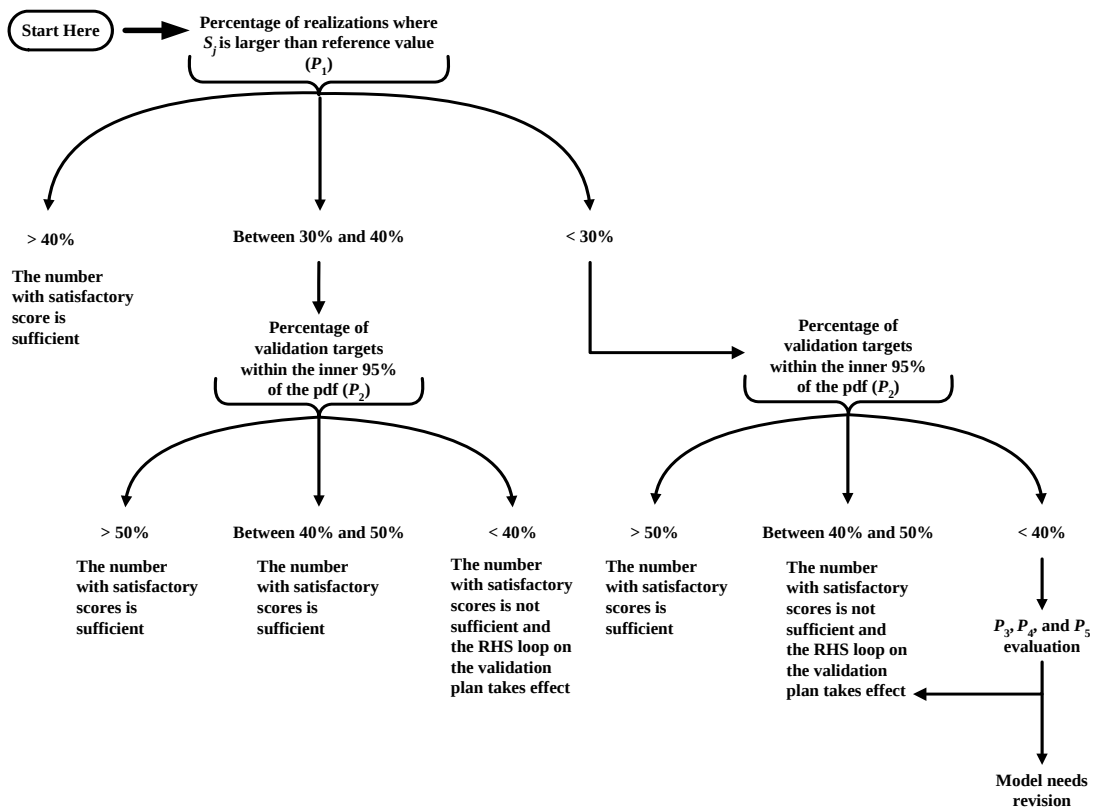

Note: A decision tree showing how the first decision (Step 5) in the validation plan will be made and the criteria for determining the sufficiency of the number of acceptable realizations

Figure 5-26
Validation decision tree chart

it may be that the model is conceptually good but the input parameter distribution is skewed one way or another and by generating more realizations and keeping the ones that fit the above criteria, the distribution attains the proper position. This can be done using the existing model without conditioning or using any of the new validation data (i.e., no additional calibration). The rationale for selecting the above thresholds (30 to 40 percent for P_1 and 40 to 50 percent for P_2) is described through an example and as these metrics are evaluated with statistical hypothesis testing later in Appendix D. The appendix contains specific details and examples of the application of the validation criteria to the Shoal flow and transport model.

5.5.3 Reporting

Several milestones will occur during the proof-of-concept process. The first major milestone will be the completion of well installation and initial data collection. The results of the drilling and well completion will be communicated to NDEP through a well completion report. Validation data collection will also continue with measurement of water levels and tritium

concentrations as part of the monitoring network. This ongoing data collection will be transmitted through annual monitoring program reports. The validation analysis will begin upon initial completion of the wells, with its exact course through the sequence shown in Figure 5-25 dependent on the match between the data and the model. The results of the validation analysis will be communicated to NDEP at Step 6 in Figure 5-25, as a major decision point in the process. It is anticipated that validation of the model can be achieved within the first two years of the proof-of-concept period.

6.0 Schedule

Figure 6-1 shows the schedule for the PSA corrective action, through the proof-of-concept period and Closure Report.

ID	Task Name	Duration	Start	Finish
1	Monitoring\validation well install	70 days	Mon 3/27/06	Fri 6/30/06
2	Well Completion Report	30 days	Thu 7/6/06	Wed 8/16/06
3	Proof of Concept	1303 days	Fri 6/30/06	Tue 6/28/11
4	Concept analysis	154 days	Wed 6/29/11	Mon 1/30/12
5	Prepare Closure report	132 days	Tue 1/31/12	Wed 8/1/12
6	Submit CR to State	1 day	Thu 8/2/12	Thu 8/2/12
7	NDEP review of CR	22 days	Thu 8/2/12	Fri 8/31/12
8	NDEP approve CR	1 day	Mon 9/3/12	Mon 9/3/12

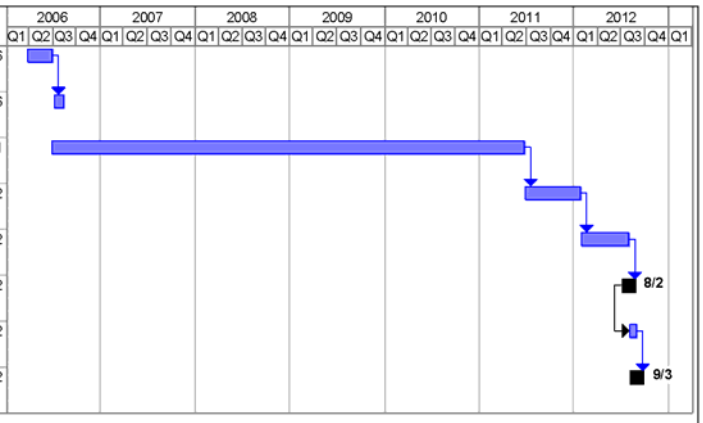

Project: shoalcadd_cap_pas
Date: Mon 3/13/06

Task | Split | Progress | Milestone | Summary | Project Summary | External Tasks | External Milestone | Deadline

Page 1

Figure 6-1
Schedule

7.0 POST-CLOSURE

Activities necessary to ensure protection of human health and the environment following PSA subsurface closure are collectively known as long-term stewardship activities. At PSA, stewardship will be designed to prevent exposure to the contamination left in place in the nuclear test cavity. Stewardship activities will include record keeping, inspections, groundwater monitoring, and controls on subsurface access and resource extraction. DOE is committed to long-term stewardship of PSA, as evidenced by baseline budget planning documents that outline 50 years of stewardship activities and the funding for those activities.

As prescribed in Rev. 1, 2000 of the FFACO, the Closure Report will establish the long-term monitoring requirements for the CAU, develop technical and administrative contingency plans for actions to be taken if long-term monitoring results are not acceptable, and define future land-use restrictions. These requirements and plans will build upon the findings and experience of the proof-of-concept monitoring. Anticipated activities are briefly described below, with details to be submitted in the Closure Report.

7.1 Inspections and Monitoring

The purpose of inspections and monitoring is to protect human health and the environment from the radionuclide hazard left in place in the Shoal cavity. Activities anticipated are as follows:

- Groundwater monitoring, and accompanying well inspections
- Land and resource use monitoring, and accompanying site inspections
- Records management

These activities are expected to continue in perpetuity, commensurate with the time span through which the Shoal cavity presents a hazard. Monitoring and inspection frequency may be decreased from the annual schedule conducted during proof-of-concept. Groundwater monitoring frequency is generally tied to transport velocities, and given the relatively slow velocities predicted for radionuclide transport from the Shoal cavity, the system is not expected to require frequent monitoring. The experience gained during the proof-of-concept will be used to determine the optimum frequency for maintaining adequate site knowledge and surveillance.

A key component of the long-term site stewardship will be institutional controls. Institutional controls can minimize the potential for human exposure and protect the integrity of the PSA closure decision by limiting resource use and providing information to modify or guide human behavior at the site. An institutional control plan will be included in the Closure Report and will

include the legal and practical limits of available tools, identification of the parties responsible for the necessary activities, and cost estimates for the stewardship activities.

The contaminant boundary presented as part of this CADD/CAP will be important in guiding the development of institutional controls for PSA. However, the boundary is based upon ambient (non-stressed) groundwater conditions. Pumping for groundwater outside the contaminant boundary has the potential to alter the hydrologic conditions that in turn can alter contaminant migration behavior. Thus, there is a need to control certain types of groundwater development activities beyond the contaminant boundary. Resource management tools will be developed as part of the closure process so that responsible parties can make permit decisions based on the knowledge developed during the CADD and validation processes. These tools evaluate whether a proposed groundwater extraction activity is consistent with the site closure, is clearly inconsistent, or whether additional evaluation must be conducted to make a determination.

7.2 Maintenance of Monitoring System

Maintenance and monitoring will occur from 2010 through 2069. The wells will be inspected annually and repaired as necessary to perform monitoring. Long-term monitoring requirements will be developed in the Long-Term Surveillance and Monitoring Plan following completion of the Closure Report. The budget is based on an average of one replacement well every 25 years.

7.3 Re-Evaluation of Model and Monitoring System

The monitoring network will continuously add to the state of knowledge about the groundwater system in the Shoal area. The new information will either support the closure decision, thus reducing the uncertainties associated with the decision, or indicate conditions that may call into question the ongoing validity of the closure decision. Essentially, the post-audit validation of the flow and transport model will continue as long as site data are collected. Data collection objectives shift from primarily model validation with attendant site monitoring during proof-of-concept, to primarily site monitoring with attendant model validation during long-term closure.

Assuming that indicator radionuclide concentrations and hydraulic head values are the primary analytes and parameters monitored, trigger mechanisms for re-evaluating the closure conditions will be upward trends in radionuclide concentrations not predicted by the model, and significant deviations in hydraulic head outside the steady-state range upon which the model is based. Re-evaluation may include revising the model and monitoring strategy. Unanticipated radionuclide concentrations may indicate a failure of the model to accurately represent flow and transport processes. Hydraulic head variations may signal a shift in the hydraulic system away

from the previous steady-state conditions. Either occurrence will trigger re-evaluation of the modeling predictions and revision if necessary. Changes in resource use in the region (e.g., groundwater development), may also trigger re-evaluation of the closure conditions, even in advance of discernable impacts on hydraulic head, in order for management options to be considered in a proactive rather than reactive timeframe.

8.0 REFERENCES

AEC, see U.S. Atomic Energy Commission.

ASTM, see American Society for Testing and Materials.

Ahlfeld, D.P., and G.F. Pinder. 1988. *A Groundwater Monitoring Network Design Algorithm*, Report 87-WR-4. Princeton, NJ: Princeton University, Department of Civil Engineering and Operations Research.

American Society for Testing and Materials. 2001. *Standard Test Methods for Determining the Liquid Levels in a Borehole or Monitoring Well (Observation Well)*, D4750.

Anderson, M.P., and W.W. Woessner. 1992. *Applied Groundwater Modeling: Simulation of Flow and Advective Transport*. New York, NY: Academic Press.

BN, see Bechtel Nevada.

Bechtel Nevada. 1995. *Nevada Test Site Performance Objective for Certification of Nonradioactive Hazardous Waste*, Rev. 0, G-E11/96.01. Las Vegas, NV.

Berkowitz, B. 2002. "Characterizing Flow and Transport in Fractured Geological Media: A Review." In *Advanced Water Resources* 25, 861-884.

Beven, K.J., and A.M. Binley. 1992. "The Future of Distributed Models: Model Calibration and Uncertainty Prediction." In *Hydrological Processes*, (6): 279-298.

Borg, I.Y. 1975. "Radioactivity Trapped in Melt Produced by a Nuclear Explosion." *Nuclear Technology*, (26): 88-100.

Borg, I.Y., R. Stone, H.B. Levy, and L.D. Ramspott. 1976. *Information Pertinent to the Migration of Radionuclides in Ground Water at the Nevada Test Site, Part 1: Review and Analysis of Existing Information*, UCRL-52078. Livermore, CA: Lawrence Livermore National Laboratory.

Bredehoeft, J.D. 2003. "From Models to Performance Assessment: The Conceptualization Problem." In *Groundwater*, 41(5): 571-577.

Bright, D.J., S.A. Watkins, and B.A. Lisle. 2001. *Analysis of Water Levels in the Frenchman Flat Area, Nevada Test Site*, WRIR-00-4272. Denver, CO: U.S. Geological Survey.

CFR, see *Code of Federal Regulations.*

Cacas, M.C., E. Ledoux, G. de Marsily, B. Tillie, A. Barbreau, E. Durand, B. Feuga, and P. Peaudecerf. 1990a. "Modeling Fracture Flow with a Stochastic Discrete Fracture Network: Calibration and Validation, 1 (the Flow Model)." In *Water Resources Research*, 26(3): 479-489.

Cacas, M.C., E. Ledoux, G. de Marsily, A. Barbreau, P. Calmels, B. Gaillard, and R. Margrita. 1990b. "Modeling Fracture Flow with a Stochastic Discrete Fracture Network: Calibration and Validation, 2 (the Transport Model)." *Water Resources Research* 26(3): 491-500.

Carroll, R., T.M. Mihevc, G.M. Pohll, B. Lyles, S. Kosinski, and R. Niswonger. 2000. *Project Shoal Area Tracer Test Experiment*, Publication No. 45177, DOE/NV/ 13609--05. Las Vegas, NV: Desert Research Institute, Division of Hydrologic Sciences.

Carroll, R., K.F. Pohlmann, G.M. Pohll, and T.M. Mihevc. 2001. *Investigation of Hydraulic Properties of a Shear Zone at the Shoal Site and Associated Groundwater Levels*, Publication No. 45183, DOE/NV/13609-12. Las Vegas, NV: Desert Research Institute, Division of Hydrologic Sciences.

Chapman, J.B., T.M. Mihevc, and A. McKay. 1994. *Groundwater Flow Near the Shoal Site, Sand Springs Range, Nevada: Impact of Density-Driven Flow*, Publication No. 45130, DOE/NV/10845-51. Las Vegas, NV: Desert Research Institute, Division of Hydrologic Sciences.

Code of Federal Regulations. 2003a. Title 40 CFR Parts 260-280, "Hazardous Waste Regulations." Washington, DC: U.S. Government Printing Office.

Code of Federal Regulations. 2003b. Title 40 CFR Part 300.430, "Remedial Investigation/Feasibility Study and Selection of Remedy." Washington DC: U.S. Government Printing Office.

Code of Federal Regulations. 2003c. Title 40 CFR Part 761.61, "PCB Remediation Waste." Washington, DC: U.S. Government Printing Office.

DOE, see U.S. Department of Energy.

Davis, P.A., N.E. Olague, and M.T. Goodrich. 1991. *Approaches for the Validation of Models Used for Performance Assessment of High-Level Radioactive Waste Repositories*, SAND90-0575. Albuquerque, NM: Sandia National Laboratories.

Dershowitz, W.S., G. Lee, J. Geier, S. Hitchcock, and P. La Pointe. 1993. *FRACMAN User Documentation*. Seattle, WA: Golder Associates Inc.

Diersch, H.-J. G. 1998. *FEFLOW Reference Manual*. Prepared by WASY Institute for Water Resources Planning and Systems Research Ltd. Berlin, Germany.

Doherty, J. 2000. *PEST - Model-Independent Parameter Estimation - User's Manual*, Fourth Edition. Watermark Numerical Computing.

EPA, see U.S. Environmental Protection Agency.

Everett, L.G. 1980. *Ground Water Monitoring*. Schenectady, NY: General Electric Company.

FFACO, see *Federal Facility Agreement and Consent Order*.

Federal Facility Agreement and Consent Order. 1996 (as amended). Agreed to by the State of Nevada, the U.S. Department of Energy, and the U.S. Department of Defense.

Federal Register. 1962a. Public Land Order 2771, "Withdrawing Lands for Use of Atomic Energy Commission," Doc. 62-9076, 11 September. Washington, DC: U.S. Government Printing Office.

Federal Register. 1962b. Public Land Order 2834, "Correcting Certain Public Land Orders; Amending Public Land Order No. 2771of September 6, 1962," Doc. 62-12191, 10 December. Washington, DC: U.S. Government Printing Office.

Franks, S.W., and K.J. Beven. 1997. "Bayesian Estimation of Uncertainty in Land-Atmosphere Flux Predictions." In *Journal of Geophysical Research*, 102 (D20): 23,991-23,999.

Freer, J., K.J. Beven, and B. Ambroise. 1996. "Bayesian Estimation of Uncertainty in Runoff Prediction and the Value of Data: An Application of the GLUE Approach." In *Water Resources Research*, 32(7): 2161- 2173.

Goishi, W., J.W. Meadows, N. Namboodiri, D.K. Smith, and J.F. Wild. 1995. *Radionuclide Inventory for U.S. Nuclear Tests Conducted Off the NTS and Hydronuclear and Safety Experiments Conducted on the NTS* (Classified), UCRL-ID- 121901. Livermore, CA: Lawrence Livermore National Laboratory

Harbaugh, A.W., and M.G. McDonald. 1996a *Programmer's Documentation for MODFLOW-96: An Update to the U.S. Geological Survey Modular Three-Dimensional Finite-Difference Ground-Water Flow Model* Open-File Report 96-486. Denver, CO: U.S. Geological Survey.

Harbaugh, A.W., and M.G. McDonald. 1996b *User's Documentation for MODFLOW-96: An Update to the U.S. Geological Survey Modular Three-Dimensional Finite-Difference Ground-Water Flow Model*, Open-File Report 96-485. Denver, CO: U.S. Geological Survey.

Harbaugh, A.W., E.R. Banta, M.C. Hill, and M.G. McDonald. 2000. *MODFLOW-2000, The U.S. Geological Survey Modular Ground-Water Model - User Guide to Modularization Concepts and the Groundwater Flow Process*, Open-File Report 00-92. Denver, CO: U.S. Geological Survey.

Hassan, A.E. 2002. "Comment on 'Determination of Particle Transfer for Random Walk Particle Methods in Fractured Porous Media' by H. H. Liu et al." In *Water Resources Research*, 38(11): 1221.

Hassan, A.E. 2003a. *A Validation Process for the Groundwater Flow and Transport Model of the Faultless Nuclear Test at Central Nevada Test Area*, Publication #45197. Las Vegas, NV: Desert Research Institute, Division of Hydrologic Sciences.

Hassan, A.E. 2003b. *Long Term Monitoring Plan for the Central Nevada Test Area*, Publication No. 45201, DOE/NV/13609-30. Prepared for the U.S. Department of Energy, Nevada Operations Office. Las Vegas, NV: Desert Research Institute, Division of Hydrologic Sciences.

Hassan, A.E. 2004a. "A Methodology for Validating Numerical Groundwater Models." In *Ground Water*, 42(3): 347-362.

Hassan, A.E. 2004b. "Validation of Numerical Groundwater Models Used to Guide Decision Making." In *Ground Water*, 42(2): 277-290.

Hassan, A.E. 2004c. *Validation, Proof of Concept, and Postaudit of the Groundwater Flow and Transport Model of the Project Shoal Area*. Las Vegas, NV: Desert Research Institute, Division of Hydrologic Sciences.

Hassan, A.E. 2005. *Long-Term Monitoring Plan for the Shoal Underground Nuclear Test*. Las Vegas, NV: Desert Research Institute, Division of Hydrologic Sciences.

Hassan, A.E., and M.M. Mohammed. 2003. "On Using Particle Tracking Methods to Simulate Transport in Single-Continuum and Dual Continua Porous Media." In *Journal of Hydrology*, 275: 242-260.

Hassan, A.E., K.F. Pohlmann, and J.B. Chapman. 2002. *Modeling Groundwater Flow and Transport of Radionuclides at Amchitka Island's Underground Nuclear Tests: Milrow, Long Shot, and Cannikin*, Publication No.45172, DOE/NV/11508--51. Las Vegas, NV: Desert Research Institute, Division of Hydrologic Sciences.

Hazelton-Nuclear Science Corporation. 1965. *Post-Shot Hydrologic Safety, Project Shoal Final Report*, VUF-1014. Prepared for the U.S. Atomic Energy Commission.

Hudak, P.F. 1994. "A Method for Monitoring Ground Water Quality Near Waste Storage Facilities." In *Environmental Monitoring and Assessment*, 30: 197-210.

Hudak, P.F. 1996. "A Method for Designing Detection Monitoring Networks in Layered Aquifers with Non-Uniform Flow." In the *Journal of Environmental Management*, 48: 341-355.

Hudak, P.F. 2001. "Effect of Groundwater Velocity on Sampling Intervals for Contaminant-Detection Networks in Aquifers." In the *Journal of Environmental Science Health*, 36(1): 117-122.

IT Corporation. 1996. *Field Instructions for Project Shoal Area Surface and Subsurface Investigation, Churchill County, Nevada*, ITLV/10972-176. Las Vegas, NV.

IT Corporation. 2000. *1999 Well Installation Report, Project Shoal Area, Churchill County, Nevada*, ITLV/13052-097. Prepared for U.S. Department of Energy, Nevada Operations Office. Las Vegas, Nevada.

Kleijnen, J.P.C. 1999. *Statistical Validation of Simulation (including case Studies): Validation of Simulation Models*. Edited by C. van Dijkum, D. de Tombe, and E. van Kuijk. Amsterdam: SISWO.

Lane, Jr., J.W., P.K. Joesten, G.M. Pohll, and T.M. Mihevic. 2001. *Analysis of Borehole-radar Reflection Logs from Selected HC Boreholes at the Project Shoal Area, Churchill County, Nevada*, WRIR-01-4014. Denver, CO: U.S. Geological Survey.

Liebendorfer, P.E., Nevada Division of Environmental Protection. 1998. Letter to M.O. Giblin (DOE/NV) entitled, "Closure Report for CAU 416, Project Shoal Area Surface," 13 February. Carson City, NV.

Liebendorfer, P.J., Nevada Division of Environmental Protection. 2000. Letter to R.C. Wycoff (DOE/NV) entitled, "Evaluation of Groundwater Flow and Transport at the Faultless Underground Nuclear Test Area, Desert Research Institute, September 1999, Publication No. 45165, CAU 443, Central Nevada Test Area, FFACO," 17 March. Carson City, NV.

Liu, H.H., G.S. Bodvarsson, and L. Pan. 2000. "Determination of Particle Transfer in Random Walk Particle Methods for Fractured Porous Media." In *Water Resources Research*, 36(3): 707-713.

Liu, H.H., G.S. Bodvarsson, and L. Pan. 2002. "Reply to Comment on Determination of Particle Transfer in Random Walk Particle Methods for Fractured Porous Media by H.H. Liu et al.'' In *Water Resources Research*, 38(11).

Loaiciga, H.A., R.J. Charbeneau, L.G. Everett, G.E. Fogg, B.F. Hobbs, and S. Rouhani. 1992. "Review of Groundwater Quality Monitoring Network Design." In *Journal of Hydraulic Engineering*, 118(1): 11-37.

Long, J., C. Remer, P. Wilson, and P. Witherspoon. 1982. "Porous Media Equivalents for Networks of Discontinuous Fractures." *Water Resources Research*, 18(3): 645-658.

Long, J.C., and D.M. Billaux. 1987. "From Field Data to Fracture Network Modeling: An Example Incorporating Spatial Structure." In *Water Resources Research*, 23: 1201-1216.

Luis, S.J., and D. McLaughlin. 1992. "A Stochastic Approach to Model Validation." In *Advances in Water Resources*, 15: 15-32.

Maize, T., Nevada Division of Environmental Protection. 2004. Letter to J. Appenzeller-Wing (NNSA/NSO) entitled, "Review of the Modeling to Support Groundwater Contaminant Boundaries for the Shoal Underground Nuclear Test Corrective Action Unit #447, Project Shoal Area, Federal Facility Agreement and Consent Order," 18 February. Las Vegas, NV.

Massmann, J., and R.A. Freeze. 1987. "Groundwater Contamination From Waste Management Sites: The Interaction Between Risk-Based Engineering Design and Regulatory Policy (1, Methodology)." In *Water Resources Research*, 23(2): 351-367.

Maxey, George B. 1968. "Hydrogeology of Desert Basins." In *Groundwater*, 6(5): 10-22.

McDonald, M.G., and A.W. Harbaugh. 1984. *A Modular Three-Dimensional Finite-Difference Ground-Water Flow Model*, Open-File Report 83-875. Denver, CO: U.S. Geological Survey.

McDonald, M.G., and A.W. Harbaugh. 1988. "A Modular Three-Dimensional Finite-Difference Ground-Water Flow Model." In *Techniques of Water Resources Investigations*, Book 6, Chapter A1, 586p. Denver, CO: U.S. Geological Survey

Meyer, P., and E.D. Brill, Jr. 1988. "A Method for Locating Wells in a Groundwater Monitoring Network Under Conditions of Uncertainty." In *Water Resources Research*, 24(8): 1277-1282.

Meyer, P.D., R. Ranjithan, A.J. Valocchi, and J.W. Eheart. 1989. "Groundwater Monitoring Network Design Using Coupled Monte Carlo Simulation and Optimization." In *Proceedings of the 1989 National Conference on Hydraulics Engineering*, M.A. Ports (Editor). New York, NY: ASCE.

Mihevc, T.M., G.M. Pohll, and B. Lyles. 2000. *Project Shoal Area Field Data Summary Report*, Publication No. 45175, DOE/NV/11508--54. Las Vegas, NV: Desert Research Institute, Division of Hydrologic Sciences.

Moltyaner, G.L., M.H. Klukas, C.A. Wills, and W.D. Killey. 1993. "Numerical Simulation of Twin Lake Natural-Gradient Tracer Tests: a Comparison of Methods." In *Water Resources Research*, 24(12): 2033-2048.

Morse, B.S., G.M. Pohll, J. Huntington, and R.R. Castillo. 2003. "Stochastic Capture Zone Analysis of an Arsenic-Contaminated Well Using the Generalized Likelihood Uncertainty Estimator (GLUE) Methodology." In *Water Resources Research*, 39(6): 1151.

NAC, see *Nevada Administrative Code.*

NNSA/NSO, see U.S. Department of Energy, National Nuclear Security Administration Nevada Site Office.

NRS, see *Nevada Revised Statutes.*

Neretnieks, I. 1993. "Solute Transport in Fractured Rock – Applications to Radionuclide Waste Repositories." In *Flow and Transport in Fractured Rock*, 39-127. San Diego, CA: Academic Press.

Neretnieks, I., T. Eriksen, and P. Tahtinen. 1982. "Tracer Movement in a Single Fracture in Granitic Rock: Some Experimental Results and Their Interpretation." In *Water Resources Research*, 18(4): 849-858.

Nevada Division of Water Resources. 2000. *Well Log Database*. State of Nevada, Department of Conservation and Natural Resources, database query on 31 July 2000.

Nevada Administrative Code. 1998. NAC 534.4365, "Monitoring Wells: Plugging." Carson City, NV.

Nevada Administrative Code. 2003. NAC 445A, "Water Controls." Carson City, NV.

Nevada Administrative Code. 2004a. NAC 444.570 – 444.7499, "Solid Waste Disposal." Carson City, NV.

Nevada Administrative Code. 2004b. NAC 444.850 – 444.8746, Disposal of Hazardous Waste." Carson City, NV.

Nevada Administration Code. 2005. NAC 445B.001 – 3497, " Air Controls." Carson City, NV.

Nevada Revised Statutes. 2003a. NRS 444.440 – 444.645, "Collection and Disposal of Solid Waste. Carson City, NV.

Nevada Revised Statutes. 2003b. NRS 459.400 – 459.600, "Disposal of Hazardous Waste." Carson City, NV.

Pan, L., H.H. Liu, M. Cushey, and G.S. Bodvarsson. 2001. *DCPT V1.0 – New Particle Tracker for Modeling Transport in Dual Continua Media, Users' Manual*, LBNL-42958. Berkeley, CA: Lawrence Berkeley National Laboratory

Pan, L., and G.S. Bodvarsson. 2002. "Modeling Transport in Fractured Porous Media with the Random-Walk Particle Method: The Transient Activity Range and the Particle Transfer Probability." In *Water Resources Research*, 38(6): 16-1 – 16-7.

Papelis, C. 2001. "Cation and Anion Sorption on Granite from the Project Shoal Test Area, Near Fallon, Nevada, USA." In *Advances in Environmental Research*, 5: 151-166.

Poeter, E.P., and M.C. Hill. 1998. *Documentation of UCODE: A Computer Code for Universal Inverse Modeling*, WRIR-98-4080. Denver, CO: U.S. Geological Survey.

Pohll, G.M. 1999. *Evaluation of Surface Recharge Flux for the Project Shoal Area*, Publication No. 45171, DOE/NV/11508--49. Las Vegas, NV: Desert Research Institute, Division of Hydrologic Sciences.

Pohll, G.M. 2004. *Radionuclide Source Term Used to Calculate the Project Shoal Contaminant Boundary* (Classified), Report CEP-04-02. Las Vegas, NV: Desert Research Institute.

Pohll, G.M., and T.M. Mihevc. 2000. *Data Decision Analysis: Central Nevada Test Area*, Publication No. 45179 DOE/NV/13609--07. Las Vegas, NV: Desert Research Institute, Division of Hydrologic Sciences.

Pohll, G.M., and K.F. Pohlmann. 2004. *Contaminant Boundary at the Shoal Underground Nuclear Test*, Letter Report DOE/NV--993. Prepared for the U.S. Department of Energy, National Nuclear Security Administration Nevada Site Office. Las Vegas, NV: Desert Research Institute.

Pohll, G.M., A.E. Hassan, and J.B. Chapman. 1998. *Evaluation of Groundwater Flow and Transport at the Shoal Underground Nuclear Test: An Interim Report*, DOE/NV/11508-58. Las Vegas, NV: Desert Research Institute.

Pohll, G.M., J. Tracy, and F. Forsgren. 1999a. *Data Decision Analysis: Project Shoal*, Publication No. 45166, DOE/NV/11508--42. Las Vegas, NV: Desert Research Institute, Division of Hydrologic Sciences.

Pohll, G.M., A.E. Hassan, J.B. Chapman, C. Papelis, and R. Andricevic. 1999b. "Modeling Groundwater Flow and Radioactive Transport in a Fractured Aquifer." In *Groundwater*, 37(5): 770-784.

Pohll, G.M., T.M. Mihevc, J.B. Chapman, B. Lyles and P. Reimus. 1999c. *Project Shoal Area: Field characterization plan, two-well tracer test deep-well characterization and monitoring*. Desert Research Institute, Division of Hydrologic Sciences, Publication No. 45168, DOE/NV/11508--45, 55p.

Pohll, G.M., K.F. Pohlmann, J. Daniels, A.E. Hassan, and J.B. Chapman. 2003. *Contaminant Boundary at the Faultless Underground Nuclear Test*, Publication No. 45196, DOE/NV/13609-24. Las Vegas, NV: Desert Research Institute, Division of Hydrologic Sciences.

Pohlmann, K.F., J.B. Chapman, A.E. Hassan, and C. Papelis. 1999. *Evaluation of Groundwater Flow and Transport at the Faultless Underground Nuclear Test, Central Nevada Test Area*, Publication No. 45165, DOE/NV/11508-41. Las Vegas, NV: Desert Research Institute, Water Resources Center.

Pohlmann, K.F., G.M. Pohll, A.E. Hassan, J.B. Chapman, and P.A. Sanders. 2002. "Integrating Numerical Modeling and Data Collection for Site Characterization at the Shoal Underground Nuclear Test Site, Nevada, USA." In the *Proceedings of SPECTRUM Conference*, August. Reno, NV.

Pohlmann, K.F., G.M. Pohll, J.B. Chapman, A.E. Hassan, R. Carroll, and C.T. Shirley. 2004. *Modeling to Support Groundwater Contaminant Boundaries for the Shoal Underground Nuclear Test*, Publication No. 45184, DOE/NV/13609-13. Las Vegas, NV: Desert Research Institute, Division of Hydrologic Sciences.

Pruess, K. 1991. *TOUGH2 -A: A General Purpose Numerical Simulator for Multiphase Fluid and Heat Flow*, Report LBL-29400. Berkeley, CA: Lawrence Berkeley National Laboratory.

Reimus, P., G.M. Pohll, T.M. Mihevc, J.B. Chapman, M. Haga, B. Lyles, S. Kosinski, R. Niswonger, and P.A. Sanders. 2003. "Testing and Parameterizing a Conceptual Model for Solute Transport in a Fractured Granite Using Multiple Tracers in a Forced-Gradient Test." In *Water Resources Research*, 39(12): 1356-1370.

Sargent, R.G. 1990. "Validation of Mathematical Models." In *GEOVAL-90, Symposium on Validation of Geosphere Performance Assessment Models*, 14-17 May, 571-579. Stockholm, Sweden.

Smith, D.K. 2001. *Unclassified Radiologic Source Term for Nevada Test Site Areas 19 and 20*, UCRL-ID-141706. Livermore, CA: Lawrence Livermore National Laboratory.

Storck, P., J.W. Eheart, and A.J. Valocchi. 1997. "A Method for the Optimal Location of Monitoring Wells for Detection of Groundwater Contamination in Three-Dimensional Heterogeneous Aquifers." In *Water Resources Research*, 33(9): 2081-2088.

Sudicky, E.A., and E.O. Frind. 1982. "Contaminant Transport in Fractured Porous Media: Analytical Solutions for a System of Parallel Fractures." In *Water Resources Research*, 18(6): 1634-1642.

Todd, D.K., R.M. Timlin, K.D. Schmidt, and L.G. Everett. 1976. *Monitoring Groundwater Quality: Monitoring Methodology*, EPA-600/4-76-026. Las Vegas, NV: U.S Environmental Protection Agency.

Tsang, C.F. 1987. "Comments on Model Validation." In *Transport in Porous Media*, 2(6): 623-630.

University of Nevada. 1965. *Geological, Geophysical, Chemical, and Hydrological Investigations of the Sand Springs Range, Fairview Valley, and Fourmile Flat, Churchill County, Nevada*: Vela-Uniform Program, VUF-1001.

U.S. Atomic Energy Commission, Nevada Operations Office. 1964. *Project Manager's Report Project Shoal*, NVO-11. Las Vegas, NV.

U. S. Department of Energy, National Nuclear Security Administration Nevada Site Office. 2003a. *Underground Test Area Quality Assurance Project Plan Nevada Test Site, Nevada*, DOE/NV--341-Rev.4. Las Vegas, NV.

U.S. Department of Energy, National Nuclear Security Administration Nevada Site Office. 2003b. *Nevada Test Site Waste Acceptance Criteria*, Rev. 5, DOE/NV--325. Las Vegas, NV.

U.S. Department of Energy, National Nuclear Security Administration Nevada Site Office. 2004. *Project Shoal Site Risk-Based End State Vision Document*, DOE/NV--955 (in publication). Las Vegas, NV.

U.S. Department of Energy, Nevada Operations Office. 1996. *Corrective Action Investigation Plan for Project Shoal Area CAU No. 416*, DOE/NV--454. Las Vegas, NV.

U.S. Department of Energy, Nevada Operations Office. 1998a. *Corrective Action Investigation Plan for Corrective Action Unit 447: Project Shoal Area, Nevada Subsurface Site*, DOE/NV--513. Las Vegas, NV.

U.S. Department of Energy, Nevada Operations Office. 1998b. *Focused Evaluation of Selected Remedial Alternatives for the Underground Test Area*, DOE/NV--465. Las Vegas, NV.

U.S. Department of Energy, Nevada Operations Office. 1998c. *Closure Report for CAU No. 416, Project Shoal Area*, DOE/NV/11718-179. Las Vegas, NV.

U.S. Department of Energy, Nevada Operations Office. 1998d. *Underground Test Area Quality Assurance Project Plan Nevada Test Site, Nevada*, DOE/NV-341-Rev. 2. Las Vegas, NV.

U.S. Department of Energy, Nevada Operations Office. 1998e. *Data Report Project Shoal Area Churchill County, Nevada*, DOE/NV--505. Las Vegas, NV.

U.S. Department of Energy, Nevada Operations Office. 1999a. *Addendum to the Corrective Action Investigation Plan for Corrective Action Unit 447: Project Shoal Area, Nevada Subsurface Site*, DOE/NV--513-ADD. Las Vegas, NV.

U.S. Department of Energy, Nevada Operations Office. 1999b. *Fluid Management Plan for the Project Shoal Area Off-Sites Project*, DOE/NV--542. Las Vegas, NV.

U. S. Department of Energy, Nevada Operations Office. 2000a. *NV/YMP Radiological Control Manual*, Rev. 4. Las Vegas, NV.

U.S. Department of Energy, Nevada Operations Office. 2000b. *Underground Test Area Quality Assurance Project Plan Nevada Test Site, Nevada*, DOE/NV--341-REV 3. Las Vegas, NV.

U.S. Department of Energy, Nevada Operations Office. 2000c. *Human Health and Safety Risk Summary Offsites Test Area* (in publication). Las Vegas, NV.

U.S. Environmental Protection Agency. 1976. *National Interim Primary Drinking Water Regulations*, EPA-570-9-76-003. Washington, DC: Office of Water Supply.

U.S. Environmental Protection Agency. 1983. *Methods for Chemical Analysis of Water and Waste*, EPA/600/4-79/020. Washington, DC.

U.S. Environmental Protection Agency. 1986. *RCRA Groundwater Monitoring Technical Enforcement Guidance Document*. Washington, DC: Office of Solid Waste Emergency Response.

U.S. Environmental Protection Agency. 1995. *Contract Laboratory Program Statement of Work for Inorganic Analysis, Multi-Media, Multi-Concentration*, EPA/540/R-95/121. Washington, DC.

U.S. Environmental Protection Agency. 1996. *Test Methods for Evaluating Solid Waste*, 3rd Edition, Parts 1-4. Washington, DC.

U.S. Environmental Protection Agency. 1997a. *Determination of Inorganic Anions in Drinking Water by Ion Chromatography*, EPA/600/R-98/118. Cincinnati, OH.

U.S. Environmental Protection Agency (EPA). 1997b. *Annual Water Sampling and Analysis Calendar Year 1997: Rulison Test Site Area, Rio Blanco Test Site Area, Faultless Test Site Area, Shoal Test Site Area, Gasbuggy Test Site Area, Gnome Test Site Area*, EPA-402-R-98-005. Las Vegas, NV: Office of Radiation and Indoor Air.

U.S. Environmental Protection Agency. 1999. *Federal Guidance Report No. 13: Cancer Risk Coefficients for Environmental Exposure to Radionuclides*, EPA 402-R-99-001. Washington, DC: Office of Radiation and Indoor Air.

U.S. Environmental Protection Agency. 2000a. "Part II. Environmental Protection Agency, 40 CFR Parts 9, 141, and 142: National Primary Drinking Water Regulations; Radionuclides; Final Rule." In *Federal Register 65*(236), 76708-76753. Washington, DC: U.S. Government Printing Office.

U.S. Environmental Protection Agency. 2000b. "Part IV. Environmental Protection Agency, 40 CFR Parts 9, 141, and 142: National Primary Drinking Water Regulations; Radionuclides; Notice of Data Availability; Proposed Rule." In *Federal Register 65*(78), 21576-21628.

Wilson, C.R., C.M. Einberger, R.L. Jackson, and R.B. Mercer. 1992. "Design of Ground-Water Monitoring Networks Using the Monitoring Efficiency Model (MEMO)." In *Ground Water*, 30: 965-970.

Appendix A
Proposed Engineering Specifications and Drawings

List of Figures

Figure A.1-1 Topographic map with the MV well locations plotted A-3

Figure A.1-2 Anticipated well design for MV-1 ..... A-4

Figure A.1-3 Anticipated well design for MV-2 ..... A-5

Figure A.1-4 Anticipated well design for MV-3 ..... A-6

Figure A.1-5 Construction of well HC-1 ..... A-7

Figure A.1-6 Construction of well HC-4 ..... A-8

List of Tables

Table A.1-1 Target Locations for the MV Wells A-1

Table A.1-2 Estimated Elevations for MV Well Completions A-1

Table A.1-3 Location and Elevation of Existing HC Wells Proposed for the Monitoring Network A-2

Appendix A Proposed Engineering Specifications and Drawings

Three new wells will be drilled as part of the corrective action for CAU 447. The logic and rationale for the wells and related testing are presented in Section 5.0 of this document.

The proposed well locations are shown on Figure 5-22. Working coordinates for the wells, in Nevada State Plane coordinates (meters) are shown in Table A.1-1 below:

Table A.1-1
Target locations for the MV wells

	UTM NAD27, Zone 11	
Name	**Easting**	**Northing**
MV-1	380924.5	4339961
MV-2	380877.8	4340041
MV-3	381024.0	4339991

The well design involves a single completion well string, with one piezometer installed in the annular space to monitor hydraulic head close to the water table. The targets for the well screen vary from well to well as dictated by the monitoring design analysis in Section 5.2. The elevations of the screened intervals are given in Table A.1-2. The well locations were plotted on a topographic map (Figure A-1) in order to estimate land surface elevation, from which the depths to the screens were estimated and used to develop well construction diagrams (Figures A-2, A-3, and A-4). The water table elevation was interpolated from other site wells (not derived from the groundwater model) and used to estimate the piezometer location for each well.

The actual locations of the well screens, and the depths of the piezometers, will depend on subsurface conditions encountered during drilling. Specifically, the upper piezometer will be located within 50 m of the water table and the well screen may be adjusted to span significant fractures, if encountered near the target horizon.

Table A.1-2
Estimated elevations for MV well completions

	Elevation, in meters above mean sea level (m AMSL)			
Name	**Land Surface**	**Water Table**	**Top of screen**	**Bottom of screen**
MV-1	1599	1286.8	1115	1065
MV-2	1603	1284.7	1050	1000
MV-3	1601	1289.1	1155	1105

Table A.1-1 In addition to the new wells, existing wells HC-1 and HC-4 are included in the monitoring network. Their construction is shown in Figures A-5 and A-6. Their locations are listed in Table A.1-3 below:

Table A.1-3
Location and elevation of existing HC wells proposed for the monitoring network

	UTM NAD27, Zone 11		
Name	Easting	Northing	Elevation, m
HC-1	380850.5	4340238.9	1618.3
HC-4	380783.5	4339520.9	1603.5

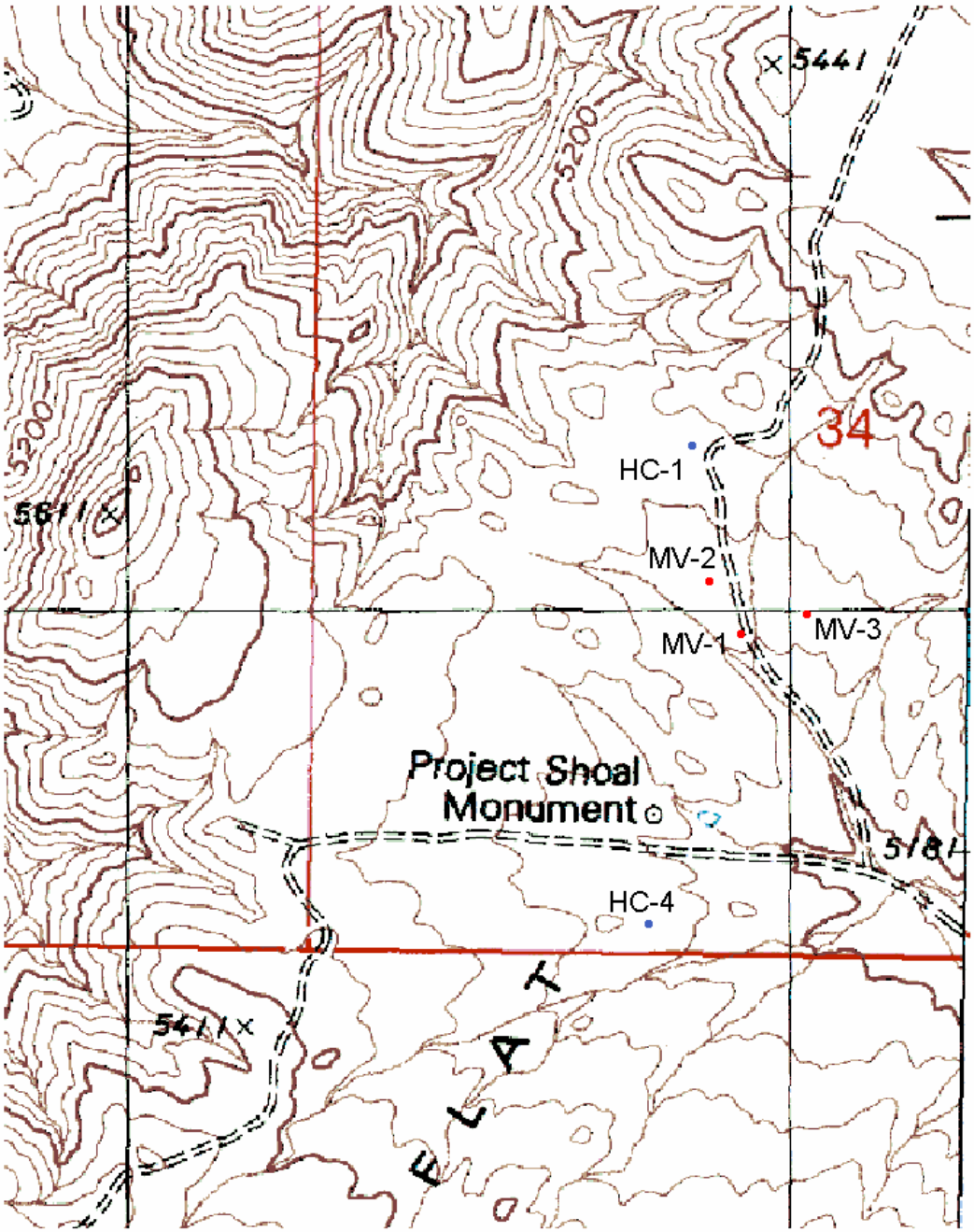

Figure A.1-1
Topographic map with the MV well locations plotted

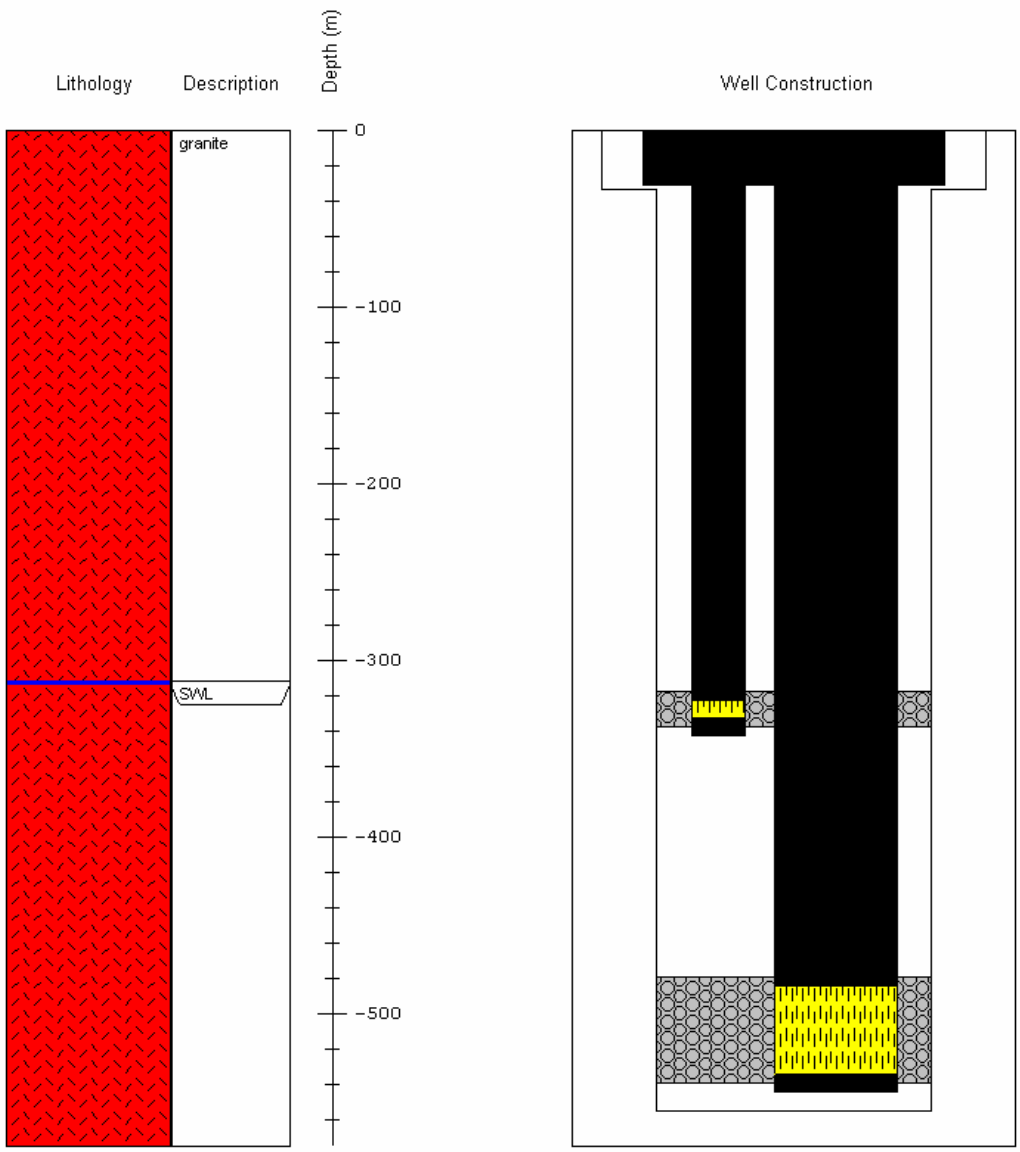

Figure A.1-2
Anticipated well design for MV-1

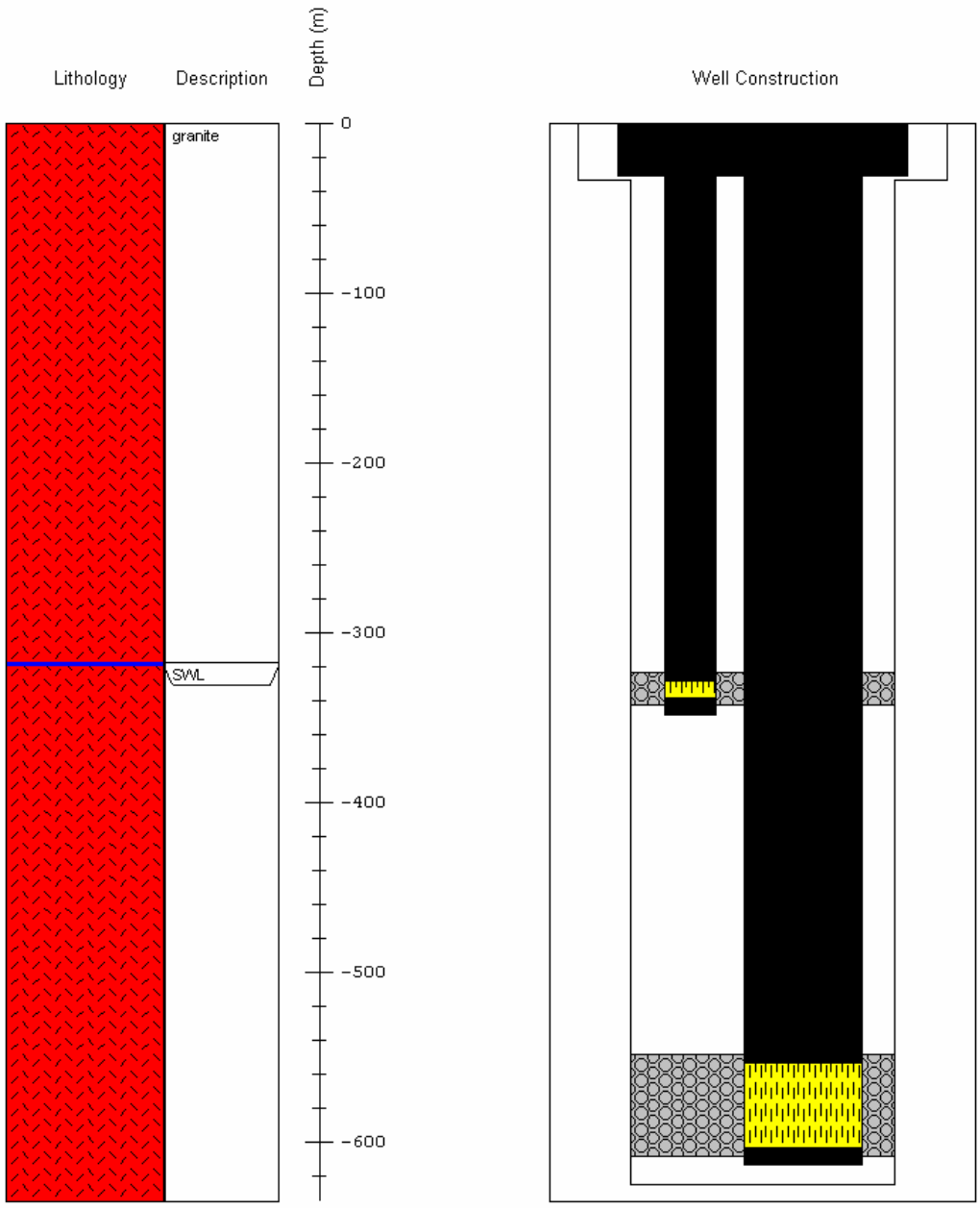

Figure A.1-3
Anticipated well design for MV-2

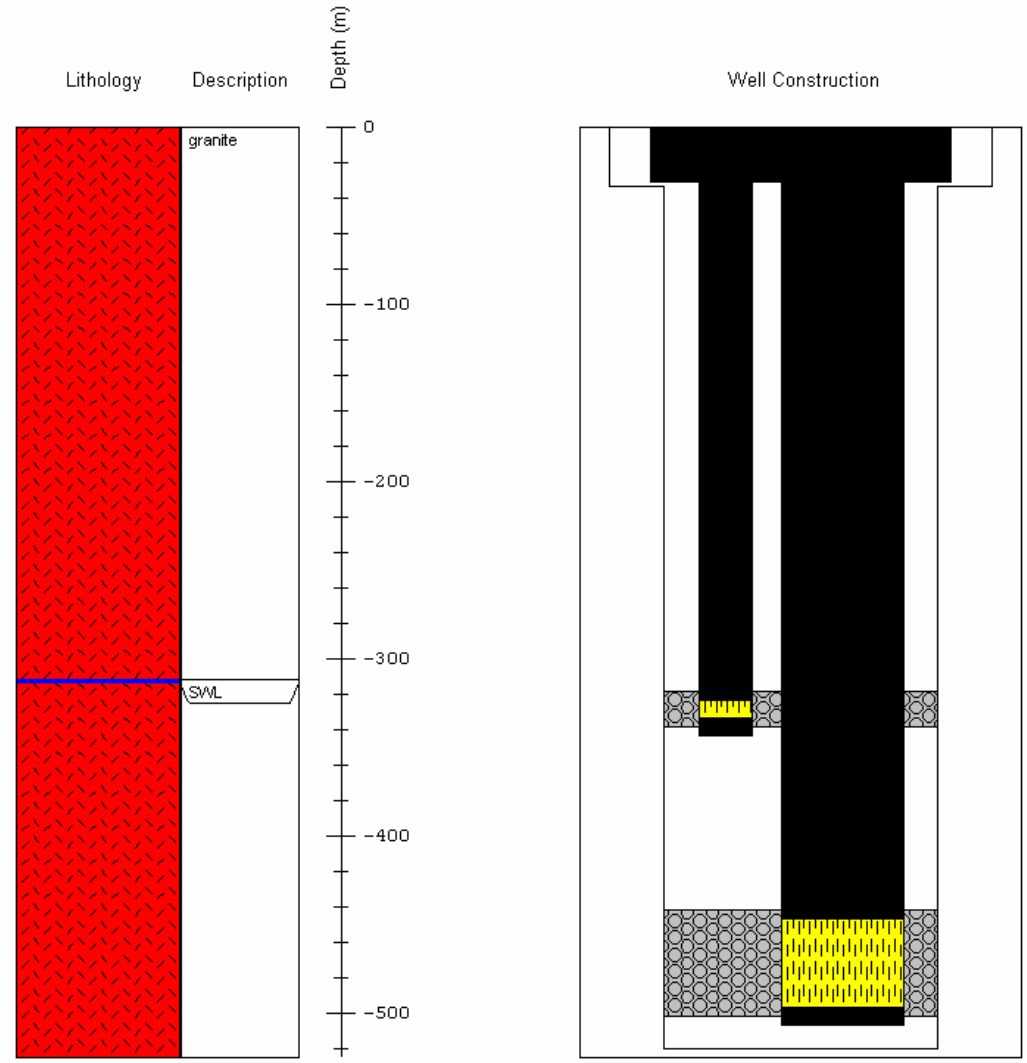

Figure A.1-4
Anticipated well design for MV-3

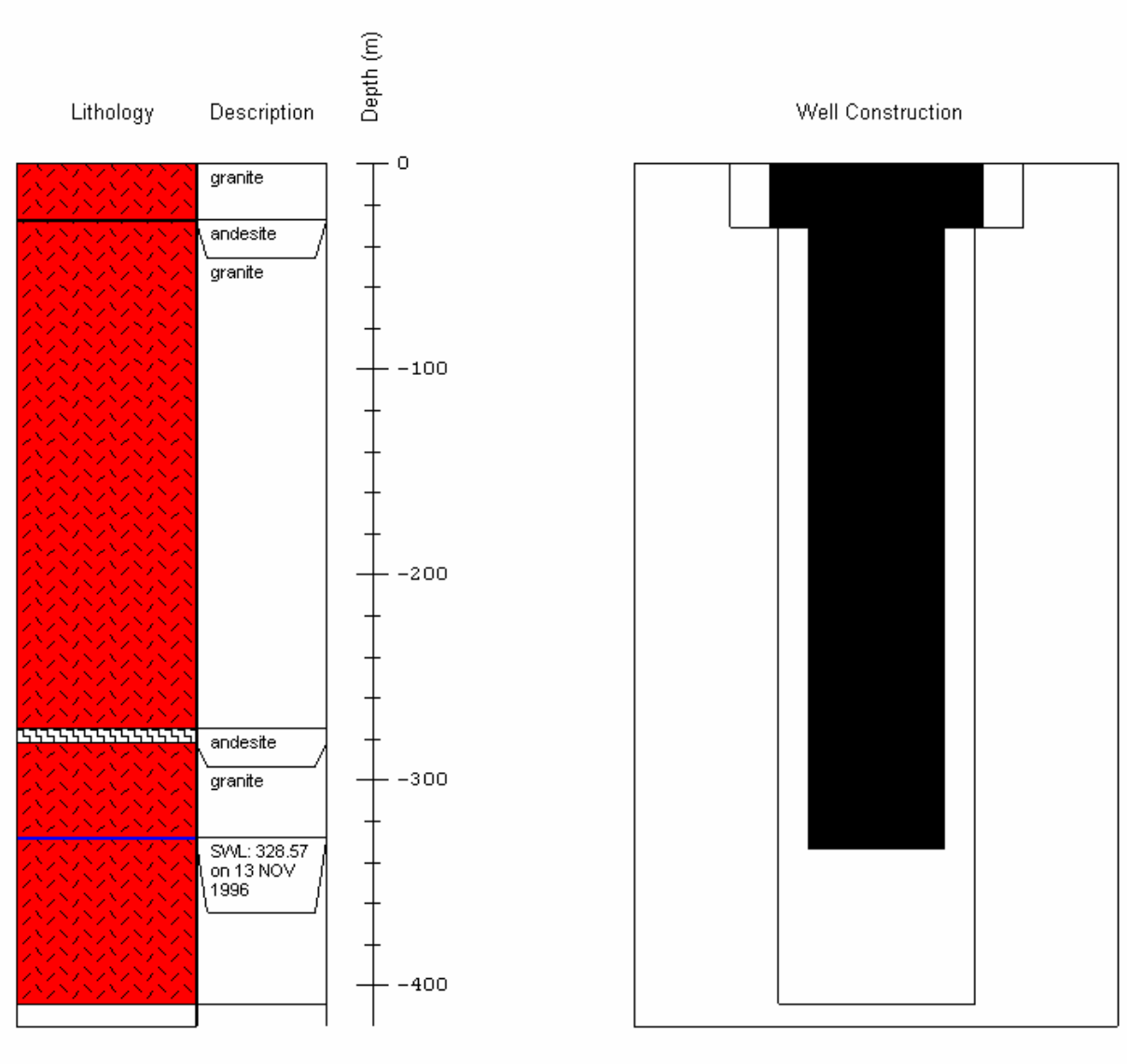

Figure A.1-5
Construction of well HC-1

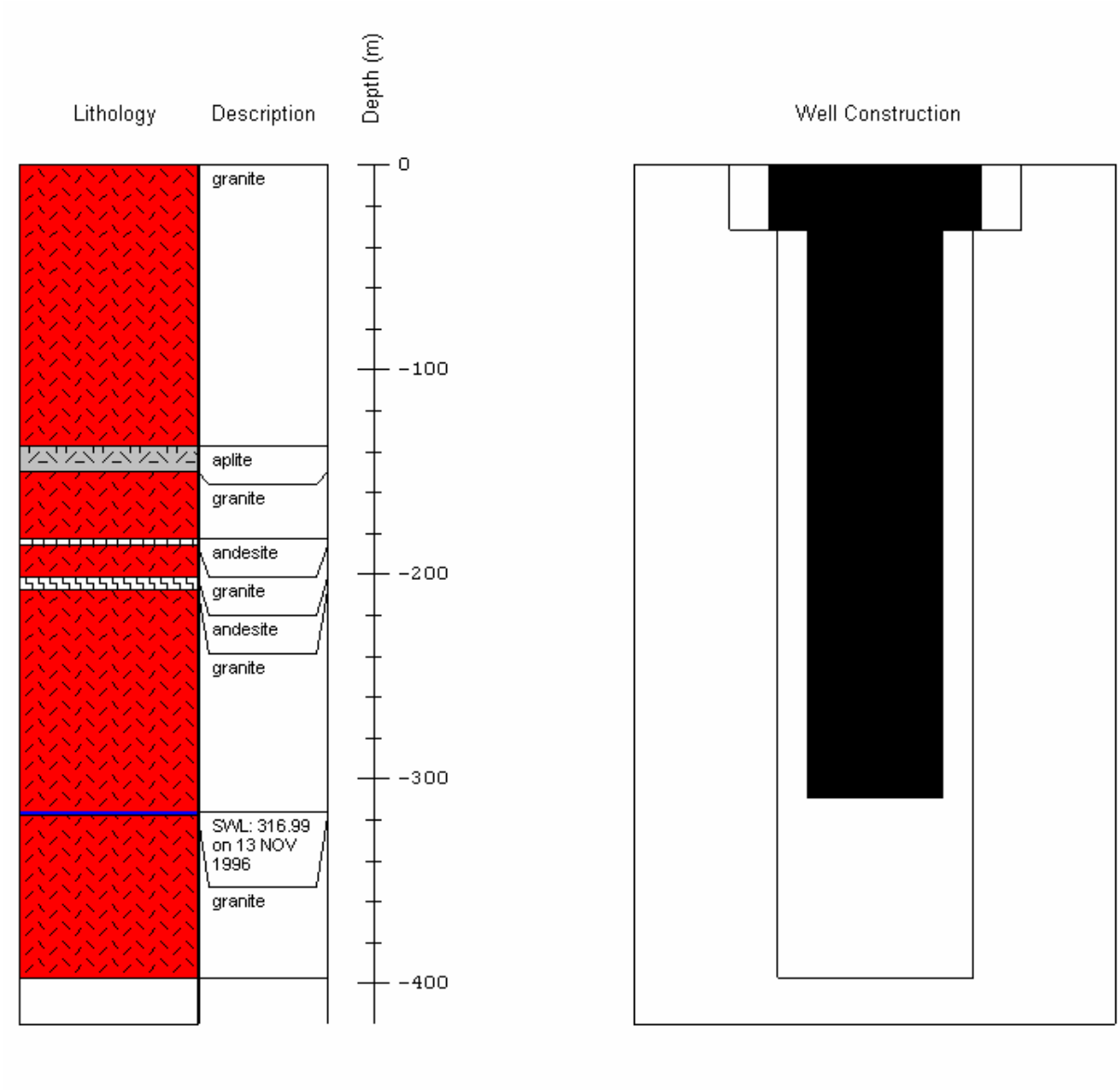

Figure A.1-6
Construction of well HC-4

Appendix B
Deviation of Existing Boreholes and Depth Correction Procedure

List of Tables

Table B.1-1 Coefficients used in the depth-correction expression for each Shoal borehole B-2

Appendix B Deviation of Existing Boreholes and Depth Correction Procedure

Accuracy of hydraulic head data, as physically measured by depth to the water level, is strongly dependent on borehole trueness. Departure of the borehole and/or casing from true vertical result in a distance from ground surface to the point of measurement that is greater than would be measured in a true borehole, thereby increasing the apparent depth to water measurement beyond the absolute vertical distance. The impact of these borehole deviations on water level measurements must be accounted for, particularly at sites having deep boreholes, where the magnitude of deviations vary widely from borehole to borehole, and where the measurements from different boreholes are routinely compared to each other. Measurements of depth to water at Shoal are corrected for departure from borehole trueness using data from borehole deviation surveys conducted after the completion of drilling. The deviation surveys provide the true vertical depth for given cable (electric tape or pressure transducer) depths at 7.62-m (25-ft) intervals. True vertical cable depth with respect to depth in the borehole is described using a polynomial expression developed specifically for the conditions observed in each well that accounts for the length of the borehole encountered during each measurement (i.e., deep water level measurements encounter a greater length of deviated borehole than shallow measurements). The general form of the expression is given by

$$D_v = \sum_{k=0}^{n} A_k D_{meas}^k \qquad \text{(B.1-1)}$$

Where D_v = vertical cable depth; D_{meas} = measured cable depth; and A_k = coefficients calculated from the deviation log.

The coefficients used in the depth-correction expression for each Shoal borehole are listed in Table B.1-1 below. The order of the polynomial was chosen based on the degree to which the deviation varied with depth (i.e. higher order polynomials were used for highly irregular boreholes). The borehole deviation data are included in the field data summary for Shoal (Mihevc et al., 2000). HC-4 does not have an access tube for water level measurements so a deviation correction was not done for this well.

Table B.1-1
Coefficients used in the depth-correction expression for each Shoal borehole

Well ID	A_0	A_1	A_2	A_3	A_4	A_5	A_6
HC-1	--	1.06	-1.20×10^{-4}	4.31×10^{-8}	--	--	--
HC-2	3.16×10^{2}	-5.48×10^{-1}	3.02×10^{-3}	-2.95×10^{-6}	1.44×10^{-9}	-2.79×10^{-13}	--
HC-3	9.82×10^{6}	-5.52×10^{4}	1.29×10^{2}	-1.61×10^{-1}	1.13×10^{-4}	-4.24×10^{-8}	6.60×10^{-12}
HC-6	--	8.43×10^{-1}	5.90×10^{-4}	-8.26×10^{-7}	5.10×10^{-10}	-1.18×10^{-13}	--
HC-7	--	1.01	-2.43×10^{-5}	3.52×10^{-8}	-2.25×10^{-11}	5.27×10^{-15}	--
HC-8	-1.29×10^{3}	5.77	-7.06×10^{-3}	5.22×10^{-6}	-1.92×10^{-9}	2.84×10^{-13}	--

Appendix C
Parametric Uncertainty Analysis for Validation Target Identification

Table of Contents

C.1 Uncertain Flow Parameters C-2

C.1.1 Case #1 ..... C-2

C.1.2 Case #2 ..... C-5

C.1.3 Case #3 ..... C-9

C.1.4 Case #4 ..... C-11

C.1.5 Case #5 ..... C-14

C.2 Uncertain Transport Parameters C-17

C.2.1 Cases #6a and #6b C-18

C.2.2 Cases #7a and #7b C-21

C.2.3 Cases #8a and #8b C-22

C.2.4 Cases #9a and #9b C-25

List of Figures

Figure C-1 Comparison between the base case model and the fracture orientation Uncertainty Case # 1 ..... C-3

Figure C-2 Comparison between the base case model and Uncertainty Case #1 in terms of a contaminant boundary and boundary uncertainty C-4

Figure C-3 Comparison between the base case model and the fracture length Uncertainty Case #2 ..... C-7

Figure C-4 Comparison between the base case model and Uncertainty Case #2 in terms of a contaminant boundary and boundary uncertainty C-8

Figure C-5 Comparison between the base case model and Uncertainty Case #3 ..... C-10

Figure C-6 Comparison between the base case model and Uncertainty Case #3 in terms of a contaminant boundary and boundary uncertainty C-11

Figure C-7 Comparison between the base case model and the fracture conductivity Uncertainty Case #4 ..... C-12

List of Figures *(Continued)*

Figure C-8 Comparison between the base case model and Uncertainty Case #4 in terms of a contaminant boundary and boundary uncertainty.....C-13

Figure C-9 Comparison between the base case model and Uncertainty Case #5 (recharge uncertainty) C-16

Figure C-10 Comparison between the base case model and Uncertainty Case #5 in terms of a contaminant boundary and boundary uncertainty.....C-17

Figure C-11 Comparison between the base case model and fracture porosity Uncertainty Case #6a in terms of a contaminant boundary and boundary uncertainty C-19

Figure C-12 Comparison between the base case model and fracture porosity Uncertainty Case #6b in terms of a contaminant boundary and boundary uncertainty C-20

Figure C-13 Comparison between the base case model and cavity porosity Uncertainty Case #7a in terms of a contaminant boundary and boundary uncertainty C-22

Figure C-14 Comparison between the base case model and cavity porosity Uncertainty Case #7b in terms of a contaminant boundary and boundary uncertainty C-23

Figure C-15 Comparison between the base case model and damaged zone Uncertainty Case #8a in terms of a contaminant boundary and boundary uncertainty C-24

Figure C-16 Comparison between the base case model and damaged zone porosity Uncertainty Case #8b in terms of a contaminant boundary and boundary uncertainty.....C-25

Figure C-17 Comparison between the base case model and matrix diffusion Uncertainty Case #9a in terms of a contaminant boundary and boundary uncertainty C-27

Figure C-18 Comparison between the base case model and matrix diffusion Uncertainly Case #9b in terms of a contaminant boundary and boundary uncertainty C-28

Appendix C Parametric Uncertainty Analysis for Validation Target Identification

The analysis of parametric uncertainty independently evaluates the selected uncertain components of the PSA model, producing a comparison of the relative contribution of each to the overall output uncertainty. The output uncertainty for the base case and for all the uncertainty cases is obtained in terms of an estimated ^{14}C contaminant boundary. However, virtually any model result can be used as the output metric. The analysis proceeds by running the calibrated model in Monte Carlo mode for each of the individual uncertain parameters that are under consideration; all of the other uncertain parameters are held at constant values that are representative of their distribution. For each uncertain parameter, the Monte Carlo values are chosen from the input parameter distributions used in the contaminant-boundary model (Pohlmann et al., 2004). However, only 500 realizations are used for this uncertainty analysis (to reduce computational time) as opposed to the 1,000 realizations used in Pohlmann et al. (2004) due to the large number of cases studied here. This does not impact the results as the relative contribution of each uncertain parameter to the overall output uncertainty of the model is the factor of interest.

For each of the uncertain flow parameters (Case 1 through Case 5; refer to Table 5-9 in the body of the report for descriptions of each case), the MODFLOW-2000 flow solver is run to generate a set of flow realizations that incorporate the uncertainty in each targeted flow parameter. These flow realizations are then used to model the radionuclide transport with the transport parameters held fixed at their mean values for all flow cases. When the effects of uncertain transport parameters are studied, a single realization of the flow field is used and the transport problem is solved 500 times with the uncertain transport parameter value being drawn from the respective parameter distribution. The selection of the flow realization to be used for these analyses is based on criteria discussed below.

The ^{14}C contaminant boundary is calculated using an unclassified estimate of ^{14}C mass for the Shoal test (0.24 curies), based on data from Smith (2001). In that report, Smith presents the average source term for the UGTA tests on Pahute Mesa. The average Pahute Mesa source term for ^{14}C is about 7.3 curies. However, when this value is scaled by the ratio of tritium source terms (the unclassified tritium estimate for Shoal relative to the average tritium source term of Pahute Mesa), the resulting ^{14}C source term for Shoal is about 0.24 curies.

C.1 Uncertain Flow Parameters

The five flow parameters considered here are the fracture orientation, the fracture length that indicates the continuity of fractures, the hydraulic conductivity, K, of the cavity and surrounding zones (three conductivity values), the hydraulic conductivity of fractures, and the recharge at the domain top. The fracture orientation plays an important role in determining how far from the cavity radionuclides can migrate. When fractures are oriented parallel to the general flow direction from the cavity outward, the migration distance increases. However, if the fractures are oriented normal to that flow direction, migration distances decrease. Therefore, the uncertainty associated with the fracture orientation may impact the contaminant boundary and lead to uncertainty in its extent. In the base case model (Pohlmann et al., 2004), four sets of fractures were chosen to represent the distribution of orientations for one of the flow categories (Flow Category 2 according to Pohlmann et al. [2004]), which represents zones of strongly oriented, large fractures. These fracture sets have the most well defined orientations and contain the highest proportion of the total fractures. Flow Category 1 (Pohlmann et al., 2004) is assumed to have no preferred spatial orientation. For those cases in which the fracture orientation was kept fixed (i.e., deterministic), conditioned fracture orientations were set to the mean orientations for each class, and unconditioned fractures were first randomly sampled to determine the class, and then the mean orientations were applied.

C.1.1 Case #1

In Uncertainty Case #1, the fracture orientation for the two flow categories are considered uncertain while fixing all other flow parameters (and subsequently transport parameters) at their best estimate or mean values. The empirical orientation distribution used in Pohlmann et al. (2004) is used here to draw the values of the fracture orientation for each realization. Figures C-1 and C-2 display the impact of the fracture orientation uncertainty on the ^{14}C contaminant boundary and the associated uncertainty. Transport simulations and contaminant boundary computation are performed in the same manner described in Pohlmann et al. (2004).

Figure C-1 shows Uncertainty Case # 1 compared to the base case model of Pohlmann et al. (2004). The uncertainty case has few realizations with larger RMSE than the base case model, but the range of RMSE for the uncertainty case is smaller than the base case. For the plume extent, it is clear that the base case model has a much larger uncertainty range compared to the fracture orientation uncertainty case. If one removes the fastest two realizations in the uncertainty case, it can be concluded that the uncertainty range of the plume extent for the base case model is at least four times larger than that for the uncertainty case. It is important to note

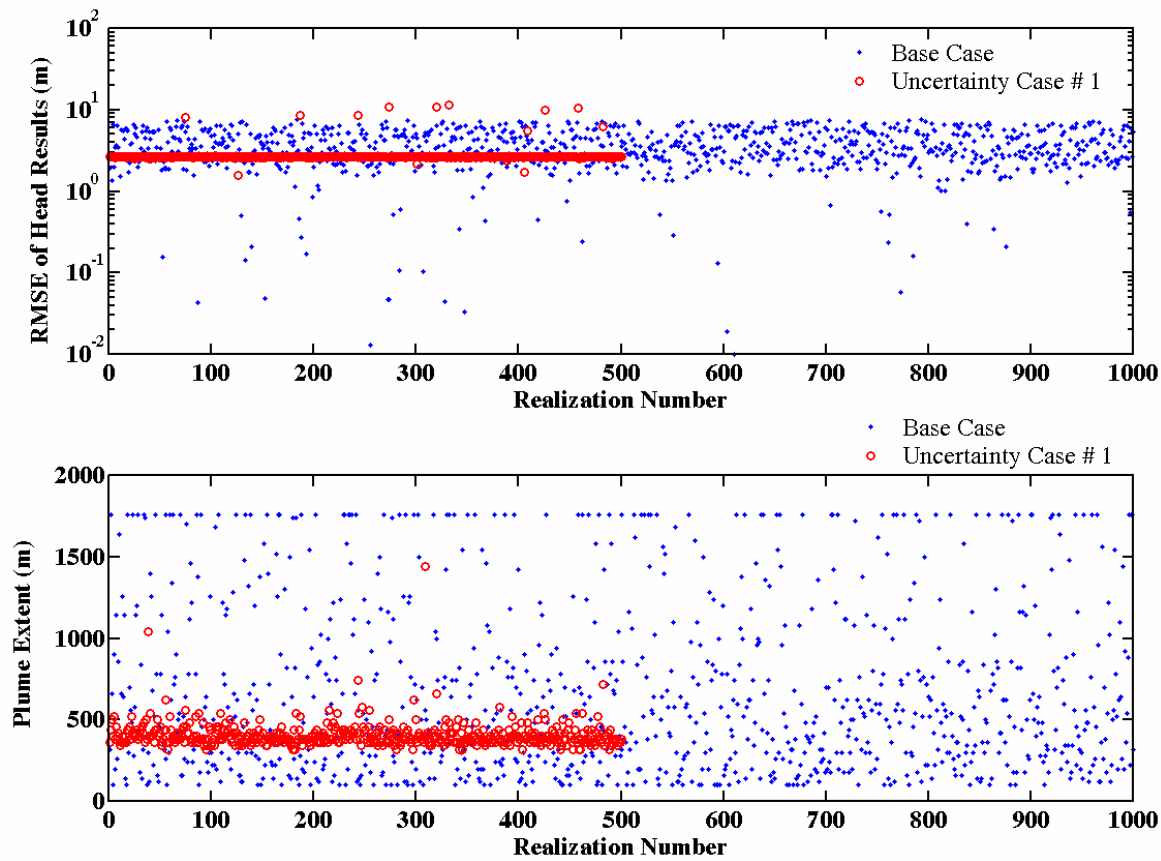

Note: Comparison is in terms of the RMSE of the head results for each flow realization and the plume extent expressed as distance between the working point and the farthest point traveled by any particle in the transport simulations.

Figure C-1
Comparison between the base case model and the fracture orientation Uncertainty Case # 1

that the plume extent is obtained by determining the y coordinate of the farthest cell where the maximum ^{14}C concentration in the x-y projection over 1,000 years is above zero and then subtracting the y coordinate of the working point.

Figure C-2 shows the impact on the contaminant boundary and its uncertainty. The subplots a), b), and c) show the different 2-D projections of the 3-D contaminant boundary volume. Again, these are computed in the same manner described in Pohlmann et al. (2004). These subplots compare the contaminant boundaries of the base case model, which are plotted to scale and in the correct cavity location indicated by the red square, to those of Uncertainty Case #1, which are shifted from their right location to clarify the comparison. The contaminant boundaries of the uncertainty case are, however, drawn to scale in terms of their size so that they could be directly compared to the base case model.

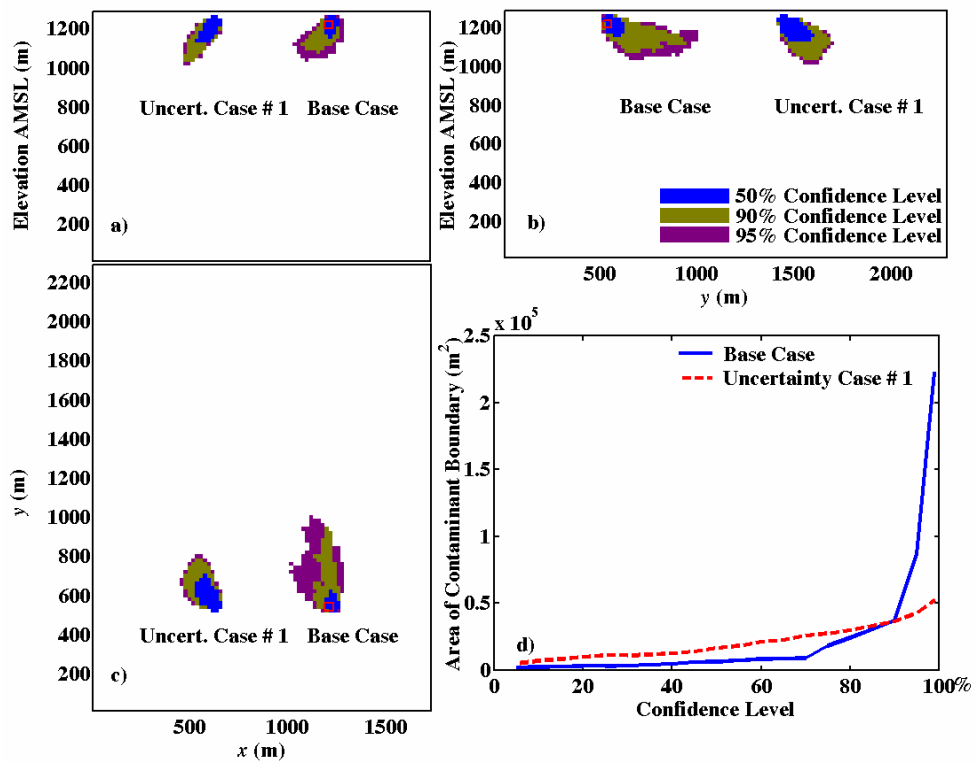

Note: Contaminant boundary maps for ^{14}C are shown, delineating the areas exceeding 2,000 pCi/L at different confidence levels. Uncertainty Case #1 is drawn to scale but is spatially shifted on the plots for comparison to the base case model. Subplot a) shows the x-z (or elevation) map, subplot b) shows the y-z map, subplot c) shows the x-y map, and subplot d) shows the x-y contaminant boundary area at different confidence levels.

Figure C-2
Comparison between the base case model and Uncertainty Case #1 in terms of a contaminant boundary and boundary uncertainty

The subplot d) shows the area of the x-y projection of the contaminant boundary obtained at the 5th, 10th, …, 99th percent confidence levels. This subplot provides an easy way to compare the impact of individual uncertain parameters to the impact of having all parameters as uncertain on the contaminant boundary uncertainty. The steeper the curve, the more uncertain the resulting contaminant boundary is. If one assumes no uncertainty, the 500 (or the 1,000) realizations will give the same exact result and the contaminant boundary area will be the same at all confidence levels (i.e., horizontal line in subplot d).

It is clear that the contaminant boundaries are smaller in area for the uncertainty case at the 90 and 95th percent confidence levels. It is also clear from subplot d) that the base case model has a much larger degree of uncertainty than the uncertainty stemming from the fracture orientation alone. Therefore, fracture orientation contributes to the overall uncertainty but to a small extent. New field data on fracture orientation would not thus yield significant reduction in the overall

model uncertainty. This aspect, added to the difficulty of better characterizing fracture orientations at Shoal, means that the fracture orientation is not a useful validation target.

C.1.2 Case #2

The fracture continuity expressed by fracture length is the second uncertain parameter that requires new flow realizations. The fractures and fracture networks are the principal pathways of water and contaminants through an otherwise impermeable or low permeability rock such as the granite at Shoal. Field and laboratory experiments in natural fractures have demonstrated strong evidence of highly preferential flow paths in individual fractures and fracture networks (Neretnieks et al., 1982; Neretnieks, 1993). Field data, for example from large-scale investigation of fracture flow in a granite uranium mine at Fanay-Augeres, France, show four orders of magnitude difference between the largest and smallest injection flow rates despite very good fracture connectivity (Berkowitz, 2002). Cacas et al. (1990a, b) concluded that the high degree of heterogeneity is due to a broad distribution of fracture conductivities, and that it overwhelmingly governs flow and transport behavior. Therefore, the nature of fractures, their connectivity and conductivity distribution, the surrounding porous rock and its characteristics, and the combined effect of fractures and porous matrix on groundwater flow and contaminant transport make the analysis significantly different than for classical porous media.

As discussed by Berkowitz (2002), studies of well tests often report that of a large number of fractures intersecting a well, only one or two actually transmit fluid. For example, at the Fanay-Augeres site in France, it was found that only 0.1 percent of the fractures contributed to flow on a large scale (Long and Billaux, 1987). Thus, the question of fracture connectivity is of prime importance to flow and contaminant transport in fractured systems and to interpretation of data from single and multiple well tests. Even domains that appear to be heavily fractured may not in fact be well connected (Berkowitz, 2002). In percolation theory terminology, the salient question one has to ask here is whether the fracture network is above the percolation threshold (i.e., connectivity of fractures is sufficient to permit flow through the network from point A to point B) or conversely near the percolation threshold and thus poorly connected. Again this question is of paramount importance when it comes to interpreting and using well test data in fractured geologic units.

At Shoal, the spatial persistence of fracture features was quantified using a digitized map of fractures observed at land surface (Pohll et al., 1998). Although fractures are not truly linear features, they were treated as linear so that an average strike could be calculated for each fracture. A bimodal distribution of strike orientations resulted and the data were grouped as follows (Pohlmann et al., 2004):

- Group 1: Strike of 0-70 and 130-180 degrees East of North
- Group 2: Strike of 70-130 degrees East of North

Fracture lengths in Group 1 are described by a lognormal distribution with mean length of 572 m and a natural log standard deviation of 0.86 m. Group 2 contained very few fractures, so a uniform distribution having a range of 100 to 750 m was used. The distribution of fracture lengths along the dip direction was assumed to be identical to the distribution of lengths along the strike direction. In Uncertainty Case #2, the fracture lengths along the dip and the strike are kept uncertain and are generated from the respective distributions, while fixing all other flow and transport parameters as seen in Table 5-9. Figures C-3 and C-4 illustrate the results of this uncertainty case.

As can be seen from Figure C-3, the base case model has a wider range of uncertainty compared to the fracture length uncertainty case. This is reflected in both the head RMSE and the plume extent. In terms of the root mean squared error, the base case model has both higher and lower RMSE than the uncertainty case. This is because the base case model has more parameter combinations that would lead to both better and worse calibration results than the uncertainty case where all parameters are fixed except the fracture lengths.

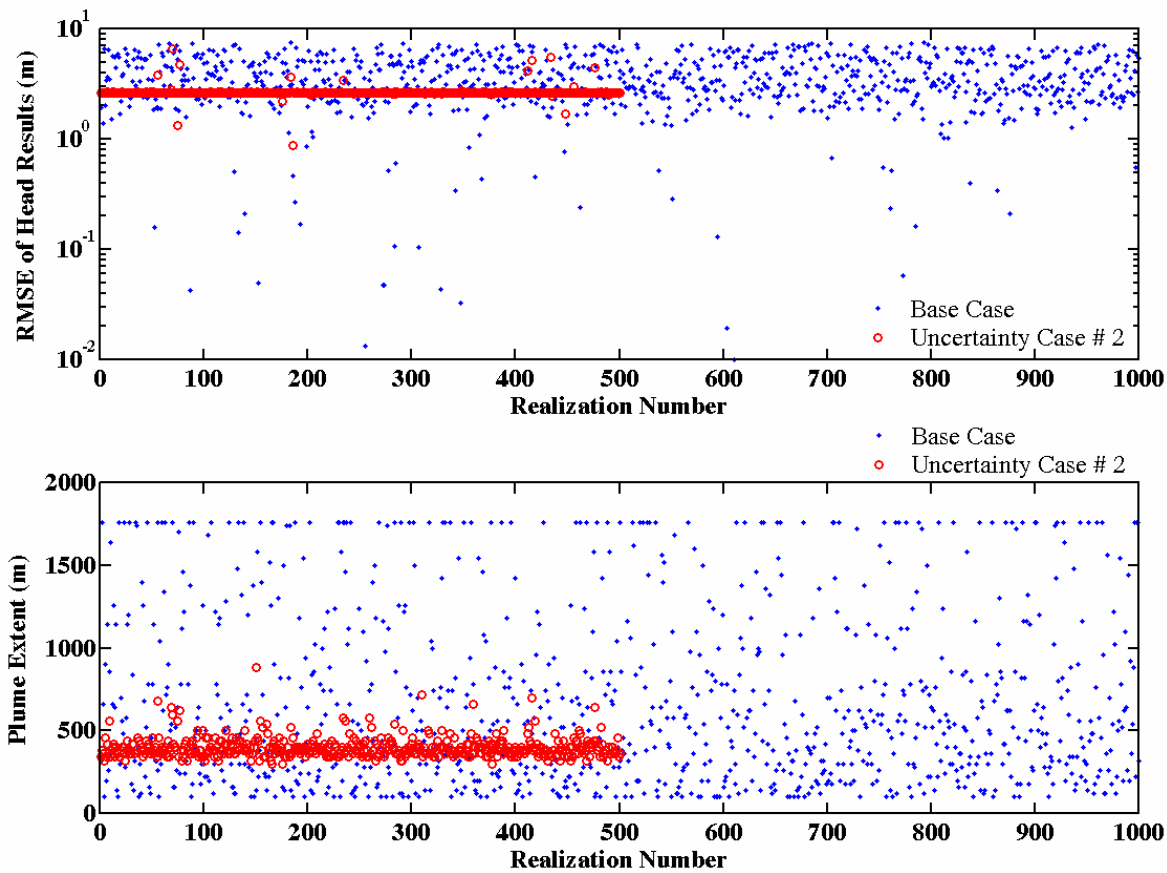

Note: Comparison is in terms of the RMSE of the head results for each flow realization and the plume extent expressed as the distance between the working point and the farthest point traveled by any particle in the transport simulations.

Figure C-3
Comparison between the base case model and the fracture length Uncertainty Case #2

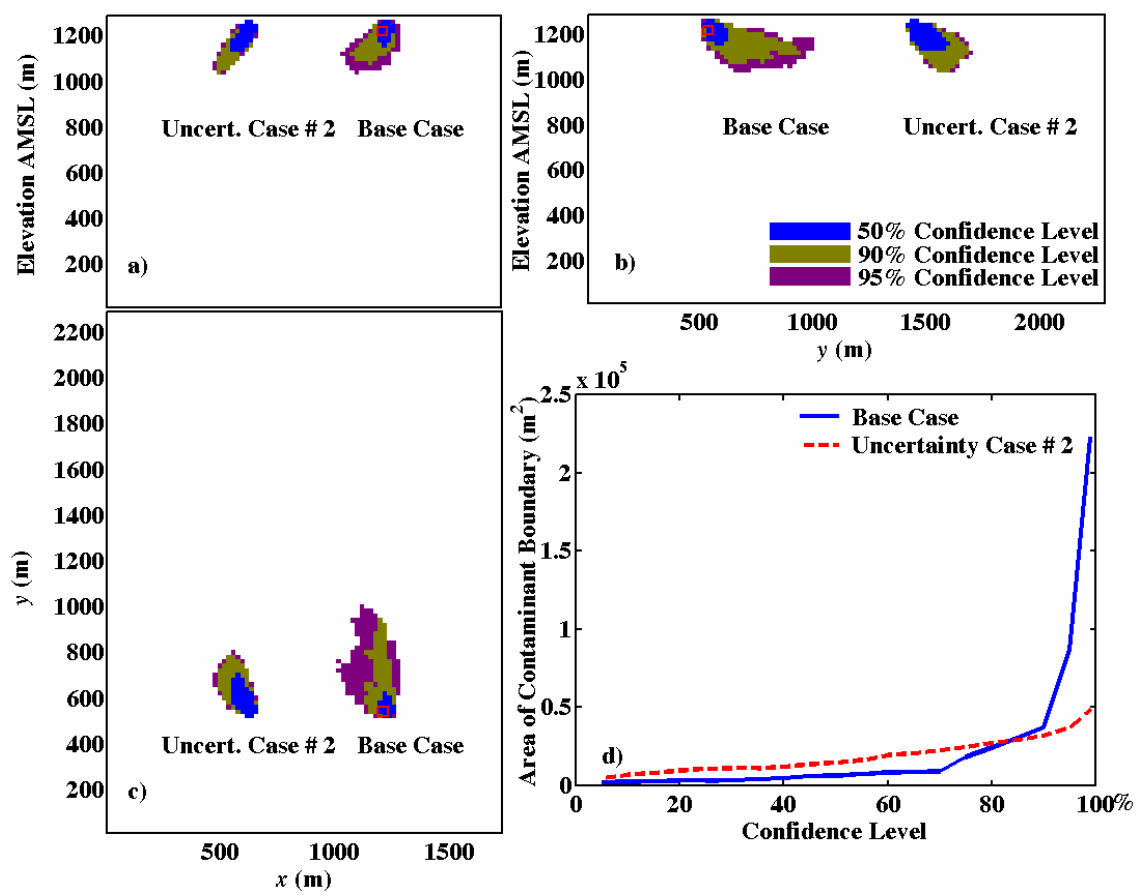

Note: Contaminant boundary maps for ^{14}C are shown, delineating the areas exceeding 2,000 pCi/L at different confidence levels. Uncertainty Case #2 is drawn to scale but is spatially shifted on the plots for comparison to the base case model. Subplot a) shows the x-z (or elevation) map, subplot b) shows the y-z map, subplot c) shows the x-y map, and subplot d) shows the x-y contaminant boundary area at different confidence levels.

Figure C-4
Comparison between the base case model and Uncertainty Case #2 in terms of a contaminant boundary and boundary uncertainty

Figure C-4 displays the contaminant boundary maps at the 50, 90, and 95 percent confidence levels (subplots a, b, and c) as well as the change in the contaminant boundary area as a function of the confidence level (subplot d). The results are very similar to Uncertainty Case #1 indicating that the uncertainty in fracture lengths minimally contributes to the overall model uncertainty. This can probably be attributed to the fact that all generated values for fracture lengths provide very well connected networks of fractures in the simulation domain (i.e., way above percolation threshold even for the smallest fracture lengths). Therefore, changing the fracture lengths above the connectivity threshold does not significantly change the migration distances away from the cavity. Given this result and the relative abundance of fracture data available for the Shoal site, the fracture length is deemed well characterized, and any new information on fracture lengths will not significantly reduce model uncertainty or help the model validation/postaudit process.

C.1.3 Case #3

Uncertainty Case #3 has the hydraulic conductivity of the cavity zone and the two zones surrounding it as uncertain. Three spherical zones are identified around the Shoal working point and are approximated in the base case model by a rectangular grid (Pohlmann et al., 2004 – Figure 3.1). The first zone represents the cavity and chimney. Values of K for the cavity and chimney are chosen from a random distribution and are assigned randomly to the cells corresponding to the cavity and chimney - no spatial correlation within this region of the model is assumed. The mean of this distribution is taken to be 43.0 m/d, which is about two and one half orders of magnitude higher than the mean of the K distribution of the undisturbed granite (the fracture conductivity studied in Case #4). A $\log_{10}$-normal distribution having a mean and standard deviation of 1.6 and 0.18 m/d, respectively, is used for the simulations. This zone is also given a porosity distribution with a higher mean as will be discussed in Case #7 below. The second zone extends from approximately 1 to 2 cavity radii (Rc) from the working point, which is about 26.0 m at Shoal. This zone is also assigned K values that are substantially higher than that of the undisturbed granite. These K values are chosen from a distribution having a mean of 8.6 m/d. A $\log_{10}$-normal distribution having a mean and standard deviation of 0.94 and 0.26 m/d, respectively, is used for the simulations. Zone 3 begins the transition from the highly disturbed, near-cavity region, to the unaffected rock. This zone extends from 2 to 4 R_C from the test and is assigned K values at the upper end of the distribution from which the K values of the undisturbed granite are selected. The distribution of K values assigned to this zone has a mean value of 0.86 m/d. A $\log_{10}$-normal distribution having a mean and standard deviation of -0.063 and 0.26 m/d, respectively, is used for the simulations.

In this uncertainty case, the conductivity values for these three zones are kept uncertain while fixing all other flow and transport parameters. For each realization, the K value for each of the three zones is drawn at random from their respective distributions as described above. The flow problem is solved for each realization followed by the transport simulations for ^{14}C. Figures C-5 and C-6 show the results of this uncertainty case. As can be seen from Figure C-5, the uncertainty in the three K values yield small range of calibration accuracy (in terms of RMSE) and a small uncertainty in the plume extent.

Figure C-6 indicates a smaller contaminant boundary for this case compared to the base case model at the 90th and the 95th percent confidence levels. The uncertainty in the contaminant boundary produced by the uncertainty in K values of the three zones around the cavity is again much smaller than the overall uncertainty built into the base case model as shown in subplot d) of Figure C-6. Since these three zones are small in scale relative to the migration distances of radionuclides from the cavity, their impact on the contaminant movement is small and thus they

contribute very little to the overall output uncertainty of the model. With the difficulty (or impossibility due to the high risk involved) of characterizing the conductivity close to the cavity and the minor impact on the model output, these K values are not suitable for being validation targets.

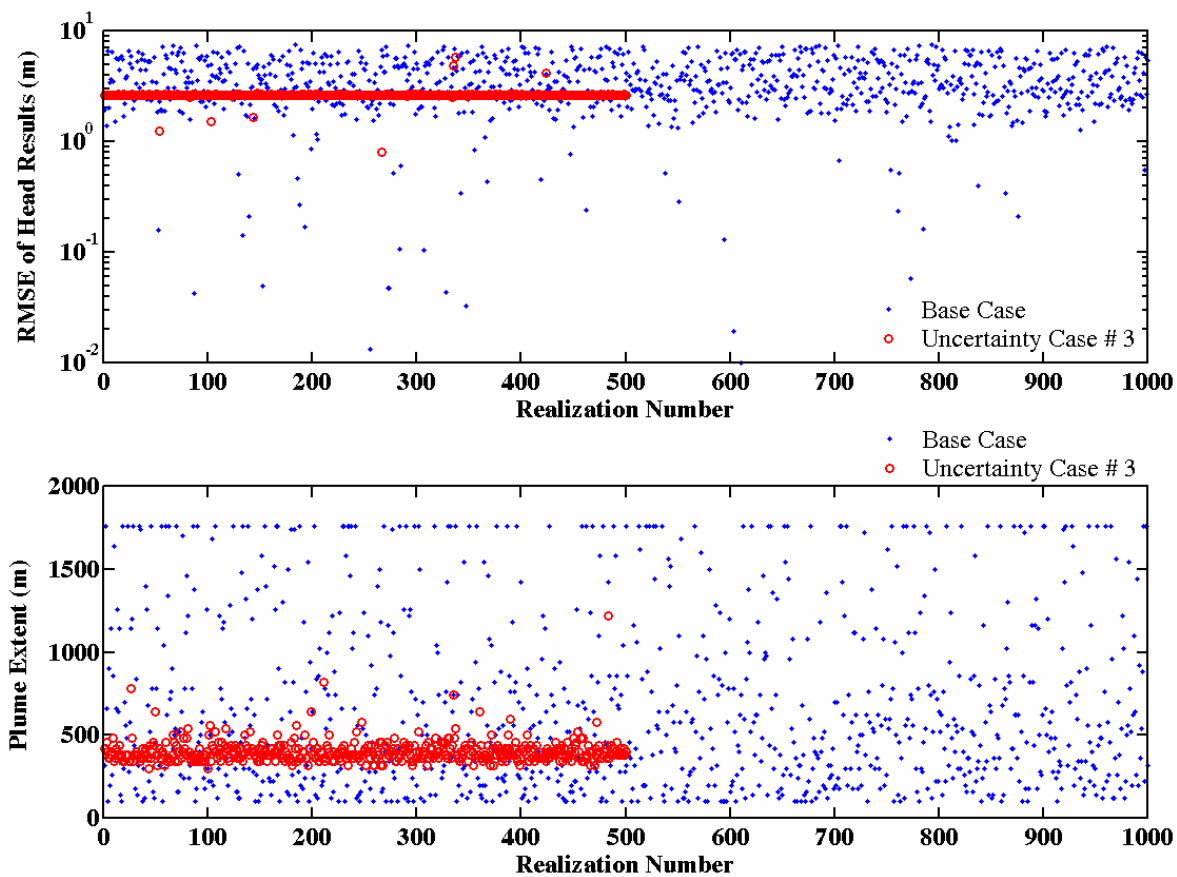

Note: Comparison is in terms of the RMSE of the head results for each flow realization and the plume extent expressed as the distance between the working point and the farthest point traveled by any particle in the transport simulations

Figure C-5
Comparison between the base case model and Uncertainty Case #3 (conductivity of cavity and the surrounding zones)

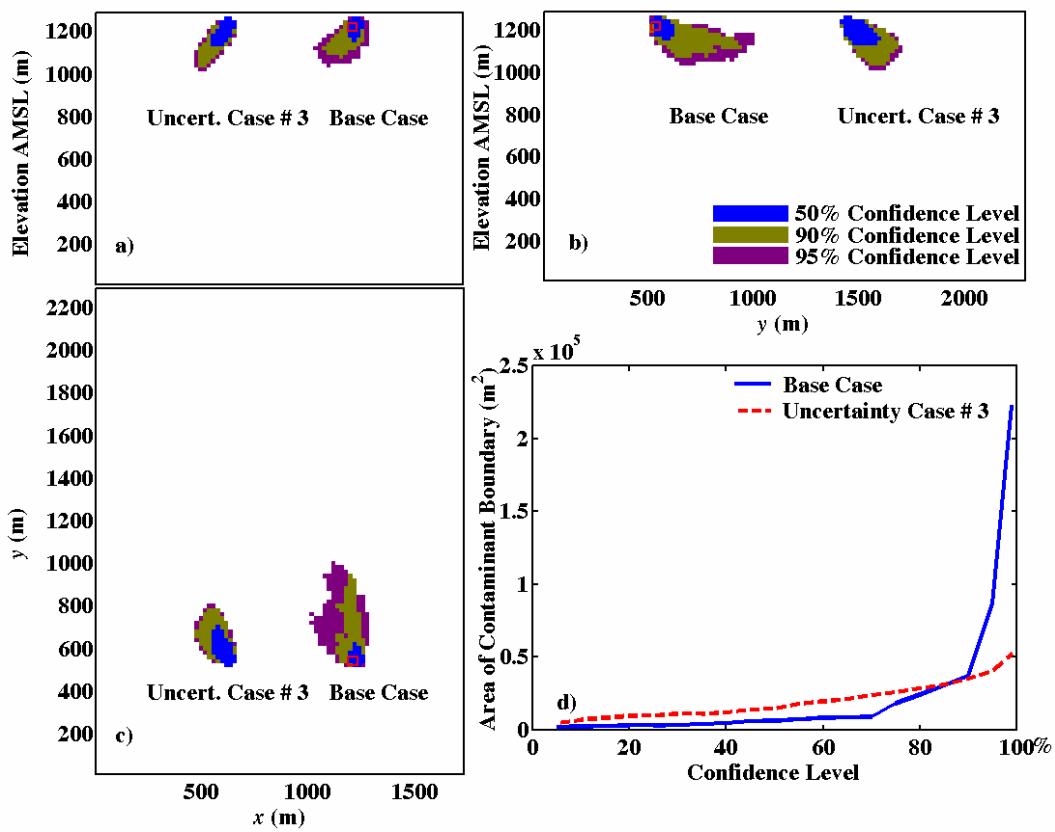

Note: Contaminant boundary maps for ^{14}C are shown, delineating the areas exceeding 2,000 pCi/L at different confidence levels. Uncertainty Case #3 is drawn to scale but is spatially shifted on the plots for comparison to the base case model. Subplot a) shows the x-z (or elevation) map, subplot b) shows the y-z map, subplot c) shows the x-y map, and subplot d) shows the x-y contaminant boundary area at different confidence levels.

Figure C-6
Comparison between the base case model and Uncertainty Case #3 in terms of a contaminant boundary and boundary uncertainty

C.1.4 Case #4

Here the conductivity of the fractured, undisturbed granite is the only uncertain parameter. In the original model, two fracture flow categories are used to characterize the fracture flow system at Shoal. Flow Category 1 represents the small and less conductive fractures, whereas Flow Category 2 is designed to represent the more conductive portions of the granite. This latter flow category is represented in the model by a $\log_{10}$-transformed triangular distribution with the minimum at -5.0 (i.e., $K_{min} = 1.0\times10^{-5}$ m/d), the maximum at 0.0 (i.e., $K_{max} = 1.0$ m/d), and the mean at -2.5 (i.e., $K_{mean} = 3.2\times10^{-3}$ m/d). The mean of this distribution is consistent with the calibrated K values obtained from the transient numerical analysis of cross-hole pumping during the 320-day tracer test conducted at HC-6 and HC-7 (3.4×10^{-3} m/d) and the regional flow model for Shoal (6.9×10^{-3} m/d). In addition, the range of the K distribution for Flow Category 2 captures the full range of the field data. The K values for Flow Category 1 were obtained during model calibration using the methodology described in Pohlmann et al. (2004).

Hydraulic conductivity values are assumed constant for each fracture in the simulated domain and no spatial correlation is assumed within either flow category. Every cell within a given individual fracture zone simulated in Flow Category 2 is assigned the same value of K that is chosen from the distribution described above. Likewise, every cell in Flow Category 1 of a given realization is assigned the same value of K as determined during model calibration that relies on the generalized likelihood uncertainty estimate methodology.

The conductivity value for the Flow Category 2 is drawn from the log-transformed triangular distribution, and during the flow simulations, the K value of Flow Category 1 is adjusted as the calibration parameter. The results of this uncertainty case are exhibited in Figures C-7 and C-8.

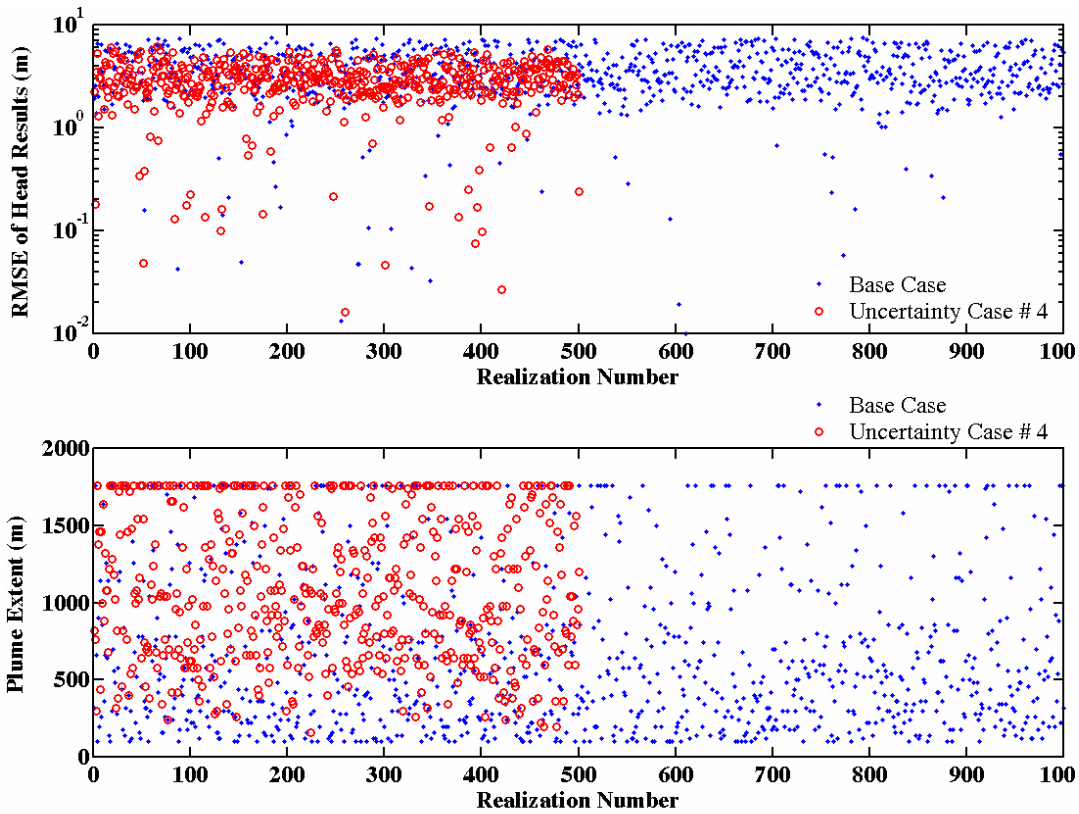

Note: Comparison is in terms of the RMSE of the head results for each flow realization and the plume extent expressed as the distance between the working point and the farthest point traveled by any particle in the transport simulations.

Figure C-7
Comparison between the base case model and the fracture conductivity Uncertainty Case #4

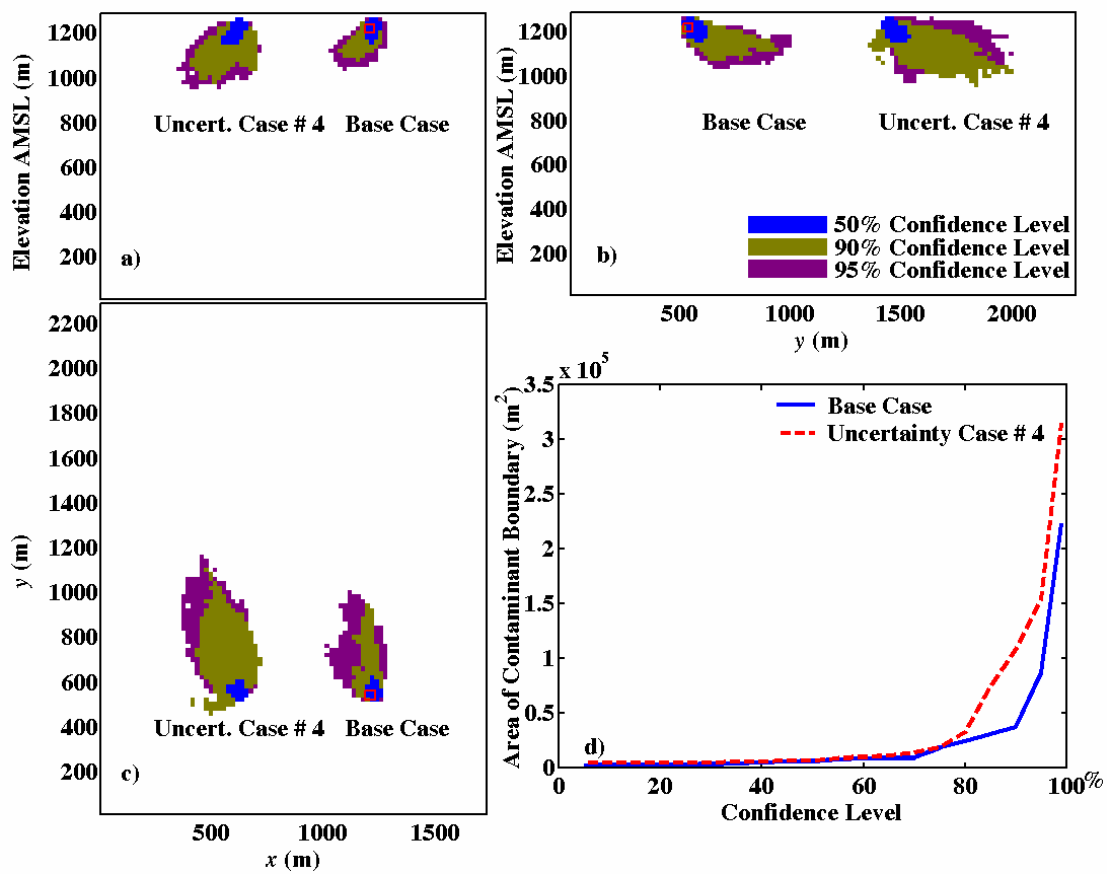

Note: Contaminant boundary maps for ^{14}C are shown, delineating the areas exceeding 2,000 pCi/L at different confidence levels. The fracture conductivity Uncertainty Case #4 is drawn to scale but is spatially shifted on the plots for comparison to the base case model. Subplot a) shows the x-z (or elevation) map, subplot b) shows the y-z map, subplot c) shows the x-y map, and subplot d) shows the x-y contaminant boundary area at different confidence levels.

Figure C-8
Comparison between the base case model and Uncertainty Case #4 in terms of a contaminant boundary and boundary uncertainty

Unlike the previous three cases, this uncertainty case shows that fracture conductivity is a major contributor to the overall model uncertainty. By far, it is the most important parameter driving the output uncertainty. As shown in Figure C-7, the fracture conductivity alone produces a range of RMSE and a range of plume extent that are only slightly narrower than the range produced by the base case model having all eleven flow and transport parameters as uncertain. Since the flow velocity in fracture Flow Category 2 is directly proportional to the hydraulic conductivity assigned to these fractures, the range of output uncertainty is derived by the uncertain velocity stemming from the conductivity uncertainty.

The unclassified ^{14}C contaminant boundaries shown in Figure C-8 indicate that the uncertainty in the fracture conductivity yields larger boundaries compared to the base case model. It also yields slightly more uncertainty than the base case model as shown by the comparison in subplot d) of Figure C-8. In the base case model, the uncertain fracture conductivity is normally combined

with other uncertain parameters, which yields different results than when all parameters are fixed at their means and only the fracture conductivity is changing. That is, when other parameters are uncertain and in the absence of any restriction on parameter correlations, high fracture conductivity values in the base case may be accompanied by high fracture velocity values and vice versa which yield less uncertainty and smaller travel distances than when the high fracture conductivity values in this uncertainty case are always associated with the mean fracture porosity.

It is apparent that the fracture conductivity is an important parameter impacting the results of the flow and transport model at Shoal. It can thus be considered as one of the validation targets for the purpose of narrowing down the range of uncertainty for that parameter and the resulting contaminant boundary uncertainty. Thus, fracture conductivity measurements should be considered as validation targets. Multiple measurements in each new well are desirable and should be considered when feasible.

C.1.5 Case #5

The recharge entering the top surface of the model domain is the last flow parameter we study in this uncertainty analysis. Recharge to the groundwater system by infiltration of precipitation through the land surface is a critical parameter controlling the velocity and direction of groundwater flow. Precipitation is thus expected to be the driving factor determining how much recharge can occur. However, recharge to the groundwater system is constrained by the observed hydraulic properties of hydraulic conductivity and head distribution. For example, a recharge rate too high relative to the hydraulic conductivity of the aquifer results in modeled water levels far higher than those observed in the field. The DDA of Pohll et al. (1999a) identified uncertainty in recharge as a significant contributor to overall model uncertainty. As a result, recharge was one of the parameters treated stochastically in the base case flow model (Pohlmann et al., 2004). Recharge is applied evenly over the top of the model domain with the value for each realization selected from a triangular distribution ranging between 0.05 and 0.70 cm/yr.

The recharge model employed in Pohlmann et al. (2004) uses the most recent and accurate recharge data in combination with a robust statistical model and it is in general agreement with the vadose zone model of Pohll (1999), which suggests that these two methods are more favorable as compared to the Maxey-Eakin recharge model and the thermal profile methods. Given the uncertainties in all models, a parsimonious model seems appropriate. Therefore, a triangular distribution is chosen to represent the potential range of recharge over the model domain as 0.05 to 0.70 cm/yr.

Using this distribution, the flow model is run with all other parameters fixed at their mean values. However, the hydraulic conductivity of fracture Flow Category 1 (small fractures) is again used as a calibration parameter and is adjusted automatically during the flow simulation. The hydraulic conductivity of Flow Category 2 is kept fixed at its mean value. The results of this uncertainty case are shown in Figures C-9 and C-10.

Figure C-9 shows that the recharge uncertainty case produces both smaller and larger RMSE than the base case model in only few realizations. In most of the realizations, the range of the head RMSE in the recharge uncertainty case is very similar to that for the base case model. The plume extent, however, does exhibit a much smaller range in the recharge uncertainty case than the base case model. Although recharge impacts the groundwater flow velocity, fixing the K value of Flow Category 2 reduces the range of velocity variability induced by the variability in recharge. It is important also to note that recharge variability alone produces a maximum plume extent of about 1000 m across all realizations, whereas the base case model produces maximum plume extent of about 1800 m. It is also of interest to note that this uncertainty case includes one realization that has a very small RMSE that is smaller than the best realization of the base case model. This realization is further analyzed in the discussion of the transport parameters uncertainty results.

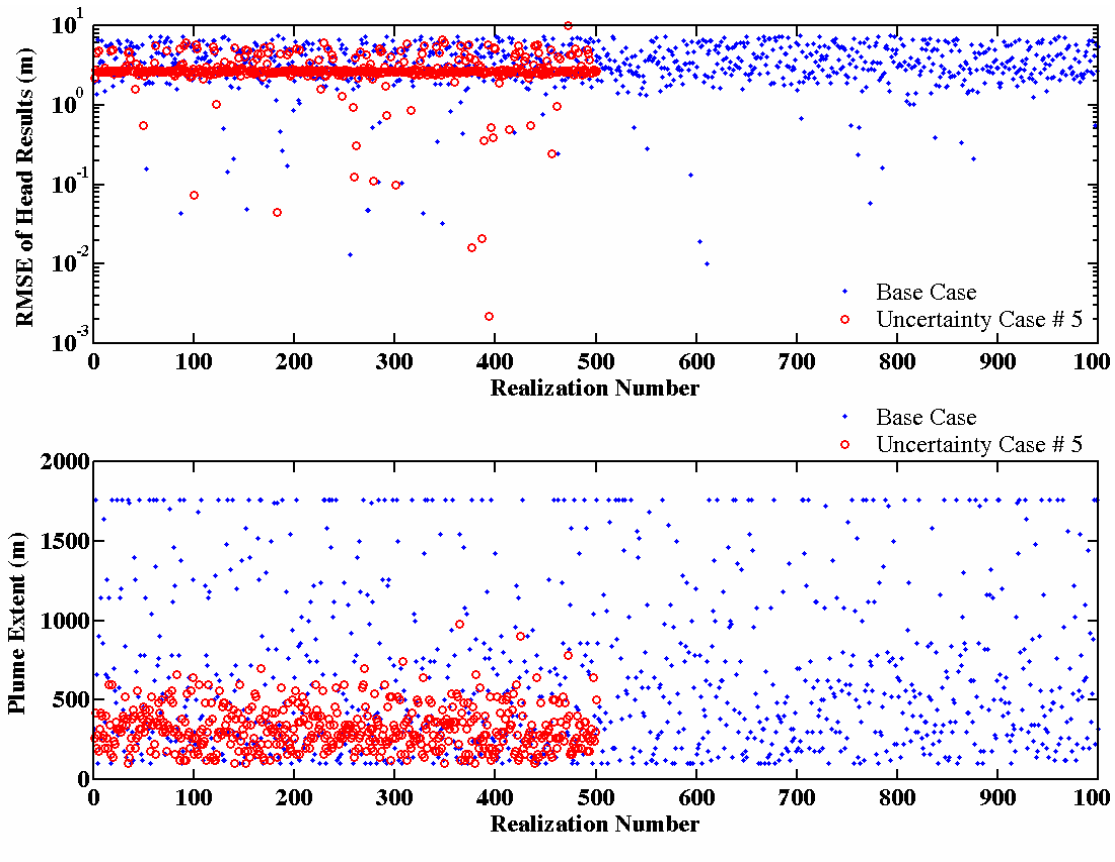

Note: Comparison is in terms of the RMSE of the head results for each flow realization and the plume extent expressed as the distance between the working point and the farthest point traveled by any particle in the transport simulations.

Figure C-9
Comparison between the base case model and Uncertainty Case #5 (recharge uncertainty)

Figure C-10 shows the resulting contaminant boundary maps and how they compare to the base case model. Interestingly, the uncertainty in the recharge value yields minor uncertainty in the contaminant boundaries. Only between the 90 and the 99 percent confidence levels does uncertainty appear in the results. So despite what one might expect, the recharge variability contributes insignificantly to the contaminant boundary uncertainty. In terms of the contaminant boundary size, the recharge uncertainty case yields very small sizes compared to the base case model. Therefore, recharge may not be considered as a validation target. However, if new temperature logs or other data provide independent recharge values, then these values could be used to confirm or invalidate the range of recharge used in the model.

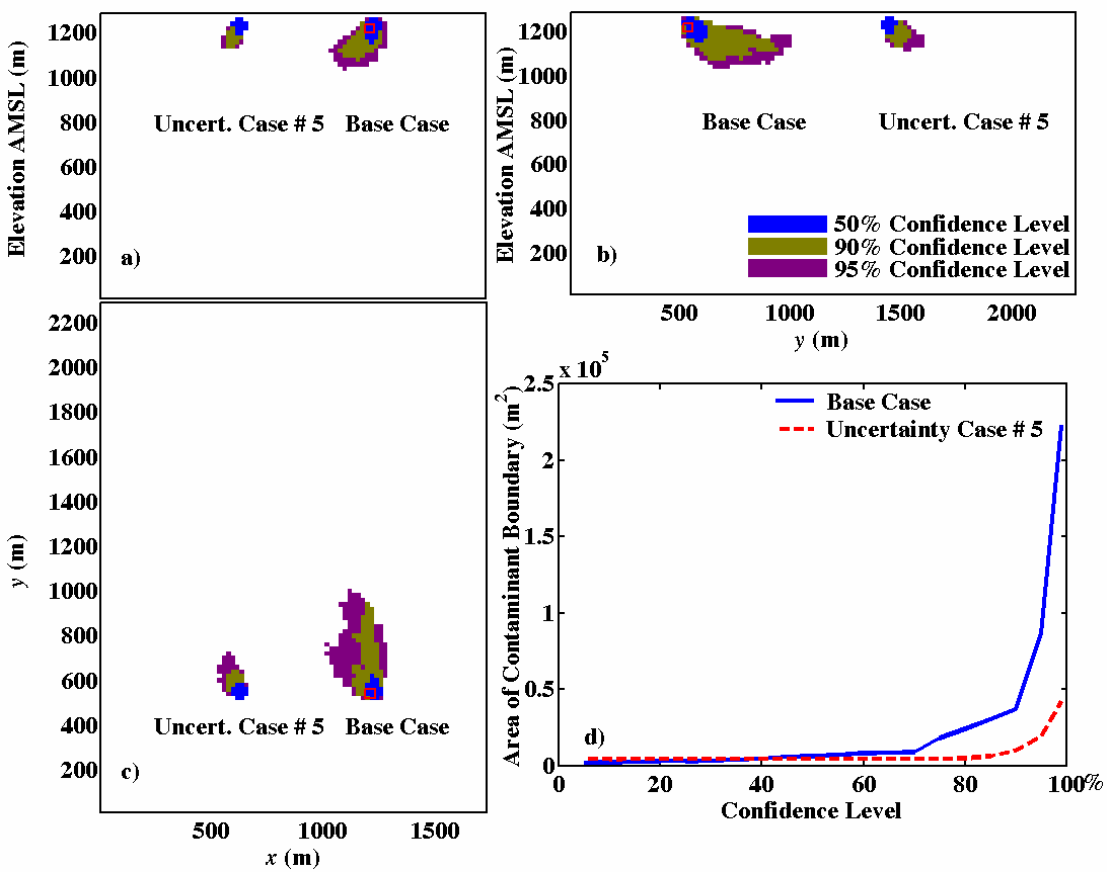

Note: Contaminant boundary maps for ^{14}C are shown, delineating the areas exceeding 2,000 pCi/L at different confidence levels. The recharge Uncertainty Case #5 is drawn to scale but is spatially shifted on the plots for comparison to the base case model. Subplot a) shows the x-z (or elevation) map, subplot b) shows the y-z map, subplot c) shows the x-y map, and subplot d) shows the x-y contaminant boundary area at different confidence levels.

Figure C-10
Comparison between the base case model and Uncertainty Case #5 in terms of a contaminant boundary and boundary uncertainty

C.2 Uncertain Transport Parameters

Four transport parameters are considered in this analysis. These are the fracture porosity, the cavity porosity, and the damaged zone porosity. These are shown in Table 5-9 presented earlier. To run the uncertainty analysis for any of these parameters, we need to select a single flow realization and solve the transport problem for different values of the parameter being studied. The flow realization selected for the analysis has a major influence on the results. Therefore, we used two criteria and selected two realizations to run the analysis for transport parameters. First, we used one of the fastest flow realizations in the base case model. We identified about 88 realizations in the base case model where particles reached the northern domain boundary. Note that individual particles reaching the end of the domain does not necessarily equate to a concentration exceeding the MCL, and thus does not necessarily lead to inclusion in the

contaminant boundary. Among these realizations, we selected the one with the least RMSE. This realization is used for cases 6a, 7a, 8a, and 9a as shown in Table 5-9.

The second criterion used to select a flow realization is the goodness of fit in the calibration process. Based on the RMSE of the modeled heads, we selected the base-case flow realization that has the least RMSE value. This realization is the basis for the transport parameters uncertainty analyses presented in cases 6b, 7b, 8b, and 9b as shown in Table 5-9 and discussed below. As mentioned earlier, one of the flow realizations in Uncertainty Case #5 attained an RMSE value smaller than this selected realization. Although not shown here, we ran the transport uncertainty analyses using that realization and found the result that the contaminant boundary did not exceed the cavity area for all cases and with no uncertainty. The reason for this result is the fact that this realization produces very flat head gradients around the cavity, which lead to very low velocities in the cavity vicinity. Therefore, regardless of the value of any transport parameter, these low velocities inhibit the particle migration and lead to small contaminant boundaries.

C.2.1 Cases #6a and #6b

In Uncertainty Case #6, the fracture porosity is considered uncertain where all other transport parameters are fixed at their mean values. The base case flow realization #284 that produces fast flow velocities is used for Case #6a, whereas realization #610 with the least RMSE is used for Case #6b. Similar to the base case model, the effective fracture porosity value is selected from a lognormal distribution that is used to describe the empirical distribution determined from the numerical analysis conducted using the tracer test results (Reimus et al., 2003). The lognormal distribution has a mean of 0.025 and a standard deviation of 0.023. The 90 percent confidence interval ranges between 0.005 and 0.07 (Pohlmann et al., 2004).

Figure C-11 shows the contaminant boundary results for Case #6a and Figure C-12 shows the results for Case #6b. These figures compare the contribution of the fracture porosity to the model output uncertainty to the contributions of all uncertain flow and transport parameters as incorporated into the base case model. It can be seen that the fracture porosity contributes significantly to the uncertainty in the contaminant boundary, especially in Case #6a with a fast flow realization. In Case #6b, however, the fracture porosity does not produce as much uncertainty as it does in Case #6a. In both cases, the flow is mainly controlled by one set of fractures that do not change between realizations as we use one flow realization and only change the fracture porosity.

To better grasp the contribution of fracture porosity (or any other transport parameter) to the overall model uncertainty, one would ideally repeat the simulations conducted here using other "representative" realizations of the base-case model that span the range of all possible flow scenarios. Then one would compute the average uncertainty by, for instance, averaging the curves in subplot d) of Figures C-11 and C-12 together with all other results based on a sufficiently large number of representative realizations. This, however, is computationally prohibitive.

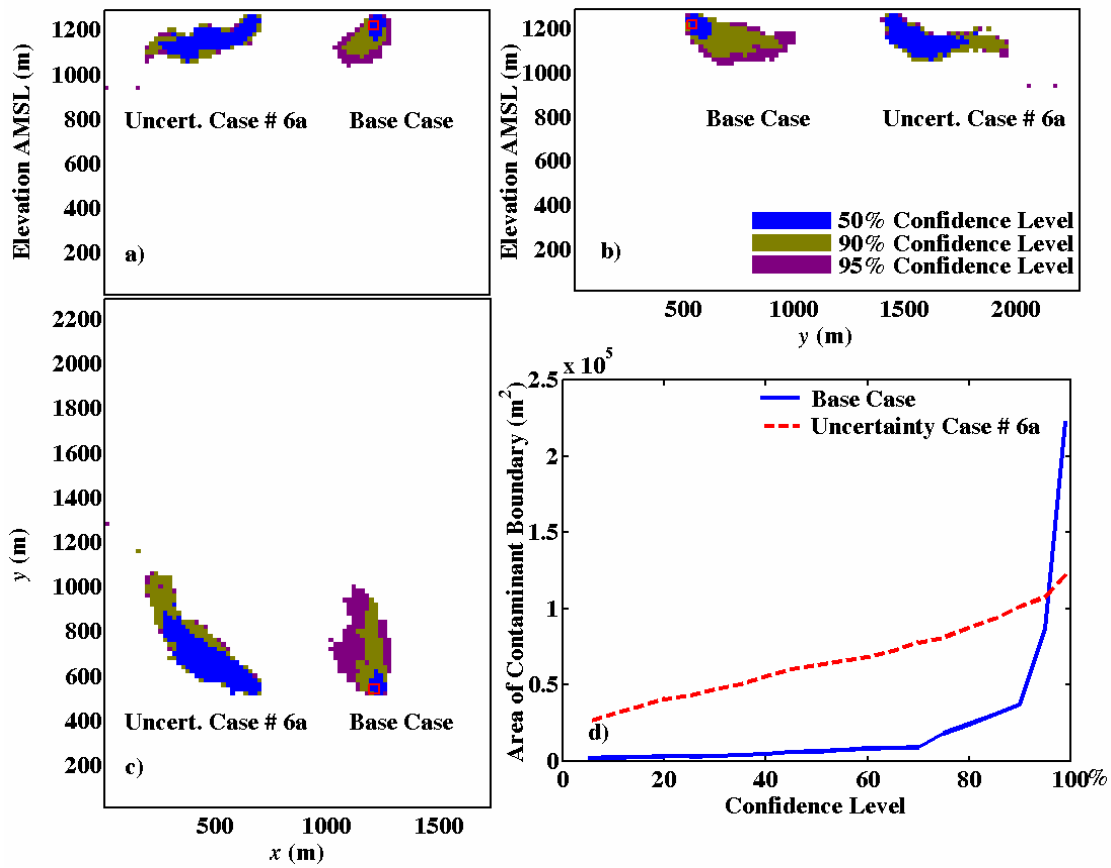

Note: Contaminant boundary maps for ^{14}C are shown, delineating the areas exceeding 2,000 pCi/L at different confidence levels. The fracture porosity Uncertainty Case #6a is drawn to scale but is spatially shifted on the plots for comparison to the base case model. Subplot a) shows the x-z (or elevation) map, subplot b) shows the y-z map, subplot c) shows the x-y map, and subplot d) shows the x-y contaminant boundary area at different confidence levels.

Figure C-11
Comparison between the base case model and fracture porosity Uncertainty Case #6a in terms of a contaminant boundary and boundary uncertainty

Field characterization efforts in 1999 and 2000 provide additional information on fracture porosity as a validation target. A long-term, sustained and substantial effort was expended through a two-well tracer test to provide information on fracture porosity and transport behavior at Shoal (Reimus et al., 2003). This effort substantially reduced prior uncertainties in porosity,

but similar reduction is unlikely in future efforts due to uncertainties in field configuration (orientation and contribution of fractures to the test) and approximations required in the analysis. Also, given that any tracer test in a fractured medium will likely span a short travel distance compared to the migration distances simulated for the 1,000-year regulatory time frame, representative fracture porosity on a large scale is very difficult to impossible to obtain. Thus, given the uncertainty of the measurement, length of time to obtain, and large cost, fracture

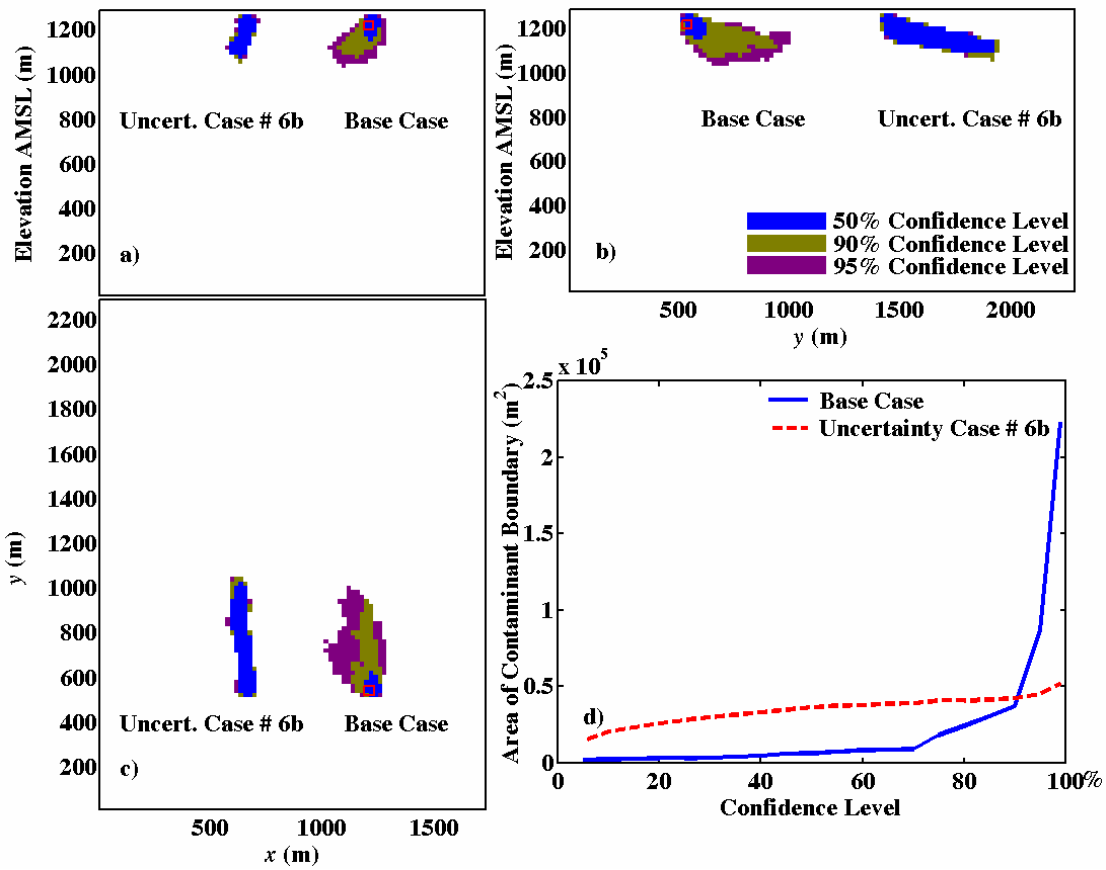

Note: Contaminant boundary maps for ^{14}C are shown, delineating the areas exceeding 2,000 pCi/L at different confidence levels. The fracture porosity uncertainty case #6b is compared to the base case model. Subplot a) shows the x-z (or elevation) map, subplot b) shows the y-z map, subplot c) shows the x-y map, and subplot d) shows the x-y contaminant boundary area at different confidence levels.

Figure C-12
Comparison between the base case model and fracture porosity Uncertainty Case #6b in terms of a contaminant boundary and boundary uncertainty

porosity is not an optimum validation target. However, other field measurements (e.g., tritium or ^{14}C concentration measurements) may indirectly help reduce the range of plausible values of fracture porosity. These measurements may confirm the predicted presence or absence of these elements in certain locations, thereby indicating what velocity range may be plausible for such findings.

C.2.2 Cases #7a and #7b

The cavity porosity is the uncertain parameter for this case. The Shoal nuclear test created a cavity that collapsed and formed a rubble chimney. The chimney did not propagate to the land surface (i.e., there is no collapse crater). The cavity radius is reported to be 26 m (Hazelton-Nuclear Science, 1965). The top of the chimney is located 108.5 m above the test location. Borg et al. (1976) reported a range for cavity and chimney porosity of 18 to 35 percent for competent rocks such as granite, basalt, and indurated tuffs. In the base case transport model uncertainty is incorporated using Borg's values as endpoints for a uniform distribution of porosity in the cavity and chimney. Thus, the porosity value is randomly selected from this uniform distribution and assigned to the eight model cells representing the cavity, and the overlying 16 cells that represent the chimney through the water table (Pohlmann et al., 2004).

Using the same flow realizations as the previous case, we obtain the results of the cavity porosity uncertainty as shown in Figures C-13 and C-14. The two figures indicate that minor differences exist between the contaminant boundaries at the 50, 90, and 95 percent confidence level. This leads to the conclusion that the cavity porosity uncertainty does not add to the model's overall uncertainty. Again, because of the locality of the cavity and chimney, the uncertainty in their porosity value does not impact far field transport as does other parameters such as conductivity and fracture porosity. This parameter is thus not a major contributor to the output uncertainty and thus cannot be considered as a validation target.

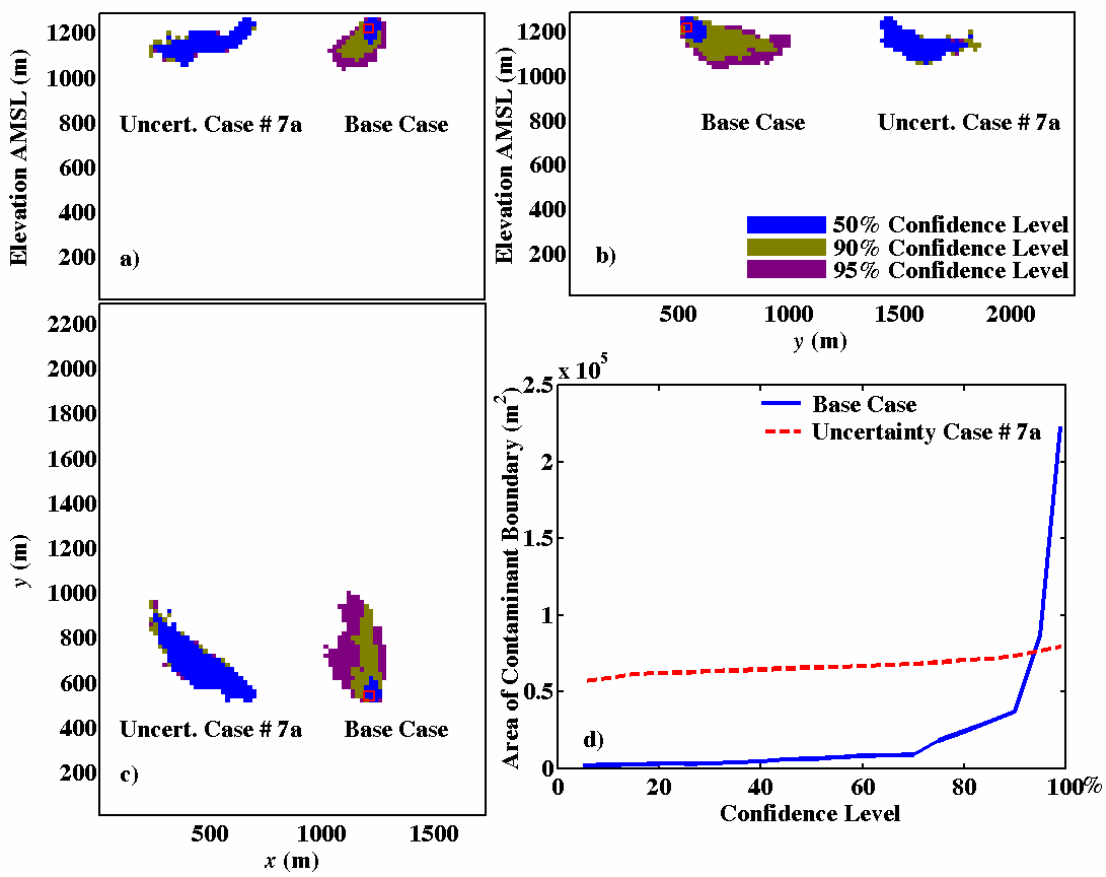

Note: Contaminant boundary maps for ^{14}C are shown, delineating the areas exceeding 2,000 pCi/L at different confidence levels. The cavity porosity Uncertainty Case #7a is compared to the base case model. Subplot a) shows the x-z (or elevation) map, subplot b) shows the y-z map, subplot c) shows the x-y map, and subplot d) shows the x-y contaminant boundary area at different confidence levels.

Figure C-13
Comparison between the base case model and cavity porosity Uncertainty Case #7a in terms of a contaminant boundary and boundary uncertainty

C.2.3 Cases #8a and #8b

The next spherical zone around the cavity represents the damaged zone of highly disturbed rock that is assigned a range of hydraulic conductivity roughly an order of magnitude higher than the highest end of the range assigned to the fractured granite. Consistent with this conceptualization of a damaged zone, the porosity of these cells are assigned random values from a uniform distribution having endpoints of 0.07 to 0.18, substantially higher than the undisturbed rock, but lower than that of the cavity (Pohlmann et al., 2004).

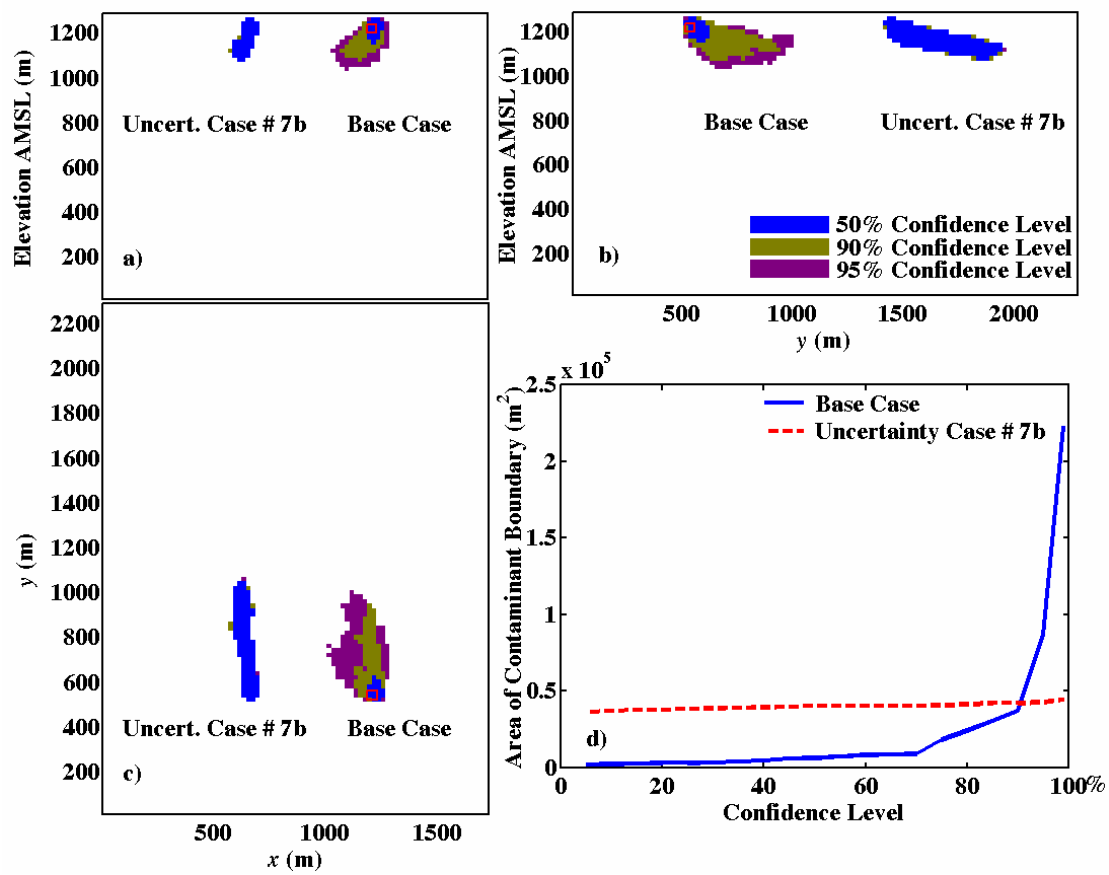

Note: Contaminant boundary maps for ^{14}C are shown, delineating the areas exceeding 2,000 pCi/L at different confidence levels. The cavity porosity Uncertainty Case #7b is drawn to scale but is spatially shifted on the plots for comparison to the base case model. Subplot a) shows the x-z (or elevation) map, subplot b) shows the y-z map, subplot c) shows the x-y map, and subplot d) shows the x-y contaminant boundary area at different confidence levels.

Figure C-14
Comparison between the base case model and cavity porosity Uncertainty Case #7b in terms of a contaminant boundary and boundary uncertainty

The uncertainty analysis for the damaged zone porosity is performed on the same two flow realizations as before. The results of the 500 realizations are summarized in Figures C-15 and C-16. Similar to the cavity porosity case, the damaged zone porosity contributes very little to the overall uncertainty of the model. However, the damaged zone porosity impacts the contaminant boundary uncertainty more than does the cavity porosity. These results added to the fracture porosity uncertainty (Case #6) are consistent with the conceptual model of Shoal. The gradual transition from the cavity outward is reflected in a gradual increase in the porosity contribution to the model uncertainty as one moves from the cavity/chimney area to the damaged zone to the undisturbed rock. Once again none of these three porosity values could be better characterized in the field and thus are not considered as targets for the validation process.

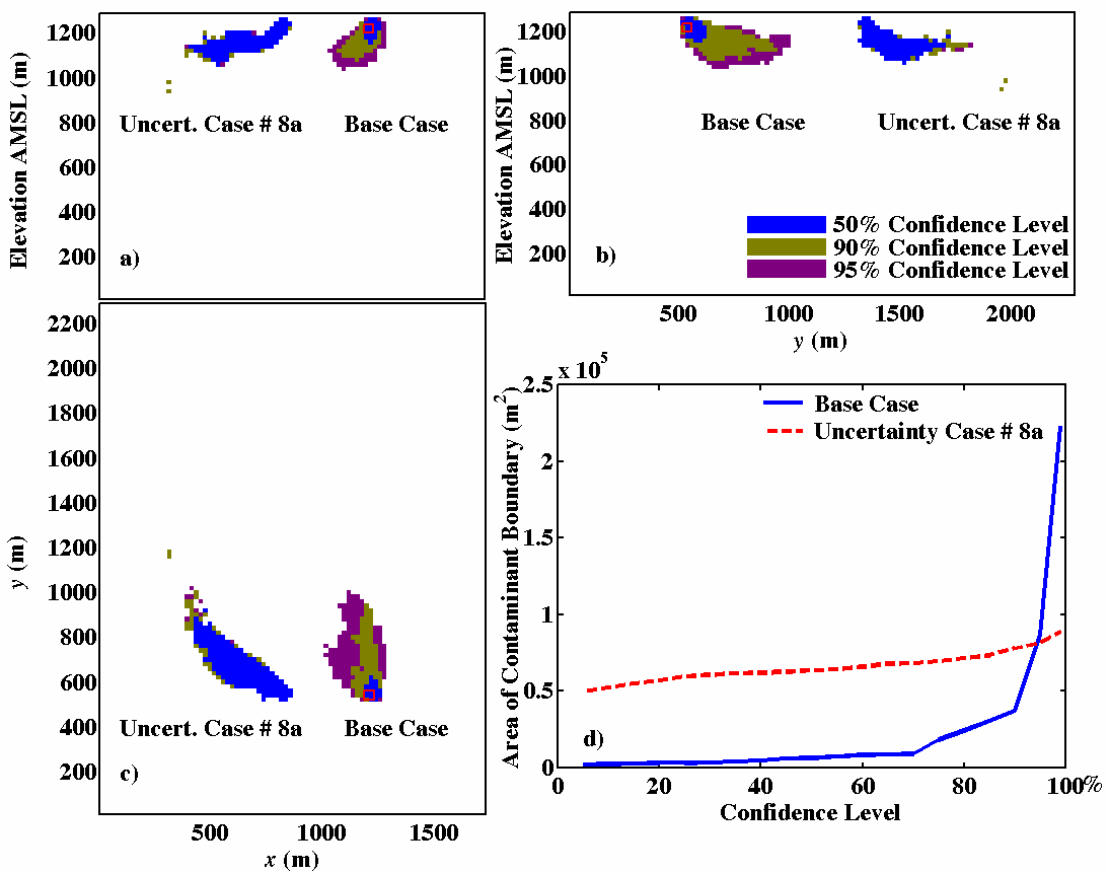

Note: Contaminant boundary maps for ^{14}C are shown, delineating the areas exceeding 2,000 pCi/L at different confidence levels. The damaged zone porosity Uncertainty Case #8a is drawn to scale but is spatially shifted on the plots for comparison to the base case model. Subplot a) shows the x-z (or elevation) map, subplot b) shows the y-z map, subplot c) shows the x-y map, and subplot d) shows the x-y contaminant boundary area at different confidence levels.

Figure C-15
Comparison between the base case model and damaged zone porosity Uncertainty Case #8a in terms of a contaminant boundary and boundary uncertainty

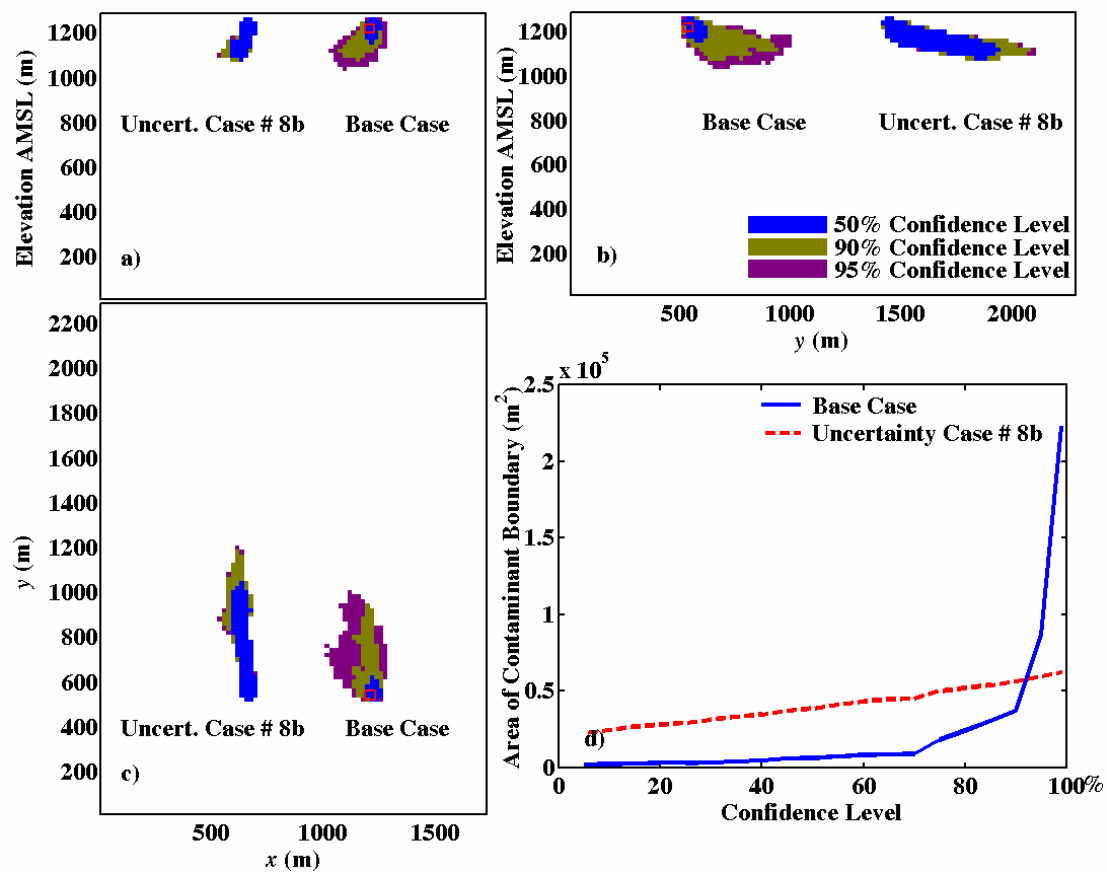

Note: Contaminant boundary maps for ^{14}C are shown, delineating the areas exceeding 2,000 pCi/L at different confidence levels. The damaged zone porosity Uncertainty Case #8b is drawn to scale but is spatially shifted on the plots for comparison to the base case model. Subplot a) shows the x-z (or elevation) map, subplot b) shows the y-z map, subplot c) shows the x-y map, and subplot d) shows the x-y contaminant boundary area at different confidence levels.

Figure C-16
Comparison between the base case model and damaged zone porosity Uncertainty Case #8b in terms of a contaminant boundary and boundary uncertainty

C.2.4 Cases #9a and #9b

The transport simulations for the base case Shoal model included the process of matrix diffusion. The process was incorporated into the RWPT method using a particle transfer approach. Although similar transport models for the Central Nevada Test Area site used the particle transfer approach developed by Liu et al. (2000), more accurate methods have been developed recently and were used in the Shoal transport model. These methods were based on the studies of Hassan (2002), Liu et al. (2002), Hassan and Mohamed (2003), Pan and Bodvarsson (2002), and Pan et al. (2001).

In the base case model, Pohlmann et al. (2004) adopted a Markov chain model to simulate the particle transfer between the fracture and matrix waters. This Markov chain model is extended to simulate the particle transfer across the fracture/matrix interface by coupling the "active diffusion range" as developed by Pan and Bodvarsson (2002) into the model. The advantage of this approach is that it allows a relatively large time interval (Δt), which dramatically reduces the computation time. The model also allows for multiple fractures within a single grid cell, which effectively increases the effective fracture-matrix interface area. As mentioned earlier, the different parameters affecting the transfer probability were obtained by calibration to the Shoal tracer test data and then kept constant in all realizations.

Here we evaluate the impact of uncertainty stemming from matrix diffusion parameters. We select the fracture spacing parameter as the uncertain parameter but any other parameter could also be used for this purpose. A lognormal distribution with mean –0.938 and a standard deviation of 0.7 is used for the fracture spacing, which yields values for this parameter with a mean of 0.5 m (equivalent to the deterministic values used in the base case) and a range of about 0.05 to 2.5 m. This range leads to uncertainty in the transfer probability and in turn it changes the strength of matrix diffusion from one realization to another. Figures C-17 and C-18 show the results of this uncertainty case.

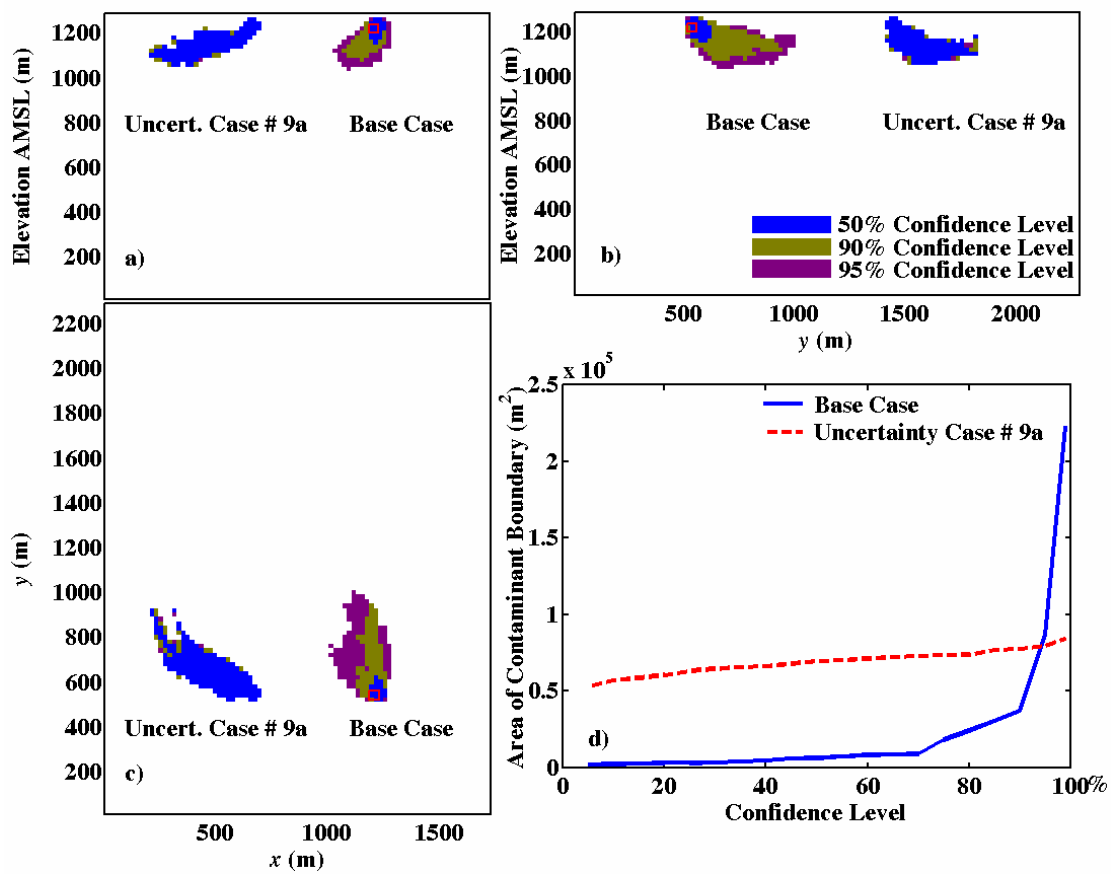

Notes: Contaminant boundary maps for ^{14}C are shown, delineating the areas exceeding 2,000 pCi/L at different confidence levels. The matrix diffusion Uncertainty Case #9a is drawn to scale but is spatially shifted on the plots for comparison to the base case model. Subplot a) shows the x-z (or elevation) map, subplot b) shows the y-z map, subplot c) shows the x-y map, and subplot d) shows the x-y contaminant boundary area at different confidence levels.

Figure C-17
Comparison between the base case model and matrix diffusion Uncertainty Case #9a in terms of a contaminant boundary and boundary uncertainty

Case 9a shows that the effect of uncertainty in matrix diffusion is enhanced by the set of strong fractures having high velocities as were the case for previous parameters (i.e., Cases #6a, #7a, and #8a). The results, however, exhibit less sensitivity to matrix diffusion compared to other transport parameters such as damaged zone porosity and fracture porosity. Case #9b that used the flow realizations having the least RMSE shows very little sensitivity to the matrix diffusion parameter. So, given these results and the fact that matrix diffusion parameters were obtained by calibration to the tracer test data, the matrix diffusion parameter would not be considered as a useful validation target.

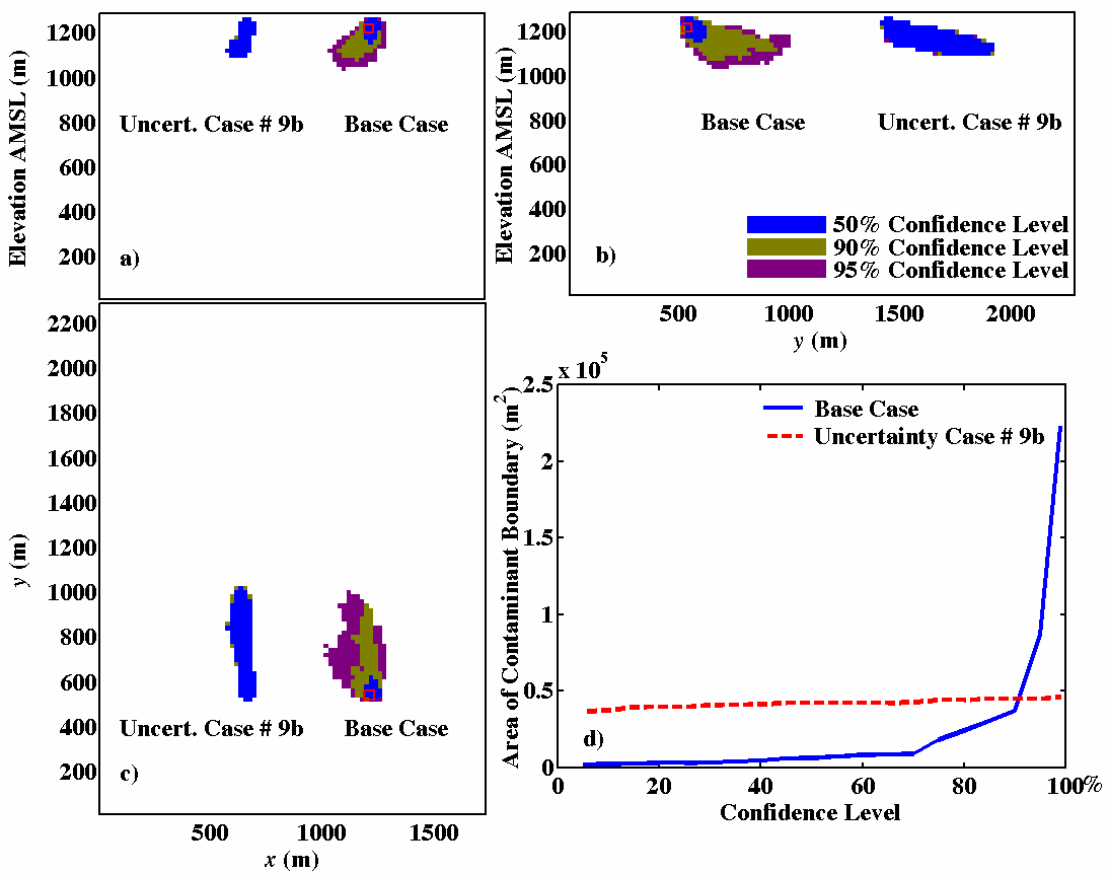

Note: Contaminant boundary maps for ^{14}C are shown, delineating the areas exceeding 2,000 pCi/L at different confidence levels. The matrix diffusion Uncertainty Case #9b is drawn to scale but is spatially shifted on the plots for comparison to the base case model. Subplot a) shows the x-z (or elevation) map, subplot b) shows the y-z map, subplot c) shows the x-y map, and subplot d) shows the x-y contaminant boundary area at different confidence levels.

Figure C-18

Comparison between the base case model and matrix diffusion Uncertainly Case #9b in terms of a contaminant boundary and boundary uncertainty

Appendix D
Validation Metrics and Application to the Shoal Model

Table of Contents

D.1 Single Validation Target Illustration D-1

D.2 Testing the Efficacy of P_1 for a Single Validation Target D-3

D.3 Multiple Validation Targets Illustration D-6

D.4 Testing the Efficacy of P_1 for Multiple Validation Targets D-12

D.5 Testing the Efficacy of P_2 for Multiple Validation Targets D-14

Figures

Figure D-1 The head distribution (or pdf) as obtained from the Shoal model for one interval in one target well D-2

Figure D-2 Realizations scores, Sj, relative to the Reference Value, RV, for the single validation target case D-2

Figure D-3 The Reference Value, RV, for the single validation target case as a function of the measured field value D-4

Figure D-4 The P_1 metric, student t distribution, and the results of hypothesis testing using the Z test D-5

Figure D-5 Example 1 showing the pdf distributions for validation targets 1 through 9 ..... D-7

Figure D-6 Example 1 showing the pdf distributions for validation targets 10 through 18 ..... D-8

Figure D-7 Example 1 showing individual realization scores, Sj, relative to the Reference Value, RV D-9

Figure D-8 Example 2 showing the pdf distributions for validation targets 1 through 9 ..... D-10

Figure D-9 Example 2 showing the pdf distributions for validation targets 10 through 18 ..... D-11

Figure D-10 Example 2 showing individual realization scores, Sj, relative to the Reference Value, RV D-12

Figures *(Continued)*

Figure D-11 The P_1 metric (blue), its mean (magenta), its best fit normal distribution (black), student t distribution (green), and the results of hypothesis testing using the Z test (red) for the multiple validation targets case D-14

Figure D-12 The P_2 metric (blue) and its mean (magenta) for the multiple validation targets case D-15

Appendix D Validation Metrics and Application to the Shoal Model

D.1 Single Validation Target Illustration

The first criterion is to compute the number of realizations with scores S_j above a reference value. To demonstrate how this reference value is computed, assume we only have one validation target (e.g., the head measurement in one interval in one well). Figure D-1 shows the pdf for this head value as produced by the stochastic Shoal model where the triangles represent the 2.5th, 50th, and 97.5th percentiles and the circle indicates a hypothesized field measurement, h_o. The reference value and the score for any individual realization for this simple case are computed as

$$RV = \exp\left[-\frac{(h_o - h_{2.5})^2}{(h_{97.5} - h_{2.5})^2}\right] \quad \text{for } h_o < h_{50}$$
$$RV = \exp\left[-\frac{(h_o - h_{97.5})^2}{(h_{97.5} - h_{2.5})^2}\right] \quad \text{for } h_o > h_{50} \qquad \text{(D-1)}$$

$$\text{Realization Score } (S_j) = \exp\left[-\frac{(h_o - h_j)^2}{(h_{97.5} - h_{2.5})^2}\right] \quad \text{for } j = 1, \ldots, NMC \qquad \text{(D-2)}$$

$$\text{First Criterion } (P_1) = \frac{\#\text{ of Realizations where } S_j > RV}{NMC} \qquad \text{(D-3)}$$

where j is the realization index and it varies from 1 to the number of Monte Carlo realizations (NMC) with NMC being 1,000 realizations for the Shoal model. This leads to all realizations with absolute errors smaller than ($|h_o - h_{2.5}|$) or ($|h_o - h_{97.5}|$), whichever is smaller, attaining a score higher than the reference value (RV). Figure D-2 shows the resulting scores and how they compare to the RV as obtained from the above equations.

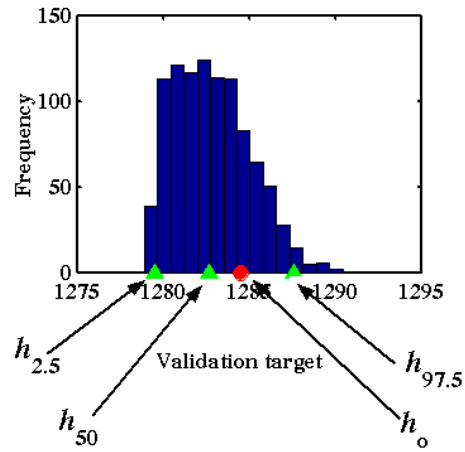

Note: The 2.5th, 50th, and 97.5th percentiles are shown by the green triangles and the hypothesized field data are shown by the red circle.

Figure D-1
The head distribution (or pdf) as obtained from the Shoal model for one interval in one target well

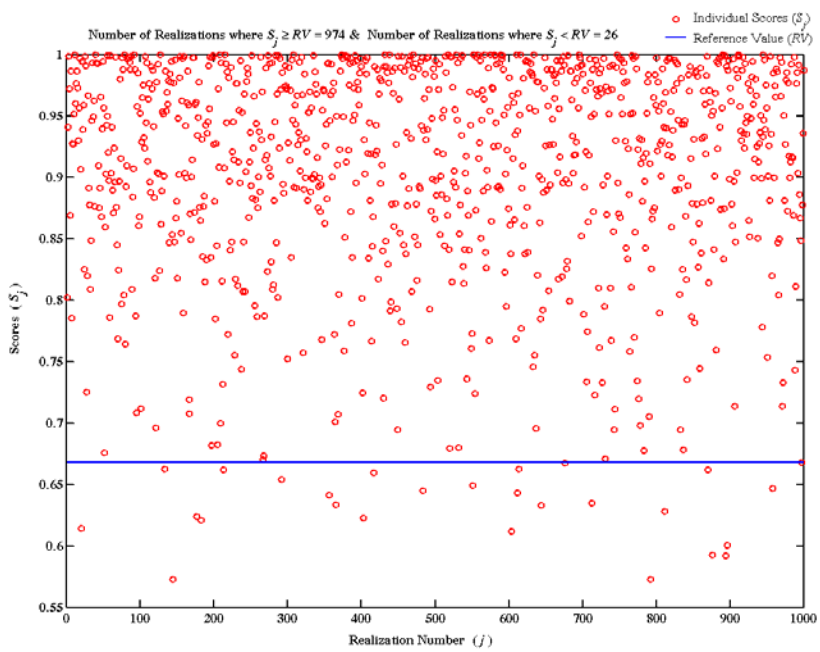

Note: The P_1 value here is 97.4 percent (= 974/1000).

Figure D-2
Realization scores, Sj, relative to the Reference Value, RV, for the single validation target case

It can be seen from Equations D-1 to D-3 that the maximum value that RV or Sj can attain is 1.0. Thus if the observed value, ho, is equivalent to the 2.5th or the 97.5th value, P_1 becomes zero because RV becomes 1.0 and all Sj values will be less than 1.0. Also, if the observed value is

found to be less than $h_{2.5}$ or greater than $h_{97.5}$, P_1 will be automatically set to zero. In such cases, one may conclude that the model output is skewed toward higher or lower values than indicated by field data. However, this does not necessarily indicate conceptual problems and it may be an indication of incorrect input parameter distributions. The other tests and evaluations can help identify the reasons for this output skewness. When the measured value coincides with the mean value (or 50th percentile) of the target output, h_{50}, then P_1 will approximately be 95 percent indicating that 95 percent of the realizations attained scores higher than RV.

D.2 Testing the Efficacy of P_1 for a Single Validation Target

To investigate the P_1 metric for the case of a single validation target, we assume a distribution form for the model output. For simplicity, it is assumed that the model predictions follow a standard normal distribution with zero mean and unit variance, so $h_{50} = 0.0$, $h_{2.5} = -1.96$, and $h_{97.5} = 1.96$. We test the performance of this metric for a range of measurement values (hypothesized values for the single field data point) between –10.0 and +10.0. For each one of these hypothesized values, the RV can be obtained according to Equation (1) and the results are shown in Figure D-3. The RV metric decreases rapidly as the observation value approaches the median, h_{50}. When the measured value lies outside the middle 95 percent of the output distribution (i.e., outside the range [-1.96, 1.96]), we do not compute the RV since P_1 becomes zero. Also, as shown in the figure, when h_o equals –1.96 ($h_{2.5}$) or 1.96 ($h_{97.5}$), RV equals 1.0. Due to the exponential form in Equation (2), all Sj values will be less than 1.0 resulting in a zero value for P_1 when h_o is at the 2.5^{th} or 97.5^{th} percentile.

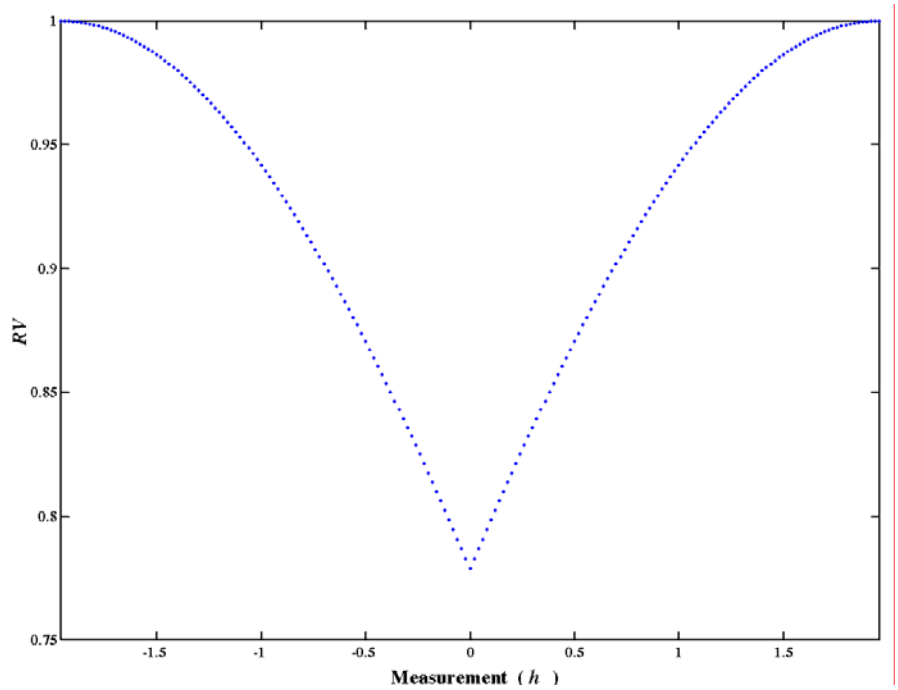

Figure D-3
The Reference Value, RV, for the single validation target case as a function of the measured field value

The next step is to calculate the Sj score for each Monte Carlo realization, with Sj being a similar measure to the RV, but using individual realization predictions. The Sj score is compared to the RV score and the relative number of Sj values that exceed the RV are tallied to obtain P_1. The Sj values and the corresponding P_1 value were tallied for a range of single observation values in the range [-10, 10] as shown in Figure D-4.

Figure D-4 also compares the P_1 metric to the t-distribution with one degree of freedom. The t-distribution is commonly used to test the statistical differences among means when the variance of the distribution is not known. The distribution plotted with green in the figure simply shows the value of the significance level, α, at which each observation on the range [–10, 10] would be rejected in a hypothesis testing that evaluates the statistical difference between the mean of the model output (assumed standard normal distribution) and each observed value (assuming that each observed value represents a distribution with only one [n = 1] sample). The one degree of freedom used in this plot is not exactly correct as the degrees of freedom are actually n - 1 = 0.

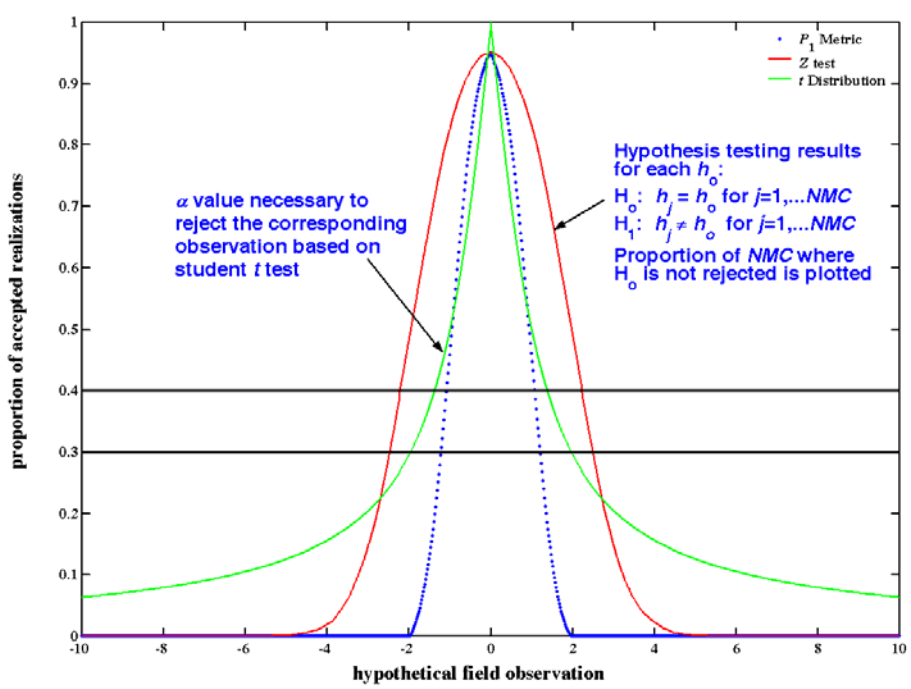

Figure D-4
The P_1 metric, student t distribution, and the results of hypothesis testing using the Z test

To avoid this limitation, we employ the Z test that is commonly used for the same purpose, but it assumes that the variances of the distributions are known. We assume that each observation is a mean of a normal distribution and each output realization represents a mean of a normal distribution. For each observation value, we then test the following hypothesis:

$$\begin{aligned} \mathrm{H}_0 &: h_j = h_o \qquad for\ \ j = 1, \ldots, NMC \\ \mathrm{H}_1 &: h_j \neq h_o \qquad for\ \ j = 1, \ldots, NMC \end{aligned} \tag{D4}$$

Then the proportion of Monte Carlo realizations where the null hypothesis, H_0, above is not rejected is plotted against each observation value as shown with the red line in Figure D-4.

The plots in Figure D-4 provide an indication of how the P_1 test compares against standard statistical tests. According to the figure, one would accept all model realizations for any of the observed values [-10, 10] based on the student t-test. In other words, if the t-test is used, one would not reject any of the model realizations until approximately the absolute value of the observation is well above 10 (at the 95 percent confidence level). On the other hand, the P_1 measure and the Z-test both indicate decreasing proportions of acceptable realizations as one deviates from the median of the model output distribution which is zero in this test case. At the five percent significance level and if the observed value coincides with the median of the model output, only 95 percent of the realizations are deemed acceptable using the P_1 measure and the

Z test. When the observed value deviates from the median, the proportion of acceptable realizations drops faster using the P_1 measure compared to the Z test. For example, 40 percent or more of the model realizations would be accepted using the Z test for any observation value in the range [-2.22, 2.22], whereas the P_1 measure gives this level of acceptance for a narrower range of observation values [-1.07, 1.07].

At first glance it appears that the two methods (the P_1 measure versus the Z-test or the t-test) are in large disagreement. But Type I error (rejecting a model realization when in fact it is a good one) versus Type II error (accepting a poor model realization) must be considered. The P_1 metric is essentially reducing the Type II error at the expense of Type I error. As discussed by Sargent (1990), the probability of Type I error is called model builder's risk, whereas the probability of Type II error is called model user's risk, and in model validation, model user's risk is extremely important and must be kept small. As a result, it is believed that the restrictiveness of the P_1 measure helps minimize Type II error and thus reduce the model user's risk (both DOE and NDEP) at the expense of increasing model builder's risk (supposedly the research team evaluating the model).

D.3 Multiple Validation Targets Illustration

For the general case of having N validation targets, the above equations should be modified to account for these different validation targets. In this case, the RV and the individual scores, Sj, will depend on the sum of squared deviations between each observation, h_o, and the corresponding $h_{2.5}$ or $h_{97.5}$. The equations thus become

$$\text{Reference Value } (RV) = \exp\left(-\sum_{i=1}^{N} \min\left[(h_{o_i} - h_{2.5_i})^2, (h_{o_i} - h_{97.5_i})^2\right] / \sum_{i=1}^{N} [h_{97.5_i} - h_{2.5_i}]^2\right) \quad \text{(D-5)}$$

$$\text{Realization Score } (S_j) = \exp\left(-\sum_{i=1}^{N} [h_{o_i} - h_j]^2 / \sum_{i=1}^{N} [h_{97.5_i} - h_{2.5_i}]^2\right) \quad \text{for } j = 1, \ldots, NMC \quad \text{(D-6)}$$

For demonstration purposes and as an example, assume the hypothetical case that data are collected on 18 validation targets. These, for example, could be conductivity data in three wells, three measurements each (i.e., 9 intervals) and head data for the same intervals. For each one of these targets, the current stochastic Shoal model provides a distribution of values, as each realization of the model has different values for these targets than other realizations. We then assume that the values of the field data are known (we pick at random one realization to provide an example observation for all targets.) Figures D-5 through D-7 show the results of this example (Example 1) where P_1 is found to be about 76.7 percent. In this case, we do not check for P_2 and

accept the sufficiency of the number of realizations having acceptable scores. Note, however, that if we were to check P_2, it would be about 94 percent (=17/18).

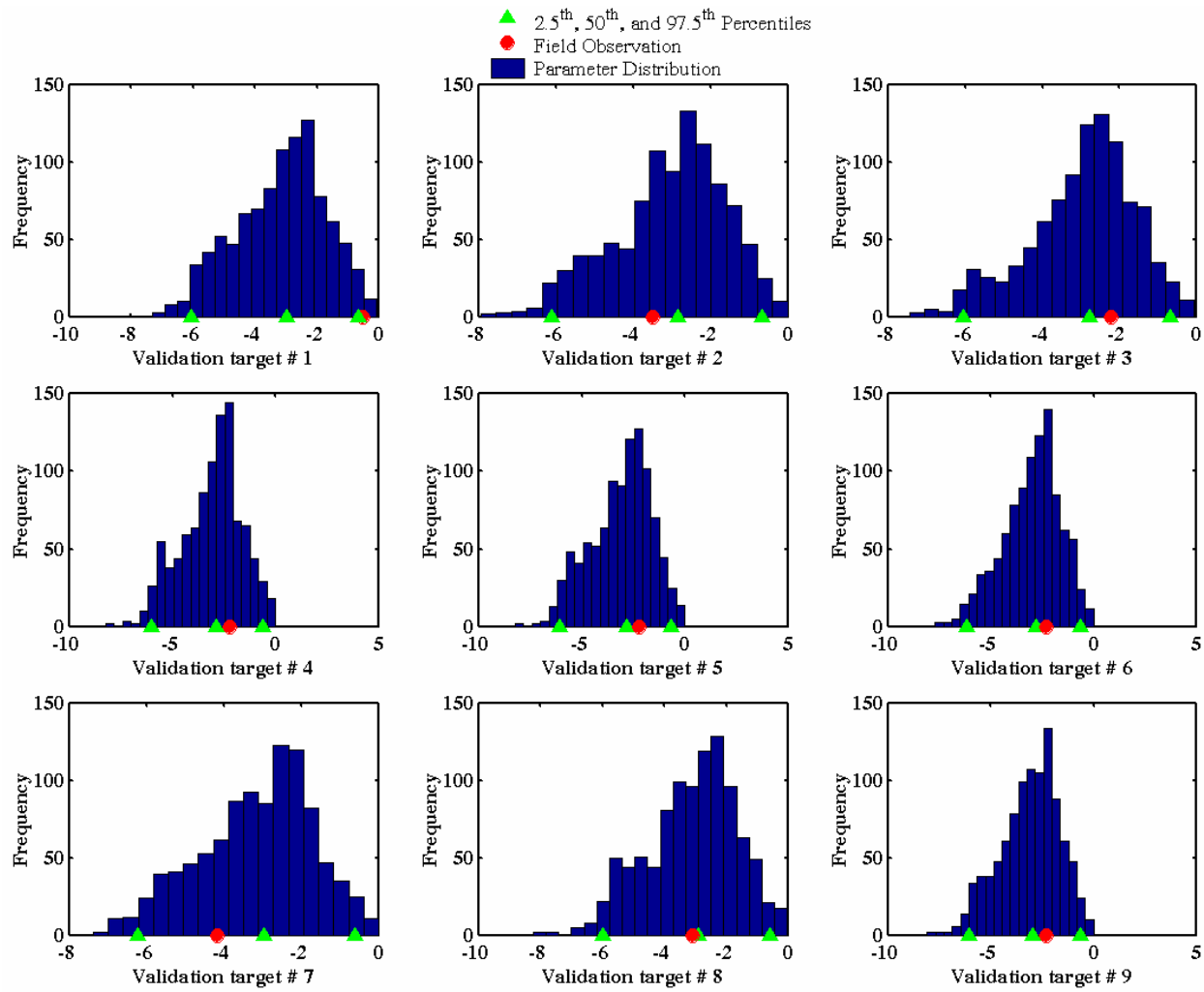

Notes: The 2.5th, 50th, and 97.5th percentiles are shown by the green triangles and the hypothesized field data are shown by the red circles.

Figure D-5
Example 1 showing the pdf distributions for validation targets 1 through 9

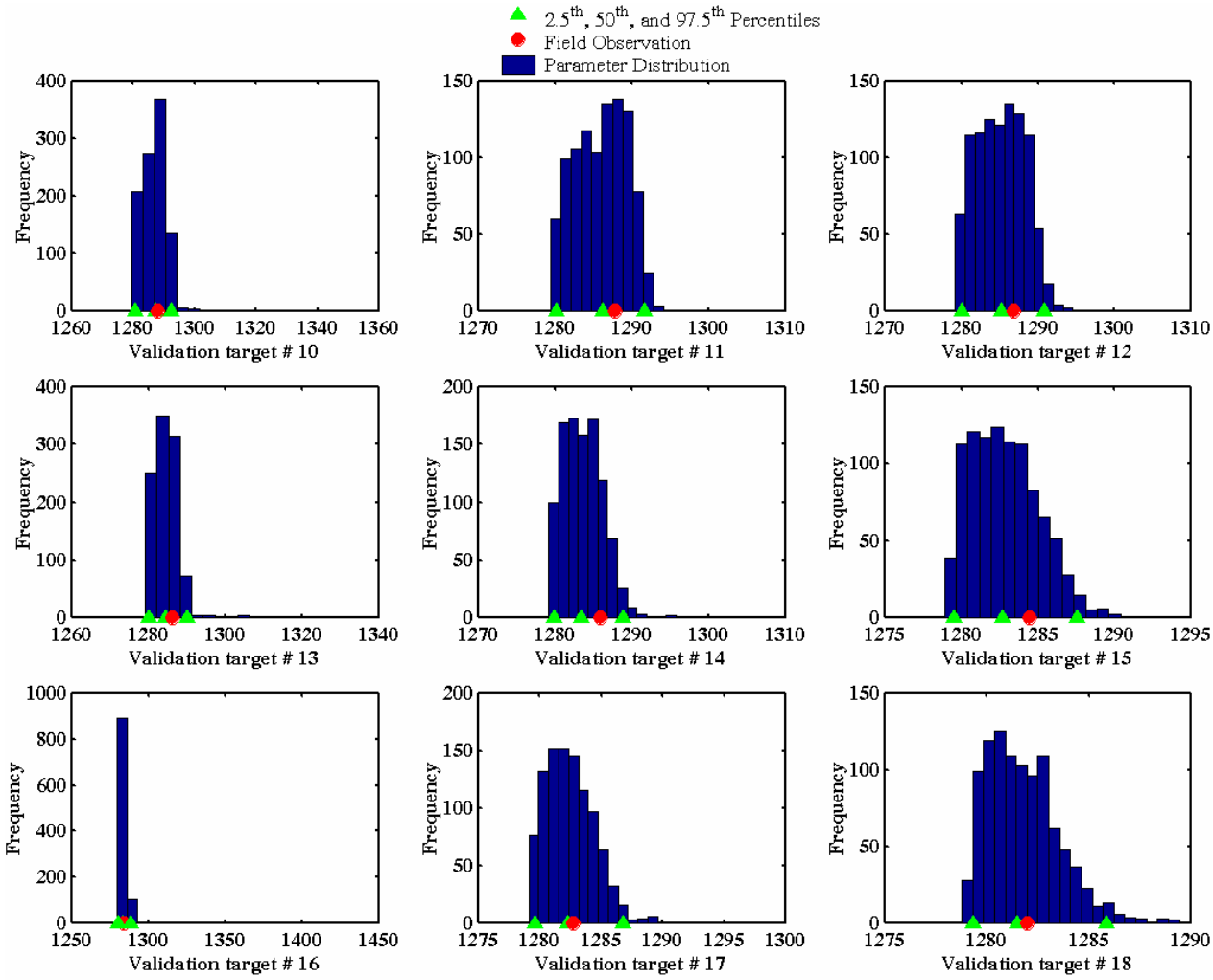

Note: The 2.5th, 50th, and 97.5th percentiles are shown by the green triangles and the hypothesized field data are shown by the red circles.

Figure D-6
Example 1 showing the pdf distributions for validation targets 10 through 18

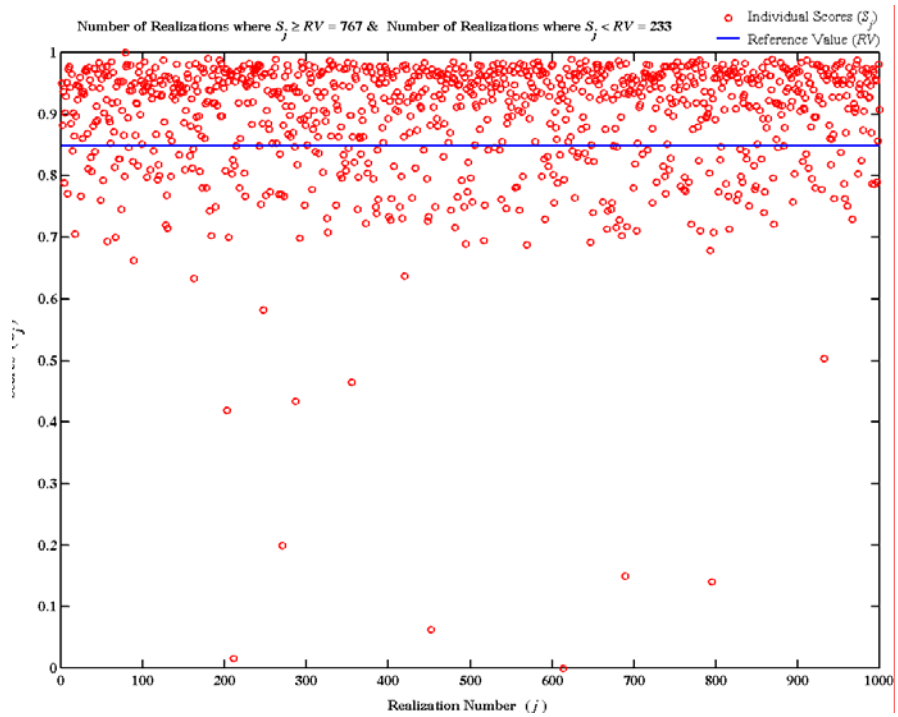

Note: The P_1 value here is 76.7 percent (= 767/1000).

Figure D-7
Example 1 showing individual realization scores, Sj, relative to the Reference Value, RV

Using another set of random values to hypothesize the field data, we obtain a different result as shown in Figures D-8 through D-10 for Example 2. In this case both P_1 and P_2 are less than 40 percent (since the number of validation targets where the red circle are between the 2.5th and the 97.5th percentiles is only 2 ~ 11 percent). In this case, the additional hypothesis tests and linear regression evaluations will be performed to assert whether the model needs to be revised or if the parameter distributions need to be modified.

In example 1 above, the field data values are hypothesized to be equivalent to one of the model realizations. That is, the values of the 18 validation targets are obtained from one single realization and assumed to represent field data collected for the validation analysis. In spite of assuming field values that exactly match one of the model realizations, the P_1 metric was found to be about 76.7 percent. This value is obviously dependent on which realization is selected. Therefore, we repeated the above example 1,000 times with each of the model realizations assumed to represent the field data in one of those times. The P_1 metric is obtained for these 1,000 experiments and its mean value was found to be about 43 percent. Given that the actual field data to be collected for the validation analysis are very unlikely to exactly match any of the Shoal model realizations, the 30 to 40 percent threshold for P_1 is considered realistic. In other

words, if one, on average, obtains 43 percent for P_1 when one of the model realizations is assumed to match real field conditions, one can safely assume the model conceptually valid if P_1 is between 30 and 40 percent when using the actual validation data.

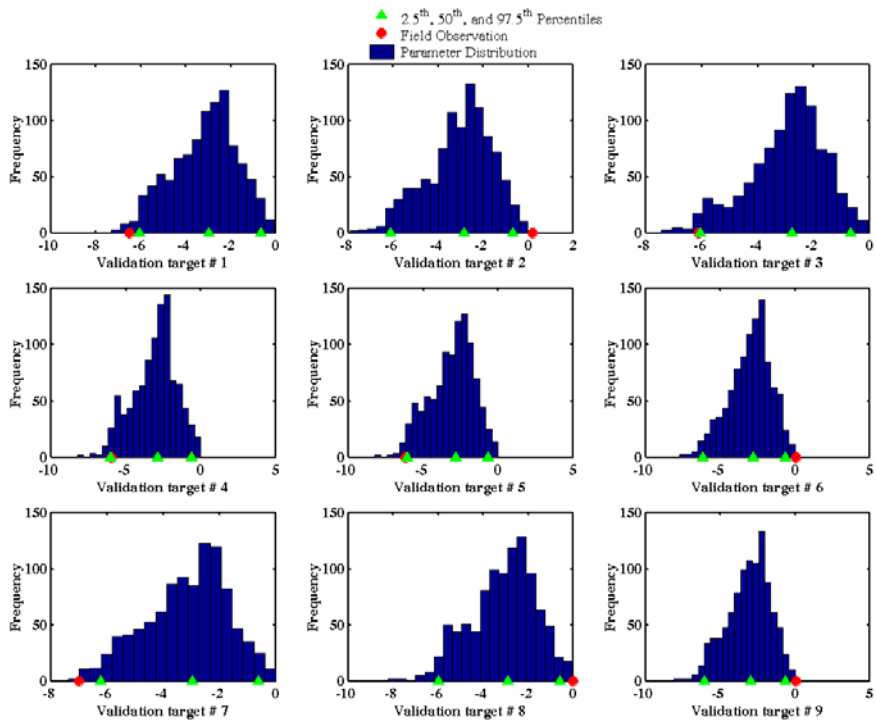

Note: The 2.5th, 50th, and 97.5th percentiles are shown by the green triangles and the hypothesized field data are shown by the red circles.

Figure D-8
Example 2 showing the pdf distributions for validation targets 1 through 9

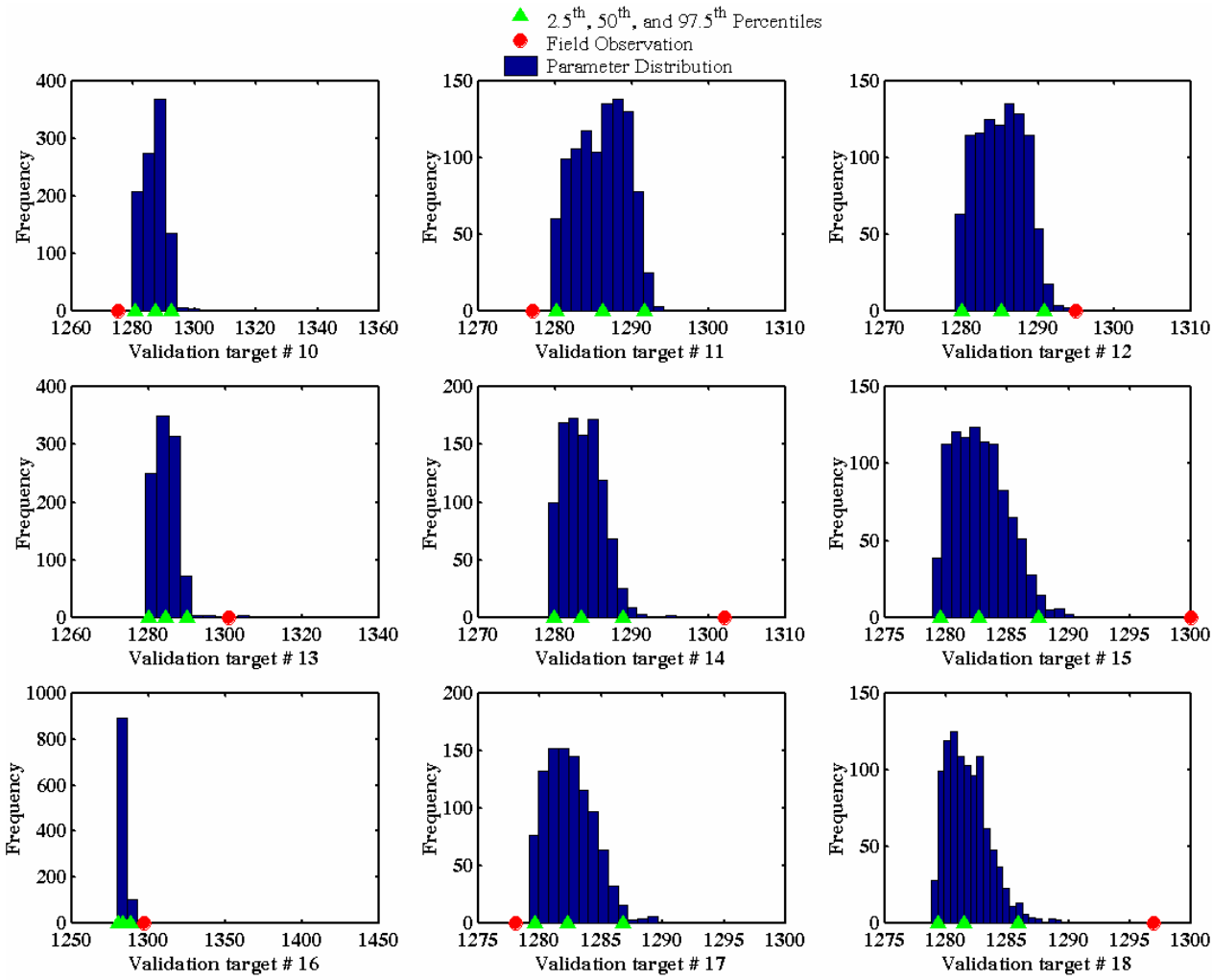

Note: The 2.5th, 50th, and 97.5th percentiles are shown by the green triangles and the hypothesized field data are shown by the red circles.

Figure D-9
Example 2 showing the pdf distributions for validation targets 10 through 18

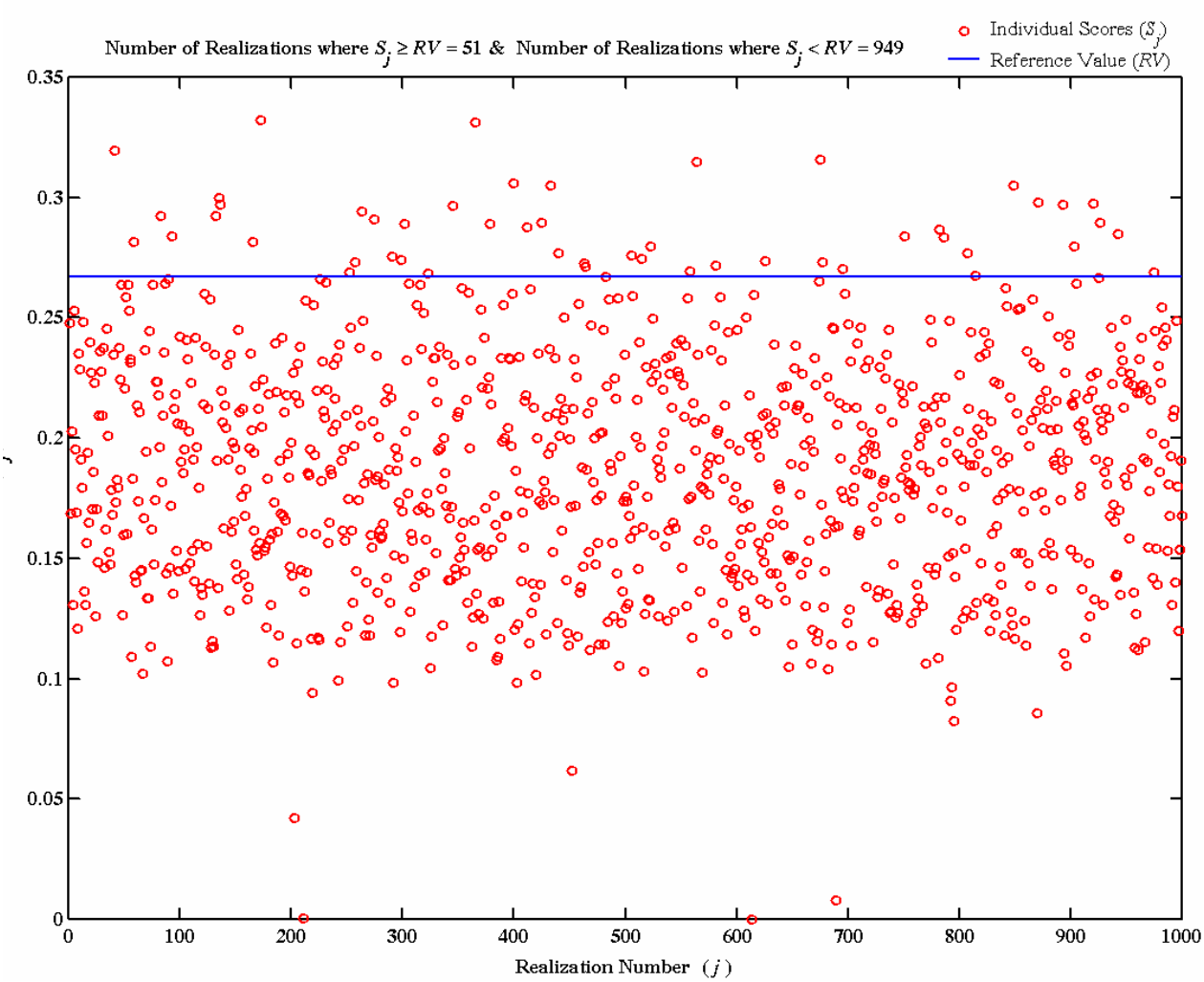

Note: The P_1 value here is 5.1 percent (= 51/1,000).

Figure D-10
Example 2 showing individual realization scores, Sj, relative to the Reference Value, RV

D.4 Testing the Efficacy of P_1 for Multiple Validation Targets

A numerical experiment is performed to evaluate the P_1 metric for the case of multiple validation targets. The experiment is run as follows:

- A model is assumed to produce multiple outputs, each following a standard normal distribution with zero mean and unit variance.
- To test the sensitivity of the P1 metric, 30 observations are randomly selected, with the mean value of each observation being constant. A range of observation means is used to determine at what point the model will be rejected. The mean of each observation set is tested over the range – 4.0 to 4.0 (i.e. – 4.0, –3.9,...,4.0).

- For each mean value, 30 observations are randomly drawn from a normal distribution with the mean equal to the current mean value (i.e., – 4.0, – 3.9, …, 4.0) and a standard deviation = 1.0.
- The RV value for the 30 validation targets is computed using Equation (D-5).
- For each observation mean, the scores Sj for 10,000 realizations of a model (model is assumed to be standard normal) are computed and the metric P_1 is obtained according to Equation (D-3).
- Steps 3 to 5 are then repeated for each observation mean in the range [– 4.0, 4.0].

The purpose of this experiment is to determine the point at which a model will be considered invalid. Each observation set represents data that is either close to the model predictions (i.e., mean values close to zero), or poor fitting data with mean values far away from zero. This experiment allows us to compare the rejection region for using a simple hypothesis test (i.e., Z-test) versus the P_1 measure.

Due to the random nature of the distributions generated in the above procedure, we repeated the above experiment 100 times and the average results are shown in Figure D-11. The blue dots in the figure represent the results for the P_1 metric, the red line shows the results of the Z test that is similar to the test conducted for the single validation target case, the magenta line represents the mean value (of 100 values) of the P_1 metric at each observation mean, and the black line represent a normal distribution that best fits the P_1 results.

For the Z test, we assume that each output realization represents a mean of a normal distribution. For each observation mean value, we then test the following hypothesis:

$$\begin{aligned} \mathrm{H}_0 &: h_j = h_o \qquad for\ \ j = 1, \ldots, NMC \\ \mathrm{H}_1 &: h_j \neq h_o \qquad for\ \ j = 1, \ldots, NMC \end{aligned} \tag{D-7}$$

Then the proportion of Monte Carlo realizations (assumed 10,000 in this experiment) where the null hypothesis, H_0, above is not rejected is plotted against each observation mean as shown with the red line in Figure D-11. According to the figure, the t test would suggest that we accept all model realizations if the mean value of the observations was inside the range [–2.2, 2.2] at 95 percent. The P_1 criterion has a narrower acceptance region ([–1.6, 1.6] according to the black or magenta line) again suggesting that the P_1 metric is overemphasizing (i.e., trying to reduce) Type II error. Therefore, the P_1 criterion is more stringent than typical hypothesis tests and provides a useful method to test multiple validation targets, which is a more difficult task with standard hypothesis test procedures.

It is important to note that according to P_1 and the Z test, decreasing proportions of acceptable realizations are obtained as one deviates from the median of the model output distribution (zero in this test case.) At a five percent significance level and if the observed mean value coincides with the median of the model output, 95 percent of the realizations are deemed acceptable using the Z test, whereas only 60 percent of the model realizations are deemed acceptable using the P_1 measure. Therefore, a rejection region of less than 30 percent for the P_1 criteria is very stringent and should not be confused with the 95 percent confidence interval used for presenting the output uncertainty.

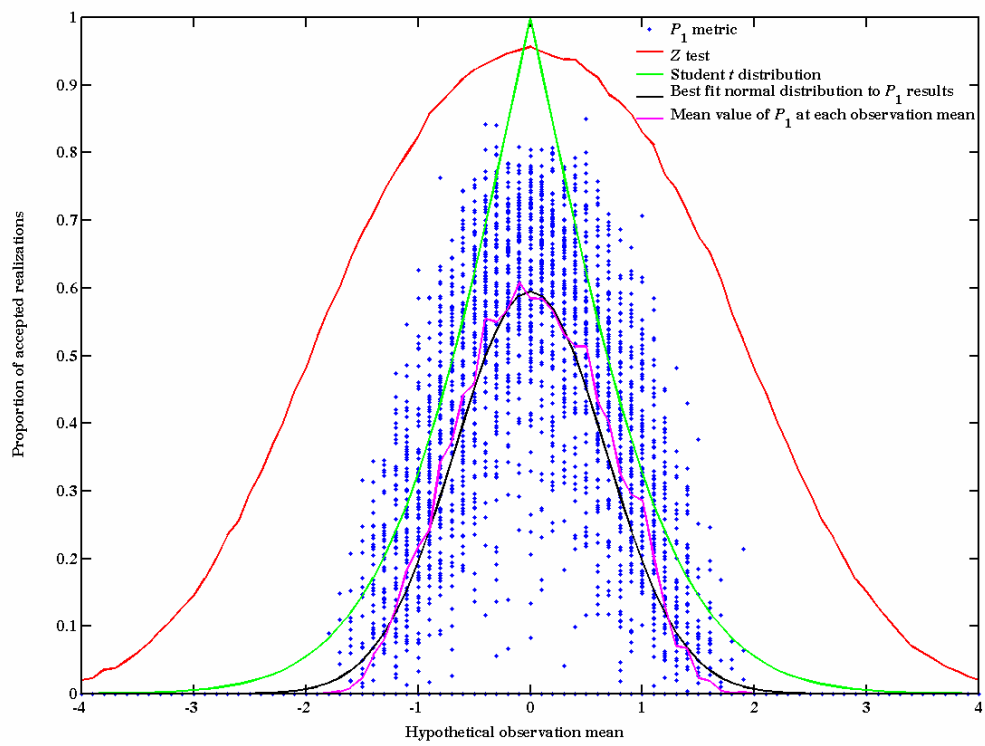

Figure D-11
The P_1 metric (blue), its mean (magenta), its best fit normal distribution (black), student t distribution (green), and the results of hypothesis testing using the Z test (red) for the multiple validation targets case

D.5 Testing the Efficacy of P_2 for Multiple Validation Targets

A numerical experiment is constructed to test the efficacy of the P_2 metric as follows:

- A model is assumed to produce output according to a standard normal distribution.
- Observations are assumed to follow a normal distribution with mean μ and unit variance. The numerical experiment chooses mean values μ from an observation distribution range – 4.0 to 4.0 (i.e., – 4.0, –3.9, …, 4.0).

- For each mean value, a random sample of 30 observations is drawn from a normal distribution with the mean equal to the current mean value (i.e., – 4.0, – 3.9, …, 4.0) and a standard deviation equal to 1.0.

- Each of the thirty observations is then compared to the model's distribution N (0,1) to determine what percentage fall outside of the 95 percent confidence interval (i.e., –1.96 to 1.96).

- The process is repeated for all observation means [– 4.0, 4.0].

Due to the random nature of the distributions generated in the above procedure, we repeated the above experiment about 100 times and the results are shown in Figure D-12. The figure shows that if 50 percent is chosen as the rejection threshold for the P_2 metric, then the model would be accepted for μ=[-1.96, 1.96]. This is a very interesting result as one might initially think that 95 percent should be the acceptance threshold, but 50 percent yields the same acceptance region as a standard t test at a 95 percent confidence level.

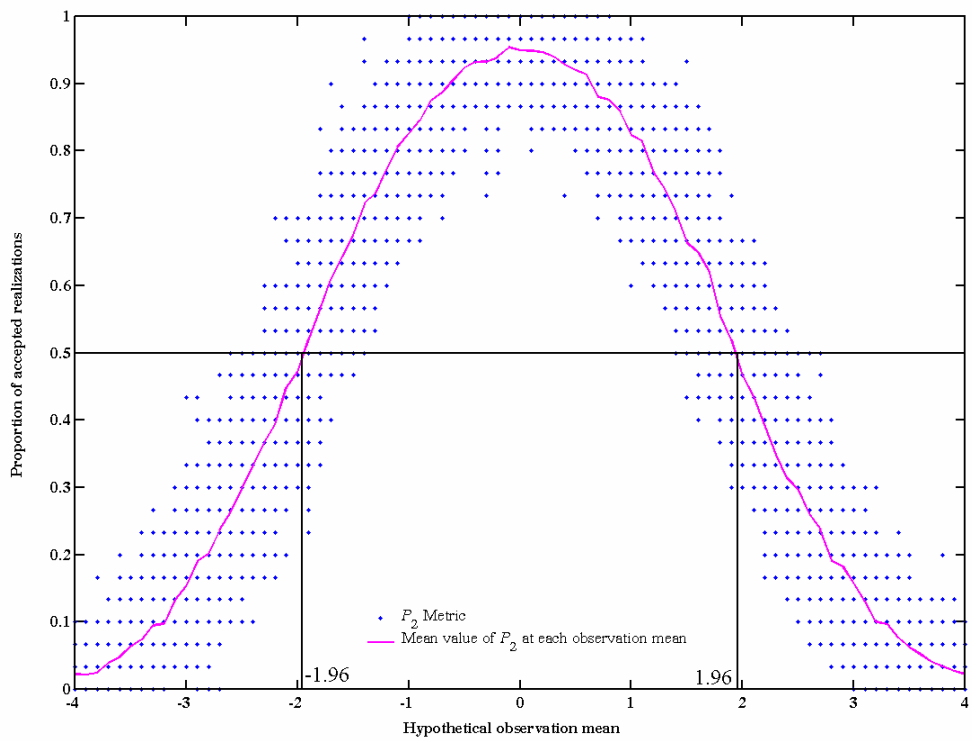

Note: The black lines show that at the 50 percent threshold, the acceptance region is [-1.96, 1.96], which is the same acceptance region for a standard t test at the 95 percent confidence level.

Figure D-12
The P_2 metric (blue) and its mean (magenta) for the multiple validation targets case

Appendix E
Nevada Environmental Restoration Project
Document Review Sheet

NEVADA ENVIRONMENTAL RESTORATION PROJECT
DOCUMENT REVIEW SHEET

1.	Document Title/Number CADD/CAP for CAU 447: Project Shoal Area – Subsurface	2.	Document Date April 2005
3.	Revision Number Rev 1	4.	Originator/Organization SNJV
5.	Responsible DOE/NV ERP Project Mgr.	6.	Date Comments Due
7.	Review Criteria _____		
8.	Reviewer/Organization/Phone No. NDEP – Chief, BoFF, (702) 486-2874	9.	Reviewer: Tim Murphy

10. Comment Number/Location	11. Type[a]	12. Comment/Rationale	13. Comment Response
1. Page 9, Section 2.1.1.1, 3rd paragraph	Specific	The document states that "field data provided definitive information regarding the central question of the location of the groundwater divide relative to the nuclear test". Please provide a reference for this definitive information.	Change sentence to "Hydraulic head data from the wells provided information regarding the central question of the location of the groundwater divide relative to the nuclear test." Note that the reference is given in the prior sentence and that the word "definitive" was removed.
2. Page 14, Section 2.1.1.5, Table 2-1	Specific	The top elevation indicator for well ECH-D is listed as "nb". Please define "nb".	Typographical error. It will be changed to "na", not applicable because borehole was uncased.
3a. Page 25, Section 2.1.2.4.1, 2nd paragraph	Specific	The document states, "… west of underground nuclear test, preventing flow from the test to Fourmile Flat." Please provide a reference for the data that demonstrates that flow is prevented from the test to Fourmile Flat.	Insert the following sentence after the commented sentence: "This divide was first recognized by University of Nevada (1965) and is consistent with basin-and-range hydrogeologic principles (Maxey, 1968). Its location west of the test was demonstrated by hydraulic heads measured in wells at the site (Pohll et al., 1998; Pohlmann et al., 2004)."

3b.		NDEP is reviewing two documents referenced in the response (2004 and 1998) to see if hydraulic head maps are provided. Also, the use of the word "prevented" indicates a high degree of certainty. The reference for the data that demonstrates that the flow is "prevented" has not been addressed in the comment response. In regards to comment 3, I have reviewed the two documents (2004 and 1998) and the hydraulic head contour maps based on measured data are not in the reports. In order to demonstrate the location of the divide west of the test, it is necessary to provide hydraulic head maps based on measured data. The second part of my comment to you in the August 18 email pertaining to comment 3 still stands that the use of the word "prevented" indicates a high degree of certainty. The reference for the data that demonstrates that the flow is "prevented" has not been addressed in the comment response.	The reference for the data requested in the original comment are given in the second sentence proposed for insertion. The data are the hydraulic heads, referenced to tables in Pohll et al. 1998 and Pohlmann et al., 2004. These heads indicate the divide is west of the test, and the divide thus prevents flow from the test from going to the west, toward Fourmile Flat. The additional comments make it clear that those data should be more readily accessible to the reader. In response, water levels will be presented for the wells on the map in Figure 2.1, and the data also listed on Table 2-1. The amount and spatial relationships of the data would render contouring deceptive, if not meaningless, which is why the flow directions are depicted in other maps by arrows approximating the direction. In regard to the last concern, the commented sentence will be changed and additional explanation added to that suggested in the original response. The text would now read: "A groundwater divide runs along the western portion of the Sand Springs Range, west of the underground nuclear test, directing flow from the test to Fairview Valley. This divide was first recognized by the University of Nevada (1965) and is consistent with basin-and-range hydrogeologic principles (Maxey, 1968). Its location west of the test was demonstrated by hydraulic heads measured in wells at the site (Figure 2-1 and Table 2-1), though evaluation of the regional hydrogeology indicates that the divide may not be a prominent, easily detectable feature (Pohlmann et al., 2004). This is due to the very low relief in the water table below Gote Flat, as a result of barriers to flow formed by a shear zone on the east and the range-front fault on the west. The groundwater divide forms…"
4. Page 37, Section 2.1.2.7, 2nd paragraph		Based on the information provided in Table 2-9, it appears the reference to Table 3-9 in this paragraph should be Table 2-9. Please check and correct if necessary.	The reviewer is correct and document will be changed.
5. Page 38, Section 2.1.2.8, 5th paragraph		The document states that "several independent methods of estimating recharge resulted in a potential range of recharge over the PSA". Please provide the methods of estimation.	After the commented sentence, the following will be inserted: "Methods used include a numerical vadose zone model (Pohll, 1999), borehole temperature profiles at Shoal (Pohll et al., 1998), an analysis based on the Maxey-Eakin method (Pohlmann et al., 2004), and a revised recharge model (Pohlmann et al., 2004), all of which are summarized in Pohlmann et al., 2004."

6. Page 38, Section 2.1.2.8, 5th paragraph		The document states that the recharge rate and incoming flux from the southwest are sampled from this distribution. Please provide the data for the distribution.	A reference for the distribution will be added at the end of that sentence. The reference is Pohlmann et al., 2004.
7. Page 39, Section 2.1.2.8, 2nd paragraph		Various models were used to investigate different aspects of the alternate conceptual models and the results used to construct the PSA flow and transport model. Please provide references in the text to the detailed discussions of the various models.	After the first sentence of this para, the following will be added: "These alternative models are described in detail in Pohlmann et al., 2004."
8a. Page 39, Section 2.1.2.8, 2nd paragraph		The document states that "The shear zone was determined to be a very low permeability barrier". Please elaborate as to how it "was determined".	The previous sentence states that hydraulic heads and tests supported a model used to evaluate the shear zone hydrologic behavior. The commented sentence will be modified to state: "From the model results based on these data, the shear zone was determined to be a very low permeability barrier."
8b.		The comment response indicates that the shear zone was determined to be a very low permeability barrier based on the results of the northern Sand Springs Range Model. If this model was run with multiple realizations and the results are still available, then is it possible to obtain an uncertainty estimate (i.e., percentage) and if so please include that in the document, because this information would aid in the elaboration of how it "was determined".	The alternate models were tested deterministically. Multiple realizations were not performed.
9. Page 39, Section 2.1.2.8, 4th paragraph		The contaminant boundary is evaluated in terms of the 95 percent confidence interval, however the document states that "the 90 percent confidence interval for the effective porosity at PSA ranges between 0.005 and 0.07." In most instances the 95 percent confidence interval is listed, thus why is the 90 percent confidence interval for the effective porosity listed? Please explain how this 90 percent confidence interval used for input parameters effect the final modeled contaminant boundary confidence interval.	The 90 percent interval was given in the text for informational purposes only; the entire distribution was sampled for the modeling. To avoid confusion, the text will be changed such that the 95% confidence interval is given. Note that this change has no impact on the results as the full pdf was used in the analysis, not the 95% confidence interval. The 95% confidence interval is 0.004 – 0.088.

10a. Page 40, Section 2.1.2.9, 2nd paragraph		The document states that the tracer test data are used for verification of the model. Please provide the actual spatial coverage of the tracer test, the area of the model influenced, and discuss the resulting influence on the model verification, because on page 42, the document states: "one can deem the flow model as successfully verified."	The following sentence will be added after the 2nd sentence in this para: "The tracer test was conducted between wells located 30 m apart. Numerical modeling suggests that the zone of influence of the year-long test was approximately 100 - 150 m."
10b.		The first two comments concerning the tracer test data spatial coverage and the area of the model influenced are addressed in the comment response. However, there is no discussion of the resulting influence on the model verification, which is the main concern of the comment.	There was specific discussion about this comment in our meeting on July 13, 2005. It is our recollection that NDEP agreed that the suitability of the tracer test for model verification was part of the model acceptance and not subject to reevaluation at this time. It was agreed that the spatial coverage of the tracer test would be presented, allowing the reader to reach their own conclusion if they wish to consider that area relative to the model.
11a. Page 47, Section 2.1.3, 2nd paragraph		The document states that "there is a strong component of vertical flow, driven by the surface recharge." Given the limited vegetation in the area there may be limited recharge. Please provide the documentation for this statement.	Though vertical recharge is low (as simulated in the model), there are essentially no sources of lateral flow because the site is located at the crest of the Sand Springs Range. Also note that the discussion at this point is regarding the model results, not the conceptual model. The sentence will be modified to read: "There is a dominant component of vertical flow in the model, driven by the surface recharge."

11b.		In the comment by NDEP, the concern is that the actual documentation stating that the vertical flow is actually driven by the surface recharge (i.e., how do we know this?) be included in the document. If this is based on a comparison of hydraulic head data in three dimensions throughout the region, then please indicate this in the document and reference the data and hydraulic head maps.	We do not think the discussion requested is appropriate in this section. This section is discussing the model results and the model does simulate vertical flow. This is simply a fact; the numerical model *does* simulate vertical flow. NDEP's comment seems directed at the conceptual model that led to the model development. We recommend they consider the text in the conceptual model section (Section 2.1.2.4.1, pages 25-27) and determine if it satisfies the concern. We are hopeful that it is satisfactory as is, but if not, the following could be added after the last sentence of the first paragraph on page 27 (after the bullets, "For example, the site presents no alternate model to that of flow through fractured granite fed by infiltration of precipitation through the surface of the range and directed toward the adjacent valleys."): "Vertical recharge from precipitation is the only source of groundwater; there are essentially no sources of lateral flow because the site is located at the crest of the Sand Springs Range." Vertically distributed hydraulic head data from ECH-D (University of Nevada, 1965) and from HC-8 and HC-5 (Pohlmann et al., 2004) support the conceptual model in that they exhibit decreasing head with increasing depth (indeed, Maxey used the data from ECH-D in his 1968 paper on the hydrogeology of desert basins); however, it is the position of the site at the crest of the range that dictates the model.
12. Page 61, Section 2.2.3, 1st paragraph		Please clarify the difference between risk and MCL.	The references to risk in this section will be replaced by MCLs. The difference will be clarified in section 2.2.2 Relationship between risk and safe drinking water act requirements, by adding the following sentence: "Lifetime excess cancer risk is calculated using radionuclide-specific cancer-risk coefficients applied to drinking water activity concentrations predicted for specific radionuclides, and estimating lifetime exposure to drinking water. Certain combinations of radionuclides in groundwater might yield estimates of lifetime excess cancer risk that could exceed a risk of 10^{-6}, even though a categorical MCL may not be exceeded. Details regarding the risk and MCL approaches are presented in Pohll et al. 2003." Ref: Pohll, G., K. Pohlmann, J. Daniels, A. Hassan, and J. Chapman, 2003. Contaminant Boundary at the Faultless Underground Nuclear Test. DOE/NV/13609-24, 52p.

13a. Page 82, Section 5.1, 2nd paragraph		The document states "The validation process is necessary for developing an effective detection monitoring system. The detection system is based on the model results. Validation of the model, and reduction of uncertainty in the model predictions in the process, is a priority for detection monitoring." Please elaborate on the interaction of the results of the preliminary model in the design of the detection monitoring system and subsequent use of the information obtained from the detection monitoring system to validate the model.	At the end of the para, the following will be added: "Details regarding the proposed validation process are given in Section 5.5."
13b.		Let me rephrase the comment: If the data from the monitoring network show that the model needs modification, and the model is modified in response to that need, how is the monitoring network going to be modified. Would this monitoring network modification be addresses in a subsequent CAP amendment?	Modifications to the monitoring network would be done with concurrence from NDEP. The mechanism (CAP amendment, technical change, etc.) used will be agreeable to all parties and based upon the situation. Note that in Section 5.2.4 Evaluation and Evolution of Monitoring Network Through Time, the last sentence on page 130 contains the following statement: "Significant changes to the monitoring system will be presented for NDEP concurrence."
14a. Page 85, Section 5.2.0.1, 1st paragraph		The document states "This quantity would mean that the maximum well spacing is less than or equivalent to the plume width in a sufficiently large number of realizations." Please clarify what is meant by sufficiently large number.	The following will be added: "The quantity needed for analysis of deterministic problems is the maximum plume width when the plume crosses a particular CP. For the stochastic Shoal model, this quantity is obtained for each realization and then the average of these plume widths are obtained and used to determine maximum well spacing. For the deterministic problem, the actual plume width (in the field) may be larger or smaller than what is used in the analysis. Thus there is 50 percent probability that the selected plume width in the monitoring design is smaller than the actual plume, and thus there is a 50 percent chance that the resulting well spacing is less than the actual plume width. To be consistent with these probabilities, the mean plume width of the stochastic model was chosen, which would mean that the resulting well spacing has a 50 percent probability to be less than the plume width (because the selected plume width is less than the plume width in 50 percent of the realizations)."

15. Page 86, Section 5.2.0.1, 2nd paragraph		The discussion of the selected CP locations should be clarified. Please explain the need to have a CP line (#2) passing through the eastern edge of the MCL boundary.	The need for considering the eastern edge (and western edge) is simply to account for the irregular shape of the boundary and the uncertainty in the plume trajectory, while considering wells within the compliance boundary. We agree the concepts can be confusing and will change the paragraph to the following (recalling that part of the explanation occurs in the prior paragraph): "The selected CPs are shown in Figure 5-2. Due to the irregular shape of the compliance boundary and the uncertainty in plume trajectory, the CPs are located relative to three different points on the downgradient edge of the boundary: the farthest (central) downgradient point, the farthest downgradient point on the western edge, and the farthest downgradient point on the eastern edge. CP#5 passes through the farthest western point, and CP#2 passes through the farthest eastern point. No plane is placed at the farthest central point because the line would pass entirely outside the compliance boundary. By taking a 50-year reaction time from CP#2, CP#5, and the farthest central point, a safeguard is provided against contaminants crossing the compliance boundary along the mean flow direction and from either side of the mean trajectory as bounded by the northwestern and northeastern points on the boundary. These "reaction time" planes are provided by CP#3 (60-m upgradient of CP#5), CP#4 (60-m upgradient of the farthest central point), and CP#1 (60-m upgradient of CP#2).

16a. Page 90, Section 5.2.0.1, 1st paragraph		The document states that "The Shoal cavity was simulated in the model as a sphere having a diameter of 40 m to match the grid size of 20 m." However, a reference to an estimate of 52 m for the sphere is given in the text. Why was 40 m used in the modeling instead of 60 m?	A detailed discussion regarding the simulation of the cavity is better conducted in the primary modeling section of the CADD, rather than here in the CAP where the monitoring analysis is presented. The exact same configuration was used in both models. The sentence beginning "The radionuclide source…" will be deleted from this paragraph, and additional clarification added in Section 2.1.2.6, page 33. It should be noted that the finite difference formulation of the flow model simulates the nuclear cavity as cubic with an edge length of 40 m. This approximation produces a simulated cavity volume that is approximately 13 percent smaller than the spherical volume associated with the estimated cavity radius, but considering the uncertainty in the estimate and the hydraulic zonation simulated around the cavity this small difference is considered reasonable. The following clarifications will be made in Section 2.1.2.6: Add figure showing cavity zones as (c) of Figure 2-8 (on page 33). Amend the last sentence in the first paragraph of Section 2.1.2.6 (page 32) with the following: "to be consistent with the scales of geophysical and hydraulic measurements at the site, to approximate the estimated volume of the cavity, and to satisfy computational considerations." Section 2.1.2.6, para. 5, sentence 1 (page 34): Follow "The test cavity and surrounding damaged zone are represented by three zones" with "that together radially span across five model cells from the simulated working point (Figure 2.8 [c])." Prepend the second sentence of this paragraph with "The configuration and properties of these zones are" Section 2.1.2.6, para. 6 (page 34): Append the paragraph with the following: "To simulate potential dispersion of radionuclides in fractures and/or prompt injection away from the cavity, 90 percent of the contaminant source is uniformly distributed in a sphere of radius 20 m, with the remaining 10 percent distributed from 20 m to 100 m in exponentially decreasing amounts."

16b.		For the comment response, Section 2.1.2.6, Paragraph 5, section 1 (p.33), does the comment response mean that the beginning of paragraph 5 should read: "The test cavity and surrounding damaged zone are represented by three zones that together radially span across five model cells from the simulated working point (Figure 2.8 (c)). The configuration and properties of these zones are based on the performance of the Shoal test and relationships observed in granite at various distances from the working points of French nuclear tests conducted in granite in the Sahara (Borg,1975)." If this interpretation is correct, then we agree with the comment response.	Yes, your interpretation is correct.
17. Page 90, Section 5.2.0.1, 1st paragraph		The document states that matrix diffusion and radioactive decay are ignored in these calculations because it is plume location, not contaminant concentrations, that is of interest. Please explain how this statement relates to locating the contaminant boundary using the MCL?	There is no relationship to locating the contaminant boundary. The sentence will be amended to read: “Matrix diffusion and radioactive decay are ignored in these calculations because it is plume location, not contaminant concentrations, that is of interest for locating the monitoring wells.”
18a. Page 91, Section 5.2.0.2, 2nd paragraph		If possible, give an example to clarify the various steps in the monitoring design tool #2 for individuals who do not have a strong statistical background, perhaps in an appendix to this document.	Supporting documents have been provided to NDEP and further discussion of this comment will occur after they have a chance to review them. In particular, DOE/NV/13609-39 presents a detailed application of tool #2 to Shoal, but that discussion may not be suitable for readers without a statistical background.

18b.		Supporting documents are currently being reviewed and we will get back to DRI concerning this comment response after the documents are reviewed. In regards to comment 18, one of the documents "Long-Term Monitoring Plan for the Shoal Underground Nuclear Test" has been reviewed for the information indicated in the comment response. The detailed application of tool #2 to Shoal in the LTMP is very similar to the material in the Draft CADD/CAP for Shoal. However, Hassan (2003) is referenced in the LTMP and in reviewing the Draft Hassan document, there appears to be a section that may aid the lay reader in understanding the use of tool #2 (see pages 25-28).	We greatly appreciate the reviewer identifying a solution to the issue. The explanatory discussion from the CNTA Monitoring Plan will be presented at the beginning of Section 5.2.0.2 on Monitoring Design Tool #2, along with a new Figure 5-4.
19. Page 101, Section 5.2.0.3		Please include an example that helps explain the meaning and use of the various alpha levels in Figure 5-10.	Various alpha values are considered because it is an arbitrary factor and the impact of its selection needed to be considered in the analysis. Though the meaning and use of alpha are described in detail in the Shoal monitoring design report (Hassan 2005), presentation of the results for the various alphas is not necessary for the CADD-CAP discussion and may contribute to confusion on the part of some readers. Rather than expanding the discussion, the figure will be changed to present the results for only one alpha, which will clarify the individual well performance values that are the point of the figure. The sentence above the figure will be changed to: "The detection efficiency for individual wells is first analyzed, setting the criterion that a plume is considered detected by a well if the vertically-integrated resident mass within the well vicinity attains a percentage mass of 0.5 percent when or before an equivalent percentage reaches the compliance boundary (Figure 5-11). This percentage is arbitrary and other values are used and discussed in Hassan (2005). The figure shows in general….."

20a. Page 112, Section 5.2.0.4, 2nd paragraph		Bottom of page: In the various sections discussing the monitoring tools the results are presented in terms of probabilities or prediction quantiles, however the comment is made "based on these results, it is reasonable to assume that one interval for each well will have a good chance of detecting the plume migration if it reaches to that particular CP." The use of the term "good chance" does not fit with the previous use of probabilities. Please modify this statement to reflect the probabilistic approach.	The sentence will be changed to: "Based on these results, it is reasonable to assume that one interval for each well is sufficient for detecting plume migration if it reaches to that particular CP."

20b.		If the results of the multiple realizations are available, then a calculation of the uncertainty can be made in terms of a percentage and this will answer NDEP's comment concerning modification of the statement to reflect the probabilistic approach.	This is difficult at this point in the discussion because the location of the recommended interval hasn't been identified yet (that happens in the next couple of paragraphs), and the statistics of detection depend on the vertical location. The quantitative performance of various intervals was computed, with some of those results shown on figure 5-19. At this point in the text, the analysis is only evaluating the number of vertical intervals, not the precise location. Another important factor on the number of vertical intervals comes from consideration of good hydrogeologic monitoring practice. Screening multiple intervals in a well is entirely possible, but isolating them from each other is very difficult. This leads to problems interpreting the results. There would be flow in the wellbore from the zone of higher to lower head (from the highest to lowest interval at Shoal) and the pump will be producing water from whichever interval is most conductive (a zone which might have experienced inflow from other horizons during the long periods between sampling). Also recall that the final zone chosen will be subject to qualitative hydrogeologic interpretation, with any large fracture zone encountered during drilling carefully evaluated as a potential screen location, whether or not it is at the exact vertical horizon indicated by the model. Ultimately, dilution is the likely result of longer screened zones. There would need to be compelling reasons for multiple zones and the statistical analysis of the particle tracking results shows that is not the case. We agree with the original comment and still seek to respond to it, but without presenting additional statistics, given the difficulties stated above. Please consider the following modification instead, again replacing the last sentence on page 117: "Based on these results, and the fact that a single completion zone prevents the possibility of cross-flow, mixing and dilution in the wellbore, a single interval is recommended for each well."

21a. Page 121, Section 5.2.2.1, 2nd paragraph		The comment is made that based on the differences between the well screen intervals and the model heads averaged through 20 cubic meter blocks, the information to be gained from very precise head measurements for proof-of-concept is reduced. Please explain how this reduction in information may impact the proof of concept and validation of the model.	The intent of the discussion was to clarify that the precision desired for trend analysis (tenth of a foot) was much greater than the accuracy needed for the validation analysis. The text will be modified as follows: Last paragraph of Section 5.2.2.1, page 125: Replace the second sentence (that begins "The model reports head…") and third sentences with the following: "The model simulates head values at the cell scale of 20x20x20 m, whereas a well provides access to a very limited portion of the aquifer directly adjoining the screen and filter pack. Thus, field measurements of heads in a fractured aquifer are much more highly resolved than model-simulated heads, and their high precision does not provide additional information for proof-of-concept when comparing them to simulated heads that can be considered averages over relatively large blocks of the aquifer." Editor Note: The following text was added after the added text above: "(The issue of different scales of measurement in the validation process is discussed in Appendix E of Hassan, 2003.)"
21b.		With the difference in scale between the model and field measurements how will the two be compared (i.e. if the measured head values are within plus or minus one standard deviation of the model hydraulic head values will this indicate an acceptable comparison)?	This response is essentially a new comment in regard to the model validation process, so we infer that the response given above was acceptable for the original comment. In regard to this question, we plan to apply multiple measures of model performance. No single statistical test is perfect, and considering the results of a variety of tests decreases the chance of accepting a faulty model. The particular issue of different scales of measurement vs. model is addressed in Appendix E of the CNTA validation report (Hassan, 2003; DOE/NV/13609-27: Appendix E Stochastic Validation Approach), which is also referenced in the Shoal Validation plan. The validation criteria analysis will also be used where the measured value at the small scale is weighted based on how far it is located from the mean head value of the stochastic realization. In regard to your specific question in parentheses, based on the validation criteria analysis performed for Shoal (measures P1 and P2 in the validation criteria section of the Shoal validation report and in Appendix D of the CADD-CAP), the answer is yes.

22a. Page 121, Section 5.2.2.2, 2nd paragraph		Based on the sentence "Subsequent sample collection from the new wells and any other well sampled using a pump, will be conducted after one well volume is purged….". Have low flow techniques been evaluated to indicate that the purging of one well volume is the appropriate approach?	We solicit input from NDEP on acceptable low-flow techniques and alternative methods may be proposed based on that dialogue. Note that HC-1 does not currently have a pump.
22b.		A list of references on the low flow techniques was emailed to Karl Pohlmann on July 14, 2005 as provided by Michelle Stamates. For further discussion on such techniques, we will need to involve Michelle. Let us know if you would like such a discussion.	The low productivity of the new CNTA wells will raise this as an issue for that site in the near future. We suggest leaving the wording as is for the Shoal CADD-CAP, pending observing the well characteristics.
23a. Page 124, Section 5.2.4, 2nd paragraph		Based on the comment that the "pump configuration in HC-4 prevents routine water level measurements", how will this fact influence the use of this well in the proof-of-concept monitoring network?	We appreciate your notation of this issue. We propose excluding HC-4 from hydraulic head monitoring until such future time as well maintenance allows a water-level access tube to be installed. The following text will be added at the end of Section 5.2.2 Monitoring Analytes and Parameters, after the sentence beginning "The system parameter…" "Due to the current pump column configuration in well HC-4, there is no access for water level measurements. It will be excluded from the hydraulic head monitoring until future well maintenance activities allow an access tube to be installed."
23b.		While we agree with your response, can you please supply a timeframe in which future well maintenance activity to install an access tube will be completed?	Well maintenance is performed on an as-needed basis, such that there is no scheduled timeframe. Whenever the pump malfunctions and needs to be pulled, the access tube will be installed.
24a. Page 125, Section 5.2.4:		Based on the water levels presented in Figure 5-22, it appears the water levels are still recovering from the tracer test. Thus the aquifer is in quasi steady state. With HC-1 included in the monitoring well network for proof-of-concept and validation of the PSA model, please elaborate as to how quasi steady state data will be used to validate the model?	From July 2002 to July 2004, the maximum water level change was about 2.5 m and the rate of water level recovery is decreasing over time as shown in Figure 5-23. Given that the uncertainty range predicted by the model is about 15 m (Figure 5-24), the use of the quasi-steady state head during the 5-year proof of concept period and the incremental change in heads are much smaller than this uncertainty range and thus are not expected to significantly influence the results of the validation analysis. (Editor note: figure numbers have changed due to additional text added in Section 5)

24b.		We agree with the response, please include this in the text of the final CADD/CAP.	The text was added on page 129 by splitting the 3rd para (the para beginning "gaining stabilized heads…") at the sentence "The fluctuations encountered in a well…" and adding the text in the comment response afterward.
25. Page 132, Section 5.4, end of paragraph		The document states that before initiating surface construction activities NNSA/NSO will obtain a Surface Area Disturbance Air Quality Operating Permit in accordance with the NAC. Please include the specific NAC citation.	The specific NAC citation will be included.
26. Page 135, Section 5.5.1.1		In the legend of Figure 5-24, a blue box is shown indicating the steps using pre-validation data only. However, there are no blue boxes in the figure, only a green one? Please correct this discrepancy.	The figure will be corrected accordingly.
27a.		The NDEP concurs with the proposed placement of the monitoring wells MV-1, MV-2 and MV-3 and the inclusion of wells HC-1 and HC-4 in the monitoring network. However, in regards to a long-term monitoring well network for this CAU, NDEP requests the inclusion of an existing well to the east of the emplacement cavity but west of the shear zone, such as well HC-7, in addition to a well to the west of the emplacement cavity, but east of the hydraulic boundary, such as well HC-2.	DOE will provide NDEP with recent LTHMP data for their consideration on this comment.
27b.		Can you supply a timeframe in which the LTHMP data will be submitted to NDEP.	The data are currently being cleared through the Safeguard and Security Division for public release. That approval is expected within 30 days. (Editor note: This data was sent to NDEP on 10/3/05).

Library Distribution List

	Copies
U.S. Department of Energy National Nuclear Security Administration Nevada Site Office Technical Library P.O. Box 98518, M/S 505 Las Vegas, NV 89193-8518	1 (Uncontrolled)
U.S. Department of Energy Office of Scientific and Technical Information P.O. Box 62 Oak Ridge, TN 37831-0062	1 (Uncontrolled, electronic copy)
Southern Nevada Public Reading Facility c/o Nuclear Testing Archive P.O. Box 98521, M/S 400 Las Vegas, NV 89193-8521	2 (Uncontrolled, electronic copies)
Manager, Northern Nevada FFACO Public Reading Facility c/o Nevada State Library & Archives 100 N. Stewart Street Carson City, NV 89701-4285	1 (Uncontrolled, electronic copy)